DEVELOPMENT OF A MUSCLE PROGENITOR CELL-BASED THERAPEUTIC APPROACH FOR THE TREATMENT OF STRESS URINARY INCONTINENCE

by

Ronald Jay Jankowski

B.S., University of Pittsburgh, 1994

M.S., University of Pittsburgh, 1997

Submitted to the Graduate Faculty of

The School of Engineering in partial fulfillment

of the requirements for the degree of

Doctor of Philosophy

University of Pittsburgh

2003

UNIVERSITY OF PITTSBURGH

SCHOOL OF ENGINEERING

This dissertation was presented

by

Ronald Jay Jankowski

It was defended on

April 17, 2003

and approved by

Harvey Borovetz, PhD, Professor, Department of Bioengineering

David Vorp, PhD, Assistant Professor, Departments of Surgery and Bioengineering

William Wagner, PhD, Associate Professor, Departments of Surgery and Bioengineering

Lars Gilbertson, PhD, Assistant Professor, Department of Bioengineering

Michael Chancellor, MD, Professor of Urology and Obstetrics and Gynecology

Dissertation Director: Johnny Huard, PhD, Associate Professor, Departments of Orthopaedic Surgery and Bioengineering and Molecular Genetics and Biochemistry

ABSTRACT

DEVELOPMENT OF A MUSCLE PROGENITOR CELL-BASED THERAPEUTIC APPROACH FOR THE TREATMENT OF STRESS URINARY INCONTINENCE

Ronald Jay Jankowski, PhD

University of Pittsburgh, 2003

The urethra serves a dual function by maintaining continence during bladder filling and aiding the release of urine during micturition. Within the urethra, a sphincter region containing both smooth and striated muscle layers normally prevents involuntary leakage of urine. However, patients with stress urinary incontinence lose this ability upon sudden increases in intravesical pressure (i.e. from coughing, straining, etc.). This condition has been associated with a decline in striated muscle, which may be susceptible to direct muscle or associated nerve damage. Cellular uromyoplasty proposes to augment this muscle layer through the transplantation of myogenic progenitors. The goal of this work was to address current deficiencies regarding the isolation and identification of efficient progenitors, and the urethral biomechanical consequences of striated muscle restoration. Both issues are essential for effective clinical implementation of this therapeutic approach.

The ability of various progenitor populations to regenerate skeletal (striated) muscle was assessed in a dystrophic mouse model. Both cell surface protein expression and behavioral characteristics were investigated for their potential use as indicators of regenerative efficiency. The results demonstrate the limited utility of surface proteins due to fluctuations in expression and lack of regenerative consistency between directly-isolated and cultured cell populations. Behavioral characteristics related to the ability of cells to maintain a proliferative phenotype under differentiation-inducing conditions appears more promising in this regard, and indicates that *in vivo* expansion of transplanted cells may be a critical variable in the regeneration process.

A new *ex vivo* method to assess the regional biomechanical function of the intact urethra, under physiologic loading conditions, was introduced and validated. Quantitative characterization and comparison of tissue responses

to applied intralumenal pressures was performed in the presence or absence of selected muscle activity. The dominant smooth muscle influence observed suggests that a large degree of striated regeneration may be necessary to impart functional changes in urethra mechanics. Importantly, these results also indicate that muscle fiber orientation may significantly impact urethra closure function.

Together, this information will be useful in progressing uromyoplasty therapy toward clinical utility, and aid the broader scientific community investigating myogenic cell transplantation and lower urinary tract function.

DESCRIPTORS

Biomechanics
Flow Cytometry
Incontinence
Isolation
Progenitors
Regeneration
Smooth Muscle
Striated Muscle
Transplantation
Urethra

FOREWORD

I would like to gratefully acknowledge the support of my thesis advisor, Johnny Huard, and all of the members of the Growth and Development Laboratory. It was truly a pleasure to work in such a friendly and supportive environment. I am sure that the relationships that I have established in the G&D lab will last long beyond my departure. Research is always a challenging endeavor, but becomes significantly easier when you are surrounded by talented and intelligent individuals with diverse research and clinical backgrounds. The diversity of the lab from a cultural standpoint was also something I truly enjoyed, although Nicole (my wife) has informed me that I am never allowed to go to Japan unaccompanied.

Sincere thanks to David Vorp, Harvey Borovetz, William Wagner, Lars Gilbertson and Michael Chancellor for willingly agreeing to comprise my thesis committee and critique the work presented here, and more. David Vorp, Michael Chancellor, and Lars Gilbertson were extremely supportive in many aspects of the urethra biomechanics work. William Wagner was particularly instrumental in helping me to develop sound research skills during my formative graduate years. Special thanks go to Harvey Borovetz for not only convincing and allowing me to re-enter the graduate program, but for allowing me to form the second half of a tremendously dynamic teaching duo for Artificial Organs (x2).

Unfortunately I cannot list all the members of the G&D lab, but I must acknowledge Dr. Zhuqing Qu-Peterson for her cell isolation wizardry and the cryostat sectioning talents of both Marcelle Huard and Jing Zhou. Also, thanks to Bob Lakomy and Alexis Styche for their flow cytometry expertise, and most of all their patience.

Last but certainly not least, I am eternally indebted to Nicole, who has endured what may have appeared to be a life-long commitment to student life. Not only did you provide me with tremendous support, you also did not lock me out of the house or hit me in the head with a shoe.

I would also like to acknowledge at this time the following sources of funding support for the work presented: the Muscular Dystrophy Association, the Parent Project (USA), the Orris C. Hirtzel and Beatrice Dewey Hirtzel Memorial Foundation, and the National Institutes of Health (RO1 DK55387, RO1 AR049398, K12 DK02656).

TABLE OF CONTENTS

LIST OF TABLES

LIST OF FIGURES

1.0 INTRODUCTION

The information presented is intended to facilitate the development of an effective method to augment or generate new functional striated (skeletal) muscle to improve the continence securing mechanism of the urethral sphincter through myogenic cell transplantation; an experimental therapy termed 'cellular uromyoplasty'. One of the main targets for such therapy is a segment of the urethra containing a striated muscle layer that has been shown to be vital in maintaining continence under both normal and stress-inducing conditions. Importantly, damage to this muscle layer, through various mechanisms, is suspected in the development of stress incontinence conditions. Implementation and evaluation of this therapy requires an understanding of the cell isolation, transplantation, and regeneration processes as well as the functional consequences of the intervention in terms of its effects on the ability of the tissue to perform its intended mechanical function.

The following background information provides the interested reader with a scientific basis behind this investigational therapy as well as updated information in the relevant areas of myogenic progenitors, myogenic cell transplantation, stress urinary incontinence pathophysiology and treatment options, and evaluation of urethral function. Current deficiencies in this knowledge that limit the progression of this experimental treatment are highlighted, and subsequently serve as the foundation for the experimental investigations performed to address these deficiencies.

1.1 Myogenic Progenitors

1.1.1 Role in Growth, Homeostasis and Regeneration Following Injury

Skeletal, or striated, muscle is comprised of a latticework of connective tissue surrounding bundles, or fascicles, of multi-nucleated myofibers. A complex structural organization exists within each myofiber (Figure 1.1), which individually contains the contractile sarcomeric proteins that interact to shorten the cellular structure, leading to the generation of force. The majority of these myofibers are formed postnatally, during development, from the

interaction of committed myogenic cells which fuse together to form new multi-nucleated myofibers or contribute to the growth of already existing fibers by providing additional nuclei and cytoplasmic content, as needed. The primary source of these committed myogenic precursors, often referred to as myoblasts, are a population of progenitors termed satellite cells. These satellite cells maintain their own cellular structure and typically reside in a position outside the sarcolemma but beneath the protective basal lamina surrounding the myofibers [1], as shown in Figures 1.2 and 1.3. They have been given this name due to their sustained position near the perimeter of the myofiber, and do not actively participate in generating force. In fact, they have been shown through microelectrode studies to develop no electrical coupling with their associated myofiber [2]. Rather, they function only to produce the cellular progeny necessary to provide nuclei to form new myofibers or to augment growing fibers [3]. Not surprisingly, they are most abundant during early development and decline in relative number concomitant with increases in myofiber-associated nuclei, although there is also evidence that actual satellite cell number may decline as well within specific muscles and with senility. Under normal conditions these cells remain mitotically-quiescent but can become stimulated to enter the cell cycle, through as yet undefined paracrine or autocrine locally-released growth factors, during the need for perceived growth or during post-natal reparative responses to stress or damage. Such conditions exist during both normal function and through overwork of muscles, although it is not yet clear whether their responses are primarily mediated by the work itself or rather as a consequence of exercise-induced myofiber damage [2].

As skeletal muscle contains several fiber types, identified primarily by the selective expression of several forms of the contractile myosin heavy chain protein and defining their relative fatigue-resistance, it is important to note that satellite cells are associated with the maintenance of all fiber types. *In vivo* labeling studies have demonstrated the satellite cell's ability to contribute myonuclei to more than one myofiber during growth, and particularly during repair, in a manner independent of fiber type [4].

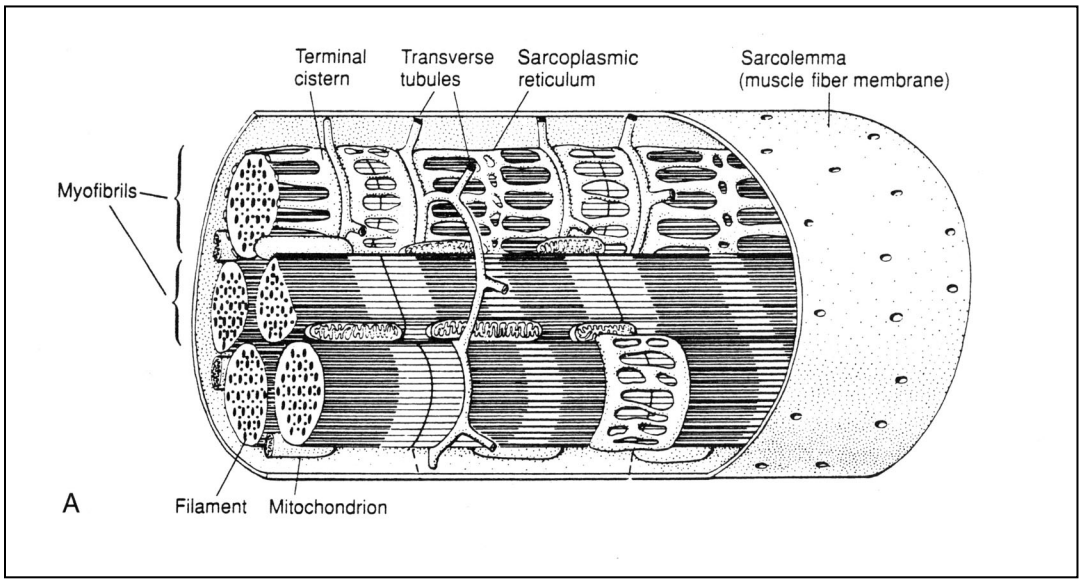

Figure 1.1 Schematic of individual myofiber structure, from [5].

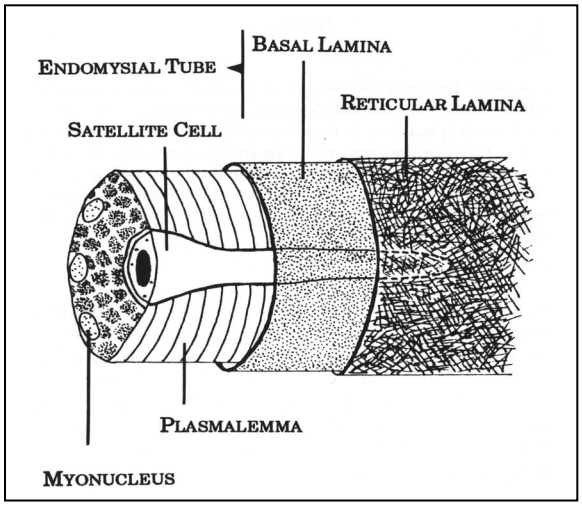

Figure 1.2 Schematic representation of satellite cell positioning in relation to the myofiber and its surrounding extracellular matrix. Reproduced with permission from The McGraw-Hill Companies [2].

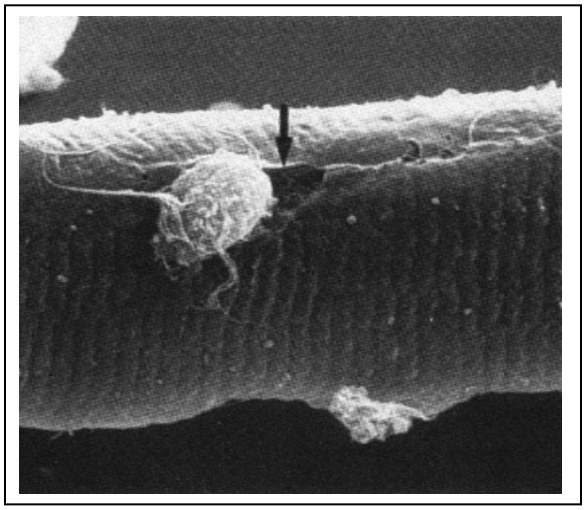

Figure 1.3 Scanning electron micrograph of a single isolated myofiber *in vitro*, in which the extracellular basal lamina matrix has been enzymatically-digested. The arrow indicates the presence of a satellite cell outside of the fiber plasmalemma. Reproduced with permission from The McGraw-Hill Companies [2].

1.1.2 Myogenic Differentiation

A family of four transcription factors, termed the myogenic regulatory factors (MRF), has been demonstrated to direct the myogenic differentiation process and has been useful in defining the developmental relationship and fundamental differences among the various myogenic cells. Fortunately these factors appear to be highly conserved among species, and thus such regulational relationships have been developed over the years as a composite of information gathered from a number of animal models. These MRFs (Myf-5, MyoD, myogenin, MRF4) and other proteins that have been associated with various stages of cellular maturation are shown in Figure 1.4, which presents a simplistic overview of skeletal muscle progenitor/precursor cell hierarchy and differentiation within the myogenic compartment [6-10]. It has been shown that these four proteins are expressed in a relatively defined sequence within all myogenic cells and can be divided into two separate groups: early stage and late stage

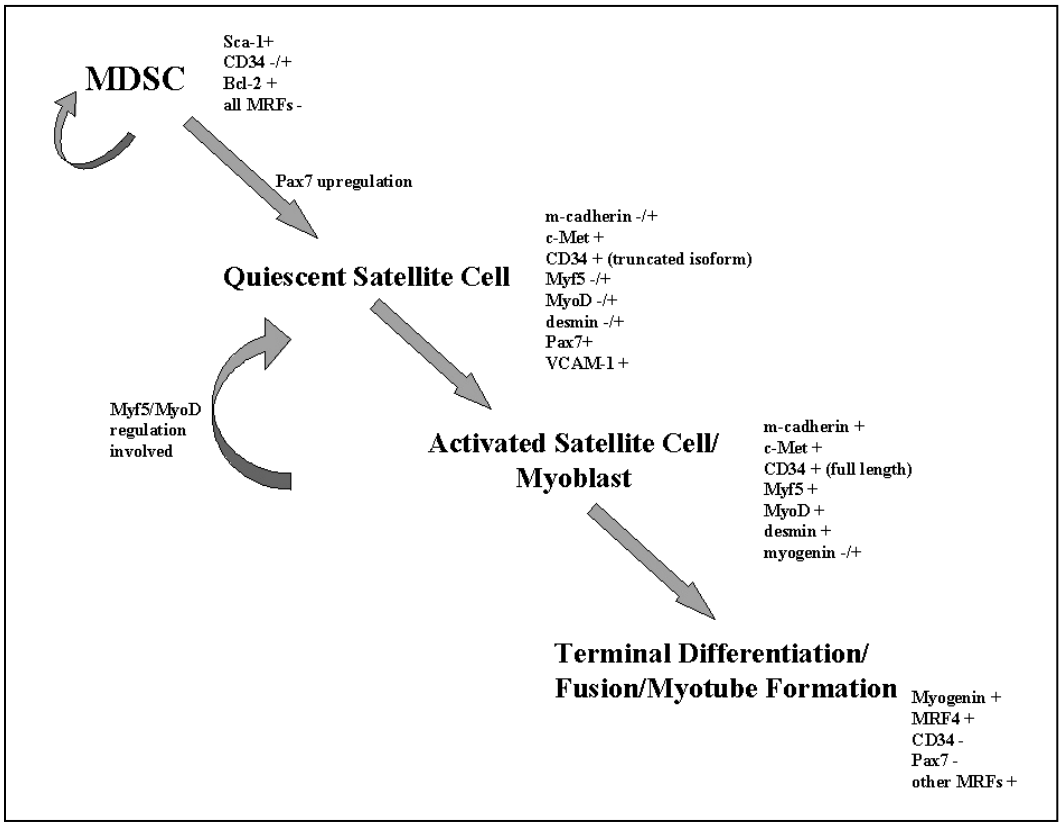

Figure 1.4 Proposed model of skeletal muscle differentiation and progenitor hierarchy, based on current published literature.

factors [11]. Myf-5 and MyoD are typically expressed at earlier stages of myogenic progression and are considered to play a role in specifying commitment to the muscle lineage, although their exact sequence of expression in relation to the progression of differentiation is still under debate [6, 12, 13]. By consensus, myogenin expression represents the earliest known event of myogenic commitment to cell cycle withdrawal and terminal differentiation followed by MRF4 which is thought to be involved in myotube maturation, and which consequently leads to the expression of all four MRFs simultaneously [8, 14].

As might be inferred, both differentiation and cell cycle processes are regulated in a coordinated fashion. One proposed overview of early stage MRF expression in relation to the regulation of such transitions is provided in Figure 1.5 [15]. Although many other proteins are involved, MyoD activity is currently considered to be one of the key mediators in the interrelation between these cellular processes. Evidence of myogenic inhibition by pro-mitotic cell cycle regulatory proteins, such as cyclin D1, has been reported. For instance, it has been observed that cyclin D1 acts to promote the nuclear translocation of cyclin-dependent kinase 4 which in turn subsequently disrupts MyoD DNA-binding activity [16]. Expression of cyclin D1 can be induced through the actions of locally released combinations of known potent myogenic inhibitors of differentiation such as transforming growth factor-β and fibroblast growth factor, to name a few [17]. Conversely, differentiation processes are coincident with both the down -regulation of cell cycle activators and the up-regulation of competitive inhibitors. In particular, expression

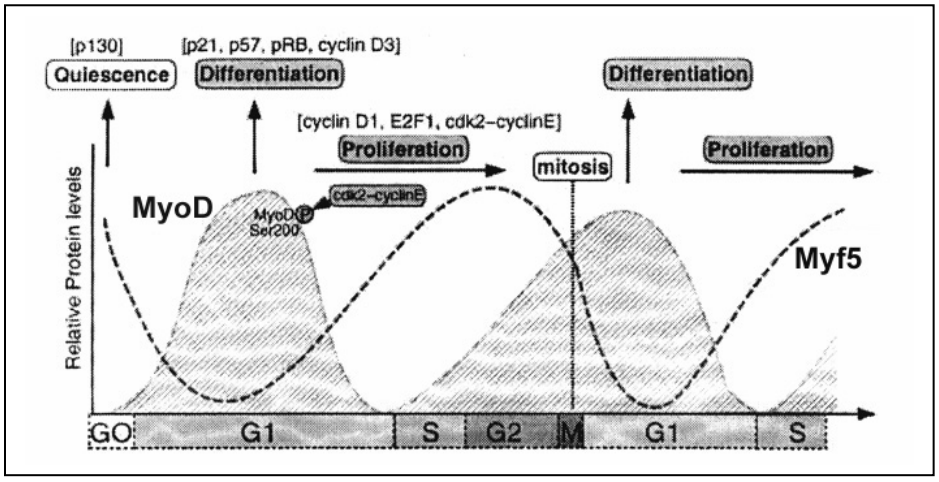

Figure 1.5 Proposed model of myogenic cell MRF expression in relation to alternative proliferation or differentiation pathways, from [15].

and activation of certain cyclin-dependent kinase inhibitors (such as p21 and p57) and the retinoblastoma protein have been shown to be induced by high levels of MyoD expression, leading to cell cycle arrest [15]. Researchers are now just beginning to understand and define this complex regulational control and many reviews detailing the numerous biochemical interactions coordinating this activity, that have been revealed thus far, are available for the interested reader [18-21].

1.1.3 Cellular Heterogeneity

Satellite cells appear to be distinct from their progeny, at the least, with regard to their self-renewal capacity. Demonstrations of this quality have been provided by assessments of satellite cell frequency, which has been shown to be relatively maintained within regenerated muscle following repeated challenges of induced regeneration by the administration of myotoxic agents [2]. Traditionally, maintenance of this cell compartment during growth and repair has been attributed to asymmetric divisions, such that a committed myoblast and a conserved satellite cell are generated following an induced cell cycle [4]. These myoblast progeny, while capable of limited proliferation, are destined to withdrawal from the cell cycle and fuse into multi-nucleated myotubes in relation to the specific sequences of MRF gene expression that regulate their progression toward terminal differentiation [22, 23].

Aside from the differences that exist between satellite cells and their myoblast progeny, compelling evidence for heterogeneity within the satellite cell compartment itself exists. *In vivo* proliferation studies have described at least two different satellite cell progenitor populations, one seemingly limited in the number of mitotic divisions and the other capable of generating larger cell populations through asymmetric cell divisions [24, 25]. Additional evidence is presented by *in vitro* studies that have reported variations in the size of colonies generated by individual satellite cells, as well as observed proliferative heterogeneity upon exposure to differentiation conditions [8, 26-28]. Interestingly, a reduction of satellite cell proliferative potential has also been observed coincident with increasing age and following numerous rounds of regenerative responses to injury [29, 30], suggesting an exhaustive quality which may contribute to this observed heterogeneity. It has been suggested that the age-induced loss of muscle mass, referred to as sarcopenia, is reflective of this diminished satellite cell capacity [31].

1.1.4 Muscle Derived Stem Cells

In addition to the satellite and myoblast cells described, recent evidence has suggested the existence of yet another distinct myogenic progenitor, the muscle-derived stem cell (MDSC). Adult stem cells have been traditionally defined by their self-renewal and multi-lineage differentiation capacity. Thus, it is important to conceptually distinguish between the MDSC and the conventional satellite cell, often referred to as 'muscle stem cells'. Satellite cells are indeed capable of regenerating skeletal muscle and demonstrate self-renewal properties, however they are considered to be restricted progenitors of the myogenic lineage only. Although such traditional concepts regarding satellite cell differentiation capacity are currently being challenged [32], the MDSC, which may represent a predecessor of the satellite cell, is currently considered to be distinct in that its ability to produce progeny may not be restricted to the myogenic or mesenchymal tissues [33].

The existence of MDSCs remains somewhat controversial; however developmental models have recently emerged attempting to address their potential origin and function. One such model is based upon the finding that satellite-like cells, sharing both myogenic and endothelial markers, can be obtained from the dorsal aorta of murine embryos [34]. This suggests that at least some portion of the myogenic progenitor cell population may develop independently of embryonic myogenesis and instead may be rooted in vascular development. Such a model predicts that progenitors associated with the vasculature may differentiate in a capacity directly related to the tissue with which the vasculature is associated [9, 34, 35]. Other evidence is supportive of a clear distinction between conventional satellite cells and MDSCs, distinguished through examination of the differential expression of the transcription factor Pax7. $Pax7^{-/-}$ mice demonstrate a complete absence of satellite cells, whereas the number of MDSCs remains unaffected. Such evidence suggests that MDSCs represent satellite cell progenitors with Pax7 expression signaling commitment to the myogenic lineage [10]. [Considering the fact that $Pax7^{-/-}$ mice display normal-appearing skeletal muscle further implies that embryonic myoblast and muscle development may occur independently of satellite cell development.]

In terms of differentiation capacity, investigators have recently demonstrated the MDSCs potential toward both the hematopoietic and osteogenic lineages [36-39]. Such differentiation ability has also sparked debate over the potential bone-marrow origin of MDSCs, and has called to question whether these cells may actually be present within the circulation and become inadvertently obtained along with the heavily-perfused muscle biopsy during

isolation. The idea of a circulating cell competent in the repair of skeletal muscle is not new [40]. However, more recent experiments utilizing localized high-dose irradiation to block myogenesis confirm that such non-muscle derived cells or compensatory mechanisms do not contribute to any significant repair or regeneration [41, 42]. In addition, at least one population of MDSC has been localized within the basal lamina of the myofiber in a position similar to the satellite cell, but also in a much lower frequency and lacking expression of at least identifying satellite cell protein [43]. Regardless of origin, and in addition to this remarkable mulitilineage differentiation capacity, perhaps the most intriguing and promising application for their potential use in clinical therapies involves the regeneration of skeletal muscle. This will be further discussed within the historical perspective of myogenic cell transplantation for the treatment of Duchenne Muscular Dystrophy in the following sections.

1.2 Myogenic Cell Transplantation

1.2.1 Duchenne Muscular Dystrophy

Much of what is known regarding myogenic cell transplantation has evolved from studies investigating the therapeutic potential of this form of cellular therapy for the treatment of the most severe form of muscular dystrophy, Duchenne muscular dystrophy (DMD). DMD is a lethal X chromosome-linked recessive disorder characterized by an absence or marked deficiency of the cytoskeletal protein dystrophin [44], shown immunohistochemically in Figure 1.6. Clinically, patients present symptoms of progressive skeletal muscle weakness within the first three years of life which primarily affect the lower limbs and later affect the upper limbs, respiratory and cardiac muscles. The latter of these symptoms contribute to patient fatality within the second decade of life. Morphologically, dystrophic muscle appears to be in a constant state of spontaneous necrosis and regeneration, with a concomitant gradual replacement of muscle fibers by fibrous tissue [45].

Dystrophin is part of a complex of cytoskeletal glycoproteins that interconnect actin with the sarcolemmal membrane, shown in Figure 1.7 [45, 46]. This membrane-association, along with other evidence of abnormal membrane function in its absence, have led to the conclusion that dystrophin is integral in maintaining the mechanical stability of the muscle cell membrane by anchoring and supporting the sarcolemma during exercise [47].

Contraction-induced sarcolemmal damage has been correlated with the magnitude of mechanical stress endured by the membrane during contraction [48, 49]. In the absence of dystrophin, it is now believed that myofiber

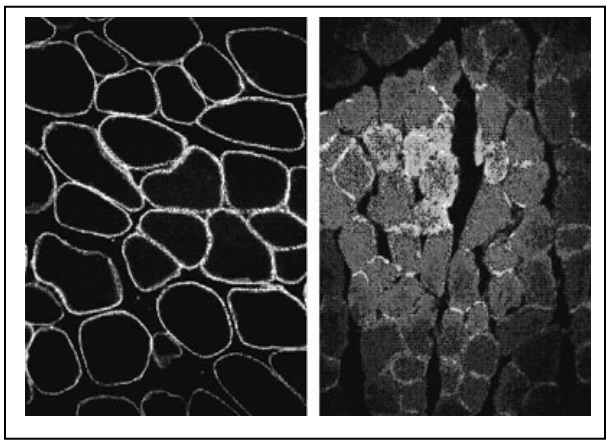

Figure 1.6 Immunohistochemical dystrophin labeling of skeletal muscle biopsies, taken from a normal individual (L) and from a patient with Duchenne's muscular dystrophy (R) [from Dr. Johnny Huard].

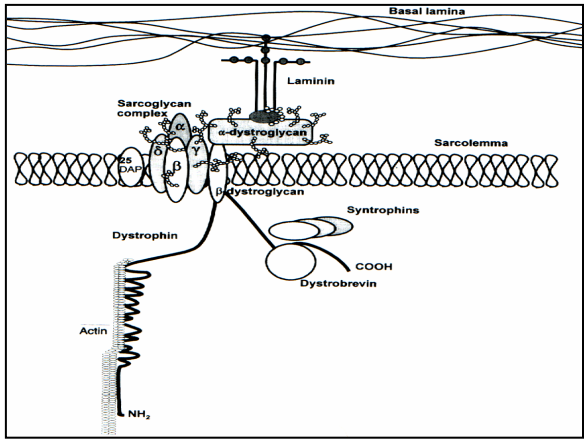

Figure 1.7 Dystrophin's role in the structural protein complex of the myofiber and connection to the extracellular matrix, from [45].

membranes are highly susceptible to the formation of small lesions in the plasmalemma, resulting in leakage of proteins and ions into the sarcoplasm and disruption of homeostasis, leading to fiber necrosis [50, 51]. Moreover, restoration of muscle strength, protection from contraction-induced damage, and histological alleviation of damage and necrosis has been observed in dystrophic animal models following viral-based gene transfer studies to restore dystrophin expression [52, 53].

1.2.2 Animal and Human Studies

The necessity of restoring dystrophin expression to alleviate the progression of DMD and its associated debilitating symptoms has led to proposed experimental therapies involving both viral and cell-based gene delivery. At the present time, viral delivery remains purely experimental. However, cell-based transplantation approaches have been investigated extensively in both animals and humans. In 1989, investigations involving the direct injection of myogenic cells derived from a normal donor into the skeletal muscle of the mdx mouse, a widely-used

dystrophin-deficient animal model for DMD, revealed that restoration of dystrophin expression could be achieved [54]. In the years that followed, a number of cell-based clinical trials were performed and were met with a very limited degree of success [55-58]. As a whole, little evidence of significant contribution to myofiber regeneration and dystrophin expression by the donor cells was observed. Poor restoration was encountered despite matching of donor-host major histocompatibility loci [59], even in a case in which donor cells were harvested from a monozygotic twin [60]. In spite of these apparent clinical failures, ongoing investigations in the mdx mouse continued. Such studies have since revealed several inherent limitations that are thought to impede the use of the direct-injection cell transplantation approach toward the treatment of DMD. These include the low migratory capacity of the cells from the injection site and potential specific and non-specific immune responses to both donor cells and the dystrophin protein itself [61]. More importantly, significant evidence for a large and rapid donor cell demise following injection had also been implicated as one of the primary reasons for the lack of clinical success [56, 62-65]. This donor cell demise, which cannot be attributed to specific cellular immune responses, has yet to be clarified by animal model experimentation and has since been observed within immunocompromised and immunosuppressed, normal and mdx models, under conditions considered optimal for muscle cell transplantation. Such conditions include pretreatment of the host muscle with myonecrotic agents and irradiation to prime the muscle for a regeneration response and reduce host cell competition with donor cells [62, 66-70]. Interestingly, the results of these studies revealed considerable regenerative competition from host cells, which additionally serves to lessen the degree of dystrophin restoration that may be achieved [55, 71].

It is apparent that the initial transplantation environment, which includes non-specific inflammatory reactions along with other necrotic and possibly yet undefined influential factors, certainly influences initial cell survival [35, 72, 73]. Improvement in transplantation efficiency within animal models has been achieved through delivery of anti-inflammatory or anti-complement agents [70, 74]. However, experimental observations regarding cell survival have forced researchers to more closely examine muscle precursor cell biology and have led to the suggestion that the success of certain transplanted cells does not appear to be by default; rather, specific populations of muscle precursor cells may be more suited to not only survive but to also flourish in the initial post-transplantation environment and contribute to the regeneration process [68, 75]. Even still, in combination with current delivery techniques, the estimated yield of new muscle and its associated nuclei formed by transplanted cells falls well short of parity and is currently not amenable to treating the major muscle groups of body, as would be

required for any genetically-inherited muscle disease [76]. The need to define and isolate efficient progenitor populations in terms of regeneration ability and dissemination quality has recently led to a focus on the MDSC.

Recently, isolated populations of MDSCs have demonstrated a remarkable ability to regenerate myofibers following transplantation into dystrophic host skeletal muscle [43], and appear to overcome several previously observed obstacles [39, 68]. Perhaps more importantly, in several studies donor-derived satellite cells are apparent within regenerated myofibers, suggesting their potential to repopulate the myogenic progenitor compartment and further supporting the claim of MDSCs as satellite cell progenitors [36, 43]. Particular attention has been paid to the systemic deliverability of such populations, and although proof of principle has been established in several cases the clinical utility of this approach still manages to fall short by orders of magnitude [36, 38]. In addition, one of the main obstacles to their continued experimental investigation remains their consistent isolation and identification, even within the mouse model in which they have originally been described. Variable isolation techniques and the lack of a commonly accepted set of identifying surface proteins, or markers, have made direct comparison of the various populations of MDSCs described within the literature difficult. Traditionally, isolation and identification of stem cell populations have relied upon a distinguishing set of characteristic proteins. In an effort to emulate this, characterization of surface protein expression is now commonly performed in MDSC studies in a manner similar to that used to describe hematopoietic stem cells. However, clear differences or similarities between the populations identified thus far have yet to be established. A summary of the defining characteristics and major findings of recently described MDSC populations is presented in Table 1.1.

Table 1.1 Summary of recent investigations and experimental results utilizing MDSC populations.

Investigators	Isolation Technique	Cell Phenotype	Major Finding/Conclusions
Gussoni, et al.[36]	FACS (Hoechst 33342 exclusion)	Sca-1+, CD34+/-, c-kit-, CD45-	Hematopoietic reconstitution, partial dystrophin restoration following intravenous delivery
Jackson et al. [37]	Brief culturing (1-24 hr adhesion) followed by FACS (Hoechst 33342 exclusion)	Sca-1+, c-kit+, CD45-	Efficient hematopoietic reconstitution of irradiated host, in competition studies
Lee et al. [39]	Preplate (variable cell adhesion)	Sca-1+, CD34-, c-kit-, CD45-, desmin+	Osteogenic differentiation, enhanced muscle regeneration, and intravenous dissemination capacity

Table 1.1 Summary of recent investigations and experimental results utilizing MDSC populations, continued.

Investigators	Isolation Technique	Cell Phenotype	Major Finding/Conclusions
Torrente et al. [38]	Preplate (variable cell adhesion)	Sca-1+, CD34+, desmin-	Hematopoietic differentiation and enhanced dissemination characteristics via arterial delivery
Qu-Petersen et al. [43]	Preplate with additional low density and long-term culture	Sca-1+/-, CD34-/+, c-kit-, CD45-, desmin-/+	Exceptional muscle regeneration, multipotent differentiation, immune-priveleged behavior

1.3 Urinary Incontinence Overview

The controlled storage and release of urine from the bladder is a complex process that requires the integrated and coordinated actions of the bladder, the urethra and its internal and external sphincters, the musculature of the pelvic floor, and a neural component comprising afferent and efferent signaling of both autonomic and somatic nerve pathways [77]. Uncontrolled or involuntary leakage of urine defines a condition called urinary incontinence. Incontinence syndromes can occur as the result of a loss of coordination or dysfunction of both the bladder and the urethra, and include: overflow, stress, and urgency incontinence. Combinations of stress and urge can occur and are often referred to as mixed incontinence.

Overflow incontinence arises from a failure of the bladder to contract adequately, resulting in urine accumulation within the bladder until it reaches an overflow pressure. This form is relatively uncommon and is frequently the result of spinal cord injury, affecting the lower motor neurons, or other disease conditions affecting bladder contraction. More common are stress and urge incontinence, particularly in the elderly population. Urge incontinence, characterized by an extremely brief warning or urge followed by immediate urination, is caused by hyperactive bladder detrusor muscle. The exact causes of stress urinary incontinence (SUI), also referred to as genuine stress incontinence, are less well-defined. SUI is characterized by the leakage of urine in the absence of bladder detrusor activity upon an increase in abdominal pressure such as from a cough, sneeze, or other source of

abdominal straining [78]. SUI is most common in elderly women but can present itself in younger women, typically following childbirth and/or menopause. This type of incontinence can also be observed in men following surgical procedures on the lower urinary tract which may damage the urethral sphincteric mechanism, such as radical prostatectomy [79].

Differences in anatomy, direct physical insult from childbirthing events, and hormonal changes associated with pregnancy and menopause, leading to alterations in the distribution of neuronal receptors, have all been suggested to contribute to the prevalence of incontinence conditions within the aging female population [80]. Incontinence conditions have been estimated to afflict 15-35% (of which 70% are female) of the non-institutionalized population over the age of 60, and over 50% of nursing-care facility residents [81]. However, due to the embarrassing nature of this condition, these figures are believed to be vastly underestimated. Direct annual costs associated with the care, not the treatment, of these patients was previously estimated at over 16 billion dollars (based on 1994 dollars) [81]. Perhaps a more devastating impact stems from indirect psychological costs, as patients often lack self esteem and have even described their symptoms as rendering life intolerable [82].

1.4 Stress Urinary Incontinence

1.4.1 Urethral Anatomy, the Role of Striated Muscle, and Pathophysiology

The urethra is a dynamic tube-shaped tissue comprised of both circumferential and longitudinally-oriented smooth and striated muscle within a connective tissue matrix. It serves a dual function by maintaining continence during bladder filling and aiding in the release of urine from the bladder during micturition, in coordination with the activities of the bladder. Both passive and active mechanisms are thought to play a role in maintaining closure of the urethra. Understanding the causes of incontinence conditions and devising potential therapies requires an understanding of the anatomical construction and function of the urethral components. Owing to the prevalence of such conditions, investigations and therapeutic strategies are often geared toward the female patient population. The following focuses on the female urethral anatomy and, in particular, how it may relate to urethral dysfunction and SUI.

Prolonged muscle tone, and the bulk of the permanent lumenal closure force, is thought to be generated from circumferentially-arranged smooth and striated urogenital sphincter muscles which are intrinsic to the urethral tissue and originate just below the base of the bladder. Unlike the smooth muscle layer, which is relatively uniform and continuous throughout the entire axial length, the circumferentially-arranged and predominately slow-twitch striated muscle layer (in humans) becomes much more dense within the mid-urethral region which has been termed the rhabdosphincter (see Figure 1.8) [83-85]. The location of the rhabdosphincter, which is separate from the periurethral skeletal muscle of the pelvic floor, corresponds with the area of highest urethral closure pressure [84] and its presence leads to a convenient anatomical separation of the urethra into three distinct regions: the proximal urethra (continuous with the bladder neck), the high stress zone (mid-urethra) containing the rhabdosphincter, and the distal urethra. The striated muscle within the proximal and mid regions is generally referred to as the external urethral sphincter and, in cooperation with the smooth muscle, the sphincteric mechanism as a whole is not considered a solitary structure or point but rather a region comprising nearly the proximal two-thirds of the urethra. Aside from permanent closure mechanisms occurring during normal resting conditions, adjunctive closure forces are also generated during conditions of increased physical activity or other events necessitating increases in these forces. The increased intraurethral pressure, shown to be highest near the mid urethral region, is attributed to both the intra and peri-urethral striated muscles as well as from passive pressure transmission from the abdominal cavity [86].

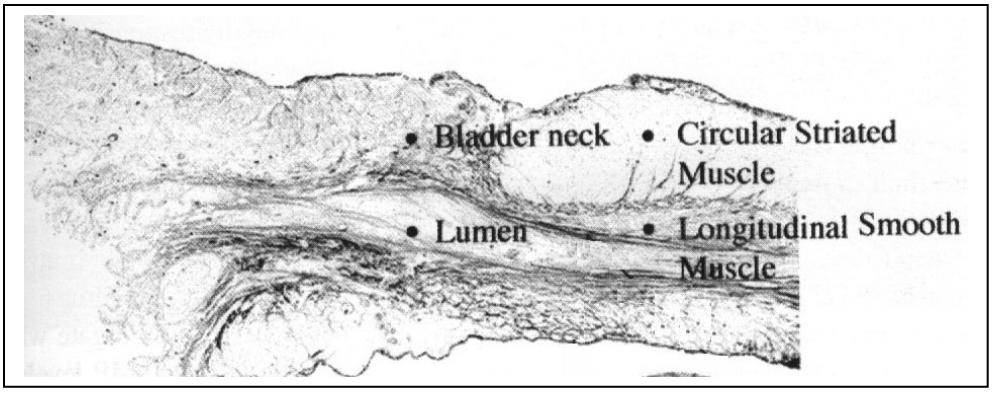

Figure 1.8 Longitudinal section of female guinea-pig urethra, illustrating the concentration of striated muscle near the mid-region in reference to the axial length. Image from [87].

With regard to pathophysiology the vast majority of the literature pertaining to incontinence conditions is clinical in nature, as gold-standard animal models have yet to be established. With respect to SUI, clinical evidence is suggestive of a weakening in the resting and dynamic mechanical and functional properties of the urethral tissue. Symptoms such as low resting urethral pressure, an inability to voluntarily increase intra-urethral pressure, and an inability to discontinue micturation midstream are clinical hallmarks of SUI [78]. Through experimental studies involving pharmacologic or neuromuscular blockage it is clear that the muscle tone provided by each muscle layer significantly contributes to closure pressure, although the quantitative contribution of each layer to the overall maintenance of the continence securing mechanism remains a subject of debate [86]. Nonetheless, it has become increasingly apparent that the striated muscle layer plays a vital role in securing continence and may be more susceptible to damage or dysfunction than other constituent urethral components. Indirect evidence of its importance is implied through measured decreases in the relative volume of striated muscle, but not smooth muscle, associated with increasing female age [88]. A 65% loss of striated myofiber number has been observed to occur between the third and eighth decade of life [89, 90], coincident with over a 50% loss in urethral closure pressure during a similar period observed in separate studies [91]. In addition, functional urethral length and closure pressure measurements are noticeably decreased by 8 weeks post-partum and implicate an inherent weakness in the urethral sphincter mechanism in the development of SUI following vaginal delivery [92]. The birthing process has long been suspected of causing either direct damage to the sphincter and/or pelvic floor muscles, or indirect damage through the compression of their associated nerves; the severity of which may impact the immediate or future development of SUI [93, 94]. Indeed, needle muscle biopsies taken from women with SUI have demonstrated a lower striated muscle content and subsequently higher connective tissue content within muscle fascicles in comparison to those taken from normal women, and combined with electromyographic parameters further suggests neurogenic damage coincident with incomplete muscle regeneration and fibrosis [95].

Studies performed on healthy women using pudendal nerve blockage, through local anesthesia or administration of somatic neuromuscular blocking agents to suppress striated muscle function, provide further evidence that the striated muscle layer's contribution to closure force is paramount both at rest and during physical or strenuous activities [86, 96, 97]. In addition, electromyography studies have demonstrated steady striated muscle firing at rest, with increases in the number of active firing units occurring concomitantly with increases in abdominal pressure [87]. Direct evidence of its role in the pathogenesis of incontinence is more elusive, although changes in

mechanical properties have been observed specifically in SUI patients. Measurement of parameters associated with changes in pressure and cross-sectional area (dP/dCA) in the resting urethra of normal and SUI patients has revealed significant differences between the respective tissue responses. Interestingly these changes were prevalent in both the mid-urethra, containing the striated rhabdosphincter, and also in the less-muscular proximal urethra [98]. Although this is suggestive of changes occurring in both the active (tension generating) and passive urethral components in association with this condition, it is generally accepted that an insufficient proximal urethra alone is not predictive of incontinence and thus shifts the focus to the mid-urethral region for devising potential therapeutic applications [98, 99].

1.4.2 Current Treatments

Since a large portion of incontinent patients suffer from some form of SUI, and as this condition is most relevant to the experimental therapy considered here, discussion will be limited to its treatment. The interested reader can find additional information regarding specific treatments of urge or overflow incontinence, typically aimed at reducing bladder activity through anti-cholinergic medications or other measures, within a number of clinical reviews [100, 101]. Despite the lack of detailed knowledge underlying the SUI condition, a number of therapies have been adopted and have been modestly successful. Such therapies can be divided into non-invasive, minimally-invasive, and surgical.

Incontinence conditions are typically treated first using conservative therapy, and thereafter using more invasive and surgical procedures. Non-invasive pelvic floor muscle exercise training programs (aimed at strengthening the striated sphincter), biofeedback, and electrostimulation, have all been suggested as potential therapies. However, only pelvic floor exercises have been shown to be effective through objective assessment of outcome data [102]. Even so, this form of treatment is usually limited to treating milder cases, as only modest increases in muscle strength can be expected and patient compliance often becomes a factor [103, 104]. Pharmacologic strategies to treat SUI include attempting to increase urethral smooth muscle and mucosal tone through the use of alpha-adrenergic agonists, in combination with estrogen therapy in post-menopausal women, or beta-adrenergic antagonists. $Beta_2$-adrenergic agonists have also been used to stimulate urethral striated and/or pelvic floor muscles. Unfortunately, little controlled clinical data to support their use is currently unavailable, risk

to benefit ratios have not been assessed and, in the case of alpha-adrenergic agonists, the drugs lack specificity for urethral tissue and thus cause a number of unwanted systemic side-effects [105]. As a whole, no effective non-invasive interventions are currently available to treat SUI.

In terms of minimally-invasive treatments, one of the most widely-used modalities involves the periurethral or transurethral injection of substances intended to add bulk to the submucosal layer, situated between the urothelium and the inner smooth muscle layer. This procedure is most often performed when SUI is believed to be caused by intrinsic urethral sphincter deficiency and/or in cases in which the patient cannot or does not wish to undergo a major surgical operation. In theory, the amount of volume occupied by the non-contractile bulking submucosal layer will directly determine the length change required by the surrounding circumferential muscle fibers to shift the tissue between the open and closed states. Thus, through simple geometry, reduction of the effective urethral luminal area will require a smaller change in fiber length by the outer muscle layers in order to facilitate closure [106]. Both autologous and non-autologous agents are currently in use or under investigation, aiming to achieve both safety and long-term conservation of augmented volume. Non-autologous agents include gluteraldehyde cross-linked bovine collagen, pyrolitic carbon-coated beads, calcium hydroxylapatite, and polytetrafluoroethylene [107-109]. Autologous agents that have been investigated include fat and chondrocytes, harvested from the abdominal wall and the external pinna or articular cartilage surface, respectively [110]. Although this outpatient procedure is associated with numerous obvious advantages, such as the lack of patient exposure to the pain and risk associated with surgery and hospitalization, unfortunately all of these injectable substances fail to meet clinically acceptable standards of both safety and long-term effectiveness. For example, polytetrafluoroethylene has been associated with observed distant particle migration and granuloma formation [111], and autologous fat is subject to considerable reabsorption and inflammatory and fibrous reactions at the site of injection [112, 113]. Bovine collagen currently remains the most popular agent and studies have shown improvement rates up to 70% (30% significant improvement/40% partial improvement) following treatment [114]. However the use of collagen often requires frequent injections due to reabsorption, and is not devoid of undesirable side effects such as allergic reactions [108, 115, 116].

More invasive surgical procedures, including anterior colporrhaphy, needle suspension, colposuspension, and the suburethral sling procedure are aimed at elevating the bladder neck and proximal urethra, thereby providing a platform for compression of the urethral wall and bladder neck in the presence of increased abdominal pressure.

These are often performed in cases in which anatomic descent of the bladder neck may have occurred or in which other treatment options have failed. A tension-free vaginal tape procedure, which provides support to the mid-urethra, is also attracting recent interest. In general, however, long-term results of surgical procedures have been disappointing, often require revision, and are more dependent upon the severity of the condition as well as the medical fitness and expectations of the patient [109].

1.4.3 Previous Work Involving Cellular Uromyoplasty

A major advantage of the bulking therapies is that they can be repeated with both relative ease and minimal irritation to the patient in order to maintain clinical efficacy. This is particularly important with this form of therapy due to the aforementioned temporal decreases in continence which are typically observed with many currently available bulking agents [109]. Using the same periurethral-injection platform, the use of autologous myogenic progenitor cells has been proposed as a new method to overcome the limitations currently observed with injectable agents. This strategy has been termed cellular uromyoplasty and aims to augment urethral sphincter muscle through the regeneration and integration of new and functional muscle. If successful, such a therapy would lead to the formation of new tissue that may be able to actively participate in the generation of closure forces, in addition to passive bulking properties. It is envisioned that this type of therapy would be applicable, at the least, to SUI patients presenting with underlying intrinsic sphincter deficiency.

Thus far, experimental observations in the mouse and rat models are very limited but have demonstrated the feasibility of this approach as well as the persistence of injected muscle-derived cells within both the urethral wall and within the bladder [113, 117-119]. Comparison of primary autologous cells to commercially-available collagen demonstrate a similar degree of persistence at 3 days post-injection, as detected by cell mass or collagen nodule formation. However, significantly larger degrees of cell persistence are observed by the 30 day timepoint. Importantly, it was further estimated through measures of reporter gene expression that approximately 88% of the cells present 3 days following treatment were also present at day 30, with no histologic evidence of inflammation or tissue damage at the injection site [118]. Donor cell-generated myofiber persistence has also been observed within the bladder and urethra of allogeneic-transplanted immunodeficient mice at 6 months post-injection, with an estimated 60% of reporter gene expression remaining at the 70 day timepoint [113].

Regenerative capability following simulated sphincteric injury has also been examined. Injection of muscle precursor cells was found to accelerate the recovery of striated muscle mass, with respect to both myofiber number and diameter, following sphincteric damage initiated by the injection of a myotoxic agent [120]. Using a sciatic nerve transection model, which denervates the striated muscle layer of the sphincter, injection of MDSCs was found to significantly improve a clinically-relevant leak point pressure parameter [121] (this parameter will be discussed in more detail in the following section). More detailed evidence of muscle functionality is currently unavailable, although some promising evidence of regenerated muscle integration has been observed in separate lower urinary tract studies. MDSC injection into the cryo-injured bladder revealed innervated donor-derived myofibers as early as two weeks post-implantation, and importantly improved the contractility of the tissue as determined through strip force measurements [122].

1.5 Evaluation of Urethral Function

1.5.1 In vivo

In the absence of a previous indication of surgical or other trauma, patients with SUI are often diagnosed as having intrinsic sphincter deficiency. However, defining the pathological changes in urethral function or the surrounding support structures that result in a deficiency are difficult to obtain in the clinical setting. Thus, at the moment, it is not possible to tailor a treatment to directly address the underlying cause of the deficiency. Nonetheless a number of standard and experimental clinical techniques have emerged to aid in diagnosis and to possibly assist in judging the severity of the condition. It should be mentioned however that these currently available techniques have shown limited value in predicting competence of urethral closure mechanisms and are often used in an integrated approach to ascertain the functional condition of the urethral mechanism.

One of the most popular urodynamic measurements is the urethral pressure profile for the assessment of sphincter function in relation to a rise in bladder pressure. As shown in Figure 1.9, both intravesical (bladder) and urethral pressures are measured as a catheter is withdrawn from the urinary tract at a set rate, resulting in a pressure profile along the axial length (shown in upper left inset). Such measurements are taken while at rest and/or during a stress event such as straining or coughing. In theory, leakage occurs when closure pressure, the subtraction of

intravesical from urethral pressure, becomes negative. It is evident that the urethral pressure is an idealized concept, in the sense that it is the hypothetical fluid pressure that would be required in order to open the intralumenal space of the urethra. Thus, applications utilizing fluid pressure measures would best reflect this concept [123]. In this regard, fluid-perfused catheter systems with side-holes have been used, along with a variety of other catheter styles such as direct-pressure microtip-transducers and intraluminal balloon catheters [124].

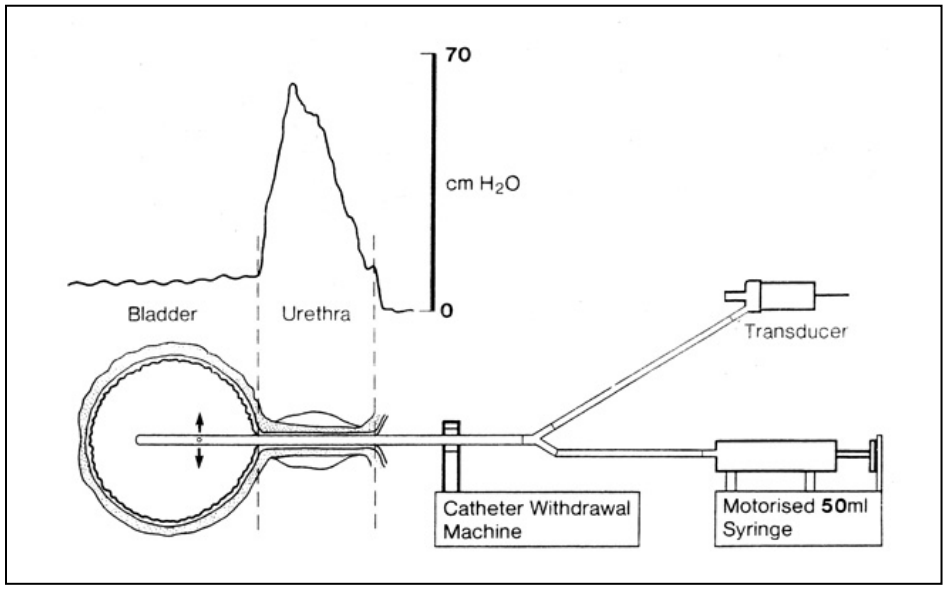

Figure 1.9 Diagram of urethral pressure profile apparatus, from [124].

Regardless of catheter style this technique has been shown to be extremely sensitive to the orientation of the catheter, and thus is associated with reproducibility problems and is particularly susceptible to experimental artifacts relating to the patient. In particular, the local interaction between the catheter and the inhomogenous inner tissue wall, known to contribute a large degree of such error, is difficult to assess and worsens as measurements during stress events are being attempted [106, 123, 125]. A less common variation of this technique has also been reported utilizing a specially-designed catheter to allow simultaneous recording of both pressure and cross-sectional area. Using this system, parameters such as compliance and resistance to dilatation have been reported, resulting in additional information used in identifying potential changes in pathologic conditions [96-98]. Such studies represent the only real effort to date to investigate urethral mechanical properties.

A variety of imaging techniques, such as ultrasonography and dynamic fastscan magnetic resonance imaging, have also been used to visualize movement of various physiologic structures during stress events. However, such studies remain descriptive rather than quantitative and are limited in most cases by resolution issues. Neurophysiologic assessment via electromyograms of sphincter striated muscle can be obtained through direct insertion of needle electrodes. Using this technique, SUI has been found to be associated with a decline in the electrophysiologic activity of the pudendal nerve, striated sphincter, and pelvic muscles [94]. However such measurements are also painful and more difficult to obtain during important physiological events such as initiation of voiding. Leak point pressure measurements are also performed in which the direct or indirect assessment of urine leakage is observed in relation to various physiologic straining events. Such measurements however lack precision, as correlation and synchronization of leakage with any definite value of pressure remains an unresolved issue [106].

Many of the same *in vivo* procedures are also performed in various animal models, with the addition of increased experimental flexibility permitting the collection of more detailed information relating to structure-function relationships. Measurements can be performed in concurrence with manipulation of physiologic components through surgical means or administration of neuromuscular blockers or other agents, which would not be ethically acceptable in humans, permitting a more direct assessment of urethral sphincter function. In addition, unlike in humans, tissue may be conveniently removed and assessed for structural or neurologic changes relating to man-made or naturally-occurring deficiencies [126, 127]. Additional advantages are seen in a method-specific manner. For instance, leak point pressure studies performed in the animal model allow for more precise control over administered intravesical pressures through the insertion of surgically-placed catheters within the bladder, as well as the elimination of contributions from intrinsic neural pathways that may lead to error in urethra-specific measurements.

1.5.2 In vitro

In vivo measurements benefit from obvious advantages in terms of physiologic significance, but also are limited in terms of the ability to gather detailed experimental information without the presence of confounding variables such as influences from surrounding structures. Although somewhat limited in scope, *in vitro* preparations using isolated segments of tissue benefit from greater experimental control and flexibility to address specific

questions. For studying urethral function, strip or ring preparations are most commonly performed, as depicted in Figure 1.10. In this setting, force displacement measurements are made in response to either electrical field or pharmacologic stimulation as a determinant of contraction and relaxation of muscle components. Such studies have been extremely instrumental in identifying receptors and pathways involved in urethral neuromuscular control, and this method continues to be the gold standard for assessing *in vitro* urethral behavior.

An *in vitro* preparation utilizing whole-mounted urethral tissue has also been previously reported. This system, shown in Figure 1.11, allows for the characterization of overall urethral closure through measured parameters such as fluid flow resistance and opening pressures. This system has been used in describing such processes as the role of calcium modulation in urethral tone as well as the effects of anoxia on closure function [128, 129]. Importantly, results obtained using this system have also been shown to be comparable to those obtained using more conventional strip methods [130].

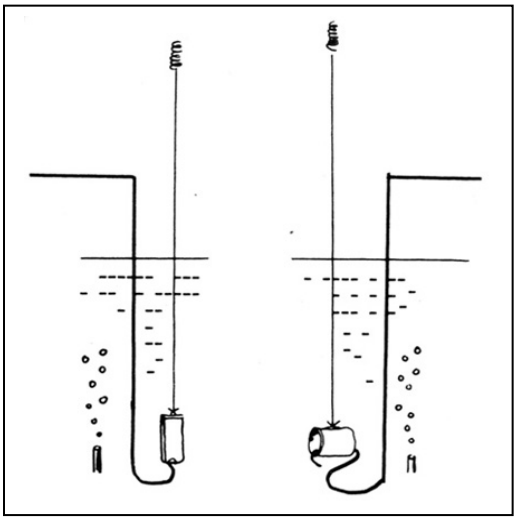

Figure 1.10 *In vitro* mounted longitudinal and circular strip preparations, from [131].

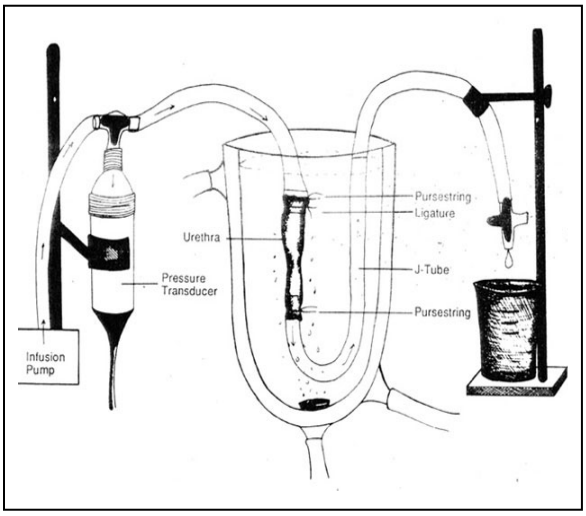

Figure 1.11 Whole-mounted, perfusion-based, urethral preparation. Image from [130].

1.6 Summary and Limitations of Previous Research

As discussed, cellular uromyoplasty as a treatment for SUI or mixed incontinence remains purely experimental. In order for this therapy to progress toward becoming an effective alternative clinical strategy to treat such conditions, a number of experimental issues must be addressed. These involve both the isolation and selection of appropriate transplantable cell populations, as well as identifying the downstream tissue effects that the generation of new striated tissue may impart. Currently, neither of these issues has been appropriately addressed by researchers in their respective fields.

1.6.1 Myogenic Cell Transplantation Efficacy

Autologous cellular regeneration efficiency is an issue of particular relevance for the treatment of incontinence, particularly when considering the documented effects of ageing on satellite cell proliferation capacity and the target patient base, which will be largely drawn from the adult and elderly populations. Practical considerations will also limit the size of the muscle biopsy that can be reasonably obtained, thus limiting the number of cells that will be available for either immediate use or *in vitro* expansion prior to transplantation. In terms of myogenic cell isolation and transplantation, nearly all of the current information available has resulted from potential applications for the treatment of muscular dystrophy. Thus, we are limited to drawing upon information gathered with regard to its application for dystrophin restoration almost exclusively, and independent of its use in the treatment of incontinence conditions. Nonetheless, the dystrophic transplantation model represents a convenient system for evaluating the regenerative response of isolated myogenic progenitor populations, since transplanted cell participation in these responses is readily identified through the appearance of dystrophin expression. Upon review of the current literature it is clear that information regarding myogenic cell transplantation, although extensive, fails to adequately address the issue of cell selection in the efficacy of this process. The transplantation process itself has traditionally been referred to as ‘myoblast transplantation’ in both the experimental animal and clinical trial literature. However, the term myoblast used in this context is misleading when considering that the vast majority of studies that have been performed to date have utilized cell populations in which little or no effort has been made to characterize them (i.e. MRFs, or other proteins). As described through numerous *in vitro* and *in vivo* studies, a

number of distinct myogenic cells, defined by differentiation state and with variable levels of myogenic gene expression and behavioral identities, have been demonstrated to exist. Despite this myogenic progenitor heterogeneity, previous cell transplantation efforts have failed to incorporate such considerations into their experimental protocols, and to the contrary, have utilized relatively uncharacterized and undefined populations. Further, this lack of information has made comparison of results between studies unrealistic, and collectively these studies have yet to identify desirable donor cell characteristics for transplantation purposes.

As described, satellite cells may be identified *in vivo* based upon their quiescence and defined location. However once they are placed in culture and replication is initiated, satellite or MDSC progenitors become rather indistinguishable from their more limited myoblast counterparts. MRFs have been useful thus far as molecular biology tools to assist in defining myogenic hierarchy and to elucidate underlying genetic differentiation processes. However, expression of such proteins cannot be easily exploited for clinical applications such as cell transplantation. The use of surface-localized proteins to characterize subpopulations of myogenic progenitor cells, particularly MDSCs, is gaining momentum within the scientific community who are hopeful that such efforts will eventually lead to more definable cell populations or provide reliable indicators to detect primitive progenitors. In contrast to nuclear-localized MRFs, these proteins may be utilized for viable cell isolation purposes through a number of sorting methodologies. However, identification of a specific protein or expression profile within any myogenic population has yet to be directly associated with differential regenerative qualities. Whether through protein expression or behavioral qualities, knowledge regarding the identification of desirable cell populations for transplantation is currently lacking but nonetheless is essential for clinical implementation of effective myogenic cellular therapies.

1.6.2 Cellular Uromyoplasty

Although a number of feasibility studies have been performed to suggest that such a therapy may provide long-term beneficial effects through transplanted-cell persistence, evidence has yet to be presented that clearly demonstrates that its intended mechanism of action, the physiologic improvement of closure force through augmented sphincteric muscle function, has been attained. Indications of clinical improvement, through *in vivo* leak point measures, cannot be attributed to a specific mechanism of cellular influence within the urethral tissue. Further,

it is currently unknown to what degree the addition of functional striated muscle tissue may impart. While it is evident from the collection of *in vivo* evidence that deficits in this muscular component result in a decreased ability to maintain continence, there is currently a lack of quantifiable experimental evidence conclusively defining its relative contribution to normal closure forces. Such information would provide a more realistic outlook as to the effectiveness of successful striated muscle augmentation therapy within the urethra when considered in combination with expected regeneration outcomes.

Currently available *in vivo* techniques, while clinically-relevant, are deficient in their ability to accurately describe structure-function relationships. Experimentation at the *in vitro* level is required to clarify such issues and will be particularly instrumental in determining the source of improved physiologic urethral function as a result of regional-specific treatments, such as the one discussed here. Strip or ring methods have proven to be very valuable for evaluation and quantification of urethral muscle contractility. They also offer the ability to investigate segmental regions of interest along the axial length of the tissue. This quality is essential for the evaluation of localized treatments, and is particularly relevant considering the possibility that such local effects may be diluted in larger-scale tissue measurements. However, force measurement techniques alone do not allow for the complete characterization of relevant tissue properties, and additionally would not adequately address the potential need for detection of non-contractile changes in tissue behavior. Furthermore, in theory, whole preparations offer advantages over conventional strip methods owing to the retention of natural tissue structure with minimal damage and disruption of muscle or structural fibers, as well as exposure of such structures to more physiologic loading conditions. Previously described whole-mounted systems have only been able to characterize the overall urethral closure function through the measurement of flow parameters that relate to whole tissue function, not unlike parameters that can be obtained through *in vivo* methods. While it is evident that each previously-utilized *in vitro* technique offers some unique experimental advantages, neither is equipped to properly address the unresolved issues at hand. Specifically, neither offers the ability to quantifiably characterize both passive and active regional mechanical characteristics of whole urethra tissue. Such information is critical for evaluation of uromyoplasty which aims to elicit a specific change in such properties through the local addition of functional muscle mass.

1.7 Specific Aims

This study aims to directly address current deficiencies in the knowledge of applied myogenic transplantation therapies for the treatment of SUI. As discussed, unresolved issues regarding the isolation and selection of cell populations and the consequences of cellular injection at the localized tissue biomechanical level must be addressed before proceeding with a reasonable assurance of success.

Currently no consensus exists as to distinguish the identity of myogenic cells that may be reliably used for transplantation and subsequent striated muscle regeneration purposes. The current study aims to address this existing gap between muscle progenitor cell biology and regeneration efficiency. This will be accomplished through direct comparison and quantification of regeneration characteristics of more homogenous and defined cell populations, in terms of both protein expression and fundamental behavioral qualities. Further it will be determined whether any such definable qualities can be exploited in order to identify and/or separate efficient populations of progenitor cells in a species-independent manner. With regard to cellular uromyoplasty, isolation and identification of efficient cell populations is of necessary practical importance for its effective clinical implementation. However, additional understanding of the underlying mechanism(s) behind enhanced cellular regenerative capacity is critical to the advancement of the myogenic cell transplantation field as a whole and the continued development of therapies directed toward other muscular deficiencies and related diseases.

With regard to urethral evaluation, experimental strategies have been devised to more adequately address questions relating to the structure-function consequences of cellular uromyoplasty therapy. It is proposed that an accurate evaluation of regional tissue properties can be obtained using a novel *ex vivo* urethral biomechanics system that combines many of the advantages of currently utilized *in vitro* methods. Validation of this system is performed by investigating regional contraction and relaxation responses in relation to naturally-occurring axial variations in urethral anatomy. This system is then utilized to investigate the normal role of the striated muscle component within the urethra to elucidate potential changes in both the passive and active biomechanical properties that may be incurred upon its manipulation through regeneration strategies.

The culmination of such experimental information will directly aid in the progression of cellular uromyoplasty therapy towards effective clinical utility, as well as aid a broader scientific community by: 1) enhancing the knowledge underlying the effective utilization of myogenic cell transplantation for therapeutic

purposes, as a whole, and 2) establishing new experimental methodologies that can be used by the urologic community to assess the functional properties of the lower urinary tract.

2.0 ISOLATION AND IDENTIFICATION OF EFFICIENT MYOGENIC PROGENITORS

As described in section 1.2.2, results of myoblast transplantation studies performed thus far suggest that the heterogeneity of donor myogenic cells may be a contributing factor to both the variability and inefficiency of the transplantation and regeneration processes. Surprisingly, isolation and separation techniques to further investigate this heterogeneity have received little attention. Only one such method, the preplating technique, has been previously shown to result in the separation of primary myogenic cells which subsequently demonstrate variable rates of reporter gene expression, along with concomitant myofiber formation, following transplantation [75]. This method was adapted from original efforts to quickly separate the majority of myogenic from non-myogenic cells (i.e. fibroblasts, endothelial cells, etc.) following the enzymatic digestion of muscle biopsies [132, 133], and utilizes an apparent variability in myogenic cell adhesion or settling characteristics to generate a number of distinct and viable cultures. This method has since been used to isolate a number of myogenic cultures and most recently has been utilized in the isolation of several MDSC candidates from the late adhering cultures [38, 39, 43]. Given its background and usage thus far, it is logical to exploit the preplating technique as a platform for further examining the potential for identification of heterogeneous cellular characteristics.

2.1 Surface-localized Protein Identification

2.1.1 Introduction

At the present time, one of the most common techniques for distinguishing and separating subpopulations of hematopoietic and other cells is through identification of cell-specific surface-localized proteins in combination with a number of sorting methodologies. In this manner, viability is maintained during the identification and separation process and cultures may be readily screened or purified for pre-determined desirable subpopulations. Proof of concept of this methodology in the myogenic community was demonstrated in previous studies investigating CD56 (neural cell adhesion molecule) expression, which was used to purify human myogenic cultures through the elimination of non-myogenic cells [134, 135]. However, expression of this protein corresponds to all

cells of myogenic origin and therefore does not prove useful in further identification of subpopulations. Recent curiosity in the isolation of MDSCs has led to enhanced interest in the characterization of myogenic cells through proteins that previously have been used to define murine bone marrow-derived hematopoietic stem cells, such as CD34, stem cell antigen-1 (Sca-1), and c-kit (CD117)[136, 137]. All of these proteins have been found to be expressed by various muscle-derived cells [37], however Sca-1 and CD34 are increasingly becoming associated with myogenic progenitor cells [36, 38, 39]. In particular, CD34, a transmembrane glycophosphoprotein known to be expressed by human hematopoietic progenitor cells [138], has recently been associated with both the quiescent and activated states of murine myogenic satellite cells [7]. Therefore, it was of interest to screen the various preplate cultures for characteristic patterns of expression of these proteins to first determine if they might be useful as identifying markers, which could then be subsequently used to purify targeted populations for transplantation evaluation. It was also essential to screen the MDSC population, which can be obtained utilizing this technique, to determine if a unique protein profile exists to identify it from the remainder of the preplated muscle-derived cells.

2.1.2 Methods

2.1.2.1 Cell Isolation: Preplate Technique. A modified version of the preplate technique [132, 133] was utilized to obtain various myogenic cultures from dissociated skeletal muscle, as previously described [75]. A single cell suspension was obtained by enzymatic dissociation of gastrocnemius muscles from adult-aged normal mice (7-9 weeks of age, C57 BL/10J; Jackson Laboratories). Muscles from four mice were digested and combined for each experiment, in order to obtain the appropriate number of cells for immediate flow cytometric analysis. Enzymatic dissociation was performed by serial digestion of hand-minced muscles in 0.2% (by weight) collagenase-type XI solution (Sigma) for 1 hour, 0.3% dispase (Gibco-BRL) for 45 minutes, and 0.1% trypsin (Life Technologies) for 30 minutes. The final cell suspension was re-suspended in serum-supplemented Dulbecco's modified Eagle's medium (DMEM, containing 10% fetal bovine serum, 10% horse serum, 0.5% chick embryo extract by volume, and also 100 U/mL penicillin and 100 μg/mL streptomyocin; Gibco-BRL), which was also used for subsequent culturing, and added to a T-75 collagen-coated flask (collagen Type I, Sigma). After 1 hour, non-adherent cells contained within the supernatant were removed and transferred to a second T-75 flask for a period of 2 hours. Fresh medium was added to the first set of adherent cells (termed preplate 1, or PP1) and this procedure was continued for PP3 through

PP6 at subsequent 24 hour periods. A smaller surface area flask, T-25, was used for PP6 as the number of remaining non-adherent cells by this point was comparatively lower. This process resulted in six primary cultures of adherent cells with increasing initial adhesion times that were subsequently used for surface protein and desmin analysis. An overview of this process and the cell populations used in the experimental investigations is shown in Figure 2.1.

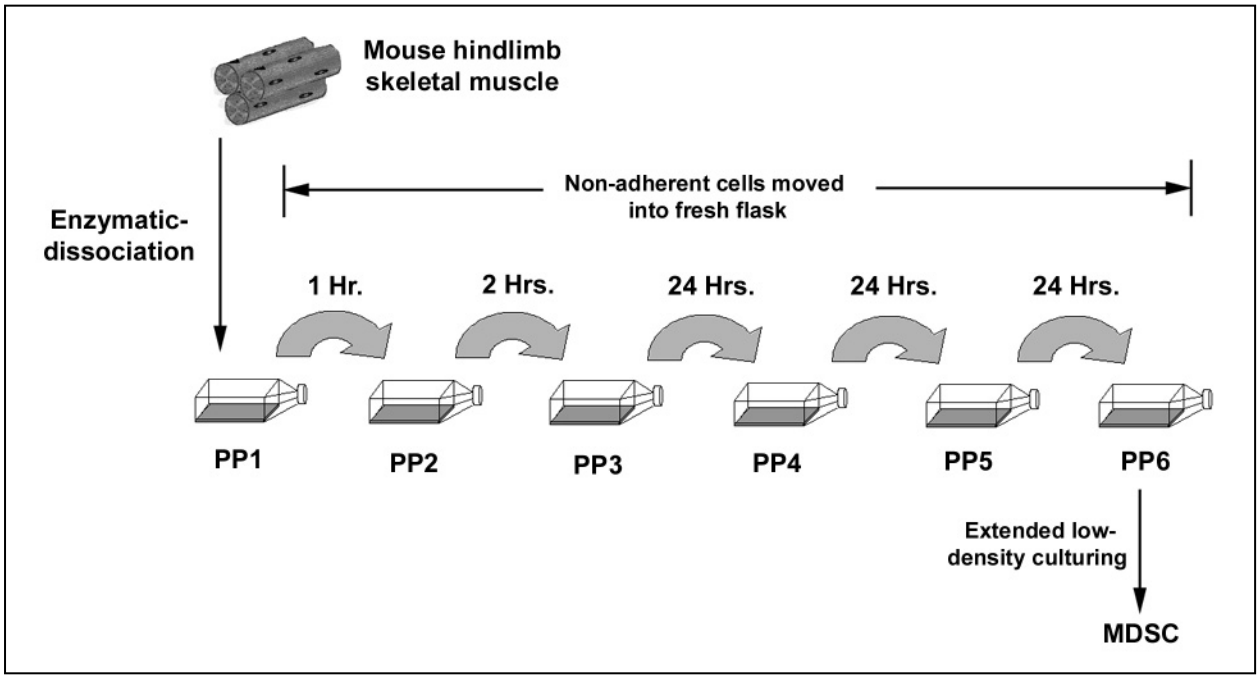

Figure 2.1 Overview of the preplating technique for the isolation of muscle-derived cell populations.

Also mentioned in Figure 2.1 is a process that can result in the isolation of MDSC candidates, obtained through extended low-density culturing of the PP6 culture. By plating 50-100 PP6 cells/well in a 12-well plate, the vast majority of cells contained within the culture perish over a 2 week period, however a few cells survive (MDSCs, < 10) and begin to form colonies during this period. Thus, delayed activation and expansion behavior is seen in the MDSC isolation process, which involves their identification and expansion only following the demise of the other progenitors contained within the mixed primary culture. These cells can then be expanded to larger quantities through extended culturing and thus have also been termed 'long-term proliferating' cells [43].

2.1.2.2 Immunofluorescence Evaluation of Desmin. Evaluation of desmin expression, an intermediate filament protein restricted to the myogenic lineage [139], was performed following fixation of cells in cold methanol for 2 minutes. Cells were then pre-incubated with 5% goat serum in PBS and were incubated at room temperature for 1 hour with rabbit IgG anti-desmin (D-8281, 1:250; Sigma) antibody diluted in 5% goat serum. Following thorough rinsing with PBS (Dulbecco's phosphate buffered saline, 1x; Mediatech), cells were incubated with biotinylated goat anti-rabbit IgG (1:250; Sigma) antibody for 30 min. Finally, cells were washed and incubated with streptavidin-Cy3 (1:500; Sigma) and the percentage of cells exhibiting positive staining was used to determine the percentage of myogenic cells within each culture through analysis of 10 random culture fields (representing >200 total cells). Control staining was performed in an identical fashion with omission of the primary antibody.

2.1.2.3 Flow Cytometry. Flow cytometry analysis of cell populations contained within the preplate cultures was performed for five separate isolations. For each separate isolation, cells were harvested from the culture flasks within 24 hours after initial adherence for flow cytometric analysis to limit potential changes in protein expression that may be induced by culturing. Cells from individual preplates were removed from the flasks with a trypsin/EDTA solution (0.25 % trypsin/2.6 mM EDTA; Life Technologies), which was quickly neutralized with cold DMEM containing 20% serum (as described). They were then centrifuged and washed in a cold PBS solution containing 0.1% sodium azide (Sigma) and 0.5% bovine serum albumin (ICN Biomedicals), to prevent cell clumping, and counted. The cells were then divided into four equal aliquots: three receiving combinations of various monoclonal antibodies, and one for control labeling. Following centrifugation, cell pellets were resuspended in a 10% mouse serum (Sigma) in PBS solution, also containing Fc Block (rat anti-mouse CD16/CD32; Pharmingen), and incubated for 10 minutes on ice. Fc Block reduces non-specific binding of antibodies via the conserved Fc region, as opposed to the specific antigen-recognizing sequence (Fab). Predetermined optimal amounts of rat anti-mouse monoclonal antibodies (Sca-1, CD34, c-kit, and CD45) were then added directly to each tube for 30 minutes. Each non-control tube received FITC-conjugated anti-CD45 antibody (Pharmingen), and one of the following combinations of monoclonal antibodies: 1) R-phycoerythrin (PE)-conjugated anti-Sca-1 and biotin-conjugated anti-CD34, 2) PE-conjugated anti-CD117 (c-kit) and biotin-conjugated anti-Sca-1, or 3) PE-conjugated anti-CD117 and biotin-conjugated anti-CD34 antibodies (all from Pharmingen). A control tube received equivalent amounts of FITC-conjugated, biotin-conjugated and PE-conjugated isotype antibody standards (Pharmingen). Following primary antibody incubation, each tube was washed in cold PBS solution and centrifuged. 20 μL of

streptavidin-allophycocyanin conjugate (SA-APC, 1:300 dilution in PBS; Pharmingen) was used to resuspend the cell pellets, including controls, and incubated on ice for 20 minutes before washing. Just prior to analysis, 7-amino-actinomycin D (7-AAD, Via-Probe; Pharmingen) was added to each tube for dead cell exclusion during analysis. A minimum of 10,000 live cell events were collected using a FACSCalibur flow cytometer (Becton Dickinson) and analyzed with CellQuest software (Becton Dickinson). Initial compensation levels were adjusted using single-labeled samples to eliminate spectral overlap in the emission wavelengths between FITC, PE, and 7-AAD labeled samples (corresponding to FL1, FL2, and FL3 detectors). Surface protein expression analysis was performed on viable and hematopoietic lineage (as recognized by CD45) negative cells by appropriate gating. Dot plot intercepts used for analysis were set using the isotype control samples obtained for each individual preplate culture. Leftover control percentages (approximately 1%) falling within the positive-staining regions were subsequently subtracted from each labeled sample during analysis.

2.1.2.4 Animals. All animals were housed in the Rangos Research Center Animal Facility of the Children's Hospital of Pittsburgh. The policies and procedures of the animal laboratory are in accordance with those detailed in the guide for the "Care and Use of Laboratory Animals" published by the US Department of Health and Human Services. Protocols used for these experiments were approved by the Animal Research and Care Committee of the Children's Hospital of Pittsburgh (Protocol 7/00).

2.1.2.5 Statistical Analysis. Percentages of each population expressing a particular protein or profile were compared among preplates by one-way analysis of variance (ANOVA), and using Student-Newman-Keuls post-hoc pairwise comparisons. This less-conservative post-hoc test, and therefore more likely to declare an observation statistically significant, was chosen for comparison of the relatively small sample sizes that were able to be realistically obtained. Analysis was performed using SigmaStat (v2.0, Jandel Scientific) statistical software.

For all analyses, results demonstrating $p<0.05$ were considered statistically significant. Data is presented as mean ± standard error of the mean (SEM).

2.1.3 Results

Many of the results and figures, where indicated, have been previously published [140] and are reproduced here with permission from Mary Ann Liebert, Inc. Publishing.

2.1.3.1 Desmin Expression. As shown in Figure 2.2, and as previously described [75, 133], application of the preplate technique results in a purification of myogenic (desmin-expressing) cells from murine dissociated skeletal muscle. The average percentage of myogenic cells, determined through visual immunofluorescence, within each preplate population from PP1 to PP6 used in this study was 4±2, 10±1, 38±8, 76±5, 94±2, and 95±1, respectively. Morphological differences in the myogenic cells isolated in the later preplates (PP4-6) were apparent as well. Later preplate myogenic cells tended to be generally round in shape, whereas the myogenic cells contained within the early preplates were more spindle-shaped (as seen in Figure 2.3). Cells within MDSC cultures displayed a round morphology similar to PP6, with no apparent fibroblast-like cells present; however only 15-30% of these cells expressed desmin

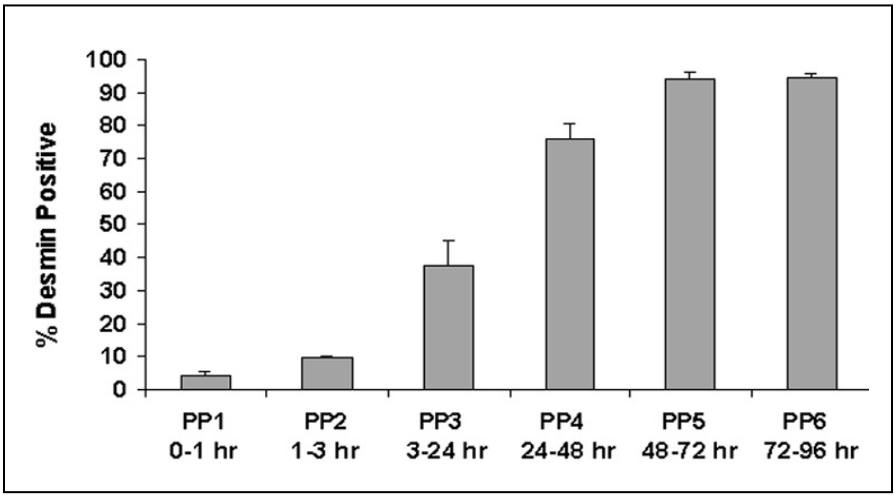

Figure 2.2 Murine muscle-derived cell cultures obtained via the preplate technique contain increasing initial percentages of myogenic cells, as determined by desmin expression. Time from isolation until initial cell adhesion is indicated.

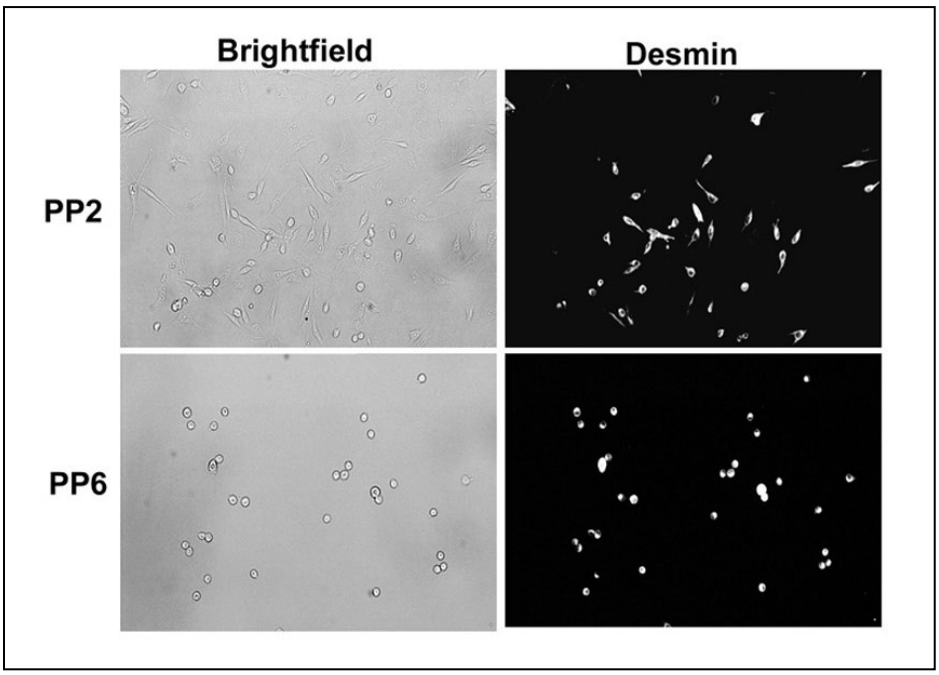

Figure 2.3 Typical morphology of myogenic cells displaying early and late adhesion characteristics.

2.1.3.2 **Flow Cytometry Analysis**. A typical flow cytometry profile used for analysis of the surface-expressed proteins Sca-1, CD34, and c-kit is shown in Figure 2.4. Similar profiles for each of the six preplate populations were generated and analyzed. Four-color fluorescence analysis allowed for the inclusion of only live cells (Figure 2.4B, R1) in the analysis, as well as the exclusion of hematopoietic cells (Figure 2.4C), while also permitting the detection of two surface proteins simultaneously (Sca-1/CD34, c-kit/Sca-1, or c-kit/CD34; Figure 2.4D-F). Separate labeling of identical aliquots taken from the same preplate cell population permitted the analysis of both the total percentage of cells expressing a specific protein and the percentage of cells co-expressing each combination of the three proteins analyzed.

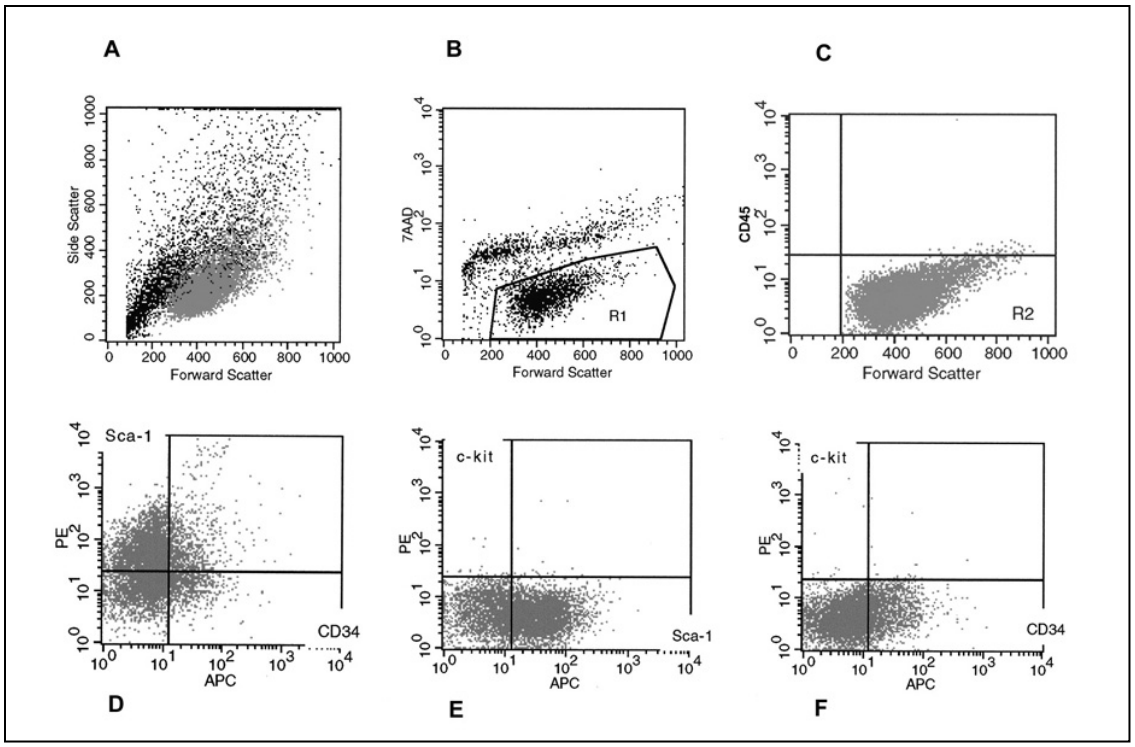

Figure 2.4 Four color flow cytometric analysis of preplates (PP6 shown), allowing the selection of viable and non-hematopoietic cells. The viable cell gate (B, R1) was first used to generate the hematopoietic lineage profile (C). Gating for non-hematopoietic cells (C, R2) was then set. The profiles and percentages for each of the three combinations of surface proteins analyzed, c-kit/Sca-1 (D), c-kit/CD34 (E), and Sca-1/CD34 (F) were then generated from an R1 and R2 boolean determination [140].

Considering each protein individually, the percentage of cells within each preplate expressing the various proteins was observed to be variable (Figure 2.5). The total percentage of cells within PP4 and PP5 expressing CD34 was found to be significantly higher when compared to all other preplates, except PP2. Expression of CD34 within PP6 was significantly lower than all other preplates. It was also observed that PP3 contained a significantly higher percentage of cells expressing c-kit, although the percentage of cells within all other preplates expressing this protein was very low (PP3, 8±1%; all other preplates, < 2%). The lack of appreciable c-kit expression by the vast majority of preplated cells resulted in a focus towards Sca-1 and CD34 expression for phenotypic characterization, particularly for the later preplates (PP4-6) which were observed to be purified for myogenic cells. Within these later-adhering cultures, the phenotypic heterogeneous nature of myogenic cells is demonstrated by the Sca-1 vs.

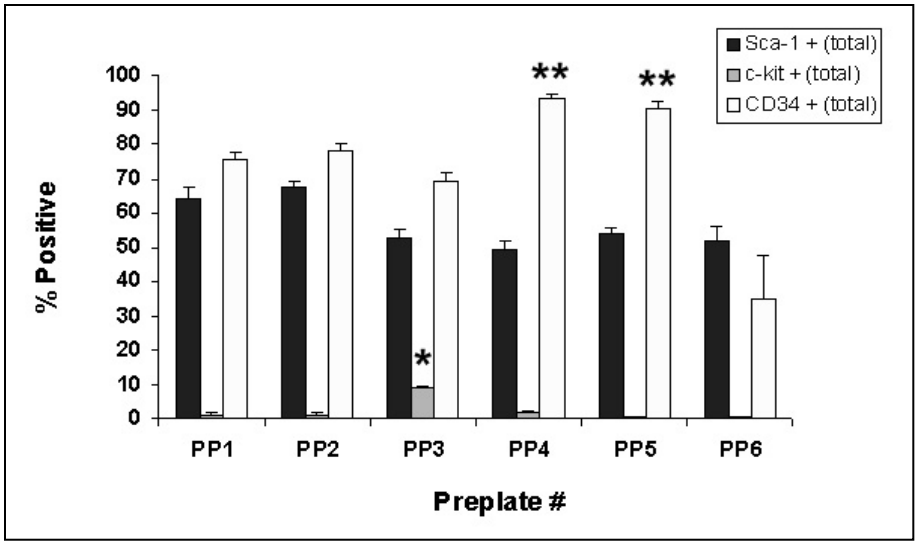

Figure 2.5 Average percentage of preplated cell populations expressing cell surface proteins Sca-1, CD34, and c-kit, determined from single color histograms (*c-kit expressed by PP3 vs. all preplates; ** CD34 expressed by PP4/PP5 vs. all preplates, except PP2) [140].

CD34 profiles shown in Figure 2.6A. Quantitative analysis of all preplates (Figure 2.6B) reveals the presence of distinct subpopulations which are found to reside exclusively within the purified myogenic cultures. A subpopulation expressing CD34 only (Sca-1-/CD34+) was found enriched within PP4 and PP5, while a population expressing Sca-1 only (Sca-1+/CD34-) was found almost exclusively within PP6. This CD34-only population was found to be significantly higher in PP4 and PP5 versus all other preplates, with the exception of PP2, and the Sca-1-only phenotype within PP6 was significantly higher in comparison to all other preplates. Statistical analysis also revealed that the percentage of cells co-expressing CD34 and Sca-1 (Sca-1+/CD34+) was found to be significantly decreased within PP6 and, consequently, cells expressing neither (Sca-1-/CD34-) were found in the highest percentage within this preplate (not shown).

The MDSC population was also analyzed for expression of these proteins, although it was not statistically compared to the primary preplates as these cells were cultured for many weeks in order to obtain adequate numbers for experimentation. As shown in Figure 2.7, these cells also did not express c-kit but did express combinations of Sca-1 and CD34 in a profile similar to that of PP6, from which it was derived.

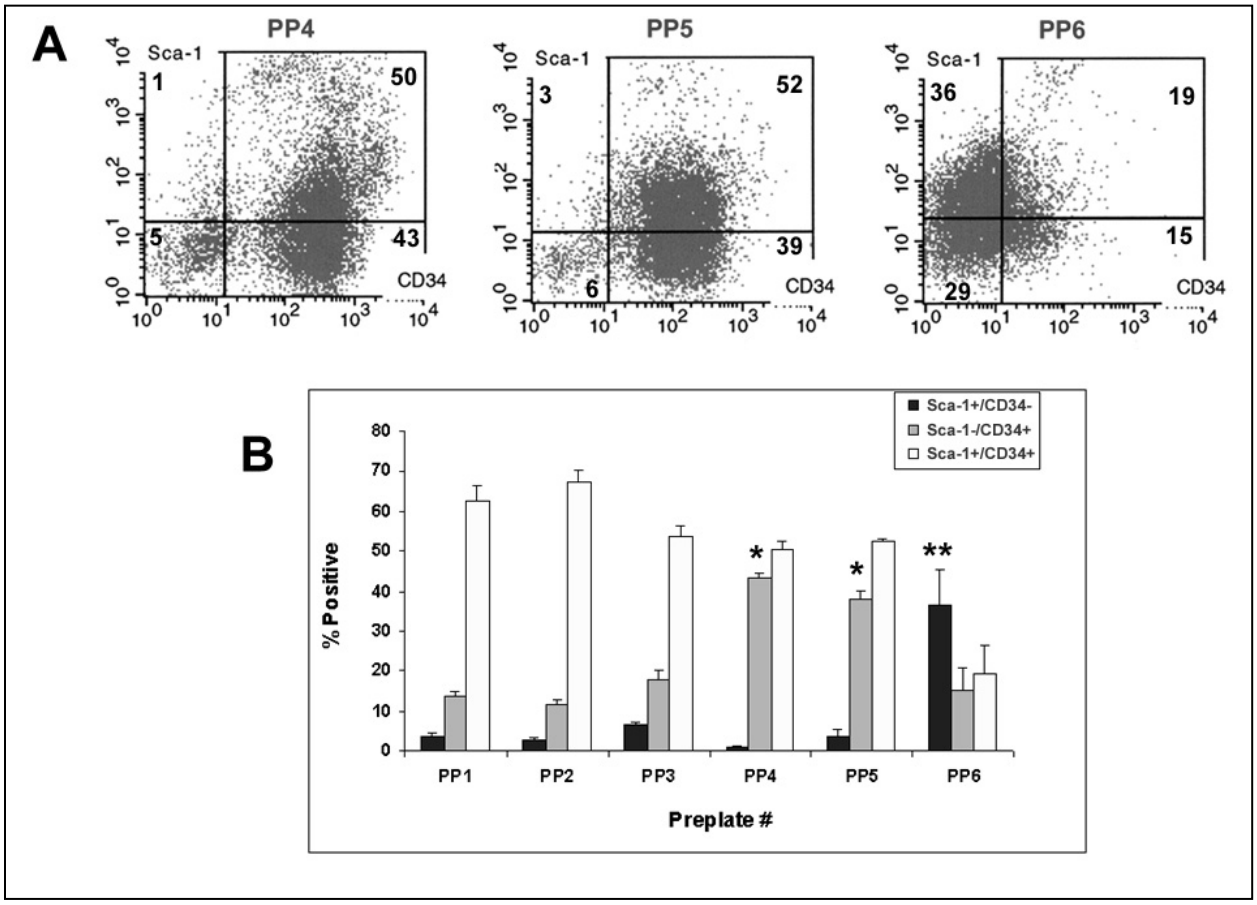

Figure 2.6 Representative Sca-1/CD34 profiles for purified myogenic preplate populations, demonstrating their phenotypic heterogeneity (A). Figures in (A) show average values of expression. (B) Subpopulations of myogenic cells expressing CD34 only and Sca-1 only are significantly higher within these myogenic cultures (*PP4/PP5, CD34 only vs. all other preplates; **PP6, Sca-1 only vs. all other preplates) [140].

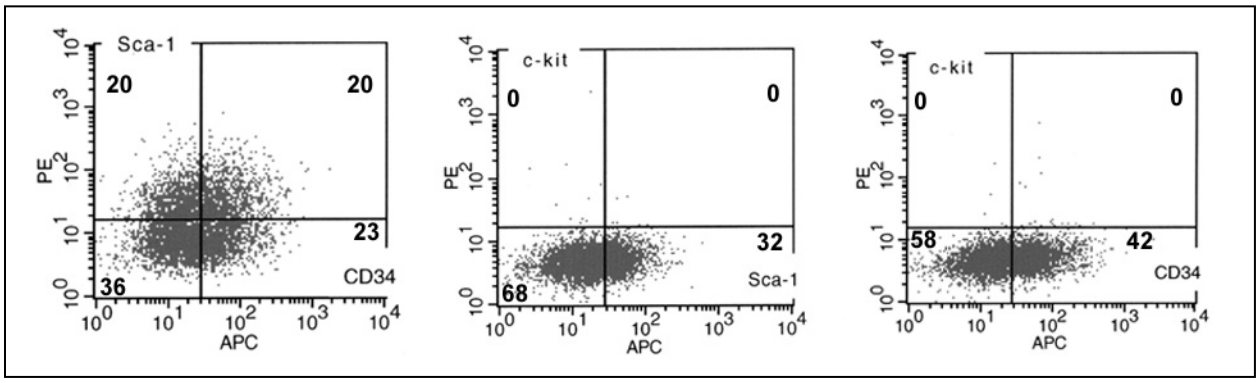

Figure 2.7 Representative protein expression profiles of an MDSC population obtained from additional purification of PP6. This population also does not express c-kit (middle, right), but does express varying degrees of CD34 and Sca-1 (left).

2.1.4 Discussion

Although preplating purifies myogenic cells that are homogeneously positive for desmin, through initial variable adhesion characteristics, distinct subpopulations of myogenic cells can be identified by flow cytometry on the basis of their phenotypic display of the surface proteins Sca-1 and CD34. The distinct patterns of expression of these two proteins within later-adhering cultures, previously described to display enhanced regenerative capabilities, merits their further investigation as efficient progenitor cell markers. c-kit was not useful in identifying myogenic cells nor was it present to any appreciable degree within the various muscle-derived cell populations.

Interestingly, a population of non-hematopoietic muscle-derived cells expressing c-kit and displaying hematopoietic differentiation capacity has been previously described [37]. In agreement with this study, these cells were also found to adhere to culture flasks within approximately 24 hours. Thus we have confirmed the presence of this population of cells based on adhesion and protein characteristics and, to the extent possible, validated our analysis through agreement with previously reported findings. However the ability of PP3, containing this c-kit-expressing population, to contribute to muscle regeneration has previously been shown to be very limited and therefore does not warrant further investigation into c-kit for our purposes of identifying efficient muscle progenitors [75].

Other similarities to previously reported muscle-derived cell populations should be mentioned. The presence of a Sca-1-positive subpopulation within skeletal muscle, identified here by the preplating technique, has been reported by others. Gussoni *et al.* isolated a phenotypically similar population from muscle using a sorting procedure identical to that used for hematopoietic stem cell isolation, the so-called 'sp' (side-population) isolation technique [36]. The rare sp population of muscle-derived cells described in this study displayed both hematopoietic potential and the ability to form muscle fibers *in vivo*, albeit only to a small degree, when injected intravenously into lethally irradiated dystrophic mice. In addition, they were found to lack expression of c-kit, CD45 and CD34, and therefore are phenotypically similar to the purified subpopulation found enriched within PP6 and also found within the MDSC population described here. These sp cells also display similar *in vitro* characteristics to the PP6 and MDSC populations, as they demonstrate prolonged initial adhesion times and maintain a round morphologically in culture.

It should not be completely surprising that we observe both Sca-1 and CD34 expression within the early-adhering, and largely non-myogenic, cultures as well. Cells from the vasculature, connective tissue, and adipose tissue are all found within skeletal muscle and primarily adhere within the first several preplates (PP1-3), as indicated by identifying morphological characteristics and their lack of desmin expression. Fibroblasts from various tissue sources have been previously shown to express CD34 [141, 142], and endothelial cells are known to express both CD34 [138] and constituitively low levels of Sca-1 [143]. In addition, a population of cells residing within the interstitial spaces of skeletal muscle, that display both vascular and myogenic characteristics and express both Sca-1 and CD34, has also been recently described [144].

Of particular interest to this evaluation are the later preplate cultures (PP4-6), containing slowly-adhering cells. These cultures have been previously shown, as a whole, to exhibit greater regenerative qualities as inferred from increased reporter gene expression [75]. Interestingly, many of these slowly-adhering cells have also traditionally been discarded by the vast majority of the myogenic transplantation community. Based on the phenotypic results of the early preplates it may be concluded that cell isolation based exclusively on the expression of only Sca-1 or CD34 will most likely yield a mixture of myogenic and non-myogenic cell types, unless a method such as the preplate technique is employed prior to separation in order to purify the myogenic fraction. Nonetheless, the heterogeneous nature of expression of these two proteins within myogenic cultures, and their expression to varying degrees within MDSC cultures, suggest that it is advisable to further pursue their value as identifying markers for cell identification and isolation purposes.

2.2 Evaluation of Surface Proteins as Indicators of Regenerative Capacity

2.2.1 Introduction

From the results of the preplate surface protein analysis, it was reasonable to proceed with further investigation of the regenerative qualities of the preplated populations in terms of the proteins Sca-1 and CD34. It was of particular interest to evaluate the expression of these proteins within the late preplates, as characteristic patterns of expression were found suggesting that distinct subpopulations of myogenic cells may be present within these cultures. Therefore, these late-adhering cell cultures were used to isolate various phenotypically-pure

subpopulations of myogenic cells, and were subsequently compared to the MDSC and early preplate populations. In addition, since the protein expression profiles were obtained through analysis performed less than 24 hours following initial cell adhesion to the culture flasks, it is reasonable to expect that such profiles may also be useful in identifying cells for sorting directly from the original dissociated cell suspension. Although direct isolation and rapid utilization of cells without culturing and expansion may not be appropriate for therapies requiring massive regeneration (i.e. muscular dystrophy), such techniques may not be as unrealistic for smaller scale regenerative applications such as uromyoplasty. Their isolation in this manner also does not preclude their potential *in vitro* expansion post-selection, if necessary.

Cells separated in both of these manners based on the expression, or lack thereof, of the two candidate proteins are therefore further investigated and compared in terms of their ability to participate in skeletal muscle regeneration within dystrophic animals. However factors that may influence protein expression, such as length of time spent in culture, are also considered within the context of their use in identifying efficient progenitors.

2.2.2 Methods

2.2.2.1 Cultured Cell Preparation and Magnetic Antibody Cell Sorting (MACS). For each separate isolation and transplantation experiment, primary cells were obtained from the combination of four gastrocnemius muscles of normal male mice (C57 BL/10J; Jackson Laboratories) between 6 and 9 weeks of age, utilizing the identical preplate procedure as described in Section 2.1.2.1. The results presented represent data collected from over 25 separate cell isolations. For convenience, PP1 through PP3 (≤27 hour initial adhesion) are referred herein as EP, for early preplate. Likewise, cells obtained from PP4 and beyond (>27 hour initial adhesion) are referred to as LP, for late preplate. Due to the difficulty in obtaining them, MDSCs however were prepared as described in Section 2.1.2.1 from separate animals (<1 week old, female, C57 BL/6J), and cultures used for transplantation were between passages 30 and 35.

For primary cell transplantation purposes, it was appropriate to compare relatively pure myogenic cell populations with initial adhesion time being the only controlled variable among the EP and LP populations. Therefore, myogenic cells were further purified from the EP cultures through an additional processing step. As described in Section 2.1, adhesion of murine non-myogenic cells to the collagen-coated culture flasks occurs at a faster rate as compared to myogenic cells, and thus EP cultures initially contained a higher percentage of non-

myogenic cells. Therefore, prior to their use, the myogenic cells found within the EP cultures were purified through a re-plating process, also described elsewhere [43, 145]. This procedure involves standard trypsinization and plating of the EP cultures, allowing the majority of the fibroblasts to adhere within the first 20-30 minutes while removing the myogenic-enriched supernatant. Using this technique, EP cultures can be purified to 80-90% desmin-positive. Although this additional step was performed to enrich the EP cultures, the time from initial cell isolation to their use in the experiments was similar for both EP and LP populations (within 2 days following initial adhesion), to eliminate any potential variability in results due to increased culture times.

LP myogenic cells were trypsinized and sorted for the presence or absence of the cell surface proteins Sca-1 and CD34, in separate experiments, using a magnetic antibody cell sorting separation system (Miltenyi Biotec Inc.) as follows, and as shown in Figure 2.8. Following trypsinization, cells were separated into labeled and control fractions and maintained on ice throughout the procedure. Both fractions were resuspended in a blocking solution (identical to that described for flow cytometry labeling in Section 2.1.2.3) for 10 minutes. For CD34 separation

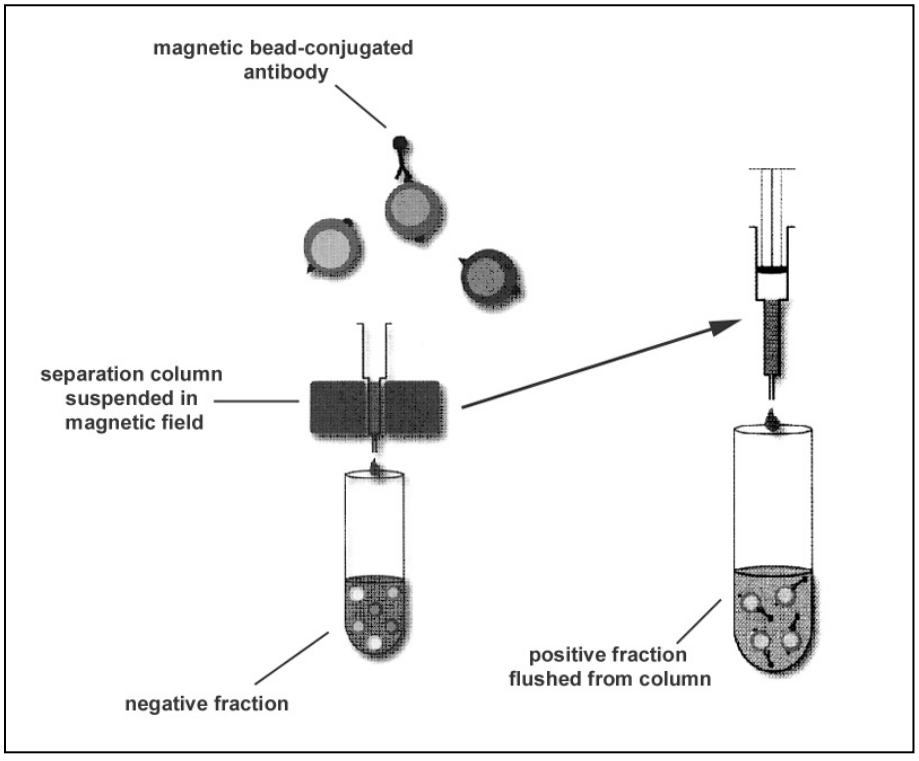

Figure 2.8 Magnetic antibody separation system.

cells were then incubated an additional 20 minutes with biotinylated rat anti-mouse CD34 monoclonal antibody (RAM34; Pharmingen), washed in Hank's Balanced Salt Solution (HBSS; Gibco), and incubated with anti-biotin antibody conjugated with magnetic microbeads per manufacturer's instructions (80μL HBSS/20μL antibody; Miltenyi Biotec). It is important to note that the antibody used recognizes both the truncated and full-length CD34 isoforms. Labeled cells were then washed and resuspended in HBSS containing 0.5% bovine serum albumin and passed through Large Cell Separation Columns (Miltenyi). Both the negative and positive fractions were collected and again passed through fresh columns, separately, in order to ensure a good separation. Purity of separation and expression of other proteins was assessed by labeling portions of both positively-selected and negative fractions with SA-APC conjugate, PE-conjugated Sca-1 (Ly-6A/E), and FITC-conjugated CD45 rat anti-mouse antibodies (Pharmingen) in an identical manner to that described in Section 2.1.2.3.

Sca-1 separation was performed in a manner similar to that described for CD34 separation. Cells however were labeled with directly-conjugated microbead rat anti-mouse Sca-1 monoclonal antibody (Miltenyi Biotec). Purity of separation and expression of other proteins was assessed by labeling portions of positive and negative sorted fractions with PE-conjugated Sca-1, biotinylated CD34 and FITC-conjugated CD45 rat anti-mouse monoclonal antibodies (Pharmingen), followed by SA-APC.

For both separations, control cell fractions used to determine background fluorescence levels were labeled with appropriately-conjugated isotype control antibodies (Pharmingen) and were treated in an identical fashion, with the exception of passing through the magnetic separation column. Separation purity was assessed using the same instrumentation as for the flow cytometry analysis (FACSCalibur flow cytometer and CellQuest software), and 7-AAD was added to all tubes for exclusion of nonviable cells in the analysis (as shown in Figure 2.9). A portion of non-injected cells was also placed back into culture and evaluated for the percentage of desmin-expressing cells, as described in Section 2.1.3.1.

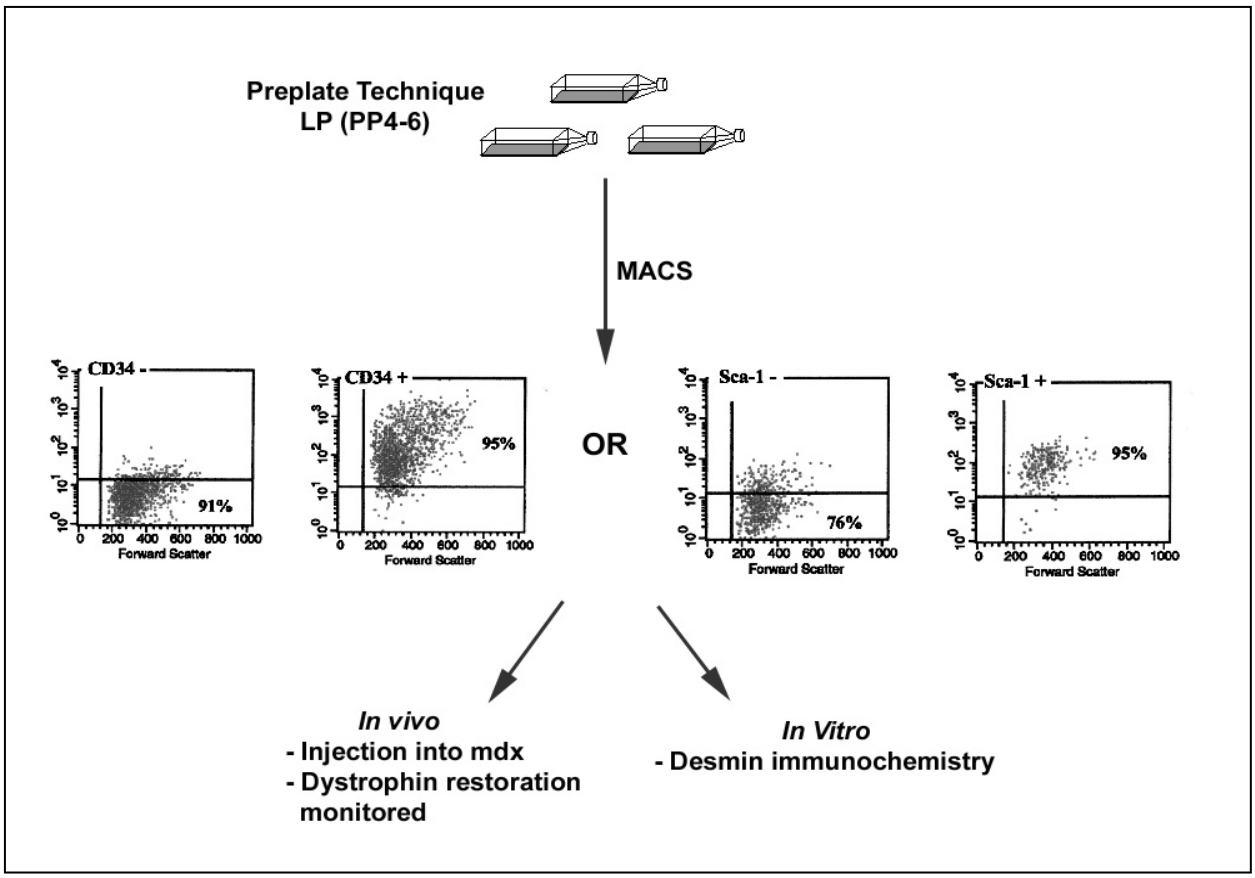

Figure 2.9 Overview of experimental procedure used for evaluating cultured LP cells sorted by MACS. LP cells were sorted based on either Sca-1 or CD34 expression, in separate experiments, prior to their utilization. Representative plots of sorted cell populations, analyzed by flow cytometry to ensure separation following sorting, are shown. These LP subpopulations were subsequently compared to EP and MDSC populations in terms of regeneration ability.

2.2.2.2 Direct Cell Isolation and Fluorescence Activated Cell Sorting (FACS). Sorting of phenotypic populations directly from dissociated cell suspensions, without culturing, was also performed using enzymatically-digested gastrocnemius muscles of normal adult-aged mice (7-9 weeks old; C57 BL/10J; Jackson Labs). A summary diagram of the experimental setup is provided in Figure 2.10.

Enzymatic dissociation was consistent with that previously described for the preplate technique in Section 2.1.2.1. In addition however, due to size limitations of the cell sorter and the presence of larger undigested connective tissue masses that are typically present despite the digestion procedure, cell suspensions were also passed through a 100 μm nylon mesh cell-strainer (Becton Dickinson). The filtered cell suspension was maintained on ice throughout the remainder of the labeling procedure. Red blood cells were removed using a lysis buffer solution

(containing 150 mM ammonium chloride in Tris-HCl buffer), followed by a washing step to remove lysed cells, prior to antibody labeling. Cells were incubated with the same blocking solution as described for flow cytometry and magnetic separation lableling (found in Section 2.1.2.3), and then labeled with pre-determined optimal amounts of rat anti-mouse CD45 (FITC-conjgate), Sca-1 (PE-conjugate) and CD34 (biotin-conjugate) monoclonal antibodies (Pharmingen). A separate cell portion received equivalent amounts of isotype control antibodies (also Pharmingen). Both fractions were then washed and labeled with SA-APC as described (Section 2.1.2.3). For non-sorted evaluation of the Sca-1/CD34 profile obtained from the directly-isolated cells, 7-AAD was added to exclude non-viable cells from analysis. This viability probe was not included in the sorted cell fractions, as it may become toxic to the cells over extended periods of time.

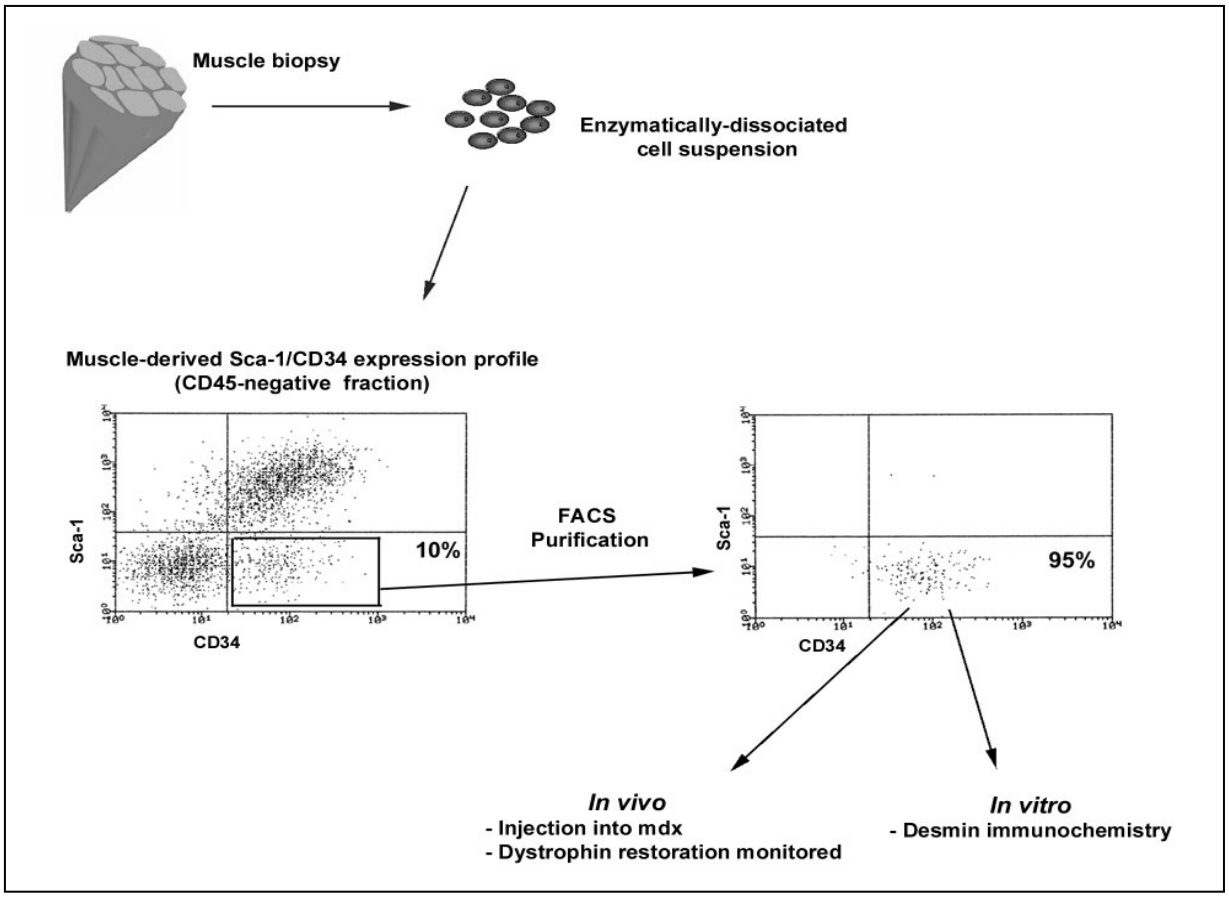

Figure 2.10 Overview of the experimental procedure used for evaluating directly-isolated muscle-derived cells by FACS.

During the sorting procedure, cells were maintained and collected in serum-supplemented DMEM culture medium (defined in Section 2.1.2.1). Appropriate gating was performed to exclude hematopoietic (CD45-positive) cells, while the remaining cells were sorted based on Sca-1/CD34 phenotype using a FACStar Plus (Becton Dickinson) flow cytometer. In general, it was observed that muscle-derived viability was influenced by the rate at which the cells were sorted, indicating an apparent shear-sensitive nature, and that viability was typically enhanced by lowering the sorting pressure.

In separate experiments, either four phenotypically-purified populations were collected using combinations of both Sca-1 and CD34 proteins (Sca-1-/CD34-, Sca-1+/CD34+, Sca-1-/CD34+, and Sca-1+/CD34-), or two populations were collected using just one of the proteins for separation, while ignoring expression of the other. A portion of each sorted population was evaluated by immunocytochemistry for the expression of desmin, similar to that described in Section 2.1.3.1, with the exception that the cells were dry-fixed with methanol immediately to glass slides. This was done to eliminate changes in the desmin percentages of each population that may occur over the time for initial cell adhesion to occur, which in some cases takes up to 4-5 days based on knowledge of the preplating process. The remaining viable cells were counted using a hemacytometer with Trypan Blue exclusion, and washed twice in HBSS to minimize any remaining serum. The average number of myogenic cells transplanted for each phenotype was 122±16, 133±21, 51±11, and 148±22 for Sca-1-, Sca-1+, CD34-, and CD34+, respectively.

2.2.2.3 Cell Transplantation. For transplantation into dystrophic mice, both MACS- and FACS-sorted cell populations were washed twice in HBSS, resuspended to a final volume of 10μL in HBSS, and transplanted using a single injection into the gastrocnemius muscle of age-matched female dystrophic mice (7-9 weeks old, C57 BL/10ScSn-DMD^{mdx}; Jackson Laboratory) using a Hamilton fixed-needle syringe (26 Gauge). Animals were sacrificed at 7, 14 or 28 days following injection and evaluated for dystrophin expression, as described in the following section. Due to the availability of an mdx/SCID cross-bred mouse at the time of experimentation, these animals were utilized for FACS transplantations intended for sacrifice at the 28 day evaluation timepoint only. A description of this breeding scheme is provided in section 2.2.2.8. It should be noted that data from several injections were excluded based on the presence of blood emanating from the injection site following removal of the needle.

For LP MACS-sorted populations, paired injections were performed with the negative-sorted population transplanted into one limb and the positive-sorted population into the other. Additional injections were also

performed in a non-paired fashion dependent upon the number of cells obtained from the isolation and separation process, which was observed to be somewhat variable.

2.2.2.4 Dystrophin Immunohistochemistry. Harvested gastrocnemius muscles were flash frozen in liquid nitrogen-cooled 2-methylbutane and serial-sectioned at 8-10 μm. Tissue was stored at -80^{o}C until processing. Sections were fixed in cold acetone for 2 minutes, incubated with a blocking solution of PBS containing 5% horse serum for 30 minutes, and then incubated with a rabbit anti-dystrophin antibody (1:1000 dilution in blocking solution; gift from Dr. Terry Partridge). Sections were then washed in PBS and incubated with biotinylated anti-rabbit IgG antibody (1:250 in PBS; Vector), followed by additional washing and incubation with SA-Cy3 or SA-FITC (1:500; Sigma). Slides were mounted in VectaShield media (Vector), to reduce quenching of the fluorescence signal during analysis.

2.2.2.5 Regenerative Index. As mentioned, portions of all cell populations utilized in the transplantation experiments were evaluated to determine the percentage of myogenic cells through desmin expression. The isolation and processing of the cells may result in variations with regard to the percentage of non-myogenic, contaminating, cells. This was of particular concern for fair comparison of cultured and directly-isolated populations, as a means for eliminating non-myogenic murine cells was not readily available (antibodies against murine CD56 were not commercially accessible at the time of experimentation). Thus, in order to more accurately assess the ability of each myogenic population to contribute to the myofiber regeneration process, the number of desmin-positive cells injected rather than the total number injected was used to define all transplanted populations. The only exception to this was the MDSC population, which may not express traditional myogenic markers but is considered a myogenic progenitor.

From dystrophin immunohistochemically-labeled sections, areas identified as containing the maximum number of dystrophin-positive myofibers for each injection were used to determine the regeneration capacity of the various myogenic cell populations, defined below.

$$\text{Regenerative Efficiency Index} = \frac{\#\,\text{dystrophin - positive myofibers}}{\#\,\text{viable and desmin - positive cells injected}} \times 10^{5} \qquad [2.1]$$

Thus, this index represents the number of dystrophin-positive fibers that can be generated for every 100,000 myogenic cells injected. Dystrophin-positive myofibers were manually counted from acquired immunofluorescence images using ImageView software (Automated Cell Technologies, Inc.).

2.2.2.6 Regenerated Myofiber Size Distribution. Dimensional analysis of immunohistochemically-labeled dystrophin-positive myofibers generated by the injection of the various donor myogenic cell populations was performed on digital images using Northern Eclipse software (v6.0, Epix Imaging, Inc.). Using a manually-set threshold to delineate the immunofluoresence signal from background, the software identifies individual myofiber boundaries and uses them to provide dimensional data for each fiber separately. An example of this is shown in Figure 2.11. Fiber size data was generated from the same images used in calculating the regenerative efficiency index, and the reported values represent the actual myofiber

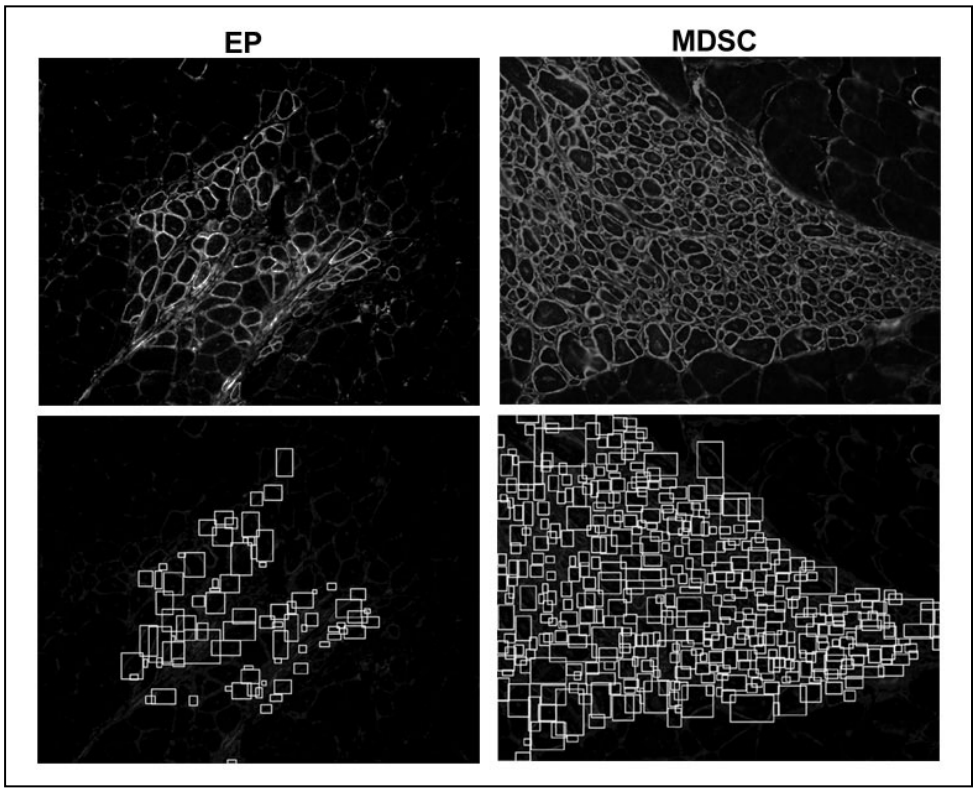

Figure 2.11 Dystrophin-positive myofiber boundaries identified from immunofluorescence images were used to evaluate size distributions generated from each transplanted progenitor population (EP and MDSC examples shown here; 200x images). A bounding box is placed around the centroid of each individual myofiber identified (bottom panels).

cross-sectional area and the maximum cross-sectional diameter. For comparison, analysis of myofiber sizes taken from non-injected areas of the same mdx muscle was also performed.

2.2.2.7 Evaluation of in vitro Protein Expression Changes. Non-injected portions of LP-sorted populations were also placed back into culture under growth conditions (high-serum DMEM as defined in Section 2.1.2.1) and their phenotype, relative to the initial sorted phenotype, re-evaluated at 2 and 5 days. Cell labeling and flow cytometry analysis procedures used were identical to that described in Section 2.1.2.3.

2.2.2.8 Animals. All animals were housed in the Rangos Research Center Animal Facility of the Children's Hospital of Pittsburgh. The policies and procedures of the animal laboratory are in accordance with those detailed in the guide for the "Care and Use of Laboratory Animals" published by the US Department of Health and Human Services. Protocols used for these experiments were approved by the Animal Research and Care Committee of the Children's Hospital of Pittsburgh (Protocol 7/00).

Dystrophic and immune deficient mice (mdx/SCID), utilized for the 28 day FACS transplantations only, were specially bred by Jim Cummins of the Growth and Development Laboratory under Protocol 33/00. In order to obtain mice that were homozygous for both the mdx and SCID mutations, the following abbreviated breeding scheme and testing regime was performed. Male C57BL/6J-Prkdc^{scid}/SzJ mice were crossed with female C57/10ScSn-Dmd^{mdx}/J mice (both from Jackson Laboratories). Brothers and sisters from the F1 generation were next crossed, and all F2 generation animals were tested for their homozygosity for the Prkdc^{scid} mutation. This mutation results in the blockage of T and B lymphocyte development. DNA for these tests was obtained from each of the F2 pups via a tail snip, and homozygosity of the scid mutation was evaluated using a PCR/Restriction Enzyme assay outlined by The Jackson Laboratory. If mice were found homozygote for the scid mutation, dystrophin expression was evaluated to determine which of these mice were homo/hemizygous for the Dmd^{mdx} mutation. An additional tail snip was obtained, snap frozen and cryosectioned. These sections were histologically stained with hematoxylin and eosin to establish the location of the muscle fibers, and then immunofluorescently labeled similar to that described in section 2.2.2.4. F2 mice that were both homozygyote for the scid mutation and negative for dystrophin expression were then inbred to expand the colony.

2.2.2.9 Statistical Analysis. Separate comparisons of regeneration indices within LP MACS-sorted subfractions and FACS-sorted fractions were made by Student's t-test or the non-parametric equivalent, Mann-Whitney Rank Sum test, for comparisons in which non-equal variance was detected. For multiple group comparisons among

cultured EP, LP-sorted, and MDSC populations, non-parametric distributions and unequal variance were detected. Therefore, comparisons were performed using Kruskal-Wallis one-way ANOVA on ranks, with Dunn's test for pairwise comparisons. Additionally, the Pearson Product Moment Correlation was used to examine the relationship between injected LP cell subfraction number and the number of myofibers generated.

All comparisons and data descriptions were performed using SigmaStat (v2.0, Jandel Scientific) statistical software, which examines both sample variance and normality of the data distributions, using the Kolmogorov-Smirnov test, prior to performing parametric comparisons. For all analyses, results demonstrating $p<0.05$ were considered statistically significant. Exact p-values are given for non-significant comparisons. Data is presented as mean ± SEM, unless otherwise noted.

2.2.3 Results

Some of the results and figures, where indicated, have been previously published [146] and are reproduced here with permission from The Company of Biologists Ltd.

2.2.3.1 Cultured Progenitor Cell Separation (MACS). The effectiveness of the separation process and the phenotypic-purity of the sorted populations can be assessed by describing the percentage of each population that emits fluorescence above or below that of the isotype control-labeled fraction. Collective results of the MACS-separated LP characteristics are described in Table 1, as well as some comparative EP and MDSC population characteristics. Separation of the Sca-1 fractions often resulted in the elution of cells expressing low levels of Sca-1 within the negative fraction (as shown previously in Figure 2.9). However, when examining the fluorescence intensity for each sorted population, it was observed that the separation occurred such that the Sca-1-positive fraction (Sca-1+) contained cells with a mean fluorescence intensity ten times greater than that of the negative fraction (Sca-1-). Separation CD34-negative and positive populations was cleaner, based on percentages above and below background levels. In either case, comparison of mean channel fluorescence between negative and positive fractions for both Sca-1 and CD34 separations was highly significant ($p<0.001$).

Overall, there was no difference in either morphology or size between the negative and positive sorted LP fractions, as seen in the forward scatter profiles in Figure 2.9. The number of cells in the positive and negative

fractions that could be obtained from sorting was variable for all isolations, however, on a consistent basis only a low number of the Sca-1+ population was able to be obtained.

For several sorts, additional characterization of expression of both sorted and non-sorted proteins was performed. For Sca-1-sorted cells, the negative fraction (Sca-1-) contained an average of 26.7±1.1% CD34-positive cells (CD34+), while the Sca-1+ fraction contained 29.6±5.2% CD34+ cells. For CD34-sorted cells, the negative fraction (CD34-) contained 49.3±3.1% Sca-1+ cells, while the CD34+ fraction contained 69.9±2.9% Sca-1+ cells.

The expression profile of the unsorted MDSC population is described in section 2.1.3.2. EP cells used in these comparison studies were also evaluated by flow cytometry and shown to express 20-30% of both the Sca-1 and CD34 proteins.

Table 2.1 Characteristics of transplanted cell populations, including sorting characteristics of LP myogenic cells separated based on either Sca-1 or CD34 expression.

	EP	**MDSC**	**LP Sca-1-sorted cells**		**LP CD34-sorted cells**	
	Non-sorted	**Non-sorted**	**Negative Fraction (Sca-1 -)**	**Postive Fraction (Sca-1 +)**	**Negative Fraction (CD34 -)**	**Postive Fraction (CD34 +)**
% Viability	**94.9** ± 1.3	**100***	**93.0** ± 1.1	**98.7** ± 0.8	**92.1** ± 2.2	**94.2** ± 2.1
% Purity	**n/a**	**n/a**	**72.7** ± 2.0	**93.3** ± 1.6	**91.1** ± 1.7	**88.3** ± 1.3
Mean Fluorescence	**n/a**	**n/a**	**16.9** ± 1.0	**171.8** ± 16.5	**12.3** ± 2.4	**217.4** ± 25.6
% Desmin Positive	**84.1** ± 4.2	**14.4***	**82.1** ± 2.4	**90.6** ± 1.5	**82.2** ± 1.5	**78.4** ± 2.4

*MDSC experiments performed using cells derived from single isolation (thus no standard error); n/a, not applicable

2.2.3.2 <u>Cultured Progenitor Cell Dystrophin Restoration</u>. In order to ensure that the number of cells injected relative to the area of injury created by the syringe needle did not limit the degree of regeneration observed, and to examine the predictability of the regeneration responses obtained with the purified LP subpopulations, the

relationship between the cell number injected and the number of dystrophin-positive myofibers generated was examined. As shown in Figure 2.12, myofiber number increased in relation to the number of transplanted cells in a relatively linear fashion for all sorted LP populations. A significant linear relationship was observed between cell number and myofibers generated for both the CD34- and Sca-1- subfractions (CD34+, p=0.0507; Sca-1+, p=0.054). Even though the number of data points collected was not extensive, these responses indicate that estimations of the regeneration response that may be expected can be made.

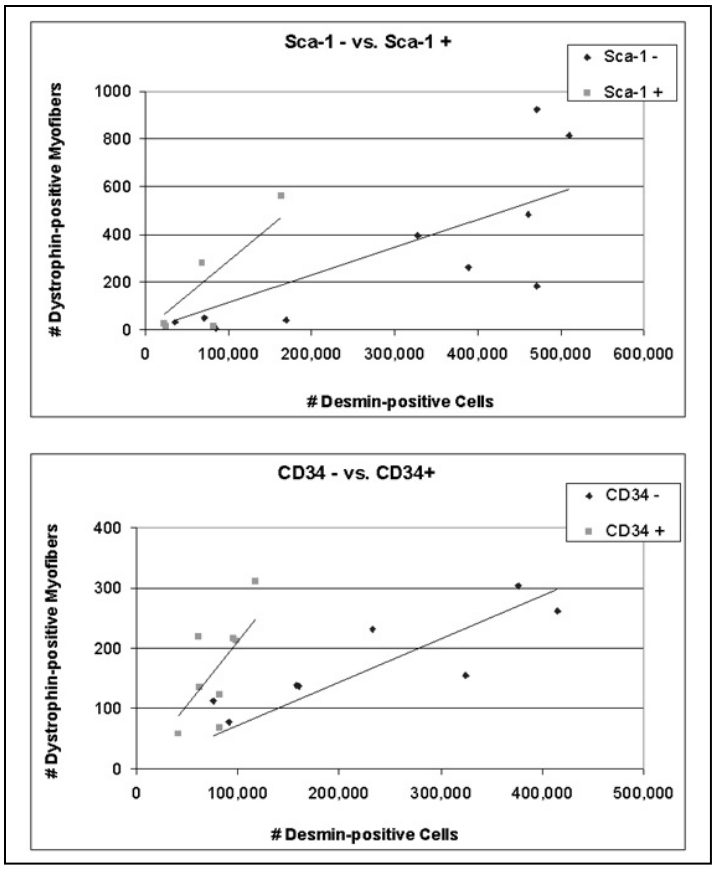

Figure 2.12 Relationship between LP cells injected and dystrophin-positive myofibers generated by 7 days post-injection. A positive linear association was observed for all populations (linear regression R^2: 0.676, 0.758, 0.736, and 0.497 for Sca-1-, Sca-1+, CD34-, and CD34+, respectively) [146].

As indicated by visual inspection of these relationships, quantitative comparison of LP subpopulations, defined by the regeneration index, revealed a variable regenerative efficiency. As shown in Figure 2.13, those

expressing the CD34 protein were significantly more efficient in generating dystrophin-positive myofibers at 7 days post-injection compared to their CD34- counterparts (n=9 and n=8, respectively; 193±30 vs. 87±10, respectively; $p<0.05$). Comparison at 28 days post-injection did not alter this finding, although the efficiency of both sharply decreased presumably due to host responses against the allogeneic cells or the dystrophin protein itself (n=5, each; 56±15 vs. 12±7, $p<0.05$). Infiltration of lymphocytes, identified by CD4 and CD8 immunostaining, within the graft site was noted by this time period. When comparing the Sca-1-sorted fractions at 7 days, there was a non-significant trend toward increased dystrophin restoration utilizing Sca-1+ cells (n=6 and n=12 for Sca-1+ and Sca-1-, respectively; 157±72 vs. 96±22, $p=0.306$). When comparing these Sca-1-sorted fractions at the 28 day timepoint, only a small number of dystrophin-positive fibers were observed for the Sca-1+ fraction (n=3 for Sca-1+ and n=8 for Sca-1-; 2±2 vs. 54±24). However, this result may be misleading due to the comparison between fractions on a per cell basis rather than absolute myofiber number, as the Sca-1+ fraction actually resulted in a lower number of dystrophin-positive myofibers at 7 days. As mentioned, an active reduction in myofiber number due to cellular responses is observed by 28 days, and thus a constant rate of elimination by host responses would facilitate a more rapid elimination of the Sca-1+ generated graft preferentially. In order to examine this further, an additional comparison at 14 days post-injection was performed, a duration in which graft rejection would be less severe. These 14 day results were indeed found to be similar to the 7 day post-injection results (n=3 for Sca-1+ and n=5 for Sca-1-; 157±45 vs. 125±13, $p=0.422$).

Efficiencies of the remaining cultured populations, EP and MDSC, at 7 days post-injection are also shown in Figure 2.13. The EP myogenic population and the MDSC population demonstrated the lowest and highest regenerative abilities, respectively (63±14 and 556±94 for EP and MDSC; n=5 and n=4). Multiple comparisons including these populations and the CD34-sorted LP subfractions showed significantly higher regeneration through utilization of the MDSCs versus all other cultured cell populations. Comparison between the EP and the CD34-sorted LP cells alone showed a significant difference between the EP and CD34+ LP fraction, but not in comparison to the CD34- fraction.

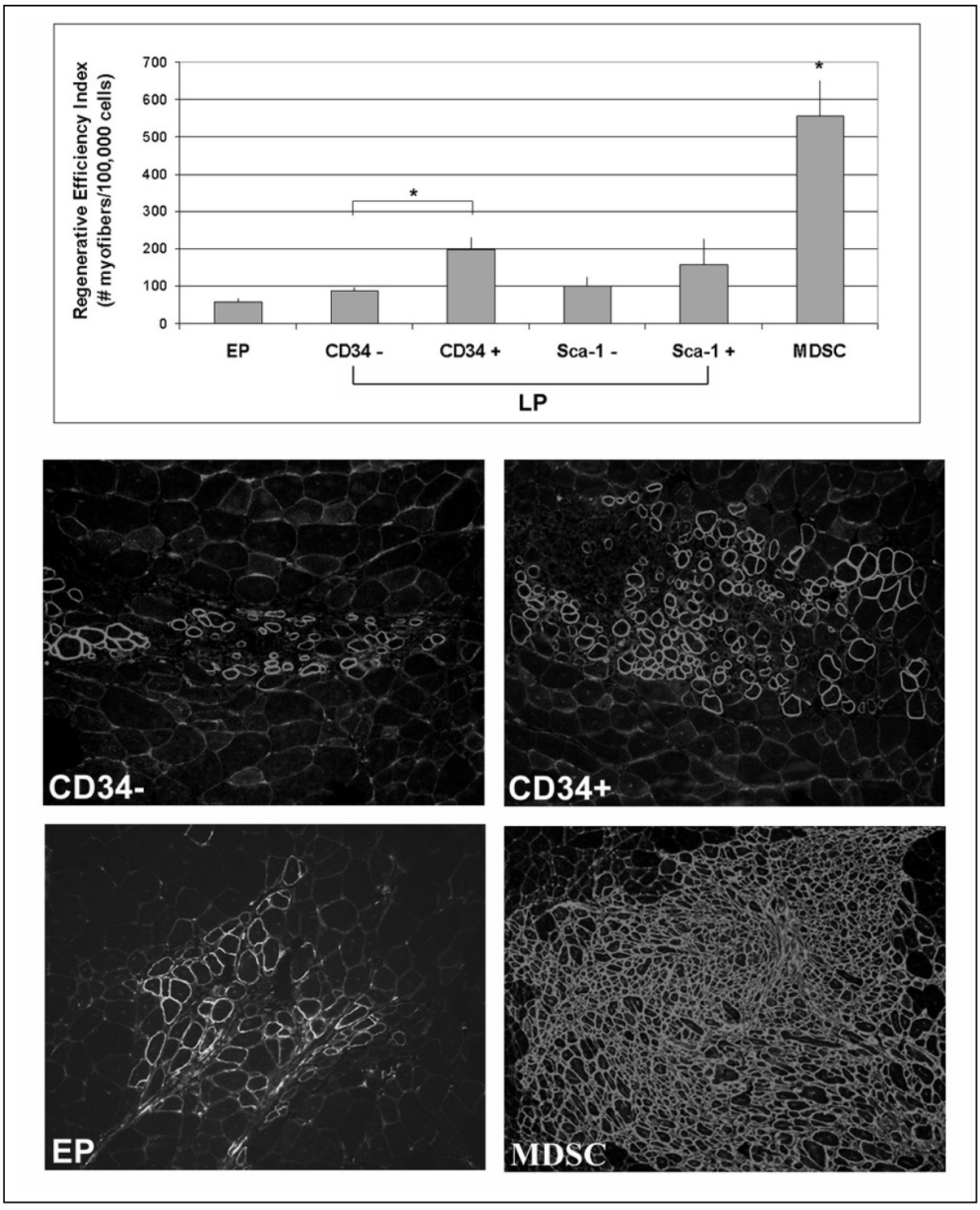

Figure 2.13 (top) Efficiency of dystrophin restoration among the myogenic progenitor populations at 7 days post-injection. CD34+ LP cells were significantly more efficient than their CD34- counterparts. MDSCs were the most efficient in comparison to all other isolated populations (*, $p<0.05$). Representative cryosections, with dystrophin expression revealed by immunohistochemical staining, following injection of EP (220,000 cells), LP CD34- and CD34 + (approximately 95,000 cells each), and MDSC (200,000 cells) are shown. All images were acquired at 200x, except MDSC which was taken at 100x to emphasize the larger graft size.

Size distributions of dystrophin-positive myofibers generated by each cell population were monitored at the 7 day timepoint, and are presented in Table 2.2. A non-parametric distribution weighted toward smaller myofiber sizes was apparent. Overall, the dimensions of myofibers among donor populations were similar, although those generated by the EP population were significantly larger in both cross-sectional area and maximum myofiber diameter. In particular, of the four progenitor populations examined, the EP population generated the lowest percentage of fibers within the 10-20 μm diameter and 0-100 μm^2 area ranges, representative of small newly-formed myofibers. The upper range of size parameters from EP-generated myofibers is seen to overlap with the lower range of that of native mdx myofibers.

Table 2.2 Dimensional characteristics of dystrophin-expressing myofibers generated by each injected myogenic progenitor cell population.

	Fiber Diameter (μm)		**Fiber Area (μm^2)**	
	Median	**Percentiles 25%-75%**	**Median**	**Percentiles 25%-75%**
mdx (non-injected)	**46.3**	**32.9 – 63.1**	**842.0**	**413.6 – 1661.8**
EP	**22.7**	**16.5 – 35.0**	**184.7**	**89.4 – 450.9**
LP CD34-	**16.5**	**10.4 – 22.7**	**108.2**	**43.4 – 220.3**
LP CD34+	**17.5**	**11.4 – 25.9**	**121.7**	**47.6 – 273.0**
LTP	**18.5**	**13.4 – 26.7**	**121.3**	**64.6 – 250.9**

2.2.3.3 Direct Progenitor Cell Separation (FACS) and Dystrophin Restoration. For evaluation of the candidate surface proteins from directly-isolated progenitors, the FACS sorting technique allowed for the comparison of cells based on the expression of a single protein similar to the MACS sorting (Sca-1- vs. Sca-1+ or CD34- vs. CD34+). However, FACS also permitted separation such that regeneration based on expression of both proteins could be

evaluated simultaneously (Sca-1+/CD34+ vs. Sca-1+/CD34- vs. Sca-1-/CD34+ vs. Sca-1-/CD34-). Figure 2.14 shows a typical muscle-derived cell Sca-1/CD34 expression profile, along with average percentages obtained from all isolations, of whole gastrocnemius muscle following enzymatic dissociation into a single cell suspension. This profile contains both non-myogenic and myogenic cells, however hematopoietic cells have been excluded based on the selection and analysis of CD45-negative cells. The percentage of excluded hematopoietic cells found within the dissociated suspension represented 26.5±9.5% of the total cells isolated. Although the remaining percentage of non-hematopoietic cells used for sorting was un-evenly distributed among the four phenotypic quadrants, this profile was fairly consistent between cell isolations.

The percentage of myogenic cells contained within sorted fractions, based only on expression of either CD34 or Sca-1, was somewhat similar (36±4% vs. 48±3% for Sca-1+ and Sca-1-, and 52±5% vs. 39±4% for CD34+ and CD34-, respectively). However, when accounting for both of these proteins simultaneously the percentages were widely variable, ranging from a very low percentage within the Sca-1+/CD34- subfraction (15-20%) to a relatively high percentage within the Sca-1-/CD34+ subfraction (>75%). Immunofluorescent desmin-labeling of non-injected portions of these sorted populations and their relative percentage of myogenic cells are displayed in Figure 2.15.

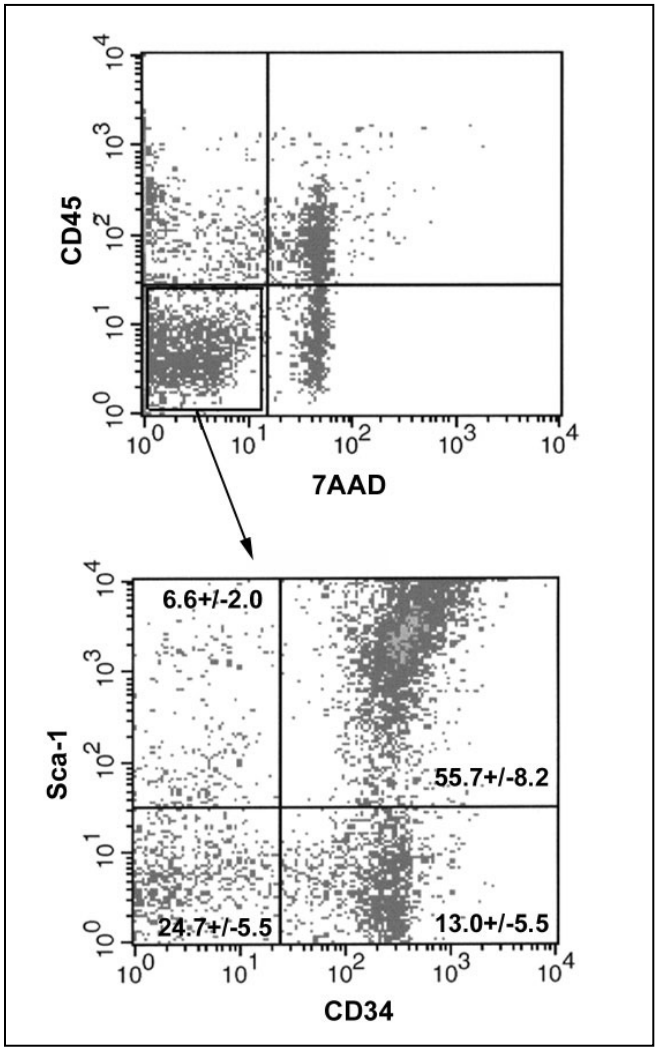

Figure 2.14 Representative Sca-1/CD34 profile of viable (7AAD-negative) and non-hematopoietic (CD45-negative) cells obtained from dissociated whole skeletal muscle. Average values from all sorts presented in each quadrant.

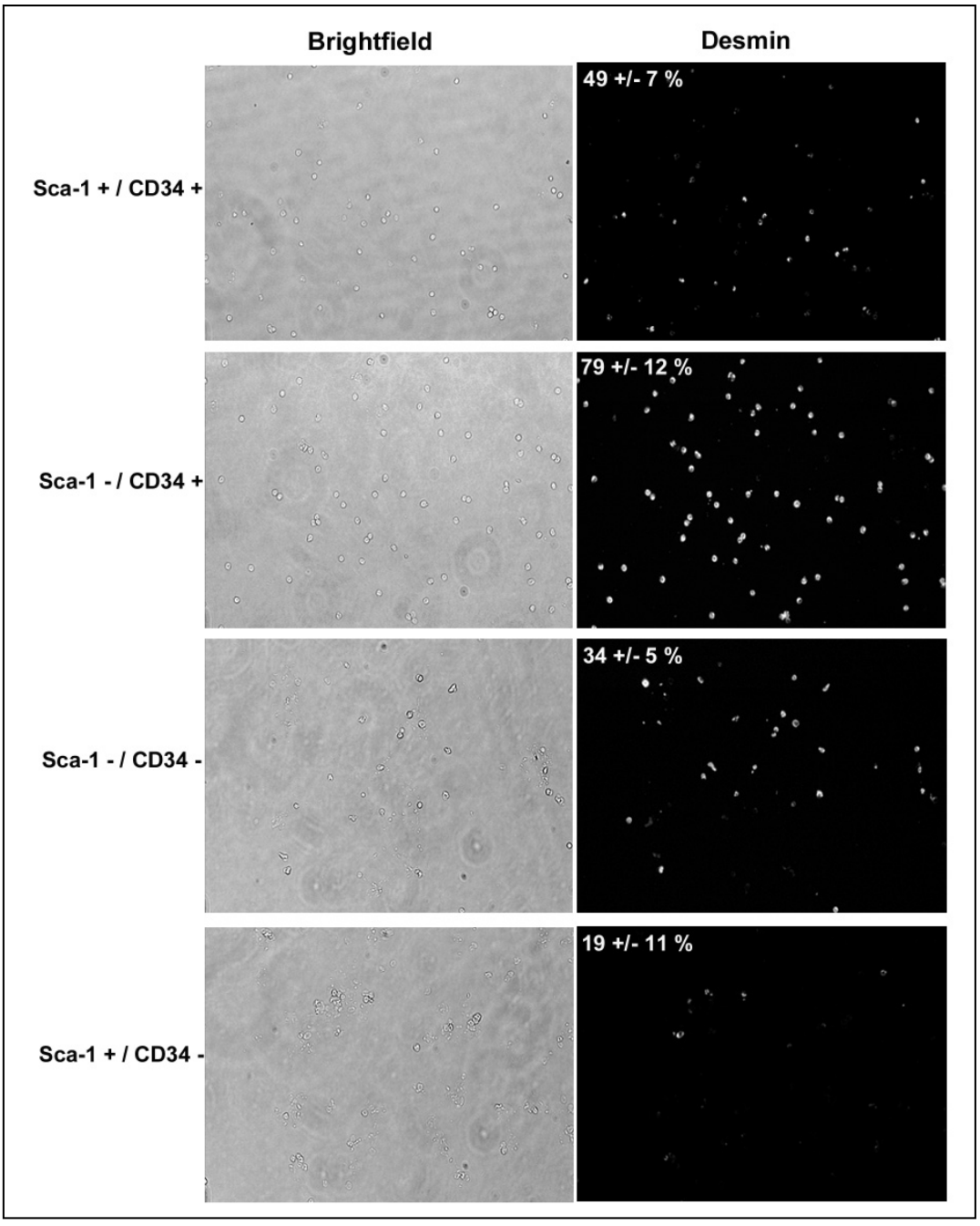

Figure 2.15 The percentage of myogenic (desmin-expressing) cells contained within each of the four sorted fractions of enzymatically-dissociated muscle (200x magnification).

Transplantation of cells into dystrophic host muscle was first performed following separation of dissociated muscle into each of the four possible Sca-1/CD34 phenotypes. Regeneration capacity was assessed at 7 days post-injection, again with respect to the number of transplanted viable and myogenic cells. As shown in Figure 2.16, variable regeneration responses were evident, with the highest degree of dystrophin restoration resulting from the utilization of the Sca-1-/CD34+ fraction (n=2 each). From these preliminary results, it was observed that cells lacking Sca-1 expression (Sca-1-/CD34+, Sca-1-/CD34-) displayed, in common, a higher regeneration response compared to their Sca-1+ counterparts (Sca-1+/CD34-, Sca-1+/CD34+). In contrast, more modest differences based on CD34 expression were apparent.

To further investigate these observations, and for a more appropriate comparison to the MACS-sorted cultured-cell results, additional transplantation experiments were performed in which dissociated cell suspensions were sorted into only two fractions based on either Sca-1 or CD34 expression. In agreement with the earlier four-fraction separation results, Sca-1- cells demonstrated a higher regeneration efficiency when compared to their Sca-1+ counterparts at 7 days post-injection (148±61 vs. 18±15, respectively; n=2 each). Also in agreement with the earlier results, two-fraction separation based on CD34 expression resulted in a similar regeneration efficiency (139±28 vs. 101±49, for CD34- and CD34+, respectively; n=3 and n=2). Taken together with the results of the four-phenotype separation, it was thus observed that Sca-1- cells displayed a significantly higher regeneration capacity compared to their Sca-1+ counterparts at 7 days post-injection (141±32 vs. 13±4; n=6 each, $p<0.05$). No significant difference was observed between CD34-sorted populations (92±29 vs. 98±34, for CD34- and CD34+, respectively; n=7 and n=6, $p=0.890$).

Continuing with the two-fraction separation, results from additional Sca-1-based transplantations evaluated at both the 14 day (107±28 vs. 46±25, for Sca-1- and Sca-1+, respectively; n=3 each) and 28 day (225±30 vs. 21±4, for Sca-1- and Sca-1+; n=3 each) timepoints did not deviate from the 7 day findings. It should be noted that unlike the MACS-sorted 28 day results, the use of the mdx/SCID host for the transplantations performed here allowed for retention of dystrophin-positive myofiber number. Nonetheless, this did not alter the observed discrepancy in regeneration between the Sca-1-separated populations. Additional CD34-based transplantations evaluated at the 14 day timepoint (231±28 vs. 244±24, for CD34- and CD34+, respectively; n=2 each) also agreed with the 7 day findings. Due to the consistency of these observations, 28 day evaluation was not performed. A summary of these results and representative dystrophin immunofluorescence-labeled sections are provided in Figure 2.17.

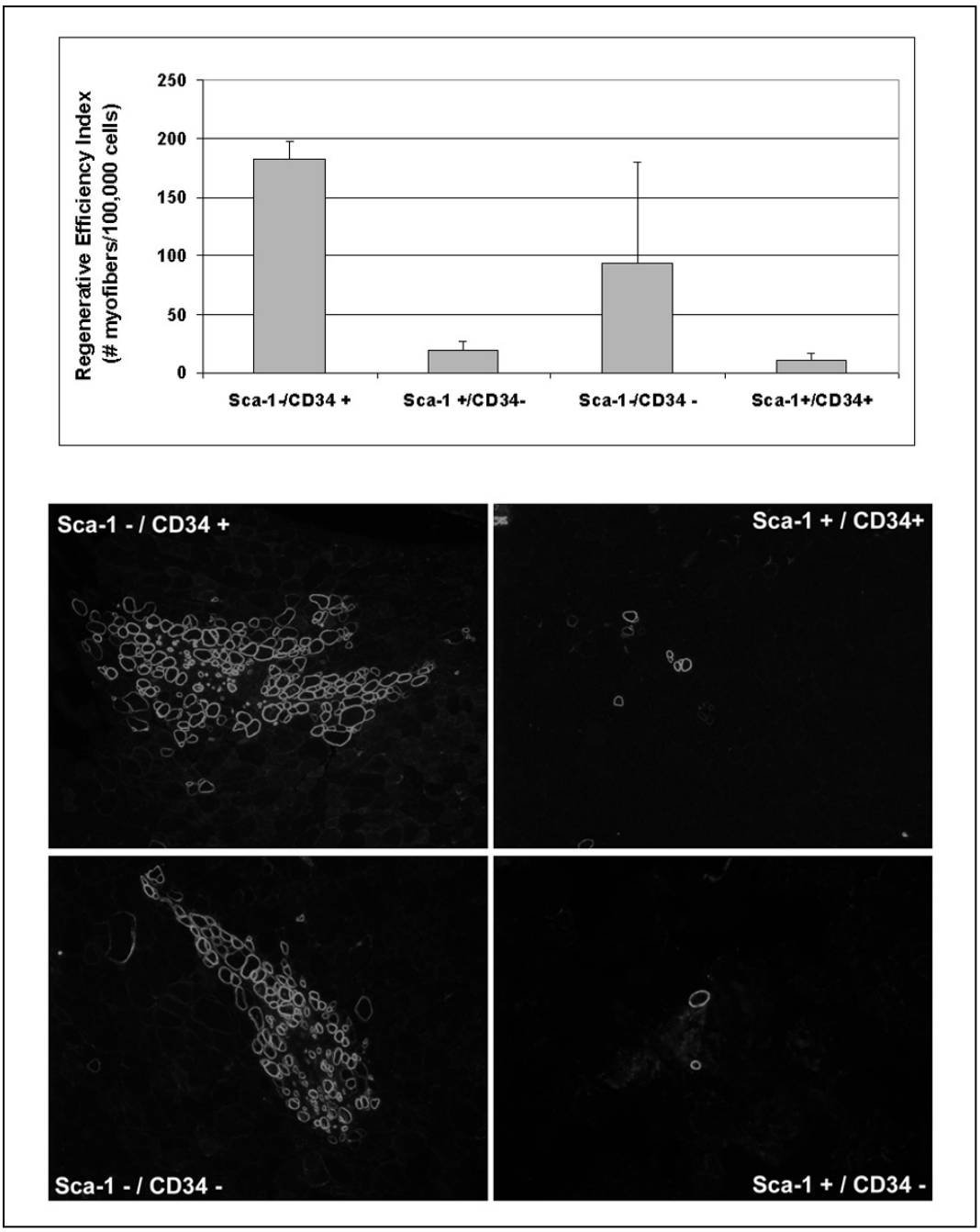

Figure 2.16 Transplantation results of four-fraction separation based on expression of both Sca-1 and CD34, evaluated at 7 days post-injection. Representative images were acquired at 100x magnification.

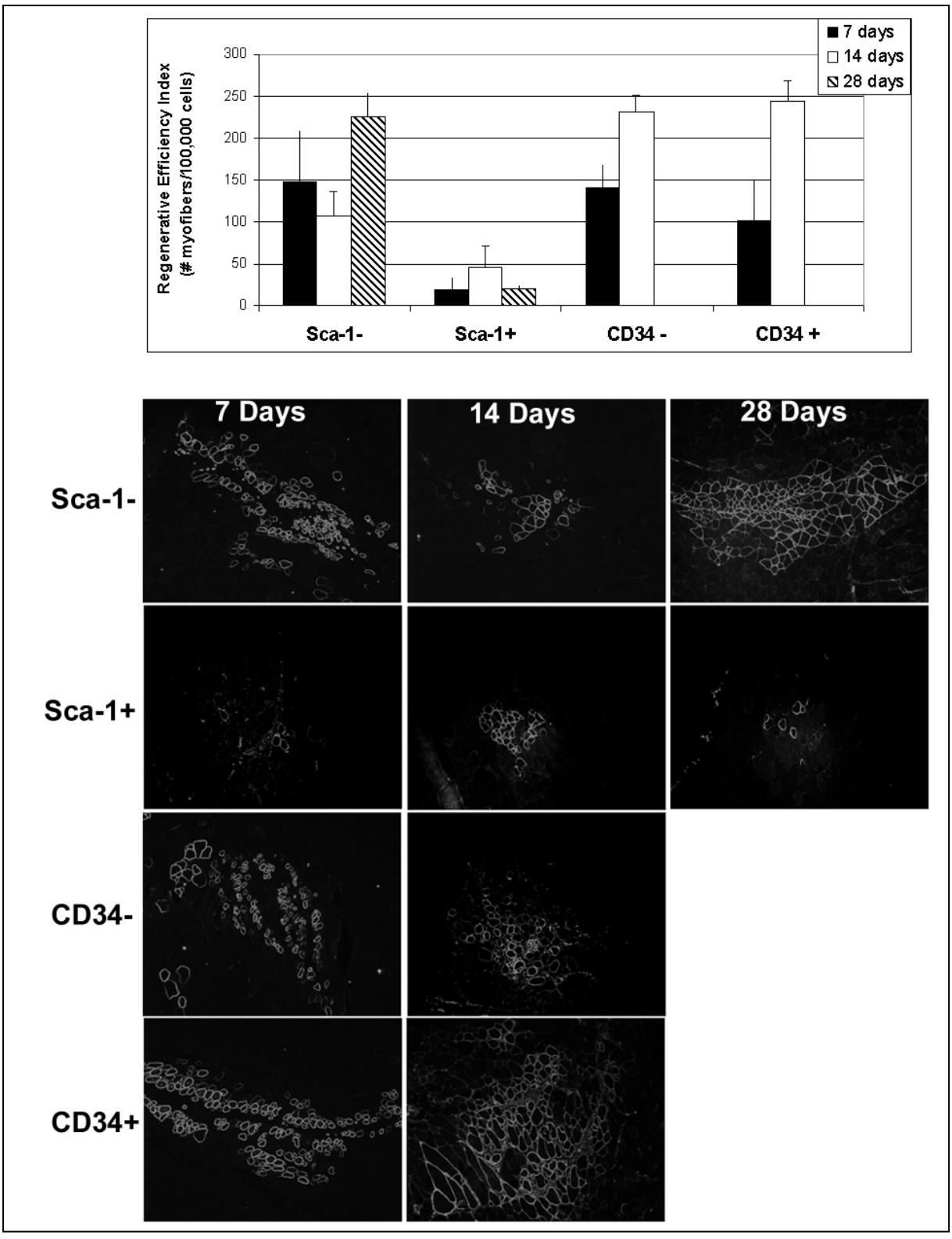

Figure 2.17 Transplantation results of two-fraction separation based on either Sca-1 or CD34. Images acquired at 100x magnification.

2.2.3.4 Stability of Protein Expression *in vitro*. The inconsistency in the transplantation results between the cultured (MACS) and directly-isolated (FACS) cell fractions obtained through surface protein sorting led to the investigation of the stability of expression of these proteins by myogenic cells. Since directly-isolated FACS cells may take extended periods of time to initially adhere to culture flasks, and are not purified for myogenic cells, LP MACS-sorted cells were used to re-evaluate surface protein expression at various timepoints following their cultivation under normal growth conditions. Overall, high levels of Sca-1 expression appeared to not be retained with time in culture, as cell populations maintained either a low level or a lack of Sca-1 expression within either purified or mixed cultures (Figure 2.18). Changes in CD34 expression were noticeably more apparent and were investigated more rigorously. In contrast to Sca-1, re-examination of expression within cultures containing a mixed population of CD34-expressing cells (Figure 2.19A) or populations either depleted (B) or purified (C) for CD34 revealed that this expression does appear to be relatively maintained over extended periods in culture (n=4). A fairly consistent level of expression was observed within mixed or CD34-purified cultures, and this expression is also quickly re-established in depleted populations and remains a mixed population within culture.

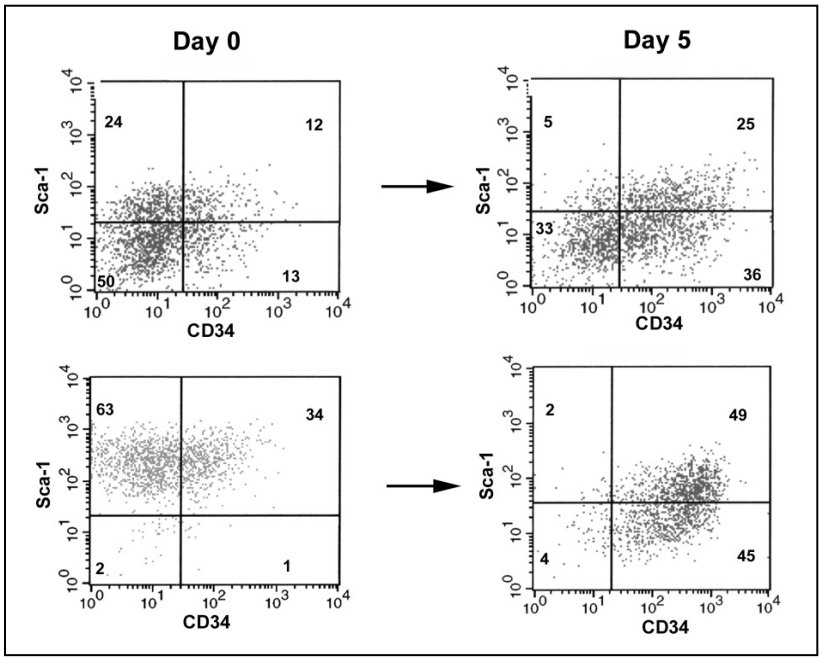

Figure 2.18 Changes in Sca-1 and CD34 expression by LP cells in culture, evaluated by flow cytometry [140].

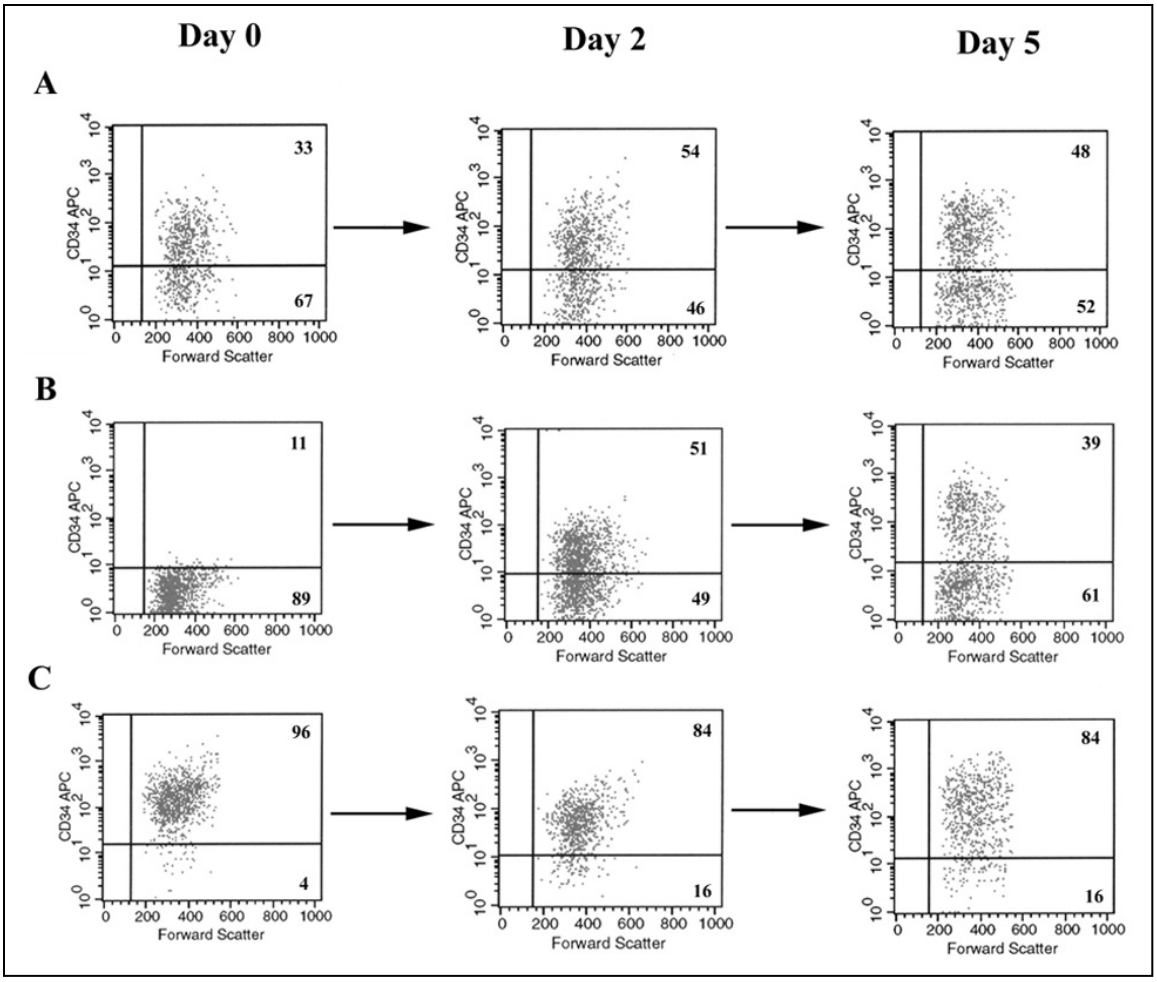

Figure 2.19 CD34 expression by cultured myogenic LP cells is maintained within purified (C) and mixed (A) cultures, and is rapidly re-established in depleted cultures (B). Values given represent averages of multiple experiments [146].

2.2.4 Discussion

The transplantation results obtained from directly-isolated (FACS) and cultured (MACS) sorted cells do not conclusively identify a single protein or expression profile, based on the two candidate surface proteins investigated here, that is exclusive to efficient myogenic progenitors. For cultured cells, CD34 expression discriminated between myogenic populations with varying regenerative efficiencies. However, for directly-isolated cells, Sca-1 expression rather than CD34 was a significant determinant in this regard. Observed shifts in expression of both of these proteins by cultured cells further suggests their lack of stability, and may help to explain the discrepancy in results

between cultured versus directly-isolated cells. Nonetheless, CD34 expression appears to have some utility with regard to cultured cell discrimination. Inclusion of CD34 expression criteria within the LP cultures allowed the identification of three separate cell populations with consistent and variable regenerative responses (EP, CD34+ LP, and MDSC). Use of these defined populations will permit an investigation into various myogenic cellular characteristics that may be considered to play a role in regenerative outcomes, as discussed in detail within the following section (2.3).

Importantly, the transplantation results presented here confirm previous observations regarding the preplating isolation technique. Specifically, myogenic cells adhering within early time points post-isolation (EP) were less capable in regenerating skeletal muscle than their later adhering (LP) counterparts [75]. Further, the MDSC population, isolated from the LP cultures, displayed a remarkable regeneration capacity [39]. Based on the size distribution of the myofibers within the dystophin-positive grafts that were generated, we can be relatively confident that the associated dystrophin expression resulted primarily from the formation of new myofibers and not the fusion of donor cells with mature host fibers. This is worth mentioning as although dystrophin restoration is an important endpoint for dystrophic therapies, regardless of the route taken by the donor cells, uromyoplasty therapy may also be reliant upon the cells' ability to form new muscle. These results may also be suggestive of variable *in vivo* behavior post-injection. Both the reduced number and larger overall size of the myofibers generated by the EP population could indicate a more preferential degree of fusion with already-existing host myofibers and/or a more rapid degree of fusion between donor cells. As fusion is associated with a post-mitotic state, such scenarios would compromise the potential for *in vivo* expansion of donor cells. With this in mind, fusion behavior is more closely examined in the following section (2.3) along with other cell characteristics that may influence regenerative capacity.

An important experimental consideration in examining regenerative quality is the post-injection evaluation period, particularly in an allogeneic transplantation setting. Unfortunately, autologous transfer is rarely feasible in the murine model, and the immunodeficient dystrophic animal model has only very recently become available. Thus, several considerations relating to the utility of extended evaluations become relevant to the conclusions drawn from these experiments. Such considerations limit the timepoints in which we are able to make realistic comparisons between populations to relatively short intervals post-injection. Aside from cellular allogenicity, over extended time periods expression of the dystrophin protein itself within dystrophic animals may serve as an

adequate antigen for antibody production and eventual myofiber destruction [61, 147]. Here the elimination of dystrophin-expressing myofibers was evident within the immunocompetent hosts, as demonstrated by both the decreased myofiber number coincident with increased duration post-injection (MACS) as well as the appearance of lymphocytes at the injection site. In addition, it has been suggested that potential differences in immunological reactions against transplanted myogenic versus non-myogenic cells may be expected [148], although we also cannot exclude potential heterogeneity among myogenic progenitor populations with regard to major histocompatibility complex antigens (investigated further within section 2.3). Thus, at least theoretically, the percentage of non-myogenic cells within each of the injected populations could potentially act as a confounding variable in the regeneration responses observed. This is obviously more relevant to the results of the FACS-isolated transplantations, as larger variations in the percentage of contaminating non-myogenic cells were inherent to the methodology. With this consideration in mind when examining the FACS regenerative responses, in relation to the number of non-myogenic cells contained within the cell injection, it was generally observed that populations with lower percentages of non-myogenic cells displayed the highest regeneration responses on a myogenic per cell basis. However, this association between regeneration and the percentage of non-myogenic cells did not appear to hold true across all populations examined (e.g. Sca-1-/CD34- vs. Sca-1+/CD34+). Additionally, previous results would suggest that through examination of early post-injection timepoints such potentially confounding immunological variables may be limited. Pavlath et al [149] previously demonstrated, in completely mismatched hosts, that allogenic myofibers are capable of being formed and visualized by 5-7 days, with little evidence of rejection. By 10-14 days a mononuclear infiltrate is observed with concomitant loss of donor myofibers. Thus, the 7 day evaluation period used in this study would limit specific cellular responses but importantly would be considered long enough to allow donor cells to be exposed to non-specific inflammatory responses, which are also thought to be extremely important in the early survival and eventual success of myogenic donor cell grafts [70, 72]. Further, the extended MACS- and FACS-sorted transplantation evaluations typically corresponded with the shorter 7 day results, and therefore the shorter evaluation period seems in most cases to be reasonably indicative of longer term results.

It is also worth mentioning that although limited to relatively short evaluation periods, the studies performed may be considered somewhat more realistic, in terms of clinical application, than many previous transplantation investigations. In the regeneration model used there was no attempt to artificially enhance the regenerative response or create host environmental conditions optimal for myogenic cell transplantation. Methods

previously described to ensure optimal transplantation efficiency include attempts to block the host regenerative responses by pre-irradiation of the muscle to be injected [55], or prior injection of necrotic agents to stimulate the regenerative response, or both [62, 150]. Additionally, the myogenic donor cells used in this study were obtained from primary cultures, as opposed to clonal cell lines, and further were derived from adult-aged skeletal muscle.

2.3 Evaluation of Cell Behavioral Characteristics as Indicators of Regeneration

2.3.1 Introduction

In the previous section the ability to separate myogenic populations with differential regeneration characteristics was shown. Building upon the information gathered with regard to the separation of what can be considered more definable myogenic progenitor populations, investigations into other potentially useful identifying characteristics of these cell populations were performed. The goal of these investigations was to further establish cellular traits that may be used to more easily identify efficient progenitor cells within culture prior to their use in regenerative therapies, and also to generate potential mechanisms that may be used to explain why discrepancies in efficiency are observed. From the myofiber distribution results following transplantation, it follows that one possible explanation for the variation in regenerative efficiency stems from heterogeneity in the proliferative and/or fusion behavior of the donor populations. Thus, a primary focus of this section is to examine the possibility that variations in inherent expansion capabilities may exist within these various myogenic progenitor populations by investigating relevant characteristics, including their: 1) differentiation status, as defined through expression of myogenic regulatory proteins, 2) stage of the mitotic cell cycle at the time of injection, 3) cell division time, 4) fraction of mitotically-active cells, and 5) their ability to proliferate and/or resist terminal differentiation when challenged with differentiation-promoting conditions. In addition, the expression of antigens associated with cellular immune recognition was examined, as this may relate to the cells ability to evade host detection prior to fusion. The LP CD34-/+ sorted populations described within the previous section were used as the focus of these investigations since they are relatively more definable, although inclusion of the EP and MDSC populations within many of these characterizations allowed for comparisons to be made across a broader range of progenitor populations with observed regenerative discrepancies.

2.3.2 Methods

2.3.2.1 Immunofluorescence Evaluation of Myogenic Commitment. Each myogenic population (EP, LP CD34-, LP CD34+, MDSC) was evaluated by immunofluorescence antibody staining for expression of the MRF proteins Myf5, MyoD and myogenin, as well as m-cadherin, in order to gauge their respective progression towards end-stage myogenic differentiation. Analysis was performed on methanol-fixed cells pre-incubated with 5% goat serum in PBS. The cells were incubated with primary antibodies at room temperature for 2 hours at the following dilutions in PBS containing 5% goat serum: mouse IgG anti-MyoD (1:250; Pharmingen), mouse IgG anti-myogenin (1:250; Pharmingen), rabbit IgG anti-Myf5 (1:300; Santa Cruz Biotechnology), rabbit IgG anti-M-cadherin (1:50; gift of Dr. Anthony Wernig). Following thorough rinsing with PBS, cells were incubated with either biotinylated goat anti-mouse IgG or biotinylated goat anti-rabbit IgG secondary antibodies (both 1:250; Vector) for 30 minutes. Finally, cells were washed and incubated with SA-Cy3 (1:500) for 10 minutes. Negative control staining was performed using an identical procedure, with omission of the primary antibody. Positive staining is indicated by nuclear fluorescence for Myf-5, MyoD and myogenin as these transcription factors are localized within the cell nucleus. M-cadherin, a cell adhesion molecule, is localized to the cell surface. As in the regeneration experiments, cells were evaluated at identical timepoints from initial adhesion to time of fixation, in order to control for differences in protein expression that may arise with time in culture. The percentage of cells exhibiting positive staining was determined within each culture through analysis of 10 random culture fields (representing a minimum of >200 total cells). Staining was performed for cell populations obtained from at least five separate isolations to determine the final range of expression of the various proteins, with the exception of the MDSC population which was derived from a single isolation but was investigated for multiple passages used in the various studies (passages 30-37).

2.3.2.2 RT-PCR. Additional evaluation of the myogenic proteins interrogated through immunofluorescence was performed for the LP CD34-/+ populations. Total RNA was isolated using TRIzol reagent (Life Technologies) and 1 μg of RNA for each cell type was used for reverse transcription (RT). RT was performed using the SuperScript™ First-Strand Synthesis System (Invitrogen) according to the manufacturer's instructions. PCR primer sequences (Integrated DNA Technologies) and reaction parameters were utilized as previously described: myogenin and MyoD [151], M-cadherin and Myf5 [6]. PCR products were obtained following 35 cycles and separated on agarose gels. Expected base pair (bp) product sizes were observed for all reactions: myogenin, 86 bp; MyoD, 147 bp; M-cadherin,

446 bp; and Myf5, 352 bp. Genomic DNA contamination was excluded by the fact that all primers spanned an intron, as well as parallel RT controls that were performed without reverse transcriptase. C2C12 cells, used as a positive control, were obtained from the American Type Culture Collection, and PP1 cells were obtained through the preplate technique as described previously within section 2.1.

2.3.2.3 Cell Cycle Status. CD34- and CD34+ LP sorted cell suspensions were centrifuged, washed in PBS and the cell membranes permeabilized by addition of 0.05% saponin (Sigma) in PBS. 20 μL of a nucleic acid dye (7-AAD; Pharmingen) was added to each cell suspension for 20 minutes prior to washing with PBS. Flow cytometry analysis was performed on histograms using a linear scale, by first gating for singlets in the forward/side scatter profile. The peak channel fluorescence for cells in the G_2/M region was confirmed to be twice that of the G_0/G_1 region.

2.3.2.4 MHC-1 Expression. Major histocompatibility complex class I (MHC-I) expression was assessed for all four progenitor populations using similar labeling and gating techniques as those described within section 2.1.2.3, and previously [43]. PE-conjugated anti-mouse H-$2K^b$ monoclonal antibody (clone AF6-88.5; Pharmingen) was utilized and reacts specifically with the MHC-I alloantigen expressed by the C57BL/10J mouse haplotype (H-2K) and allelic specificity (b). PE-conjugated isotype controls were used for determining background fluorescence.

2.3.2.5 Division Time and Mitotic Fraction. A novel microscopic imaging system was used to acquire data pertaining to LP CD34-/+ cell population division and mitotic fraction characteristics through time-lapsed brightfield imaging [152, 153]. As shown in Figure 2.20, this system houses cell culture plates within a mini-incubator, termed the biobox, which is mounted to the stage of an inverted microscope and linked to a CCD camera to track cell behavior (Automated Cell Technologies, Inc.). In order to generate time-lapsed images, user-determined coordinate positions were selected that corresponded to multiple view fields within the cultures. Each view field was recorded by the CytoWorks software program that subsequently controlled both the time and position of the microscope stage movement, allowing the system to retrieve original pre-established view field positions within the cultures. Images of the selected view fields were acquired at 10-minute intervals using a 20x objective (approximately 10 cells/field at t=0 hrs) over a period of 4 days.

For cell division analysis, cells were plated at an initial density of 1,000 cells/well on a collagen Type-I coated 12-well plate in high serum growth medium, described in section 2.1, with medium changes every other day. In terms of proliferation kinetics the total cell number is dependent upon two parameters, the division time (DT) and the mitotic fraction (α). DT was measured directly from the acquired images through individual observations of

cytokinesis. α, defined as the fraction of cells within the population actively entering the mitotic cell cycle, was calculated from experimental data using a previously described non-exponential growth model [153, 154]. This model requires experimentally-determined values for cell number and a DT determined for each population

$$N = N_o\left[0.5 + \frac{1-2\alpha^{(t/DT)+1}}{2(1-2\alpha)}\right] \qquad [2.2]$$

where N is the number of cells at any time t, N_o is the initial number of cells, and both DT and cell number at each time point are determined through image analysis. A brief derivation of this model, including assumptions inherent to its use, is provided in Appendix A. A non-linear least squares regression was used to determine the best fit to the growth model equation, performed using a statistical software package (SigmaStat v2.0). DT data was collected from observations of individual cell divisions within all view fields examined and was combined for statistical comparison between populations. Median DTs, determined for each cell population, along with corresponding cell counts were then used to determine an α value for each view field and well interrogated. Data from multiple wells were used for statistical comparison and are the result of duplicate experiments.

2.3.2.6 Proliferation and Differentiation/Fusion Characteristics. The same microscopic imaging system and imaging parameters described in the previous section were used to examine cell proliferation and both the rate and degree of cell fusion and differentiation, when challenged in a low serum assay, for each of the four progenitor populations. Cells were plated at an initial density of 1,250 cells/cm^2 in multi-well plates containing high-serum growth medium. A period of 3-4 hours was allotted for cell adhesion, at which time the growth medium was replaced with a low serum fusion-medium consisting of DMEM containing 1% each of fetal bovine and horse serum along with penicillin/streptomycin, as described previously.

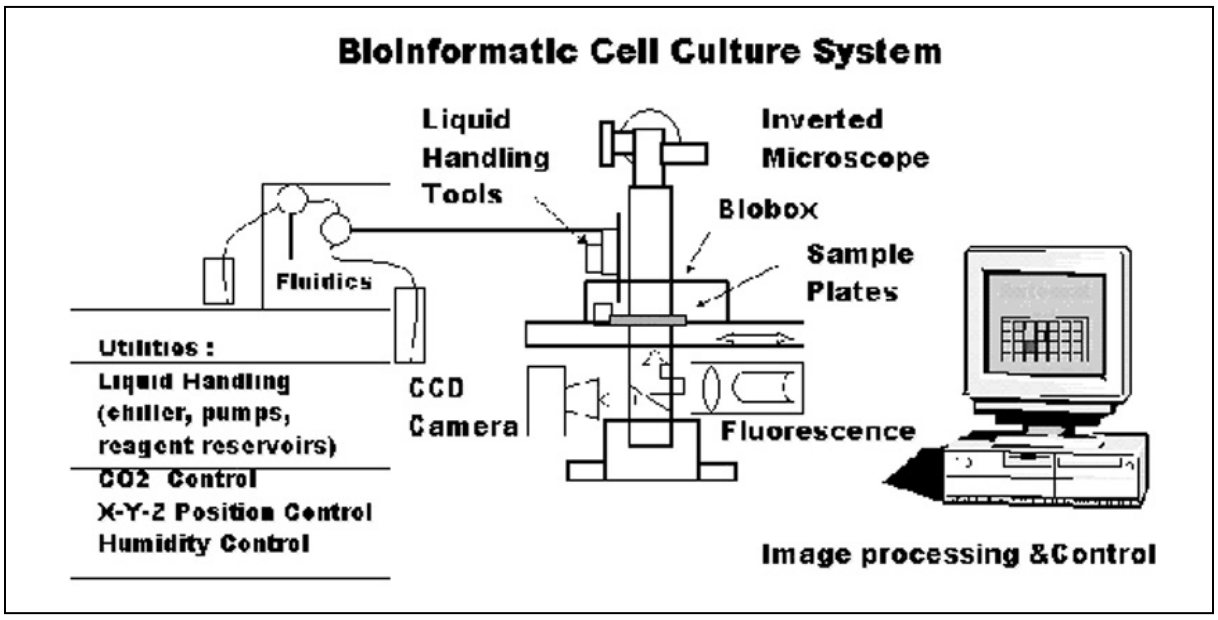

Figure 2.20 Schematic representation of the bioinformatic cell culture imaging system, allowing time-lapse image analysis of myogenic cell behavior, including cell division time and fusion behavior.

Medium changes were conducted every other day. It has been previously shown using mixed cultures of myogenic progenitor cells that induction of fusion occurs within the first two to three days in culture [155]. Therefore, cell

fusion into multinucleated and elongated myotubes was monitored over a 96 hour period, along with total cell number. As individual nuclei counts within the myotubes were difficult to assess by brightfield, each myotube was counted as a single cell. Individual values for each well were determined through manual scoring of time-lapsed images (ImageView software; Automated Cell Technologies). As the actual starting cell number within each view field varied slightly, cell numbers for the first time point and each subsequent timepoint were adjusted by the appropriate factor to achieve a normalized starting number of 20 cells per field. The actual starting cell number in each field was not significantly different among the four groups.

Immediately following this 96 hour imaging observation period, dual immunofluorescence staining was performed for evaluation of desmin and myosin heavy chain (1:250; clone MY-32, Sigma). Myosin staining was performed first though incubation of the primary antibody (mouse anti-myosin) for 1 hour in 5% goat serum followed by utilization of biotinylated goat anti-mouse IgG secondary antibody (1:250; Vector) for 30 minutes and incubation with SA-Cy3 (1:500) for 10 minutes. Desmin staining was performed as described in 2.1.2.2, with the

exception of SA-FITC (1:500; Sigma) for immunofluorescent labeling. The potential existed for undesired cross-labeling of SA-FITC to the biotinylated myosin antibodies, and thus myosin labeling was performed first. As all cells that express myosin must also express desmin, but not necessarily the reverse of this statement, this potential dual-labeling is rendered irrelevant. All cells were also counterstained with Hoechst (33328; Sigma) dye to reveal nuclei. Random fields in each well were evaluated at 200x magnification for: the total number of myogenic nuclei (determined though desmin expression), the number of mononuclear myogenic cells, the number of myotubes (determined through dual criteria of myosin heavy chain expression and displaying ≥2 nuclei), and the number of nuclei comprising these myotubes. This information was used to generate a fusion index, described below, as previously defined [156].

$$\text{Fusion Index} = \frac{\#\text{ of nuclei within myosin - expressing myotubes}}{\text{total }\#\text{ of myogenic nuclei}} x100 \qquad [2.3]$$

Thus, the fusion index represents the percentage of myogenic nuclei that have undergone terminal differentiation and have participated in myotube formation. Individual fusion indices were generated for each well through the averaging of values obtained from 5 fields/well viewed under 200x magnification (representing approximately 75-100 myogenic nuclei/well for EP and LP populations). Ratios of the number of mononuclear myogenic cells to the number of myotubes are also reported. In all, for both time-lapsed and immunofluorescence investigations, data was generated from over 20 individual wells for the EP, CD34- and CD34+ cell types from experiments that were performed in triplicate. For MDSCs, data was generated from 10 different wells from experiments performed in duplicate.

In a separate immunofluorescence labeling protocol, LP CD34-/+ populations were evaluated for desmin and CD34 (biotin conjugated mouse anti-CD34; clone RAM34) expression. Following incubation with the primary CD34 antibody (1:250), expression was revealed with SA-Cy3. Desmin staining was performed as described, however FITC-conjugated anti-rabbit IgG was utilized as the labeling antibody to avoid dual-staining. Cells were also counterstained with Hoechst to reveal nuclei.

2.3.2.7 Statistics. As one of the main focuses of the studies performed was further delineation of the CD34-sorted LP subfractions, direct comparison between these populations was performed for each parameter by paired or

unpaired Student's t-test, where appropriate. However, non-parametric distributions for both division times and mitotic fraction were observed, both of which were subsequently compared using the Mann-Whitney Rank Sum test. Multiple comparisons between all four cell populations (EP, LP CD34-/+, MDSC) were performed by ANOVA, with Student-Newman-Keuls post-hoc pairwise comparisons for cases in which a significant F-value was obtained. Comparison of myotube percentages from brightfield observations revealed unequal variance for several timepoints, and thus were subsequently compared by Kruskal-Wallis one-way ANOVA on ranks, with Dunn's test for pairwise comparisons. Unequal variance was also detected for the ratio of mononuclear cells to myotubes during comparison of immunofluorescence data and was therefore compared non-parametrically as well.

The Pearson Product Moment was used to determine the strength of association between the regeneration index and the parameters obtained from the fusion assay. This test determines if a linear relationship exists between the variables, without regard to the assignment of a specific independent and dependent variable. All data is expressed as mean ± SEM. P-values less than 0.05 were considered statistically significant, and exact p-values are given for non-significant differences. All comparisons were made using SigmaStat (v2.0, Jandel Scientific) statistical software.

2.3.3 Results

2.3.3.1 Myogenic Commitment. As shown in Figure 2.21, results of MRF immunofluorescence labeling demonstrate clear differences in the myogenic phenotype expressed by the various progenitor populations. The EP myogenic population (top rows) is observed to contain a high percentage of cells expressing both early-stage Myf-5 and MyoD proteins, as well as at least half typically expressing the late-stage regulatory factor myogenin. The CD34- and CD34+ subfractions of the LP cultures displayed a similar degree of expression of these proteins, and thus are represented only as LP in the figure (CD34+ images displayed for representative staining). In contrast to the EP progenitors, LP cells (middle rows) displayed lower percentages of both early and late-stage MyoD and myogenin regulatory proteins. The MDSC population (bottom rows), while expressing a high percentage of Myf-5, did not express MyoD or myogenin to any appreciable extent. M-cadherin expression, a traditional satellite cell

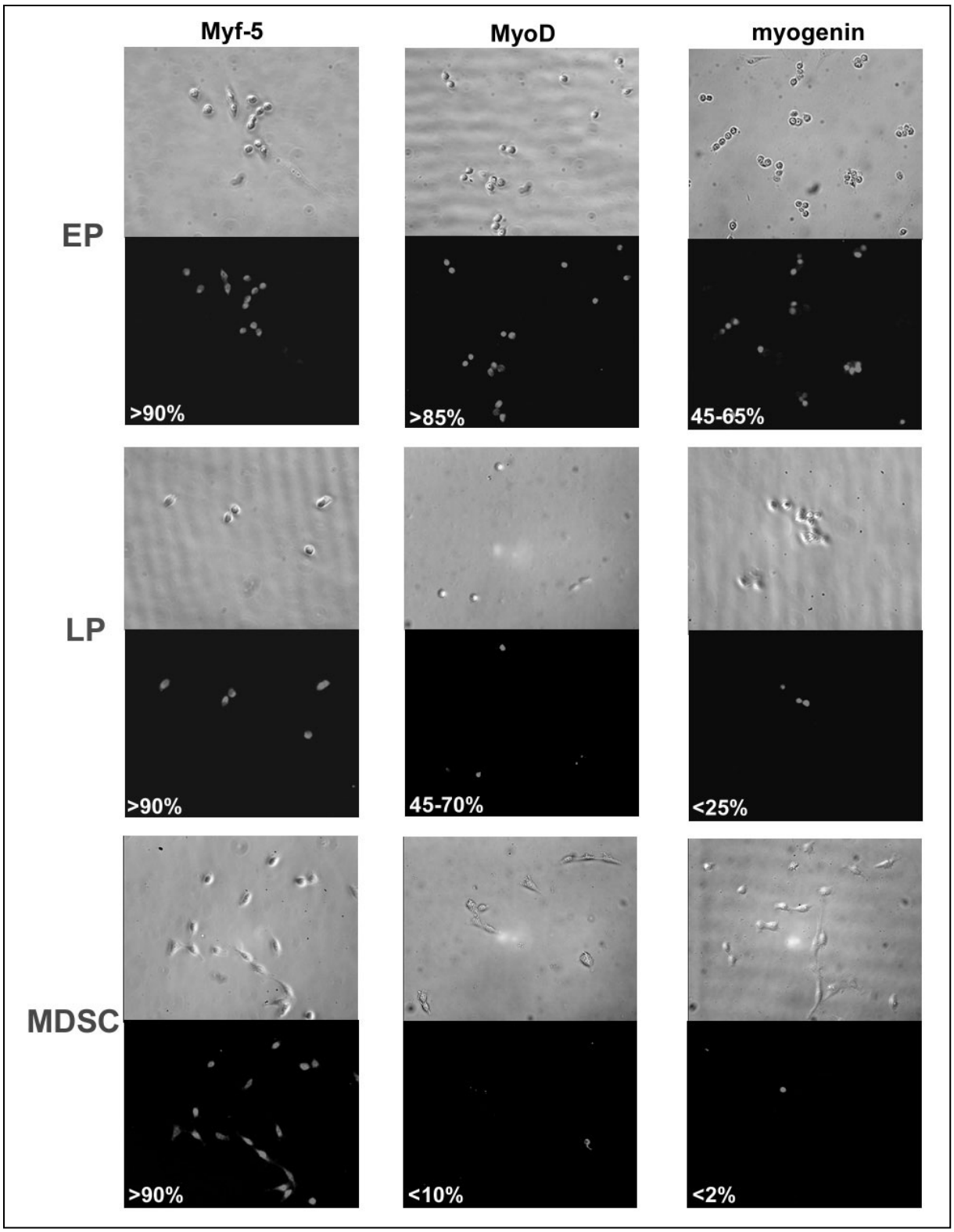

Figure 2.21 Immunofluorescence evaluation of MRF protein expression by myogenic progenitor populations (200x).

marker, was also examined (not shown) within the EP and LP cultures and found to be expressed by the majority of these cells (EP, 70-80%; LP, >90%).

2.3.3.2 RT-PCR. As both CD34- and CD34+ LP subfractions were found to express similar levels of the myogenic proteins, by immunofluorescence staining, RT-PCR was also performed to verify these results (Figure 2.22). C2C12 cells and PP1 cells were included as positive and negative controls, respectively. Although non-quantitative, both LP subpopulations expressed similar levels of all of the MRF mRNA examined as well as the satellite cell-associated m-cadherin, thus confirming the immunofluorescence observations. C2C12 cells are shown to express similar levels of all MRFs. PP1 cells, containing primarily fibroblasts (>90%), did not express m-cadherin but did display some level of expression of the MRFs, presumably due to the presence of the small percentage of desmin-expressing cells found within these early-adhering cultures.

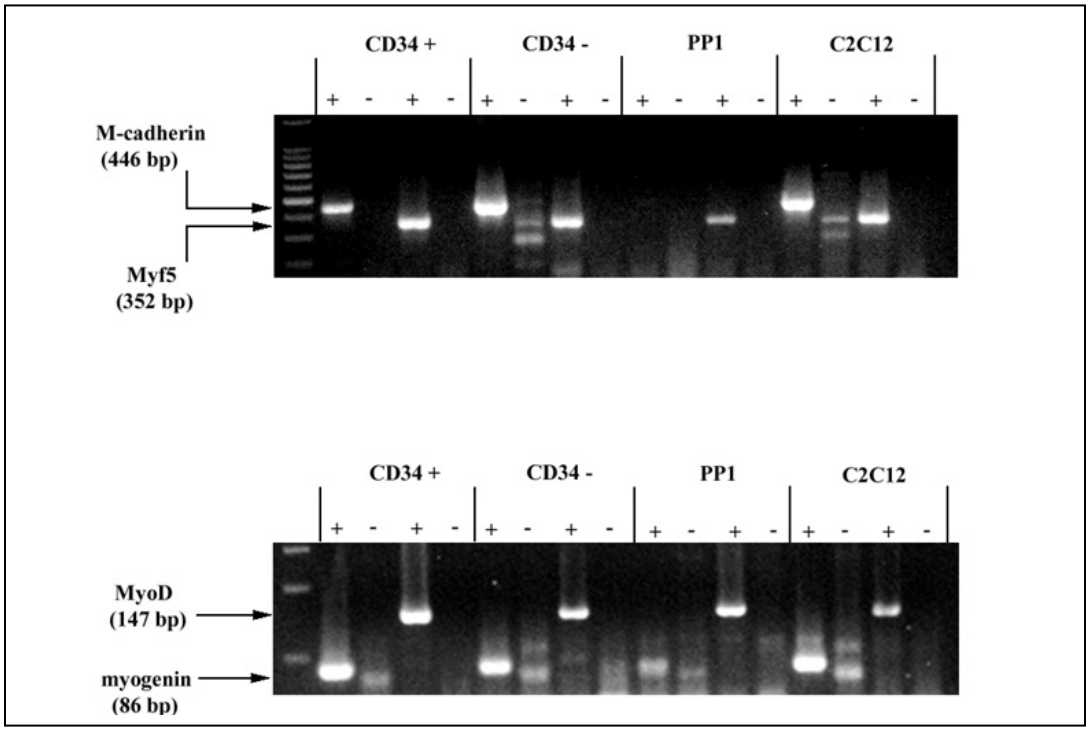

Figure 2.22 RT-PCR performed on both CD34- and CD34+ LP cells, along with PP1 and C2C12 clonal cells as controls. Lanes in which reverse transcriptase (RT) was added (+) or omitted (-) are indicated.

2.3.3.3 Cell Cycle Status. As the LP CD34- and CD34+ populations displayed a very similar degree of myogenic commitment, additional cell characteristics were examined to determine if any underlying behavioral differences could be detected. In this section and the next, their proliferative behavior was further examined in an attempt to further delineate potential differences between these two cell populations.

Results of the cell cycle analysis show no statistical difference between the CD34-sorted LP subfractions in terms of the percentage of cells in any particular stage of the mitotic cycle ($p=0.505$, $p=0.921$, and $p=0.436$ for G_0/G_1, S, and G2/M; n=4 each). The percentage of cells in the G_0/G_1, S, and G2/M stages, respectively, for CD34- cells was found to be 75.9±1.4, 12.1±2.2, and 12.0±1.2. Similarly, for the CD34+ population the percentage of cells in each stage was found to be 73.4±3.2, 11.8±1.4, and 14.8±3.0.

2.3.3.4 Population Division Characteristics. Information regarding individual cell DTs under normal growth conditions (high serum) was collected from analysis of the time-lapsed videos obtained from the microscopic imaging system. Median observed division times for dividing cells within each CD34 fraction were determined to be 14.1 (n=64) and 13.8 (n=48) hours for the CD34- and CD34+ fractions, respectively ($p=0.988$). In addition, from information gathered regarding the total cell numbers present at 12 hour intervals, the mitotic fraction of each population was calculated using the non-exponential growth model described by equation 2.2. A relatively good fit to the growth model was observed ($R^2=0.90\pm0.05$ and 0.86 ± 0.04 for CD34- and CD34+), and no difference in the estimated mitotic fraction could be determined between the two populations ($p=0.455$; median $\alpha=0.425$ and 0.393 for CD34- and CD34+ respectively; n=7 each).

2.3.3.5 Proliferation and Differentiation/Fusion Characteristics. Although still not completely understood, growth factor signals play a significant role in the maintenance of myogenic cells within a proliferative, rather than a differentiated, state. Thus, removal or reduction of such factors from media serum supplements is a common method to induce cell cycle withdrawal and differentiation [157]. Under such low serum (2%) conditions, brightfield observations regarding both proliferative capacity and cellular fusion and formation of multinucleated myotubes were also made using the time-lapsed imaging system for each of the four progenitor populations. An example of such images at 12 hour intervals is provided in Figure 2.23 for the EP, LP CD34+, and MDSC populations.

Averaged normalized cell number and myotube formation for each cell type over the 96 hour observation period is shown in Figure 2.24. Direct comparison between the CD34 LP subpopulations revealed a significantly

higher percentage of CD34- cells fusing into myotubes at all timepoints beyond 72 hours when compared to the CD34+ population, (from 72 to 96 hours; n=26 and n=22 for CD34- and CD34+). However, a significantly higher number of total cells were also observed for the CD34- population at 84 and 96 hours.

Multiple comparison of all four progenitor populations in terms of cell number during this 96 hour evaluation period revealed a significant expansion of the MDSC population above all other cell groups at the 12 hour timepoint and at all subsequent timepoints examined (with the exception of CD34+ at the 12 hour timepoint only; n=10 and n=22 for MDSC and EP, respectively). Concomitantly, myotube formation was also found to be significantly lower within the MDSC cultures when compared to EP (for all timepoints beyond 36 hours) as well as CD34- LP cells (for all timpoints beyond 72 hours). MDSC myotube formation was not significantly different from that of CD34+ LP cells at any timepoints evaluated.

Further evaluation of these cultures, at the conclusion of the 96 hour time-lapsed observation period, was performed by immunofluorescent antibody labeling. This was done to verify the final results obtained through the brightfield imaging as well as to provide more accurate data pertaining to the differentiation state of the myogenic cells, as expression of proteins confirming myotube formation could not be assessed through evaluation of brightfield images alone. As shown in Figure 2.25, immunofluorescence analysis of desmin and myosin heavy chain (MHC) expression allows easy identification and quantification of individual myogenic nuclei and their fusion state. In agreement with the brightfield observations, comparison of the LP subpopulations by immunofluorescent staining at the 96 hour timepoint revealed that the fusion index (% of total myogenic nuclei contained within myotubes) was significantly higher for the CD34- population compared to its CD34+ counterpart (Fig. 2.26; 47±4 and 36±3 respectively, n=12 each). Correspondingly, the ratio of mononuclear myogenic cells to the number of myotubes formed was significantly lower for the CD34- population (Fig. 2.26; 7±1 and 13±2 for CD34- and CD34+).

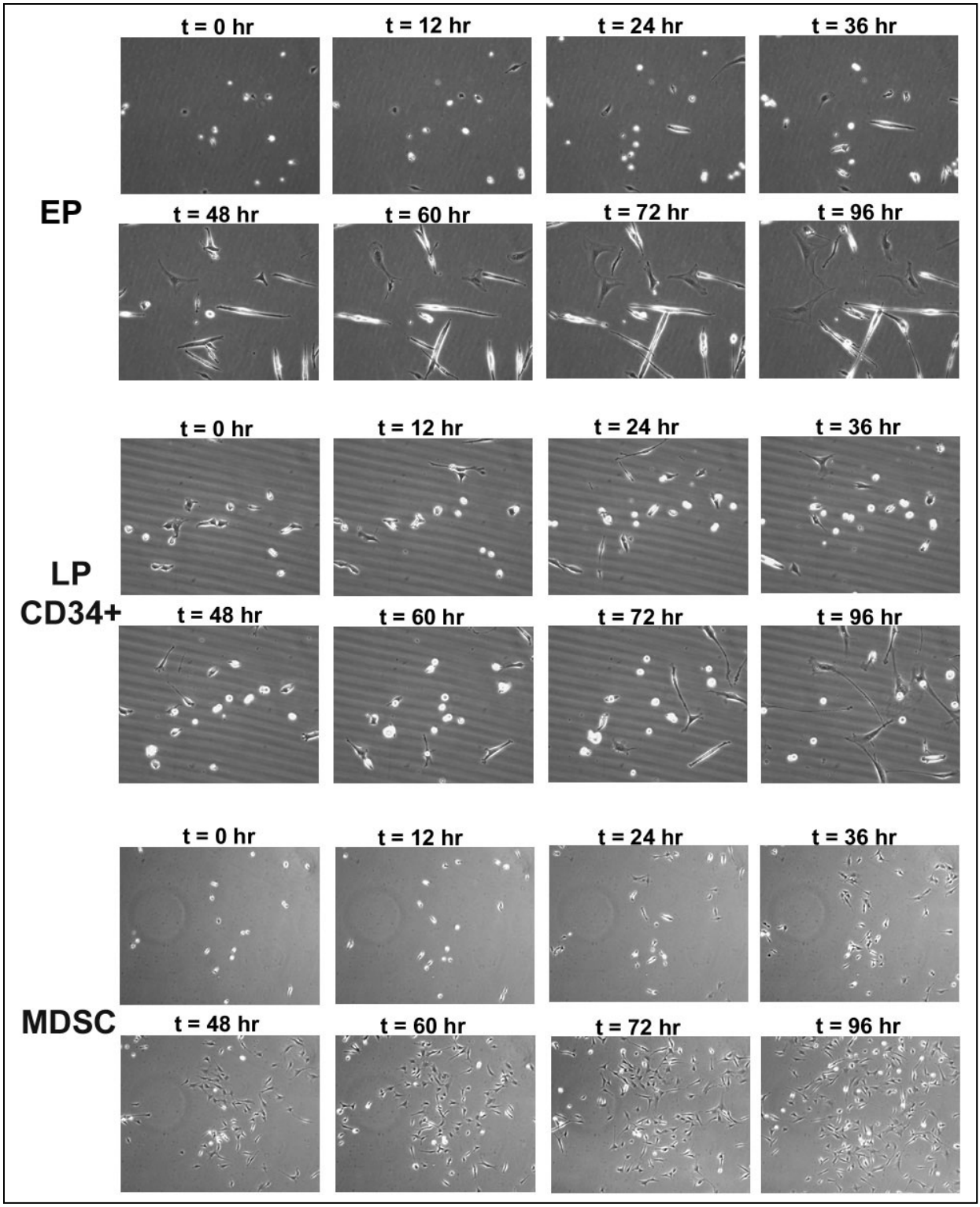

Figure 2.23 Representative time-lapsed images of EP, LP CD34+, and MDSC progenitor populations in culture under low serum 'fusing' conditions. Images were obtained from the bioinformatic cell culture system (200x magnification).

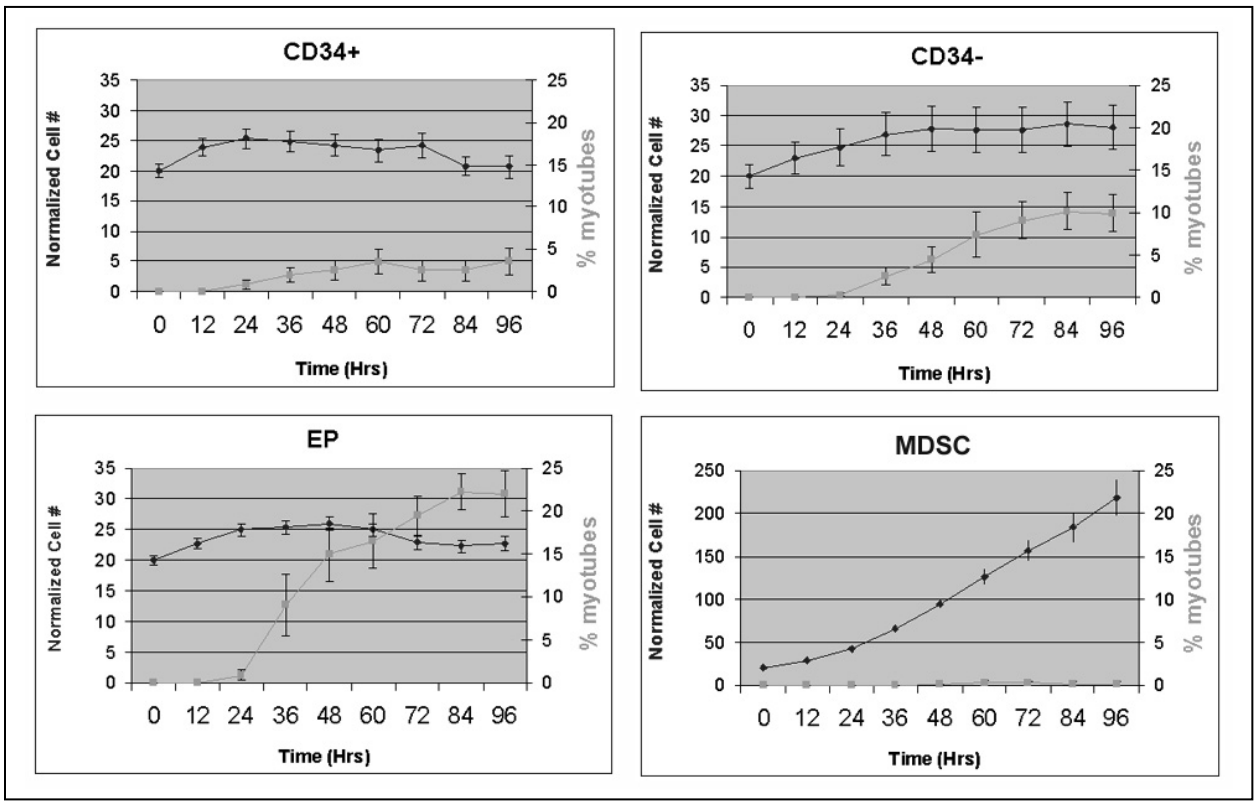

Figure 2.24 Cell expansion and fusion behavior of each progenitor population under low serum conditions, as determined from brightfield observations. Note the normalized cell number scale change for the MDSC population, demonstrating a large degree of expansion under these differentiation-inducing conditions.

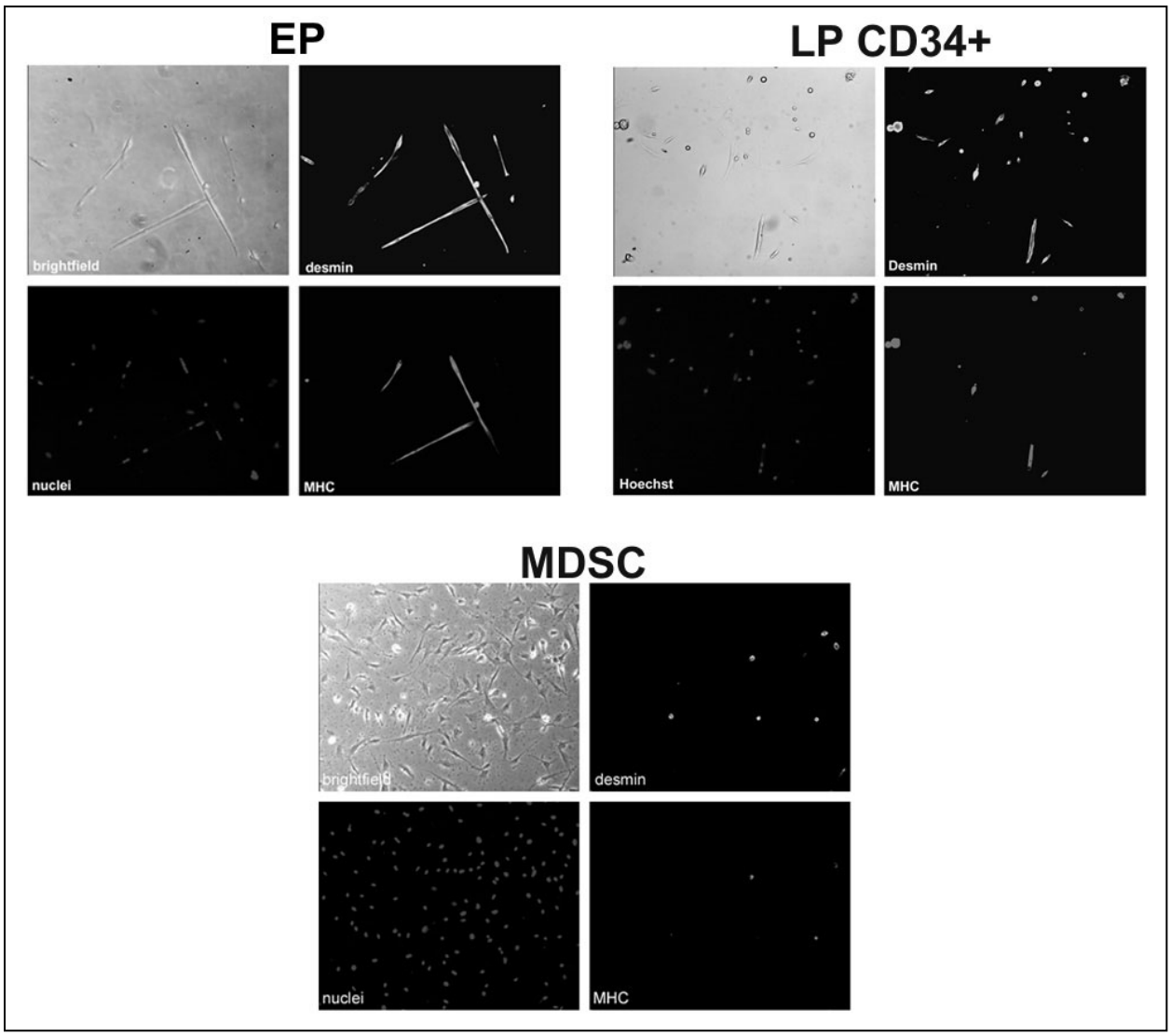

Figure 2.25 Representative images of EP, LP CD34+ and MDSC progenitor populations following 96 hour culture under low serum conditions. Cultures were immunofluorescently-labeled to reveal individual nuclei, cells of myogenic origin (desmin), and terminally-differentiated multinuclear myotubes (myosin heavy chain, MHC). Images taken at 200x magnification.

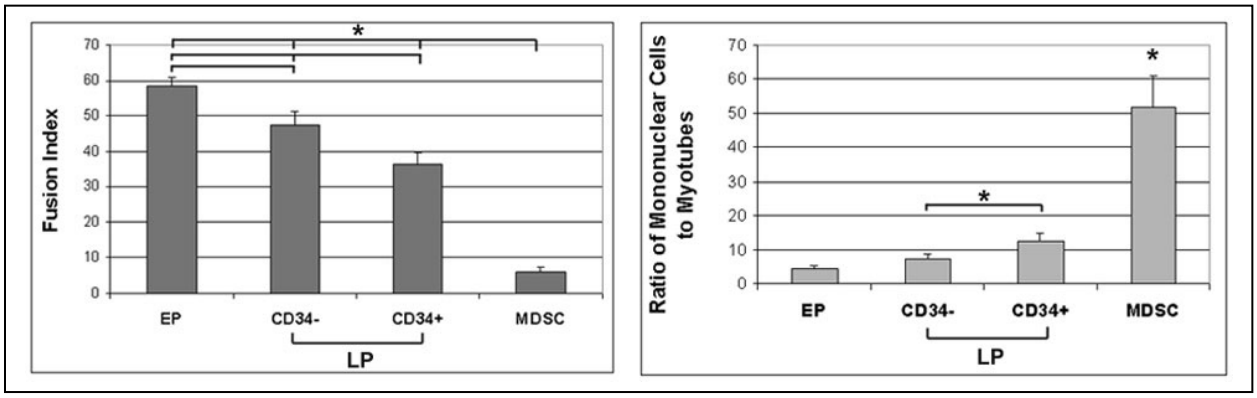

Figure 2.26 From immunofluorescence analysis, comparison of fusion indices revealed significant differences (*) between all populations examined (left). Ratios of the number of unfused myogenic cells compared to the number of multinucleated myotubes were significantly different in direct comparison between the LP subfractions (right). This ratio was also significantly higher for MDSCs when compared to all other populations.

Also shown in Figure 2.26, comparison of all four populations revealed that the EP and MDSC cells displayed the highest and lowest extent of cell fusion (fusion indices, 58±2 and 6±1 for EP and MDSC respectively; n=10 and n=12). The MDSC population fusion index was significantly lower than all other populations, and significant differences were also detected in comparison between all other populations as well. MDSCs also displayed a significantly higher ratio of mononuclear cells to myotubes in comparison to all other populations (MDSC, 52±9; CD34+, 13±2; CD34-, 7±1; EP, 4±1) corresponding to the significantly larger degree of expansion of this population observed over the 96 hour evaluation period.

Based on the differential fusion characteristics displayed by the LP subpopulations, and on earlier observations of changes in CD34 expression in culture, the CD34 status of the non-fused cells remaining in culture at the conclusion of the 96 hour fusion study was also examined through immunofluorescence. As may be expected, the non-fused myogenic cells within the CD34+ LP cultures were found to express CD34 (>95%). Interestingly though, in cultures comprised initially of CD34- LP cells it was observed that the majority (>90%) of unfused myogenic cells that remained following 4 days of low serum conditions expressed CD34 (Figure 2.27). Thus, within CD34-depleted cultures, the CD34+ subpopulation that is re-established represents the majority of the non-terminally differentiated, mononucleated fraction.

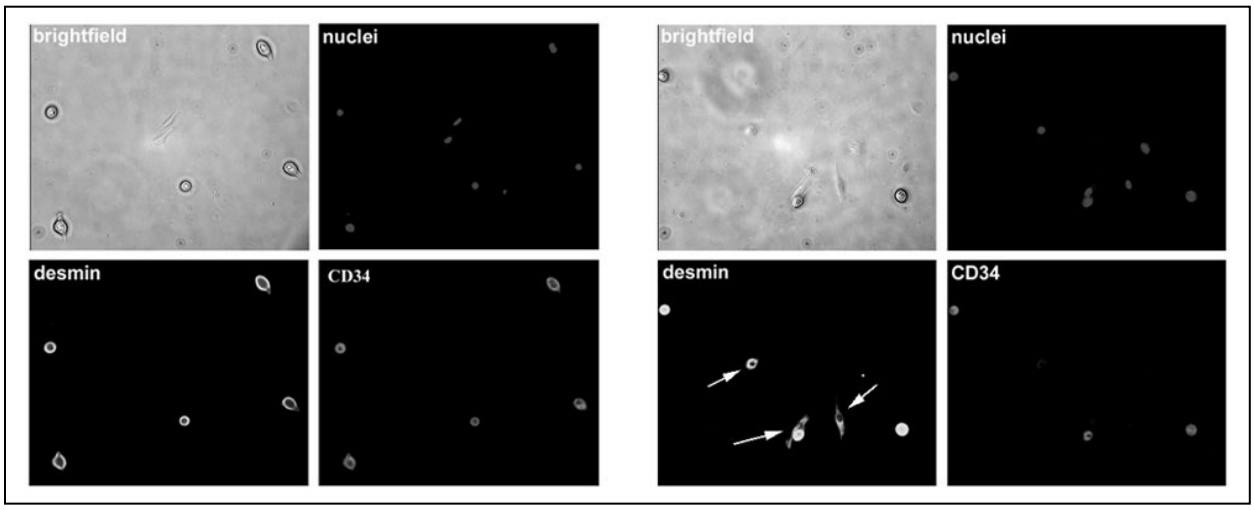

Figure 2.27 CD34 immunofluorescence labeling of mononuclear myogenic cells found within CD34-depleted LP cultures exposed to low serum 'fusion' conditions. The majority of the undifferentiated myogenic cells were found to express CD34 (left), although some CD34- cells are present (right, arrows; 200x magnification) [146].

2.3.3.6 Correlation Between Regeneration and Fusion Parameters. Associations between the regeneration properties and the fusion parameters, obtained from the fluorescence observations, were subsequently examined. A significant negative linear relationship between the regeneration and fusion indices was observed (correlation coefficient, r=-0.985), as well as a highly significant positive linear relationship between the regeneration index and the mononuclear to fused cell ratio ($p<0.01$, correlation coefficient, r=0.993).

2.3.3.7 MHC-I Expression. Since the transplantation experiments described within section 2.2 were performed in an allogenic setting the various cell populations were examined for expression of MHC-I, which is known to play a dominant role in the success or failure of allografts [158]. Statistical differences in MHC-I expression between the LP subpopulations could not be detected by flow cytometric analysis; the percentage of cells with detectable levels of expression were 13.0±6.3 and 19.1±8.3 for the CD34- and CD34+ subfractions, respectively ($p=0.594$, n=4 each). Interestingly, examination of all four populations revealed heterogeneity in expression, with the EP population containing the highest percentage of cells with detectable levels of expression (65±9, n=2). In contrast, the MDSC population contained less than 2% of cells expressing MHC-1, as shown in Figure 2.28 (n=2). Due to the limited number of evaluations however, no statistical comparisons among all groups were performed.

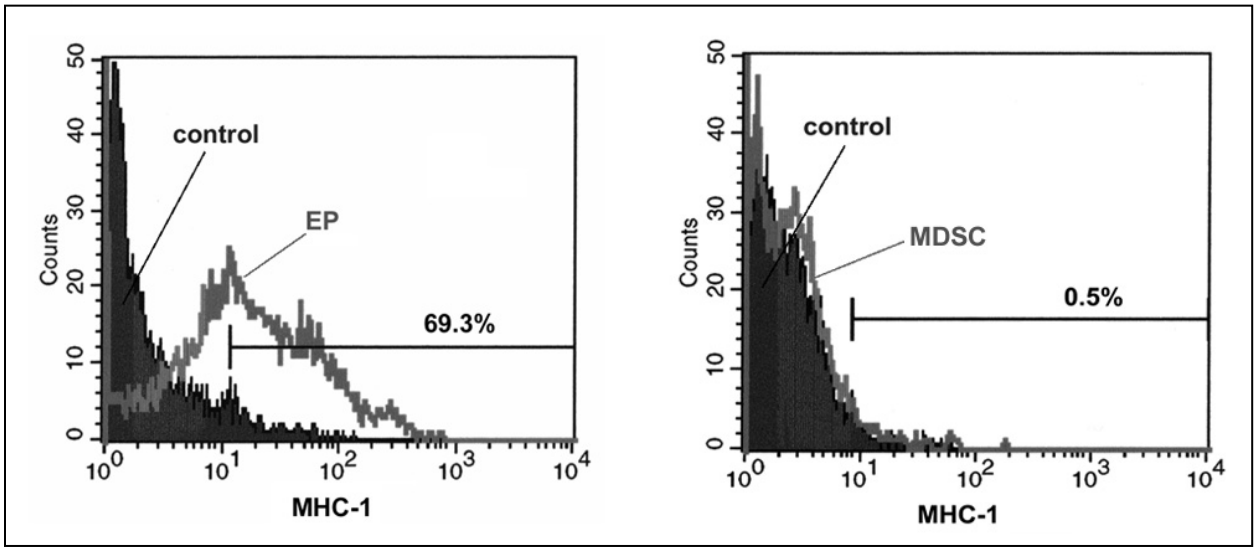

Figure 2.28 Flow cytometry histogram of MHC-1 expression by EP and MDSC progenitor populations.

2.3.4 Discussion

Among the various cellular characteristics examined, variations in expression of proteins known to influence myogenic differentiation (MRFs) were evident among the cellular populations examined. These variations in protein expression translated into measurable differences in cellular behavior as assessed through simple quantifiable parameters defining cellular proliferation and progression toward terminal differentiation. Taken together with previous knowledge of transplantation outcomes, these results suggest that proliferation and fusion behavior may have a significant impact upon a given myogenic progenitor population's ability to efficiently regenerate skeletal myofibers.

In terms of MRF expression, myogenin has previously been shown to be a key indicator of cell cycle withdrawal and coinciding obligate terminal differentiation, as supported by both *in vitro* and *in vivo* observations [159, 160], and was demonstrated to be highly variable among the populations examined here. Interestingly, although the MDSC population displayed a very low percentage of cells expressing the generic myogenic intermediate filament protein desmin, it displayed a very high percentage of the myogenic-specific early stage MRF protein Myf-5. This contradiction in expression is currently unresolved, although the lack of expression of the remainder of the MRF proteins examined further implies that this population is relatively primitive in terms of

myogenic lineage commitment. Taken together in context to the patterns of expression of these proteins and their relation to the progression of the myogenic differentiation program, as discussed in greater detail within section 1.1.2, these data suggest that on a relative scale the cells contained within the EP population display the highest degree of myogenic commitment. This is evident by the coexpression of multiple MRF proteins and a larger percentage of cells that have entered the terminal differentiation phase as signaled by myogenin expression [8, 14, 161]. While the majority of the LP cultures do coexpress the early stage regulatory proteins, importantly, a smaller percentage of cells appear to be reaching the terminal differentiation stage within culture compared to those found within EP cultures. MDSC cultures express only one early-stage regulatory protein and thus can be considered as a whole to be the least myogenically-committed among the progenitors examined here.

Observations with regard to the myogenic cell separation that occurs during the preplating process suggest that early adhesion is associated with a more progressive state of differentiation, as defined by MRF expression. It is tempting to speculate that differentiation status could be responsible for changes in cellular density, which in turn would directly affect cell settling rate following isolation. Other differences that may account for the preplating effect, such as variable cell surface protein expression, also cannot be ruled out at this time. However, it should be noted that expression of CD29, a surface integrin β_1 chain responsible for cellular adhesion to collagen, does not correlate with the observed variable adhesion, and further the preplating process is also observed in the absence of a collagen-coating on the culture flasks (personal observations and communication with other lab personnel).

As mentioned in section 1.1.2, MRF-regulation of myogenic differentiation has also been shown to influence expression of proteins regulating cell cycle status [15]. Aside from myogenin, MyoD expression, which has been positively linked to the up-regulation of cell cycle inhibitors, was variable among the four populations examined. Confirmation of proliferation and differentiation behavior among these populations, through *in vitro* analysis, was found to coincide with MyoD expression. This reaffirms previous observations of MRF-determined levels of myogenic commitment in association with both variable rates of fusion and cell expansion characteristics, as expected. Indeed, large disparities in differentiation status can result in drastic behavioral differences, as observed here between the EP and MDSC populations. However, within the LP cultures there appears to be subpopulations of cells that can be identified by differential CD34 expression with seemingly similar levels of myogenic commitment, but with variable fusion characteristics. Although mechanisms to explain this differential regulation require further investigation, similar observations have been reported previously in the literature.

Through *in vivo* proliferation studies, Schultz [25] described two different satellite cell progenitor populations: one termed the reserve population and the other the producer population. According to this model, a producer population is identified as providing nuclei directly to growing myofibers through fusion following a limited number of mitotic divisions. In contrast, a reserve population is believed to generate the producer population through asymmetric cell divisions. Additional evidence is presented by *in vitro* studies that have reported variations in the size of the colonies generated by individual satellite cells and behavioral heterogeneity upon induction of differentiation [8, 27-29]. Here it is demonstrated that CD34 expression, within mouse LP cultures displaying satellite cell characteristics, may be useful in identifying such subpopulations. Furthermore, taken together with the transplantation results involving all four progenitor populations, these variations in fusion characteristics may be implicated in the regenerative abilities of such cells following transplantation into dystrophic hosts. Corroborating evidence of such an effect is implied from a previous study in which pre-treatment of myoblast cultures with basic fibroblast growth factor, a potent myogenic differentiation inhibitor, resulted in up to four-fold increases in donor-labeled myofiber regeneration [162]. Taken together, it is logical to envision a scenario in which transplanted populations demonstrating both a rapid and high degree of fusion would limit donor cell availability to proliferate and further enhance the regeneration process, as myogenic cells that have participated in the formation of a myotube are considered terminally differentiated and permanently withdrawn from the cell cycle [2, 155]. In combination with potentially poor survival rates, as mentioned within section 1.2.2, such behavior would severely compromise the donor regenerative response. In contrast, cells that remain in an undifferentiated mononuclear state may retain the potential to proliferate and thus increase the yield of myogenic nuclei derived from an initial donor injection once exposed to host growth factors. Ironically, high fusion capacity within culture has previously been considered a desirable trait within cellular preparations for previous muscular dystrophy clinical trials [64, 65].

Potential deleterious effects of delayed fusion in the *in vivo* allogeneic setting must also be considered. It has been previously suggested that the rate of donor cell fusion *in vivo*, may play a role in host recognition of non-self antigens [163]. Following transplantation, the antigen which dominates the graft rejection process is the integral membrane glyocoprotein MHC-I [164], which both inhibits the action of natural killer cells and mediates the T-cell immune responses seen in allograft rejection [72]. Constituitive expression of this histocompatibility antigen has been previously demonstrated on human myogenic precursors [165-167], and is subsequently down-regulated with the formation of mature myofibers in normal muscle [148, 168]. Even though regenerating myofibers within

diseased tissue (such as those observed within dystrophic muscle) display some increase in MHC-I expression [169, 170], the fusion of donor cells could serve to protect them from host immune destruction. Indeed, even in fully mismatched hosts, transient immunosuppressive treatment has been found to be effective in the long-term retention of donor-host hybrid myofibers [149]. An ability to proliferate for extended periods prior to fusion would seemingly enhance the regenerative response; however, it could subsequently lead to exposure to cytotoxic host cell responses as well. Interestingly, the variation in MHC-1 expression observed corresponded with the transplantation results, such that low expression coincided with increased regeneration. Changes in MHC expression with exposure to tissue culture conditions has been described [72] although this alone would not appear to account for the differences in EP and LP expression reported here, since both were maintained in culture for a similar period of time. It should also be noted that a variable regenerative response was observed even when transplantations were performed in immuno-deficient dystrophic mice (i.e. FACS-sorted Sca-1-/+), and thus specific immunological responses alone do not seem to account for these discrepancies. Further, as variable levels of MHC-1 expression could theoretically have both advantageous and deleterious short-terms and long-term effects, it is difficult to ascertain the potential role of such expression without a properly controlled investigation. Nonetheless, the balance between proliferation and exposure to host defenses would appear to be critical only within early timeperiods post-injection, unless future damage and regeneration is initiated. From the transplantation results presented in section 2.2, it is apparent that the substantial degree of regeneration and myofiber formation occurs within the first week, a result that has been confirmed previously [133]. Thus, it appears that if a donor cell proliferation phase is taking place, it is occurring within this time frame. At least one other report of a myogenic population demonstrating highly prolific behavior upon engraftment and within this time frame has been described previously, through an elaborate *in vivo* labeling technique that allowed quantification and tracking of transplanted precursors [68].

The CD34+ phenotype investigated here has been recently described as representative of the majority of satellite cell progenitors within murine skeletal muscle [7]. Our findings demonstrate some important similarities with those previously described; primarily the satellite cell description of these populations by the observed expression of both Myf5 and M-cadherin, and their relatively low level of fusion into myotubes within culture. However some important differences must be discussed as well. Association of the CD34+ state with quiescence is not consistent with our observations. According to this previous model, activation from a quiescent state causes the CD34 isoform to switch from the truncated to the full-length transcript, followed by complete transcriptional

shutdown. Although our surface antibody labeling could not distinguish between these two isoforms, the observed shutdown of CD34 transcription (reported to occur within approximately 24 hours in culture) was not observed. This is demonstrated by maintenance of the CD34+ phenotype with extended culturing, described in section 2.2.3.3. In addition, the description of a satellite cell minority that lacks both CD34 and Myf5 expression is inconsistent with both the quantity of CD34- cells that were able to be isolated as well as the immunofluorescence and RT-PCR results described here. Thus, it is apparent that we are just beginning to uncover the intricacies in the regulation of CD34 expression by myogenic progenitors.

Although yet to be fully understood, observed phosphorylation of the cytoplasmic domain in other cell systems suggests that CD34 plays a role in signal transduction. In addition, with respect to various hematopoietic cells, CD34 has also been suggested to play a role in cellular adhesion to the endothelium [171, 172]. Interestingly, CD34 function with regard to the myogenic lineage is currently unknown. It has been previously suggested that the timing of its upregulation and downregulation may play a role in the prevention of myogenic differentiation [173]. In a non-myogenic setting, CD34 expression has also been suggested to play a role in the inhibition of hematopoietic differentiation [174]. Such observations are in agreement with the results of the *in vitro* differentiation studies presented here, and would support the hypothesis that the CD34+ cells may be associated with delayed myogenic differentiation and fusion upon injection *in vivo*. The association of the CD34+ phenotype with undifferentiated primary myogenic cells, exposed to differentiation-inducing conditions *in vitro,* has also been observed in studies utilizing myogenic cell lines [7]. However, it was further shown here that in a growth culture setting, a dominant CD34 phenotype seems to be relatively conserved. This does not appear to be the case with CD34-depleted cultures, which quickly re-establish a CD34-expressing subpopulation. This emerging CD34 subpopulation also seems to display delayed fusion characteristics when challenged to differentiate *in vitro*, further suggesting a potential role for either direct or indirect CD34 involvement in the regulation of differentiation within myogenic cells.

As a final thought, it is worth mentioning that even though the difference in the apparent fusion rate between CD34- and CD34+ cells was statistically significant, it is difficult to interpret the *in vivo* biologic significance that such relatively small *in vitro* detected differences may impart. It is much more reasonable to envision major *in vivo* behavioral differences between cell populations on either end of the observed *in vitro* fusion spectrum, such as the EP and MDSCs described here. Such large discrepancies in behavior do not require the

scientific leap of faith needed to connect *in vitro* and *in vivo* findings, and it would thus be logical to perform more in depth *in vivo* experimentation utilizing such cell populations to further strengthen the hypothesis connecting fusion behavior to regeneration capacity.

2.4 Species-Independent Evaluation of Cell Behavior and Regeneration

2.4.1 Introduction

From the results of sections 2.1-2.3, the preplating technique has been shown to be useful in separating various myogenic populations, distinguishable by combinations of their: surface protein expression, abilities to regenerate dystrophin-expressing myofibers, and proliferation and fusion characteristics when challenged in a low-serum differentiation assay. Specifically, from these observations it is proposed that the ability of a myogenic progenitor population, as well as their progeny's ability, to expand in number while consequently maintaining an undifferentiated and unfused state is reflected in their capacity to regenerate new myofibers following transplantation. However, application of the techniques and isolation strategies discussed thus far toward eventual clinical utilization requires that such observations not be limited in a species-dependent manner. Thus, within a rat animal model evaluation of both regeneration and fusion parameters, as previously established for the murine model, are presented. The presence of CD34 expression was also examined to determine the degree of conservation within the myogenic lineage, as this marker was useful to some extent within the murine setting in distinguishing subpopulations of progenitors with the proposed desirable cellular characteristics and enhanced regenerative qualities.

2.4.2 Methods

2.4.2.1 Cell Isolation: Preplating. Both hindlimb gastrocnemius muscles from a single female rat (Sprague Dawley, 6-10 weeks old; Harlan Sprague) were combined for enzymatic digestion and cell isolation. The preplating cell isolation technique, including adhesion times and supplemented culture medium, was performed using the same

materials and in an identical fashion to that described within section 2.1.2.1. However, for PP1 and PP2, larger flasks (T-175) were used to accommodate the number of cells adhering during these time periods. Evaluation of the percentage of myogenic cells initially contained within each preplate culture was performed via desmin immunocytochemistry, in an identical manner to that described within section 2.1.2.2. For transplantation and fusion assay experiments, some preplate cultures were replated in order to obtain desmin percentages of greater than 70%, also as described previously within 2.2.2.1.

A previously prepared rat MDSC population was thawed from liquid nitrogen-stored frozen stock and also utilized in the experiments (prepared by Zhuqing Qu-Peterson). This cell population was obtained following a similar isolation procedure from newborn hindlimb muscle (<2 weeks old) and derived from a PP6 culture using the method described within section 2.1.2.1. MDSC cells were cultured in a similar manner as the primary cultures, using identical medium and collagen-coated flasks.

2.4.2.2 Flow Cytometry. Flow cytometry analysis of CD34 expression within each preplate was performed similar to that described in 2.1.2.3. In addition to the mature rats used for cell isolation, preplated cells derived from a single newborn (7-10 days old) female rat were also analyzed. Labeled cell aliquots and controls were prepared and incubated with a blocking solution, as previously described, prior to addition of primary antibodies. Cell suspensions were labeled directly with both mouse IgG FITC-conjugated anti-rat CD34 and mouse IgG PE-conjugated anti-rat CD45 antibodies, or equivalent amounts of isotype control antibodies (all from Pharmingen). 7-AAD was added for dead cell exclusion and live cell events were collected and analyzed using identical settings and methods as previously described. For some cell populations, forward scatter settings were adjusted to accommodate differences in cell size. Surface protein expression analysis was performed on viable and hematopoietic lineage (as recognized by CD45) negative cells by appropriate gating. Consistent with the mouse cell analysis, rat-derived cells were analyzed within 24 hours of initial adherence to the culture flasks. However, for several isolations, cells were also re-analyzed following culture for 5-7 days.

2.4.2.3 Immunofluorescence Evaluation of Myogenic Commitment. Each preplate population was also evaluated by immunofluorescence labeling for expression of the MRF proteins Myf5, MyoD and myogenin in order to gauge myogenic differentiation status. Analysis was performed on methanol-fixed cells exactly as described within section 2.3.2.1. Staining was performed on preplates obtained from three separate isolations to determine the

final range of expression of the various proteins, with the exception of the MDSC population which was derived from a single isolation but was investigated for multiple passages used throughout the various studies.

2.4.2.4 Cell Transplantation and Dystrophin Restoration. As a dystrophic rat model does not currently exist, evaluation of myofiber regeneration through dystrophin restoration was performed by rat cell transplantation via single direct injection into gastrocnemius muscles of dystrophic and immune deficient mice (mdx/SCID), described within section 2.2.2.8.

MDSCs or individual preplates, containing greater than 70% desmin expression through direct isolation or replating, were utilized for transplantation experiments. Transplantation and evaluation of dystrophin restoration was performed at 7 days post-injection, as previously described within sections 2.2.2.3-2.2.2.5. Similar to the mouse-derived MDSCs, the regeneration index reported for the rat MDSC population was based on the total number of cells injected rather than the number of desmin-expressing cells. The data presented represents cumulative results obtained from six separate isolation procedures.

2.4.2.5 Proliferation and Fusion Characteristics. The bioinformatic cell culture system described within section 2.3.2.5 was utilized to evaluate the proliferation and fusion characteristics of the various myogenic populations under low serum (2%) conditions. Brightfield observations regarding both proliferative capacity and formation of multinucleated myotubes were made using the time-lapsed imaging system, and followed by the immunofluorescence evaluation of myogenic status at the conclusion of the 96 hour culture period. Experiments and analysis were performed exactly as described within section 2.3.2.6, however it was observed that an initial cell density of 2,500 cells/cm^2 (twice that of the mouse experiments) was required to prevent massive cell death within culture. Immunofluorescence data is again presented through the fusion index and the ratio of the number of mononuclear myogenic cells to the number of myotubes.

For time-lapsed brightfield observations, data was generated from 8 separate wells for each preplate from experiments performed from two separate isolations, or from data performed in duplicate for MDSCs. Immunofluorescence data was generated from 9 individual wells for each preplate from experiments that were performed from four separate isolations. MDSC data was generated from 9 different wells from experiments performed in duplicate.

2.4.2.6 Animals. All animals were housed in the Rangos Research Center Animal Facility of the Children's Hospital of Pittsburgh. The policies and procedures of the animal laboratory are in accordance with those detailed in

the guide for the "Care and Use of Laboratory Animals" published by the US Department of Health and Human Services. Protocols used for these experiments were approved by the Animal Research and Care Committee of the Children's Hospital of Pittsburgh (Protocol 24/01).

2.4.2.7 Statistics. Multiple comparisons were made between all four cell populations in terms of regenerative efficiency and proliferation and fusion behavior from brightfield and immunofluorescence observations. All comparisons were made by one-way ANOVA, with Student-Newman-Keuls post-hoc pairwise comparisons for cases in which a significant F-value was obtained. For comparisons in which unequal variance or a non-parametric distribution was detected, Kruskal-Wallis one-way ANOVA on ranks was used, with Dunn's test for subsequent pairwise comparisons. The Pearson Product Moment was also used to determine the strength of association between the regeneration index and the parameters obtained from the fusion assay. All data is expressed as mean ± SEM, and p-values less than 0.05 were considered statistically significant. All comparisons were made using SigmaStat (v2.0, Jandel Scientific) statistical software.

2.4.3 Results

2.4.3.1 Preplating, Desmin Expresesion, and CD34 Evaluation. Similar to the mouse, application of the preplate technique results in a purification of myogenic cells from dissociated rat skeletal muscle. The average percentage of myogenic cells, as determined through desmin expression, within each preplate population from PP1 to PP6 was 14±2, 34±13, 58±4, 86±4, 86±2, and 81, respectively. Interestingly, morphological differences between myogenic cells isolated in the earlier and later preplates were apparent, similar to that observed in the mouse, with late adhering myogenic cells displaying a round morphology as opposed to the spindle-shaped earlier adhering myogenic cells. MDSC cultures contained an average percentage of 66±1 desmin-expressing cells, displaying both types of morphologies.

In contrast to the mouse, flow cytometric evaluation of non-hematopoietic cells contained within the rat cell cultures revealed very little CD34 expression. Less than 2% of the cells within each preplate (PP1-PP6) expressed CD34, regardless of donor age (7-10 days or 6-10 weeks) or the length of time spent in culture (less than 24 hours or 5-7 days). Further, within the positive fraction, CD34 expression was very low and only slightly above background fluorescence. Such levels of expression would be difficult to assess through visual

immunofluorescence. Both of these observations were consistent with the results of the analysis performed on the rat-derived MDSC population as well.

2.4.3.2 Evaluation of Myogenic Commitment. PP3 through PP5, as well as the MDSC population, were further examined for their respective expression of MRF proteins. Ranges for the percentage of myogenic cells within each population expressing the protein of interest are provided within Table 2.3. It is seen that Myf-5 expression, unlike the other MRF proteins, was more variable among the various preplates. Overall, the MDSC population demonstrated a comparatively low myogenic commitment, with a small percentage of cells expressing both early and late stage MRF proteins MyoD and myogenin. The remaining preplates contain cells which are similar in their expression of these proteins, however PP4 contains slightly higher percentages of cells expressing early stage MRFs Myf-5 and MyoD. Thus, unlike the mouse, clear EP and LP population differences were not evident within the rat cultures, and each preplate was subsequently evaluated on an individual basis for their respective regeneration and fusion characteristics. Only on one occasion were enough cells present within PP6 to perform any experiments, and thus such cultures were omitted from the remaining analyses. In addition, a high percentage of myogenic cells could not be obtained from PP1 and PP2 through replating, and thus were also omitted from MRF expression analysis and further evaluations of transplantation and fusion characteristics.

Table 2.3 Expression of MRF proteins by various rat myogenic populations isolated via the preplate method.

	Myf-5	**MyoD**	**myogenin**
PP3	40-90	50-60	20-30
PP4	60-90	60-80	20-30
PP5	60-70	50-60	20-30
MDSC	80-90	< 5	< 1

2.4.3.3 Dystrophin Restoration. Utilizing the same regeneration evaluation strategy for the rat, the number of dystrophin-positive myofibers generated following injection of the various myogenic populations was used to generate a regeneration index. As shown in Figure 2.29, the efficiency of regeneration among the preplates and the

MDSC population was again highly variable. The MDSCs (392±55, n=5) demonstrated a clear and significantly greater efficiency when compared to all other preplate populations examined (PP3, 81±18, n=9; PP4, 40±10, n=9; PP5, 62±60, n=4). No other significant differences were detected through multiple comparisons.

2.4.3.4 Proliferation and Fusion Characteristics. From brightfield time-lapsed video observations, average normalized cell number and myotube formation was tracked for each cell population over the 96 hour observation period and is shown in Figure 2.30. Initial raw cell numbers (at t=0 hours) within each field were not significantly different among the four groups. MDSC normalized cell number was significantly higher than all other preplates (PP3-PP5) at both the 12 and 24 hour timepoints, indicating a rapid MDSC population expansion, and was also significantly higher than both PP4 and PP5 for all timepoints beyond 24 hours. Only one other difference was revealed, as PP3 cell number was also significantly higher than PP5 for all timepoints beyond 72 hours. In terms of cellular differentiation and fusion, MDSCs displayed a significantly lower percentage of myotube formation compared to both PP4 and PP5 at the 60 hour timepoint and beyond, and versus PP3 for the 60 through 84 hour timepoints. By 96 hours, PP3 myotube formation was also significantly lower than PP4.

Results of the immunofluorescence analysis at the 96 hour timepoint further confirmed these brightfield observations, as shown in Figure 2.31. The percentage of myogenic nuclei contained within myotubes, as indicated by the fusion index, was significantly lower for MDSCs (6±1, n=9) when compared to all other preplate populations (PP3, 15±3; PP4, 25±3; PP5, 19±2; n=9 each). In addition, this index was also significantly lower for PP3 in comparison to PP4. It followed that the ratio of mononuclear to fused cells was significantly higher for MDSCs (62±10) compared to both PP4 and PP5 preplates (13±2 and 14±2, respectively), reflective of the combined discrepancies in their respective expansion and fusion behavior.

2.4.3.5 Correlation of Regeneration and Fusion Parameters. The results of the regeneration and fusion assays again appeared to parallel each other, similar to that observed for the mouse model, such that increased dystrophin restoration was observed with populations exhibiting increased proliferative capacity while maintaining a low level of terminal differentiation. Some discrepancies in the significant findings between these parameters are noted, such as the non-significant relationship between PP3 and MDSC with regard to the ratio of mononuclear to fused cells, and the significant difference between PP3 and PP4 with regard to the fusion index.

The linear statistical association between the regeneration and fusion parameters was subsequently examined. From the results obtained utilizing the rat populations alone, no significant relationship between the

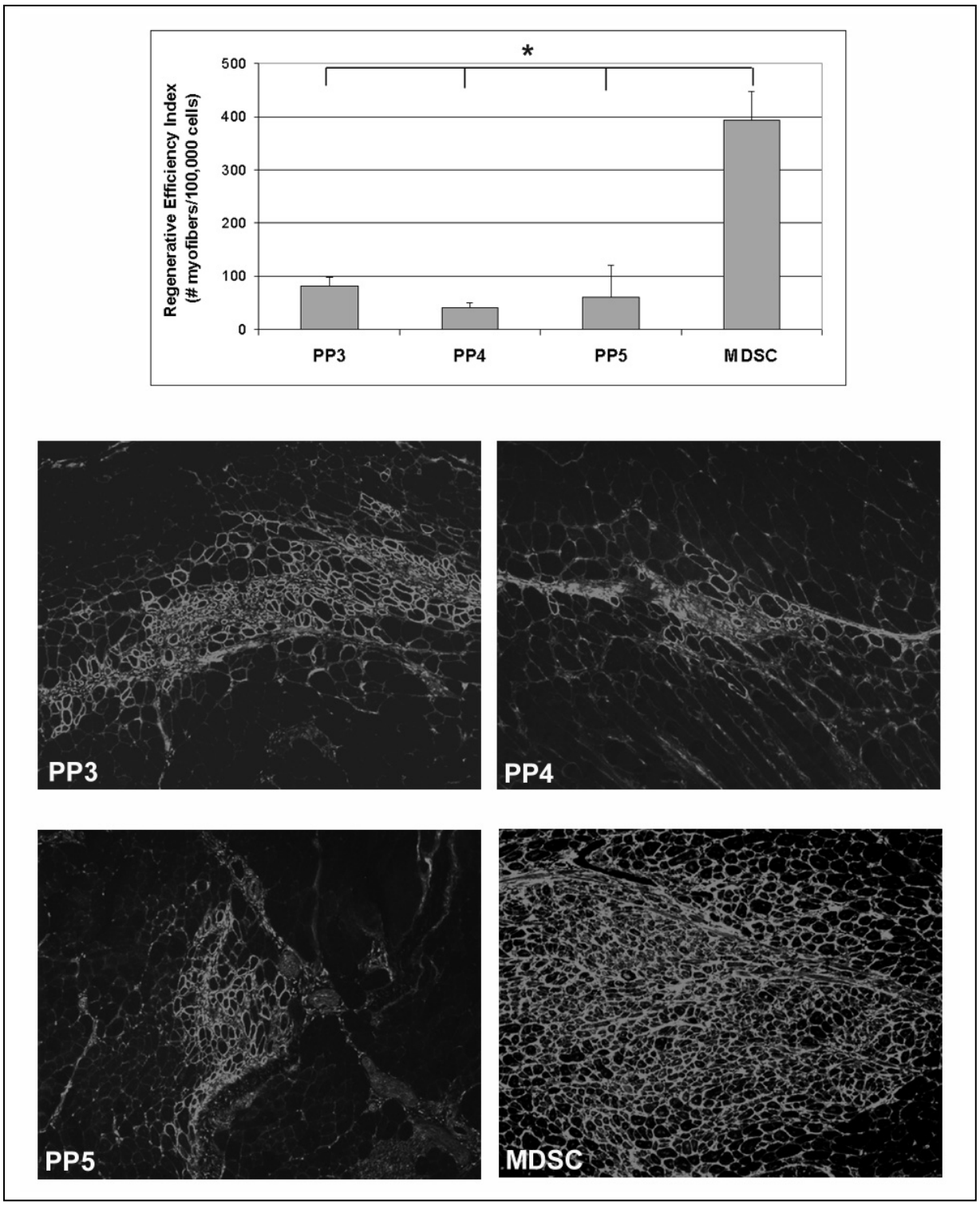

Figure 2.29 (top) Efficiency of dystrophin restoration among preplated rat myogenic populations at 7 days following injection. MDSCs were the most efficient in comparison to all other populations (*, $p<0.05$). (bottom) Representative cryosections with dystrophin expression revealed by immunohistochemical staining following injection of PP3 (400,000 cells), PP4 (300,000 cells), PP5 (100,000 cells), and MDSC (300,000 cells) populations. All images are 100x magnification.

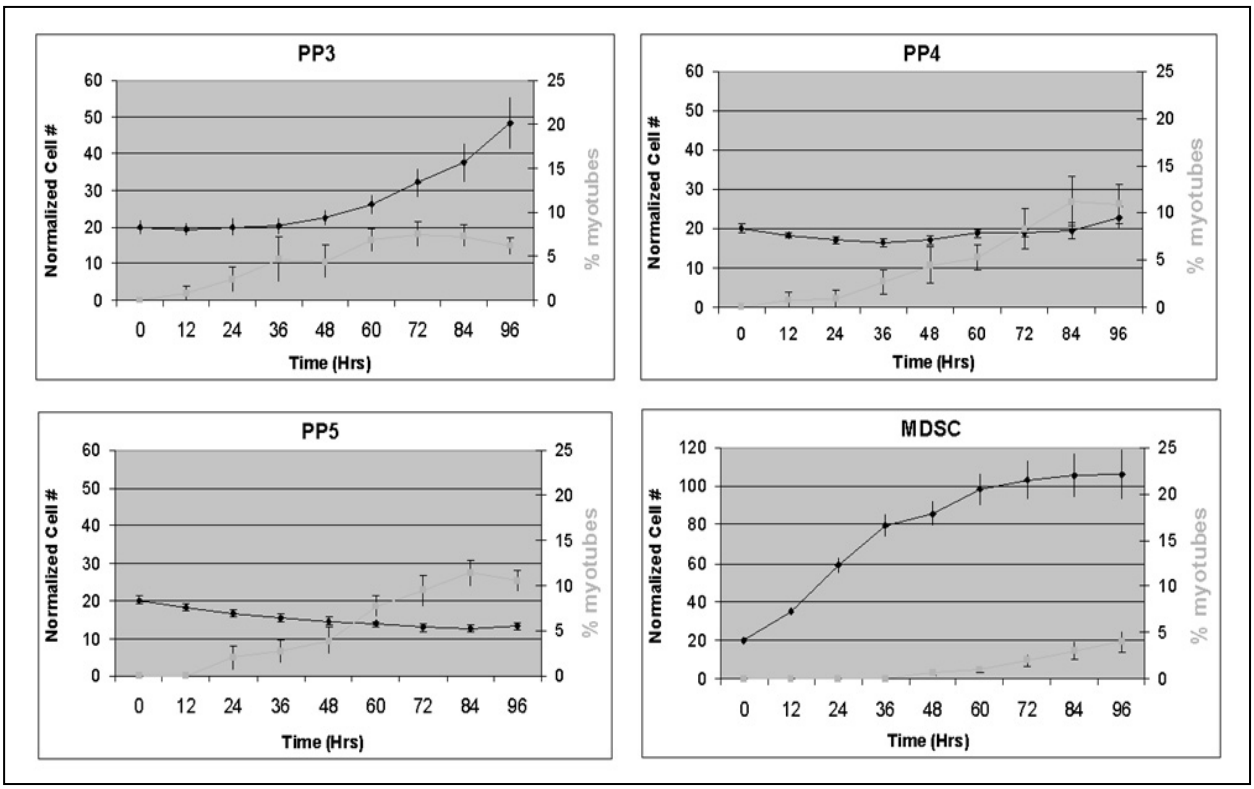

Figure 2.30 Cell expansion and fusion behavior of each rat myogenic progenitor population under low serum conditions, as determined from time-lapsed brightfield observations. Note the normalized cell number scale change for the MDSC population, demonstrating the large degree of cell expansion even under these differentiation-inducing conditions.

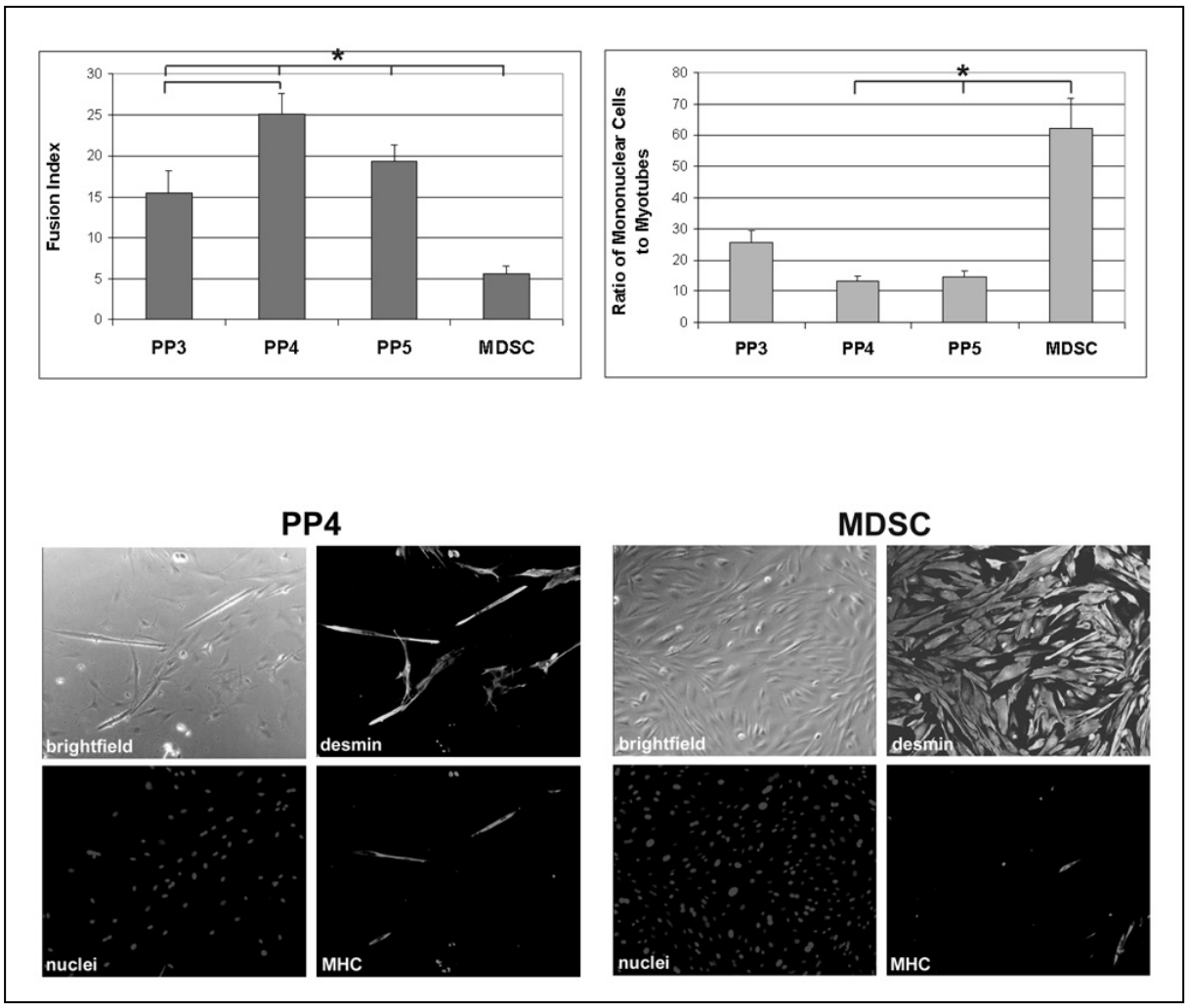

Figure 2.31 (top) From immunofluorescence analysis, comparison of fusion indices revealed a significant difference (*) between MDSCs and all other preplate populations examined. Ratios of the number of unfused myogenic cells to multinucleated myotubes were also significantly higher for MDSCs compared to both PP4 and PP5. (bottom) The contrast in cellular expansion and fusion behavior is clearly seen in the representative PP4 and MDSC images (all images taken at 40x magnification).

regeneration and fusion indices was observed ($p=0.08$). However, the mononuclear to fused cell ratio did correlate significantly to the regeneration index (correlation coefficient, $r=0.987$).

Combining both the mouse and the rat data together, a non-significant linear relationship between the fusion and regeneration indices was again observed ($p=0.105$). Likewise, a strong positive linear relationship between the regeneration index and the mononuclear to fused cell ratio was evident ($p<0.01$; correlation coefficient, $r=0.865$), such that increasing regeneration correlated with increases in this ratio.

2.4.4 Discussion

Smaller discrepancies in regeneration efficiency among the preplate populations examined were evident, mirroring the subtle differences in MRF expression. It followed that myogenic determination as predicted by MRF expression again corresponded to regeneration capacity such that, overall, cellular populations that were within earlier stages of the differentiation pathway demonstrated higher efficiency. The most noticeable example of this relationship was seen through the characterization and transplantation of the MDSC population, which again displayed the highest level of regeneration among the populations examined. Utilizing the same parameters obtained from the low serum assay, established within the mouse model, it was seen that MRF expression patterns generally paralleled fusion behavior as predicted through accepted MRF differentiation models. In addition, description of cellular expansion and differentiation behavior through the mononuclear to fused cell ratio again displayed a significant correlation with regeneration, thus independently confirming this association within a second animal model.

Application of the preplating method to rat dissociated skeletal muscle, in comparison to mouse, resulted in several important similarities and differences with regard to isolation of efficient progenitors. A similar delayed adhesion of myogenic cells resulted in an enrichment of such cells within later adhering cultures. However, in terms of perceived differentiation status, no clear EP and LP distinction could be drawn based on initial adhesion time corresponding to differential patterns in MRF expression. Wide ranges in preplate cellular percentages of expression were observed for early MRF proteins, Mfy5 and MyoD, with only PP4 cultures containing a higher portion of cells in what could be considered a more progressed differentiation state. Analysis of the MDSC population, isolated from PP6 are similar in behavior to that obtained from the mouse, clearly indicated a less myogenically-committed and distinct phenotype from the preplated populations. Isolation of the MDSC thus provided an opportunity for comparisons of regeneration and fusion to be made across populations exhibiting a broader range of cellular characteristics, which was critical for challenging the observations made within the mouse model.

In contrast to the mouse-derived cultures, CD34 expression was almost entirely absent within all rat preplate cultures examined. Thus, no further partitioning of cell cultures or investigation of CD34 potential involvement in myogenic cellular differentiation and fusion processes was possible. This observation is also

significant in terms of future isolation strategy as it suggests that investigation of surface protein expression as a means for identification and rapid selection of specific myogenic progenitor populations, for a given species, may need to be performed on an individual basis.

Evaluation of MHC-I expression by the four rat populations investigated was not performed. As the rat cell injections were performed within a SCID model, more appropriate for xenogenic transplantation, variable expression of MHC-I presumably would not impact specific lymphocytic cellular recognition and longer-term regenerative outcomes. However shorter-term variable responses to donor cells due to interactions with NK cells, although present at lower levels, are possible within the SCID host and thus potential effects due to variations in MHC-I expression in this regard cannot be excluded. In addition, inflammatory cellular constituents and mediators are also functional within the SCID model [175]. Taken together with the regeneration results, longer-term regeneration outcomes would not be expected to deviate significantly from those obtained using the short-term evaluation performed, and these short-term results should be representative of those that would be expected within a non-SCID host. These results also provide further evidence that factors influencing differential regeneration are acting within the first week following transplantation, and in all likelihood within the first few days.

2.5 Conclusions

Strategies for the identification and separation of rare or desirable cells from within a mixed population have traditionally focused on the use of cell-specific surface proteins. Historically CD34 has been utilized, at least in part, as an identifying marker found on subsets of both murine and human hematopoietic progenitors [176, 177] as well as in combination with Sca-1 and c-kit with regard to specific murine long-term reconstituting stem cells [137, 178]. Among these three candidate surface proteins investigated here as potential isolation markers, only Sca-1 and CD34 were expressed by murine myogenic progenitors. Among these two proteins, lack of Sca-1 expression by directly-isolated populations and CD34 expression by cultured cell populations were found to be associated with a significant difference among progenitors in terms of their ability to regenerate skeletal myofibers and restore dystrophin expression within the dystrophic transplantation model. Although CD34 expression has now been confirmed to be associated with at least a subset of murine myogenic ‘satellite cell’ progenitors, its potential function within this microenvironment has yet to be specifically investigated. Characterization of both the

differentiation and regeneration capacity of myogenic progenitors distinguishable only by their CD34 status (and indistinguishable in their initial adhesion, division time, mitotic status, and MRF differentiation status) suggest that its involvement within the myogenic compartment may impact cellular fusion and myotube formation. Although future elucidation of such involvement remains, it is becoming increasingly apparent that continued investigation of CD34 expression within the murine model of progenitor hierarchy may play a future role in expanding the knowledge of both fundamental myogenic development and regeneration processes. Unfortunately, in contrast to hematopoietic progenitors, it is also unlikely that such a marker will be useful for the identification and isolation of efficient adult human myogenic progenitors. Conservation of CD34 expression among myogenic cells isolated from the mouse and the rat was not observed, and reports of human myogenic expression have thus far been limited almost entirely to fetal-derived tissue [179, 180]. Further, discrepancies in the regeneration results obtained through utilization of both cultured (MACS) and direct (FACS) cell selection methods, as well as confirmed alterations of surface protein expression within sorted cultures, further suggest that such proteins may also be subject to temporal changes.

In the quest to identify a usable surface marker(s) associated with efficient myogenic progenitor populations, experimental observations from both animal models examined suggest that differential cell behavior, likely dictated by intrinsic disparities in regulated MRF protein expression, may impact regeneration outcomes by up to ten-fold or more (eg. murine EP vs. MDSC and rat PP4 vs. MDSC). A low cellular density and serum assay exposed these disparities and allowed for direct measures (brightfield and immunofluorescence) of cellular behavior to be made through simple parameters defining cellular progression toward differentiation. These parameters proved valuable in describing each isolated population's overall differentiation status, analogous to MRF expression patterns dictating myogenic progression. Specifically, the ratio of mononuclear to fused cells, which is reflective of a given cell populations ability to both expand in number while at the same time remain in an undifferentiated state, allowed for accountability of cell proliferation potential not readily evident through MRF analysis alone. Significant correlation between this parameter, obtained from an *in vitro* assay, and the regeneration index, obtained through *in vivo* transplantation, suggests that proliferation and fusion behavior may potentially be used as an *a priori* indicator of a donor population's regenerative quality. This association spanned both animal species investigated and implies that from a therapeutic standpoint isolation strategies aimed toward obtaining efficient myogenic progenitors should,

in the absence of a reliable surface marker, focus on identifying cell populations displaying the desirable combination of both high expansion capacity and low fusion behavior.

From a scientific standpoint, results taken from both the *in vitro* and *in vivo* experimentation provide further evidence of the decidedly heterogeneous nature of myogenic progenitors in terms of their behavior as well as their gene and antigen expression. Correlation of *in vitro* behavior with transplantation outcomes provides for a convenient and straightforward explanation for the disparities in regeneration efficiency. However, this process is most likely the culmination of a number of interrelated factors that allow the transplanted cells to interact with the host and respond in a variable manner when placed within the injury-induced environment imposed by their transplantation. Thus, a more complete understanding of the myoblast transplantation process requires that the impact of all such factors on donor cell regenerative performance be investigated in an appropriate manner through further experimentation.

3.0 FUNCTIONAL AND BIOMECHANICAL CONSEQUENCES OF CELLULAR UROMYOPLASTY

The ability to properly characterize fundamental mechanical tissue properties can be very powerful in understanding normal tissue function as well as in elucidating underlying causes of dysfunction and the pathological progression of disease states. Despite the principal mechanical function of the urethra, in particular the generation of controlled resistance for the prevention of urine leakage from the bladder, its biomechanical properties have remained largely unexplored. As mentioned previously, in section 1.4, only a few studies attempting to characterize the mechanical behavior of this tissue have been performed to date. Further, the anatomical basis for previous physiological studies remains unclear because, to date, the mechanical contributions of the various components of the urethra have yet to be clearly defined [106]. This lack of characterization may be attributed, at least in part, to the lack of appropriate experimental systems to perform these kinds of investigations. *Ex vivo* experimental systems have been extensively utilized to examine the relationship between tissue microstructure and mechanical function of vascular segments, and have assisted in the development of working hypotheses regarding the initiation and progression of vascular diseases [181-184]. Application of such experimental devices, modified specifically for the study of the urethra, could yield similar success. Specifically, this may permit a more thorough investigation of structure-function relationships compared to that attainable through current methodologies. Such information is essential to adequately address currently unresolved issues pertaining to the consequences, and ultimately the potential clinical effectiveness, of cellular uromyoplasty therapy.

3.1 *Ex vivo* Assessment of Regional Contractile Function

3.1.1 Introduction

The fundamental goal of the work that follows was to develop, validate, and utilize an *ex vivo* model to evaluate both the physiological and biomechanical properties of the intact urethra. Model development was achieved through utilization of the female rat urethra and modification of a well-established *ex vivo* vascular

perfusion system. The female rat is often utilized for experimental urological studies as a model for the human female and, in particular, for studies focused on investigation of urethral function due to similarities in anatomical structure [185, 186]. In particular, the clinical utility of the female rat model has been demonstrated through simulations of SUI, showing both decreasing striated muscle volume and development of stress incontinence symptoms following pudendal nerve injury [187, 188].

As a first step toward validation, the initial goal of the experiments described within this section was to first explore the utility of this model to detect variations in contraction and relaxation responses against applied intalumenal pressures in relation to regional variations in local tissue structure. As described previously in section 1.4.1, natural axial variations in the degree of muscle content are inherent to the urethra and are exploited here for this purpose. Control over individual muscle contractile responses was also explored through various routes of pharmacologic manipulation. Importantly, in addition to their validation of the experimental model, these studies provide the physiologic foundation for the characterization of urethral properties in the presence or absence of active contributions from the various muscle components, described within the following section.

3.1.2 Methods

3.1.2.1 Urethra Isolation. Whole and intact urethras were isolated from halothane-anesthetized (4%), adult female, Sprague-Dawley rats (260-320g, corresponding to approximately 8-10 weeks of age; Harlan). The bladder and urethra were exposed via a lower midline incision and catheter tubing (PE-50, OD=0.965 mm) was inserted into the urethral lumen, extending the entire urethral length, and exiting from a hole placed in the bladder dome. The tissue was secured to the tubing with sutures at the mid-bladder and at the most distal portion of the urethra, in order to maintain *in vivo* length following dissection. The ureters were ligated with sutures and served as anatomic landmarks by which the *in vivo* length was measured (typically 21-22 mm). This measured length was also used for positioning of the laser for regional measurements as described below. The pubic bone was cut at a position lateral to the urethra, and then separated and resected. The exposed urethra was gently removed from the ventral vaginal wall and the whole bladder-urethra unit was immediately placed into cold Medium 199 (Sigma) that had been bubbled with oxygen (95% O_2/5% CO_2) until same-day testing could be performed.

3.1.2.2 Experimental Apparatus. Prior to testing, the sutures securing the dissected urethra at *in vivo* length were cut and the catheter removed. The urethra was then secured with 4-0 sutures to stainless steel tubing and restored to

in vivo length inside the experimental apparatus, which was a modification of an *ex vivo* vascular perfusion system previously described [189]. Specifically, this system, used to accommodate a range of larger vascular tissue segments under continuous perfusion, was modified to accept the small-diameter urethras and to provide controlled fixed intraluminal pressures via an adjustable static fluid reservoir (Figure 3.1A). Zero pressure was set with the fluid reservoir level to the top of the bathing chamber, thus the applied pressure reported is equal to the transmural pressure. The mounted urethra (Figure 3.1B,C) was enclosed within an 800 mL bathing chamber for maintenance of temperature and oxygenation via a 37^{o}C circulation loop and connection to a physiologic blood-gas mixture (21% O_2, 5% CO_2, 74% N_2). Samples of bathing medium were periodically monitored for pH and oxygenation (pH, 7.34-7.55, pO_2, 165-187 mmHg, and pCO_2 20-30 mmHg; Radiometer ABL5), and tissues were allowed to equilibrate for a minimum of 30 minutes prior to testing. Medium 199 was utilized for both the bathing medium and to fill the hydrostatic pressure column. Air was removed from the urethral lumen by briefly unclamping the distal tubing and applying a small proximal pressure (typically 6-8 mmHg for visual fluid flow in the distal tubing) before returning to 0 mmHg pressure. A laser micrometer (Beta LaserMike) was positioned to measure urethral outer-diameter (OD) at chosen locations along the axial length, and was calibrated to provide measurements accurate to a thousandth of a millimeter. Proximal, mid, and distal regional measurements were performed by positioning the laser at axial positions 25%, 50%, and 75%, respectively, from the apex of the bladder (assumed to start 3 mm below the ureters), based on *in vivo* length. Both pressure and OD measurements were recorded simultaneously using LabView data acquisition software.

3.1.2.3 <u>Pharmacologic Testing Protocols</u>. Tissue responses were measured following addition of muscle agonists or antagonists. For these experiments, the urethra was exposed to a fixed intraluminal pressure of 8 mmHg, which caused the tissue to be pre-dilated and allowed for contraction. The deformation caused by this 8 mmHg applied pressure was measured at a single axial location (proximal, mid, or distal) 30 minutes following pressurization, and was subsequently used in determining the relative percentage change in OD measured following the addition of muscle-responsive agents, added consecutively: Nω-Nitro-L-arginine, a nitric oxide synthase (NOS) inhibitor, 100μM; phenylephrine (PE), a nonselective alpha-adrenergic receptor agonist, 40 μM; acetylcholine (ACh), a nicotinic receptor agonist, 10 mM; and ethylenediamine tetraacetic acid (EDTA), a calcium chelator, 3 mM (n=5-14; all chemicals obtained from Sigma). Dilation caused by EDTA was determined relative to the original 8 mmHg baseline.

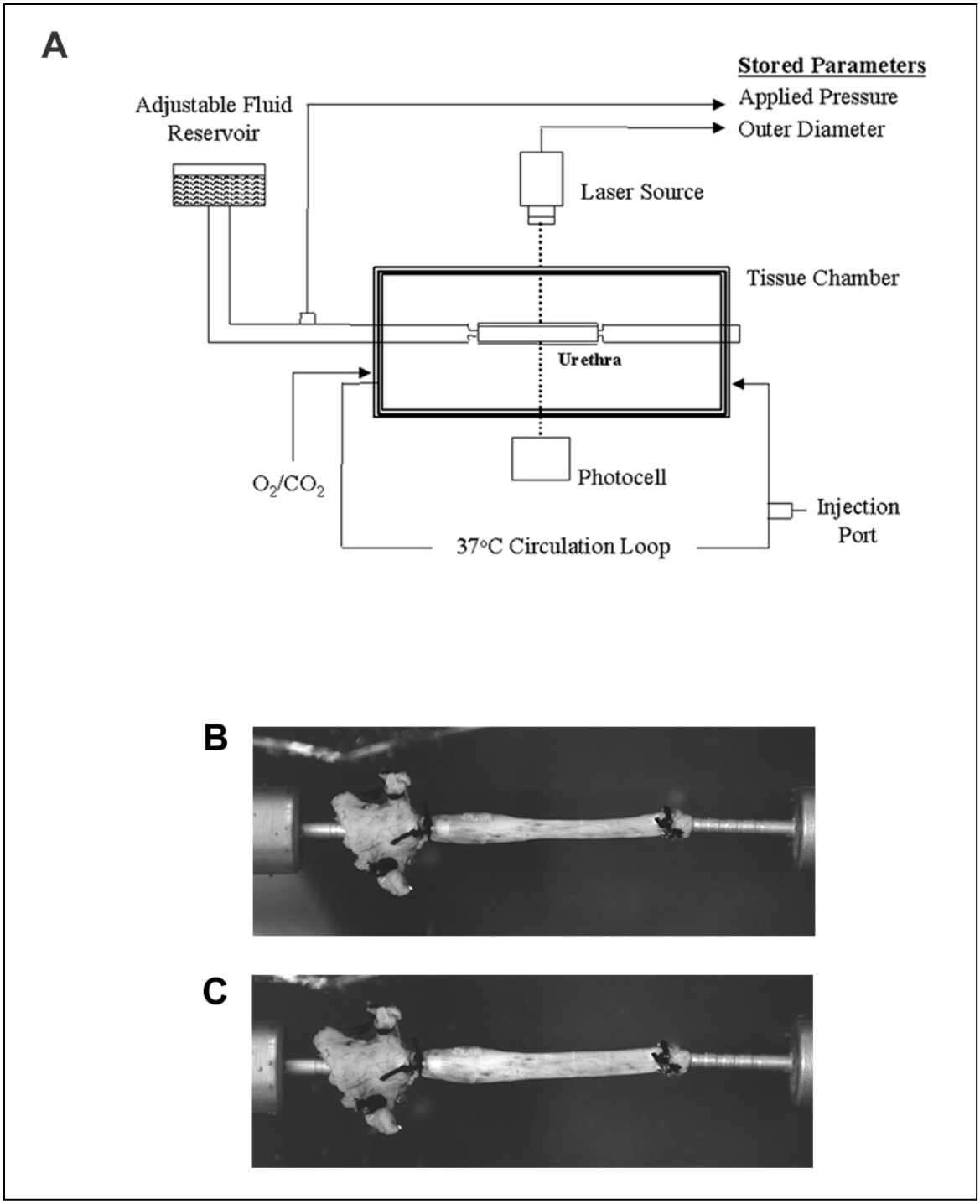

Figure 3.1 (A) Schematic of *ex vivo* experimental system. The urethra is secured within the physiologic bathing chamber at *in vivo* length and applied intralumenal pressure is controlled via a height-adjustable fluid reservoir connected to the proximal portion of the tubing. The distal tubing is clamped. (B-C) Viewing the whole-mounted urethra from the top of the chamber, it is positioned such that left is proximal (with a portion of the bladder remaining) and right is distal. The laser can be seen cutting perpendicular to the axial length of the tissue. Obvious differences in outer diameter are seen in induced contracted (B) and relaxed (C) states.

Additional studies were also performed with the following agents to examine their ability to block the chemically-evoked contractile responses: sodium nitroprusside, a nitric oxide (NO) donor, 10μM (n=5); atropine sulfate, a nonselective muscarinic antagonist, 1μM (n=12); hexamethonium, a ganglion blocking agent, 100μM (n=12); and d-tubocurarine, a selective nicotinic antagonist, 100μM (n=2) (all from Sigma). All concentrations were used at or near maximal responsive levels based on previous *in vitro* urethral studies [131, 190-193], and each solution was prepared on the same day of use.

All agents were added to the bathing medium circulation loop via an injection port and allowed 30-minutes to equilibrate prior to measurement of a new OD, as follows. The last 100 OD data points (collected at 1 Hz) of this equilibration period were averaged in the calculation of each representative OD change, as follows:

$$\%\,\text{OD change} = \frac{\Delta OD}{\Delta OD_{0\text{-}8}} \qquad [3.1]$$

where ΔOD is the difference between the new averaged OD following the addition of an agent and the previous averaged OD, and $\Delta OD_{0\text{-}8}$ is the initial dilation of the tissue caused by the application of the 8 mmHg intralumenal pressure. In addition, a 50 data point average OD change was calculated in response to ACh, taken at the peak OD inflection point observed immediately following its addition to the bath. The lower number of data points averaged here was reflective of the shortened duration of the sustained peak contraction observed, typically lasting only 1½ - 2 minutes. The % OD change reported is a quantitative measure of the ability of each agent to induce the tissue to contract toward the original pre-dilation OD baseline.

3.1.2.4 <u>Immunohistochemistry</u>. Following diameter measurements, the urethra tissue was removed from the stainless steel cannulae and again restored to *in vivo* length by securing it to the catheter tubing with 4-0 sutures under non-pressurized conditions. It was then placed in a 2% paraformaldehyde (in PBS) solution for 24 hours, rinsed briefly in PBS and placed in a 30% sucrose solution for an additional 1-2 hours. Samples from the region of interest were then cut perpendicular to the axial length and the tubing removed from the lumen of each tissue segment. Each segment (approximately 2 mm axial length) was placed in cryomolds containing TBS Tissue Freezing Medium (Triangle Biomedical Sciences), carefully removing the air from the lumen, and flash frozen into blocks for sectioning by immersing directly in liquid nitrogen for 15 seconds. Frozen sections, 8 μm in thickness, were cut transverse to the longitudinal urethral axis using a cryostat (HM 505E, Microm) and mounted onto microscope slides for immunohistochemical labeling.

Striated and smooth muscle composition was determined from serial sections as follows. Sections were blocked with 5% goat serum and incubated with 1:250 dilutions of either mouse IgG anti-skeletal slow myosin heavy chain (clone N0Q7.5.4D; Sigma) or a mixture of both anti-skeletal slow and fast (clone MY-32; Sigma) myosin heavy chain monoclonal antibodies for 2 hours. For smooth muscle, sections were blocked with 5% goat serum and incubated with a 1:250 dilution of mouse IgG anti-alpha smooth muscle actin (Sigma) monoclonal antibody, also for 2 hours. All sections were then washed with PBS, incubated with a Cy3-conjugated anti-mouse IgG antibody (1:250; Sigma) for 30 minutes and washed again prior to immunofluorescence imaging. Negative control sections were treated in an identical fashion, with omission of the primary antibody.

3.1.2.5 Muscle Volume Fraction. For determination of total muscle area and fractional composition of each tissue region, digitized immunofluorescence images were acquired (Spot; Diagnostic Instruments, Inc.) at low magnification (40x; Nikon E800) and analyzed using Northern Eclipse software (v6.0; Epix Imaging, Inc.). Actual tissue cross-sectional area (CSA) for each section was calculated as the difference in the areas enclosed by manually-drawn borders of the lumenal and ablumenal surfaces. Prior calibration of the software, performed for each magnification, allowed the conversion pixel number to real length units. A threshold parameter was applied to the image in order to distinguish the labeled-muscle immunofluoresence signal from background. Both smooth and striated muscle area fractional composition was determined by dividing the immunofluorescent-labeled muscle area by the actual tissue CSA. The percentage of each striated muscle fiber type was also determined individually from serial sections labeled with either slow or fast myosin heavy chain antibodies. For smooth muscle, areas occupied by large blood vessels were visually identified and excluded. For each region (proximal, mid, distal), values from individual sections (one from each end and one from the middle of the tissue segment; n=3) were averaged to obtain a single volume fraction representative of each tissue specimen and corresponding region.

$$\text{Specimen Regional Volume Fraction} = \frac{\sum_{i=1}^{n} (\text{Section Area Fraction})_i}{n} \qquad [3.2]$$

Individual specimen values were then averaged for all analyzed tissues (m=4-6) to obtain the single reported value for each region.

$$\text{Regional Mean Volume Fraction} = \frac{\sum_{j=1}^{m} (\text{Specimen Regional Volume Fraction})_j}{m} \qquad [3.3]$$

3.1.2.6 Animals. All animals were housed in either the Rangos Research Center Animal Facility of the Children's Hospital of Pittsburgh or at the University of Pittsburgh Biomedical Science Tower under the supervision of the Department of Laboratory Animal Resources. The policies and procedures of the animal laboratory are in accordance with those detailed in the guide for the "Care and Use of Laboratory Animals" published by the US Department of Health and Human Services. Protocols used for these experiments were approved by the Animal Research and Care Committee of the Children's Hospital of Pittsburgh and the Institutional Animal Care and Use Committee of the University of Pittsburgh (Protocols 24/01 and 0208766, respectively).

3.1.2.7 Statistics. Multiple comparisons of % OD tissue changes, induced by the various pharmacologic agents, between the three tissue regions was performed using one-way ANOVA with Student-Newman-Keuls post-hoc pairwise comparisons, or an equivalent nonparametric test (ANOVA on ranks with Dunn's post hoc analysis). Direct comparison between ACh-evoked contractions in the presence or absence of antagonists (atropine and hexamethonium) was performed by unpaired Student's t-test. P-values less than 0.05 are reported as significant, and data is expressed as mean ± SEM. All comparisons were performed using SigmaStat (v2.0; Jandel Scientific) statistical software.

3.1.3 Results

3.1.3.1 Pharmacologic-induced Contraction, and Relaxation. Examples of tissue contraction, reflected as decreases in OD, in response to smooth and striated muscle stimulation are shown in Figure 3.2. Contraction results obtained from the cumulative pharmacologic protocol are provided in Figure 3.3.

The initial tissue dilation caused by the applied 8 mmHg pressure was similar between regions (26±4%, 18±2%, and 16±3% for proximal, mid, and distal, respectively; p=0.147). Addition of a NOS inhibitor (Nω-Nitro-L-arginine) resulted in a nonsignificant trend toward contraction at the proximal and mid regions (-19±11% and -16±7%, respectively) which was not apparent within the distal region (5±10%; p=0.212). Following inhibition of NOS, stimulation with PE caused a similar degree of contraction within all three regions of the urethra (p=0.732), which was sustained over the entire 30 minute evaluation period. Subsequently, a biphasic response to ACh was observed, as both immediate (< 2 minutes) and sustained (30 minutes) contractions were apparent for the majority of the tissues. A significantly greater degree of contraction was observed within the mid region at both timepoints

(immediate, -36±4 %; sustained, -17±4 %) compared to that observed in both the proximal (immediate, -8±3 %; sustained, -2±5 %) and distal (immediate, -3±2 %; sustained, 10±3 %) regions. The degree of tissue strain at the time of ACh addition, as determined through changes in OD relative to the 0 mmHg baseline, was not significantly different among the three regions (p=0.332) and thus reduces the possibility of variations in contractile ability due to length-tension considerations. At the conclusion of this contraction protocol, addition of EDTA resulted in a rapid abolition of all contractile function with a relaxation of the tissue above the pre-established 8 mmHg baseline condition at all three regions, indicating a level of basal muscle tone prior to stimulation with the various agonists (p=0.129).

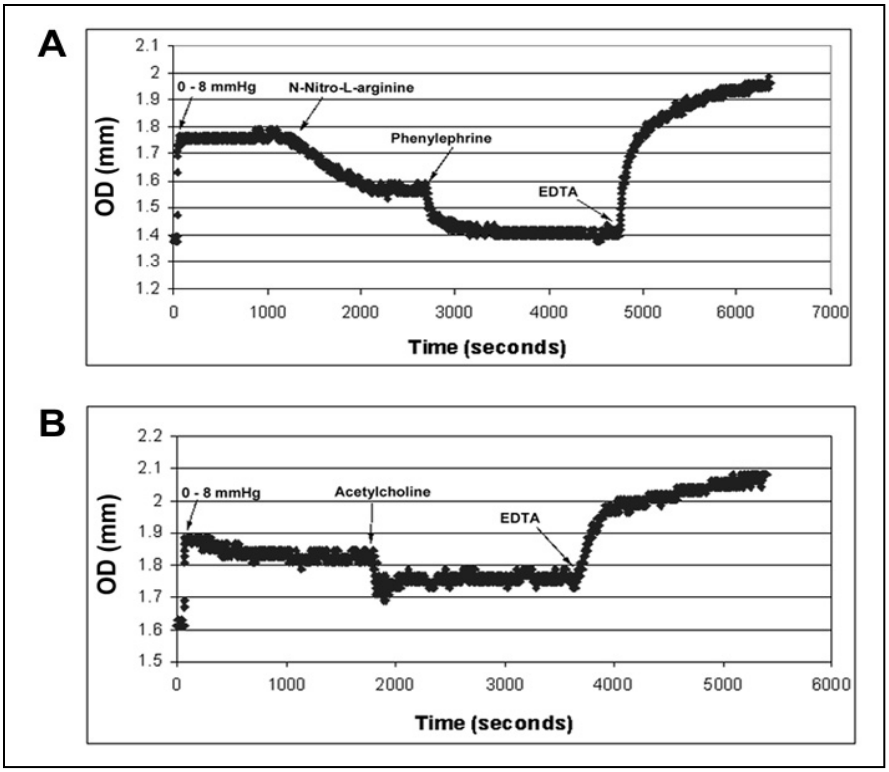

Figure 3.2 Examples of changes in measured urethral OD, at the mid region, following nitric oxide inhibition and adrenergic stimulation (A), as well as separate cholinergic stimulation (B).

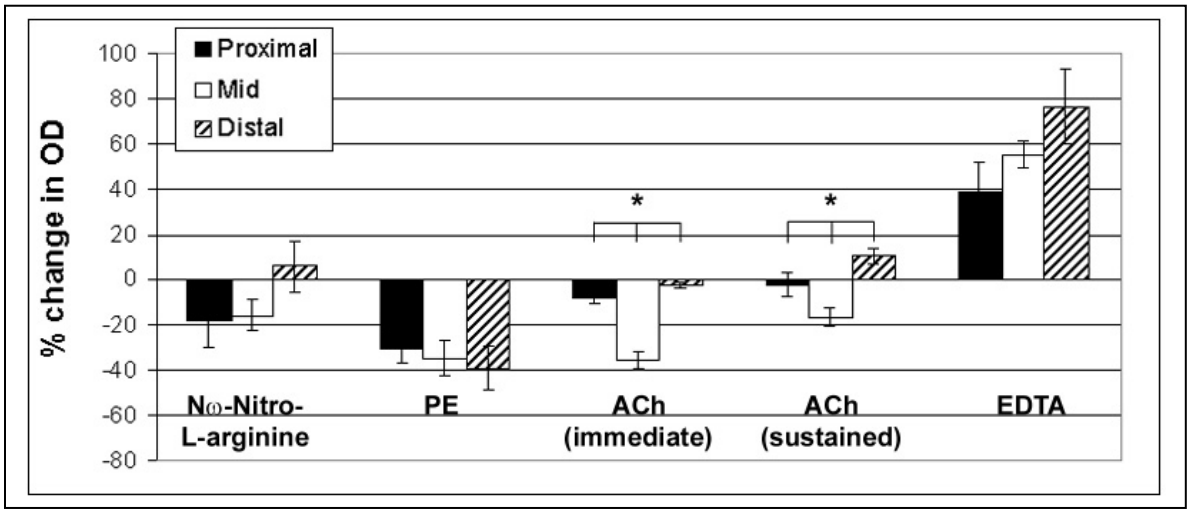

Figure 3.3 Comparison of regional contractile and relaxation responses against an applied 8 mmHg pressure within a cumulative and consecutive pharmacologic preparation (*$p<0.05$, mid vs. proximal and distal).

3.1.3.2 **Smooth and Striated Muscle Inhibition**. The ability of drugs to modulate smooth or striated muscle activity, as well as the biphasic ACh-induced contractile response, was examined. Addition of sodium nitroprusside (Figure 3.4A) eliminated 90±8% of the basal muscle tone, through comparison of subsequent OD changes following the addition of EDTA. In the presence of sodium nitroprusside (see Figure 3.4B), ACh-evoked immediate contractions were reduced and sustained contractions were almost completely eliminated within the mid region (-11±4% immediate and -3±4% sustained; compared to ACh-alone; see Figure 3.3).

The nature of these reduced responses in the absence of smooth muscle activity, and the elimination of the normal biphasic response to ACh stimulation, was further investigated in separate studies within the mid region. In particular, the role of muscarinic or ganglionic neuronal nicotinic receptor activation in the ACh-induced contractions was examined through the use of specific inhibitors to these receptors. Prior addition of atropine (muscarinic) and hexamethonium (ganglionic) (Figure 3.4C) reduced the immediate ACh-evoked contractions (-36±4%, ACh alone vs. -25±4%, blocked; $p=0.111$) and almost completely eliminated the sustained contractions (-17±4%, ACh alone vs. -1±5%, blocked; $p=0.061$). ACh-induced contractions were completely eliminated by blocking both nicotinic and muscarinic receptors with d-tubocurarine and atropine, respectively (Figure 3.4D).

3.1.3.3 Smooth and Striated Regional Content Immunohistochemical staining revealed a similar amount of total smooth muscle within each region (Figure 3.5, left column). However, when accounting for differences in tissue thickness, the smooth muscle component represented a larger fractional percentage of the tissue within the distal region. In contrast, a heterogeneous distribution of striated muscle was observed in terms of both total muscle and fractional composition within each region (Figure 3.5, right column). The largest amount (0.33 ± 0.02 mm^2) was contained within the mid region, and the vast majority of this muscle was circumferentially-oriented. The smallest amount (0.08 ± 0.01 mm^2) of striated muscle was found within the distal region, which also demonstrated a discontinuous and mixed arrangement of myofibers oriented in both the circumferential and longitudinal directions. Results of immunolabeling performed with mixtures of both slow and fast myosin heavy chain antibodies (Figure 3.6) revealed that the striated myofibers contained within each of the three regions predominantly expressed the fast myosin heavy chain isoform (proximal and mid, <10% slow; distal, 15-30% slow).

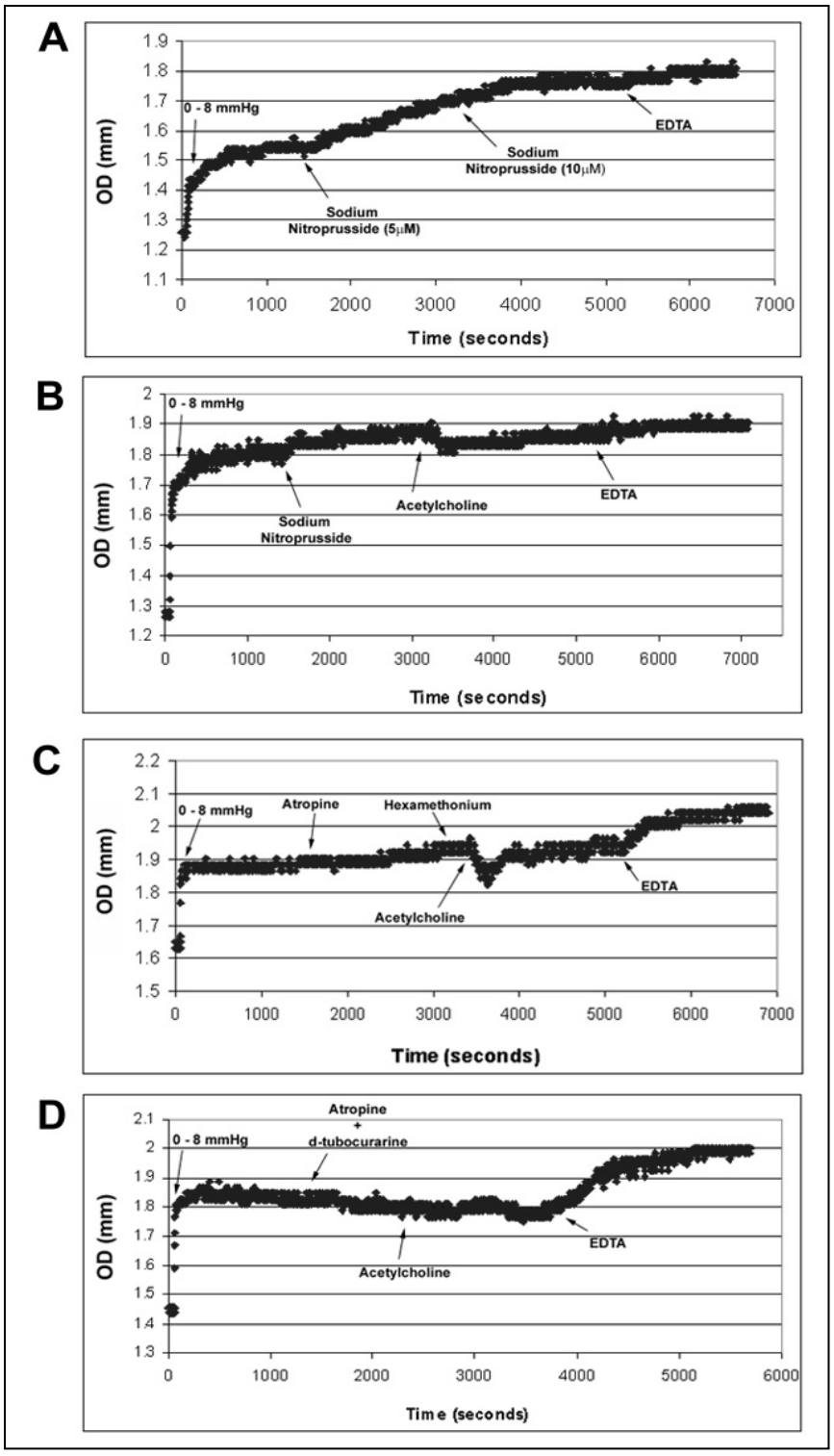

Figure 3.4 Following elimination of smooth muscle activity (A), ACh-induced immediate contractions were reduced and sustained contractions were essentially eliminated (B). Similar results were obtained following specific blockage of ACh-mediated smooth muscle activation (C). Both smooth and striated ACh-induced contractions were abolished through prior addition of nicotinic and muscarinic blockers (D).

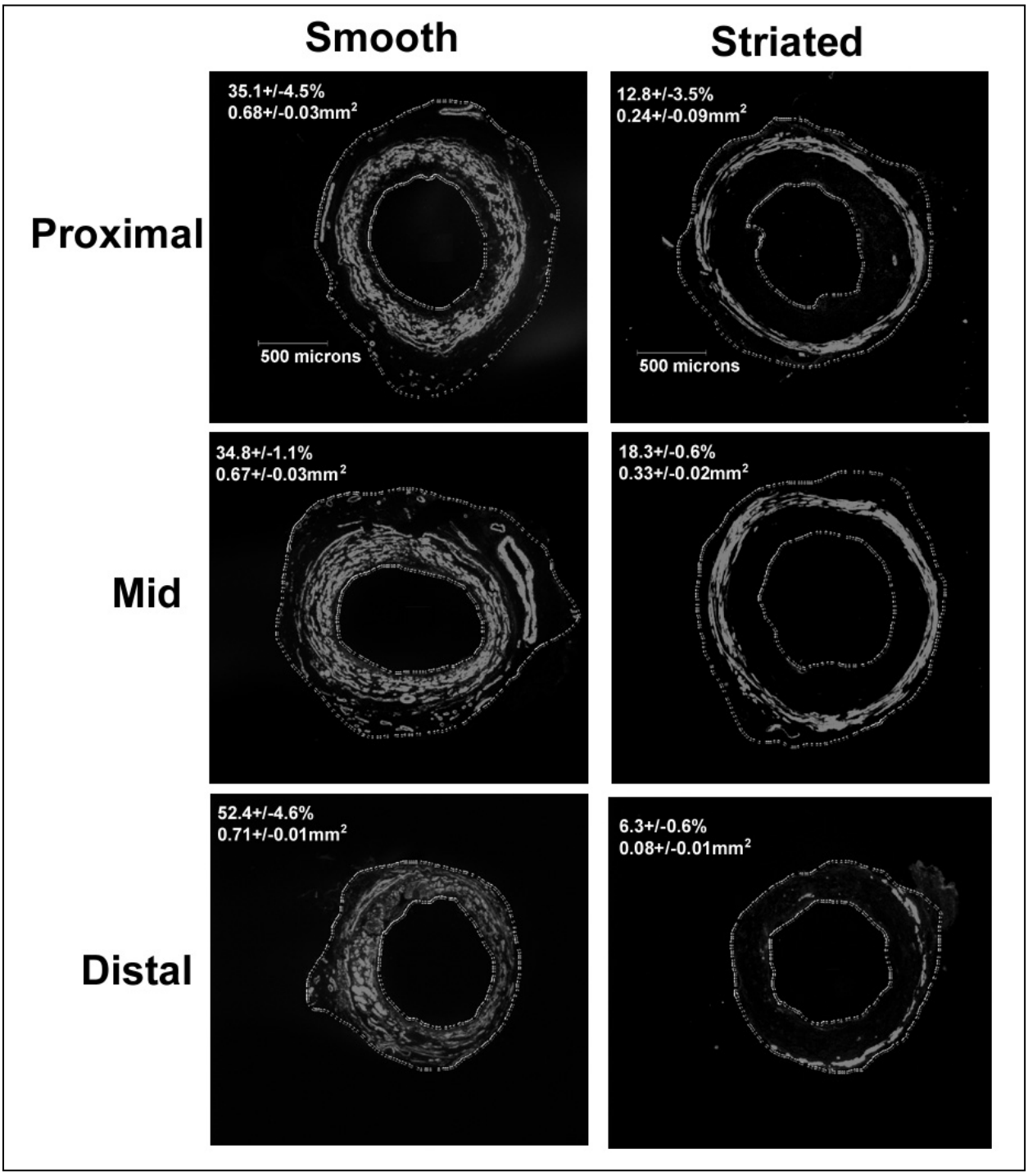

Figure 3.5 Anatomical changes in muscle composition along the urethral axial length. Total smooth muscle content (left column) remains relatively constant, while its fractional area varies between regions. Striated muscle (right column) is most prominent within the mid region, in terms of both total and fractional area. All images taken at 40x magnification.

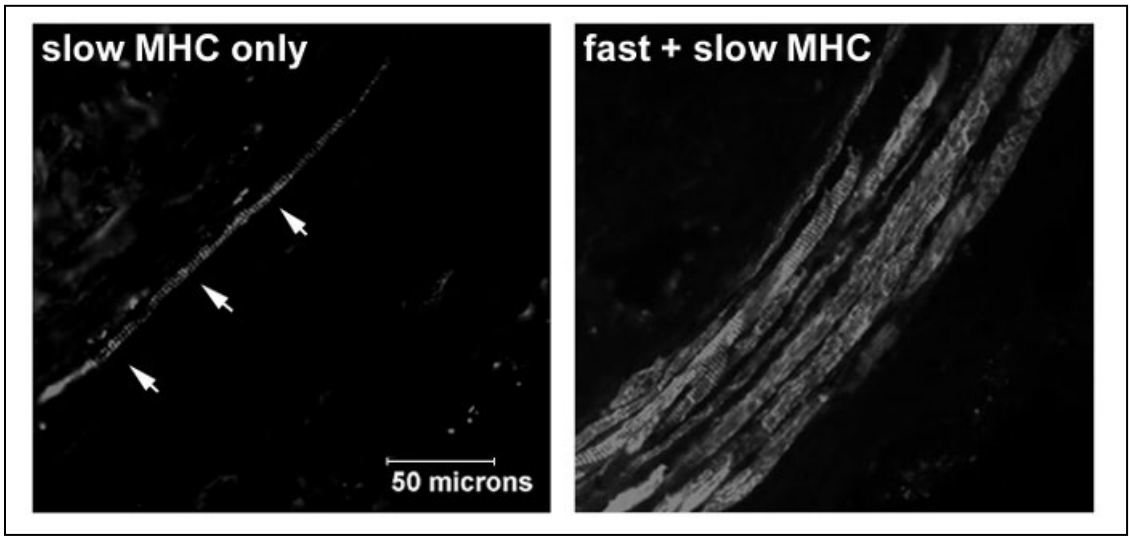

Figure 3.6 Immunofluorescence labeling of serial sections within the mid region. The striated muscle layer is primarily composed of myofibers expressing fast myosin heavy chain (MHC), as demonstrated by the sharp reduction in the number of myofibers labeled by slow MHC antibodies (left, arrows highlight labeled fiber) as compared to simultaneous labeling with both fast and slow MHC antibodies (right). Images taken at 400x magnification.

3.1.4 Discussion

An experimental technique that had been previously employed for the investigation of blood vessel mechanics was adapted for similar study of the urethra, and the feasibility of this approach was demonstrated. In validating this model, tissue tone as well as induced smooth muscle- and striated muscle-contractile responses, against applied intralumenal pressures, were recorded. Blocking studies demonstrate pharmacologic control over specific activation or inactivation of these constituent muscle elements. Differential physiologic responses were observed between the three axial regions examined, and these regional responses are consistent with respective variations in local tissue structure.

Despite removal of the surrounding external tissue support structure and neuronal input, our whole-mounted urethral preparation demonstrated a substantial basal muscular tone in the absence of applied stimulation. This tone was primarily identified by the dilation of the tissue OD above the original baseline, established following initial pressurization and prior to addition of muscle agonists. The smooth muscle nature of this tone was

demonstrated through its near complete elimination following addition of the NO donor, sodium nitroprusside. Additionally, the EDTA-induced relaxation responses observed in each of the regions corresponds to the histological findings of smooth muscle fractional composition, which was largest within the distal region. Although not statistically significant, that this region subsequently displayed the largest average degree of relaxation again implicates the smooth muscle as the source of this tone. This however also assumes that variations in passive structural components did not contribute to this variable relaxation effect, which cannot be eliminated at this time.

Aside from this endogenous smooth muscle tone, intrinsic smooth and striated muscle tissue components also demonstrated distinct and measurable abilities to contract against applied intralumenal pressures when pharmacologically-stimulated, either jointly or independently. Smooth muscle activity in this model was demonstrated by tissue responsiveness to NOS inhibitors and NO donors (Nω-Nitro-L-arginine and sodium nitroprusside, respectively) and an alpha-adrenergic agonist (PE). Homogeneity in contractile function in response to PE stimulation corresponded with immunohistochemical observations of a constant and continuous smooth muscle component throughout the female rat urethral axial length. Similar histological findings have also been reported elsewhere [194]. In regard to the observed contractile effects of NOS inhibition (Nω-Nitro-L-arginine), prior *in vivo* studies in the female rat have shown that urethral smooth muscle relaxation during reflex bladder contractions is at least partially mediated through the actions of NO [195]. NOS has been localized within several different cell types of the lower urinary tract and neurons innervating the smooth muscle [196, 197], and thus should be intrinsic to our whole specimen preparation. However, contractile responses to NOS inhibition observed here, within the proximal and mid region, would suggest a constituitive release of NO within these regions in the absence of bladder activity and neuronal input from the spinal cord. This is inconsistent with previous *in vivo* work demonstrating stable baseline urethral pressures in the presence or absence of NOS inhibitors, which thus could not detect tonic NO inhibition of urethra smooth muscle activity [198]. However for many of the specimens examined here, responses to NOS inhibition were also not observed (5 out of 11 for proximal, and 5 out of 14 for mid), even though subsequent responses to both PE and ACh were detected. The source of this inconsistency, which contributed to a large degree of variability in the reported responses to NO inhibition in this study, is currently unresolved.

Striated muscle activity in this model was demonstrated by tissue responsiveness to a nicotinic receptor agonist (ACh) alone, and in the presence of both muscarinic (atropine) and ganglionic neuronal (hexamethonium)

antagonists. Further, prevention of contractile activity was demonstrated in the presence of both specific nicotinic (d-tubocurarine) and muscarinic (atropine) blockers. Results of the blocking experiments, taken together with the observed biphasic response following ACh stimulation alone, suggest a combined ACh-evoked smooth and striated activation. It follows that the immediate contractile response was the result of nicotinic receptor-mediated striated contraction superimposed upon muscarinic-mediated smooth muscle contraction. Following subsequent fatigue of the striated muscle and/or nicotinic receptor desensitization, only the sustained smooth muscle activity remained (visible at the 30 minute time point). In agreement with the results presented here, cholinergic-mediated excitatory mechanisms of both urethral striated and smooth muscle has also been demonstrated in previous *in vivo* studies in the rat [198]. Interestingly, although smooth muscle composition was relatively constant, variability in sustained contraction between regions was also observed here and may be indicative of distinct regional neuro-pharmacological excitatory properties. A separate report of axial variations in smooth muscle contractility in the presence of muscarinic blockage (atropine) has also been described in the male greyhound urethra [199].

Heterogeneity in immediate ACh responses corresponded with total striated muscle content and fractional composition within the local axial regions of the tissue, as demonstrated histologically here. Interestingly, previous histologic observations in older (12-36 months) female rats generally verify these striated volume fractions, although slow-type fibers were found to predominate [194]. Conversion of skeletal (striated) myofiber protein expression from fast to slow myosin has been previously observed in response to normal muscle development, and with prolonged alterations in muscle usage, and thus may help to explain this conversion in the urethra with age [200, 201]. Although the slow and fast myofibers generate approximately the same amount of peak force [201], the predominantly fast (fatigueable) nature of the myofibers within the urethra may have additionally contributed to the abbreviated duration of peak contraction observed here (<2 minutes).

Taken together, these results demonstrate the ability to pharamacologically-manipulate contraction of both the smooth and striated intrinsic muscle components of the urethra within the novel experimental system developed. Importantly, this may be performed in a regional manner, as detected through local measures of tissue diameter. This information provides a foundation for the use of this system in the basic characterization of both active and passive urethral tissue properties in relation to both natural and therapeutically-induced structural changes.

3.2 *Ex vivo* Biomechanical Assessment of Urethra Properties

3.2.1 Introduction

Several theoretical issues, essential to the effective clinical implementation of the proposed cellular uromyoplasty therapy, remain unresolved. It is proposed that the *ex vivo* experimental system developed, and validated within section 3.1 using intact urethral tissue, will be useful in addressing each of these issues.

Foremost, it is fundamentally-essential to determine the magnitude of the effect caused by alterations of the striated muscle component with regard to the overall mechanical properties of the tissue. Previous urodynamic studies intended to examine the contributions of the various urethral components toward overall urethral closure pressure have not provided a sound anatomical basis for their observations, primarily due to the fact that the mechanical properties of the constituent components of this tissue have not yet been clearly defined [103, 106]. The relative importance of each active muscle component in this regard remains a subject of continued debate within the urologic community [86]. Thus, in terms of uromyoplasty therapy, estimates of the clinical impact imparted by increases in striated muscle cannot be gauged simply from evaluation of the currently available literature. This leads to considerable uncertainty concerning the expectations of such a therapy in relation to the amount of regeneration which can be realistically attained through current cellular transplantation techniques.

Up to this point, it has been theoretically assumed that the regenerated tissue will act in a manner similar to the native striated tissue. However, the confirmed mechanism of action of newly-created tissue remains an important issue. Primary active or passive functions of such tissue may have important implications as to the proper method and placement of the cellular injections. For example, although not readily discussed in the literature, the intended function of injectable agents and their subsequent success may be highly dependent upon their radial placement within the tissue. Physiologically, the most efficient manner in which to create sphincter-like closure function is for the muscle fibers to be arranged near the perimeter of the cylindrical-shaped tissue. Arranged in such a manner, smaller changes in relative circumferential fiber length will result in larger changes in lumen cross-sectional area. If muscle layers were to be positioned near the inner circumference they would be required to shorten to a much larger extent, and most likely to unrealistically short lengths, in order to achieve complete lumenal closure [106]. In this manner, bulking agents are most efficiently placed within the inner submucosal layer which

normally fulfills a 'space-filling' function in the native tissue. In contrast, regeneration or augmentation of circumferentially-arranged functional muscle tissue would provide the most benefit through placement at positions furthest away from the inner submucosal layer. In any case, through currently available tissue-strip force measurement techniques, passive contributions of new tissue could not be directly measured. Rather, they could only be implied through the lack of improvement in contractile force generated by treated tissues.

As a first step toward addressing these issues, experiments were performed to characterize both the passive and active mechanical properties of normal, untreated female rat urethra. Active characterization was performed following induced contraction of either smooth or striated components alone, or collectively. Prior to delving into the study of cellular-transplanted tissue, it appeared more reasonable, at least from a theoretical standpoint, to first examine potential structure-induced changes in measured parameters through exploitation of the naturally-occurring variations in striated composition that occur along the axial length of normal tissue (see Figure 3.5). Parameters derived from P-D responses, and subsequent incorporation of tissue thickness measurements, allowed investigation into the mechanical properties of the tissue to determine effects of activation of each of the active muscle elements. This study was thus intended to enhance the overall understanding of the structure-function relationship of the individual components comprising the urethra and, in relation to cellular uromyplasty therapy, to further examine the relative importance of the striated muscle layer.

3.2.2 Methods

3.2.2.1 Urethra Isolation and Experimental Apparatus. Tissue source, isolation procedure, and experimental equipment utilized in the following studies were identical to that previously described within sections 3.1.2.1 and 3.1.2.2, with the following exceptions. Time intervals for subsequent data collection following addition of pharmacologic agents were adjusted in some instances, and not standardized to the 30 minute incubation period, since previous experience indicated that many agents did not require this extended time in order to exert their maximal effects on the tissue. In addition, to more adequately ensure oxygenation of the muscle layers, and to more closely mimic standardized physiological strip studies, a 95% O_2/5% CO_2 gas mixture was used to perfuse the bath media. Periodic samples drawn from the bathing media confirmed this increased oxygenation but also revealed slightly acidic conditions (pH, 7.1-7.33, pO_2, 613-760 mmHg, pCO_2, 43-70 mmHg). However, previous studies

have demonstrated normal contractility of both smooth and striated muscle within this pH range [202, 203]. Additional discussion of this issue is provided within section 4.4.2.

3.2.2.2 Active and Passive Pressure-Diameter (P-D) Measurements. P-D responses for both active and passive states of the excised urethra were evaluated. For simplicity, an active tissue state herein refers to that following induced contraction of the urethral muscle components in either a separate or concurrent fashion. The passive state refers to the subsequent elimination of all induced contractions, as well as any endogenous tissue tone that may have also been present.

Activation of smooth and striated muscle components was based on the pharmacologic responsiveness of the tissue observed within section 3.1, resulting in three separate muscle activation protocols. For smooth muscle activation alone (n=9 total), Nω-Nitro-L-arginine (100μM) was first added to the tissue bath in order to eliminate endogenous NOS activity, which was previously observed within some isolated tissues. Following a 20 minute incubation period PE (40μM) was added to specifically stimulate smooth muscle contraction, which was verified through stabilization to a new and lower OD value. For tissues in which concurrent smooth and striated muscle activation was desired (n=8 total), an identical smooth muscle protocol was followed by the addition of ACh (5mM) immediately after verification of the PE-induced contraction. For striated muscle activation alone (n=10), sodium nitroprusside (10μM) was first added to the tissue bath for a period of 30 minutes, and dilation of the tissue to a new stable baseline OD was confirmed. To further eliminate the possibility of previously observed (section 3.1) cholinergic-induced smooth muscle activation, both atropine (1μM) and hexamethonium (100μM) were also added along with the sodium nitroprusside, prior to stimulation with ACh (5mM). In the presence of these antagonists, nicotinic-mediated striated muscle activation alone is ensured. A schematic of the various cholinergic-induced pathways is provided within Figure 3.7.

For all active tissue experiments, immediately following confirmation of contraction, the intralumenal pressure was increased from 0 to 20 mmHg at 2 mmHg increments. P-D data was collected at a 20 Hz sampling rate over a 10 second period for each 2 mmHg pressure step. The OD data was then averaged (20 Hz x 10 seconds = 200 data points) at each incremental pressure step to obtain discrete values associated with each applied pressure. The 20 mmHg pressure range utilized was selected based on previous reported mean values of female rat bladder pressure (3.4 kPa ≈ 25 mmHg) [204]. Pressure steps were applied through manual height adjustment of the fluid reservoir based on calibration markings (2 mmHg = 1.07 inches water), which were also separately verified with a

manometer. As the sensitivity of the pressure transducers could not accurately measure low pressure readings, the actual pressure values collected were only used to verify where step increases had occurred.

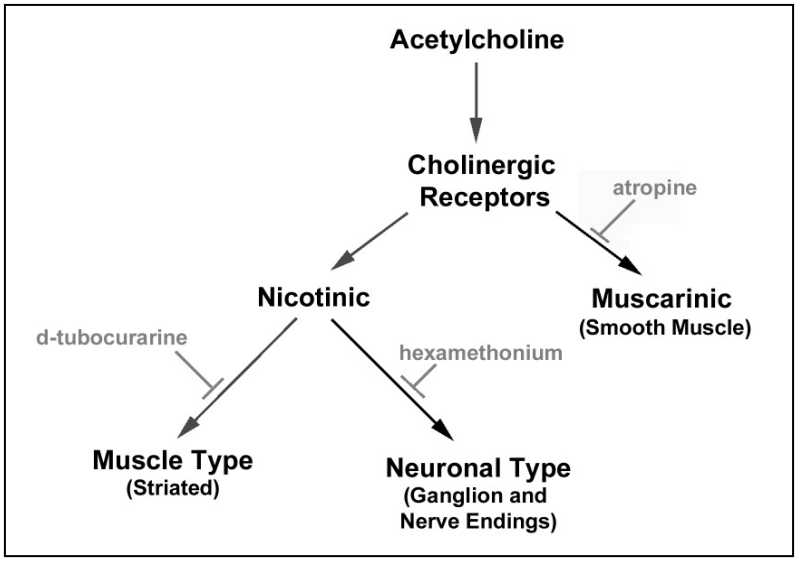

Figure 3.7 Mechanisms of potential ACh-induced muscle activation. Previous use of the blocking agents, detailed within section 3.1, confirm the specific nicotinic-mediated striated muscle activation produced by the protocol used to examine striated mechanics.

Immediately following collection of active-state data, a passive state devoid of muscle tone was induced by addition of EDTA (3mM final concentration) to the bath, allowing a 30 minute equilibration period for elimination of muscle activity based on previous observations. In order to minimize viscoelastic effects, a mechanical preconditioning protocol, consisting of 10 pressure cycles from 0 to 4 mmHg at 5 second increments, was performed prior to collection of the passive P-D data only (see Figure 3.8). Note that preconditioning was not performed prior to the collection of active-state data, and is commonly avoided in studies of active mechanics due to concerns of compromising contractile function with repetitive stretching [205-207]. Based on previous studies, this concern is greater for the striated muscle component than for smooth muscle [53, 208]. However, for studies involving striated muscle contraction, both preconditioning and subsequent testing would not be possible due to the limited duration of chemically-evoked maximal contraction (see Figure 3.9). Thus, aside from previous concerns reported in the literature, appropriate comparison of mechanics between smooth and striated muscle components dictated the omission of such a protocol in the active state.

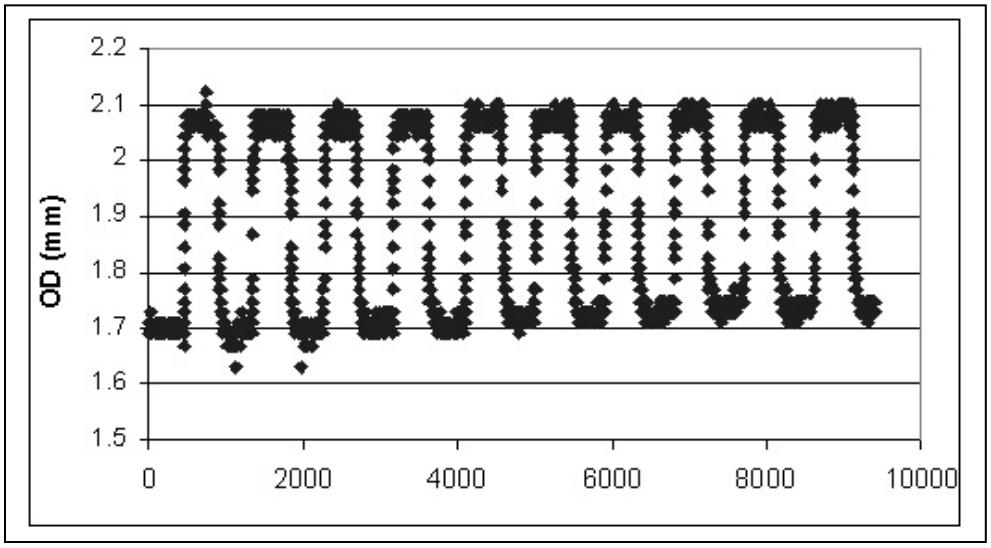

Figure 3.8 Preconditioning of passive tissue minimizes the viscoelastic stress relaxation effect, reflected as a shift toward a stable increased tissue OD with progressive pressure cycles.

Paired active and passive data was collected in this manner primarily within the mid region (laser positioned at 40-60% of axial length; corresponds to positioning within a region ~ 4-5 mm in length) for comparison between smooth and striated muscle responses. Several tissues were also evaluated at the distal region (laser positioned at 75% of axial length) in a deliberate attempt to obtain active responses corresponding to a wide range of striated muscle content (based on previous histological findings demonstrating decreased striated volume fraction from mid to distal axial locations; see Figure 3.5). All experiments were performed separately, in that tissue samples were used in the collection of only one set of paired active and passive P-D data.

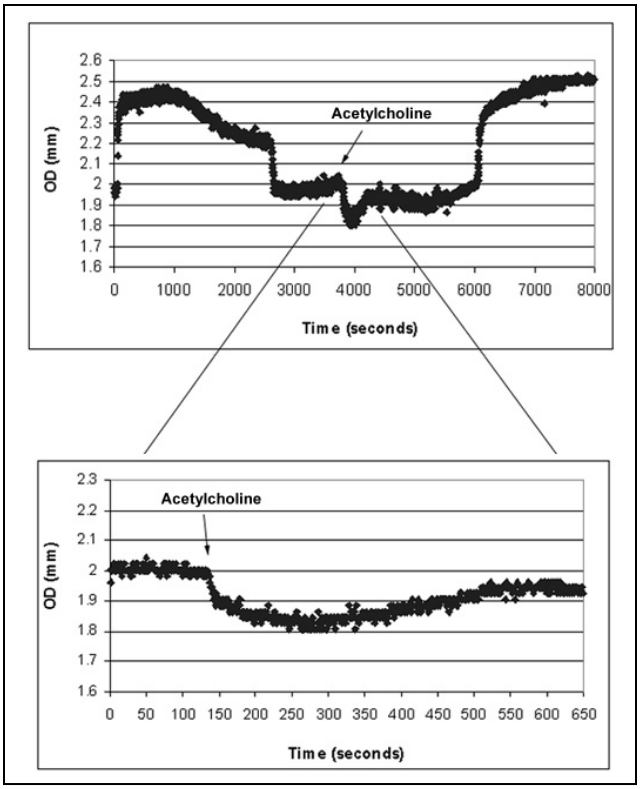

Figure 3.9 Typical duration of acetylcholine-induced maximal striated muscle contraction.

3.2.2.3 <u>Muscle Volume Fraction and Tissue Thickness</u>. Immediately following collection of P-D data, and prior to tissue removal for histological processing, the location at which the laser was positioned for OD measurements was identified by marking the outside of the tissue with a permanent ink pen. The local content of smooth and striated muscle at the axial point of measurement was determined through immunofluorescent labeling of fast and slow myosin heavy chain and α-smooth muscle actin, identical to that described in section 3.1.2.4. For each specimen, local muscle content and tissue thickness were determined by averaging values obtained from three cryosections taken near both ends and the middle of the marked segment of tissue (approximately 1 mm axial length), as described in equation 3.2 in section 3.1.2.5. Also in an identical manner, the actual tissue cross-sectional area (CSA) for each section was determined from the difference in the areas enclosed by manually-drawn borders of both the lumenal (CSA_{lumen}) and ablumenal (CSA_{total}) surfaces. Tissue thickness, h, was calculated as the difference between the estimated outer radius (R_o) and inner radius (R_i) based on these CSA measurements and an approximation of the tissue to a cylindrical geometry, as described in the following equations.

$$R_o = \sqrt{CSA_{total} / \pi} \quad [3.4]$$

$$R_i = \sqrt{CSA_{lumen} / \pi} \quad [3.5]$$

$$h = R_o - R_i \quad [3.6]$$

This tissue thickness, obtained at a reference pressure of 0 mmHg, was subsequently used in calculating the inner diameter and inner radius from OD data collected for each pressure step, as described in the following section.

3.2.2.4 Estimation of Innner Radius. The tissue inner radius, R_i, cannot be measured directly using the experimental apparatus described here. Therefore, application of the incompressibility assumption, which has previously been proven valid for similar arterial mechanics studies [209], allows for the estimation of R_i at each pressure step (P_x) based on corresponding OD measurements and from known tissue dimensions taken at a reference pressure (P_o= 0 mmHg). The outer radius (R_o) at this reference pressure was obtained directly from experimental OD measurements, and a corresponding R_i value was determined as the difference between this R_o and the tissue thickness, which was obtained from histology (tissue fixed at the 0 mmHg reference pressure) as described in section 3.2.2.3. Since the tissue was tethered at both ends, changes in axial length were not permitted. This constant tissue length, along with conservation of tissue volume, dictate that the tissue maintain a constant wall cross-sectional area (i.e. $WCSA_{Px} = WCSA_{Po}$). Thus, assuming an approximate cylindrical geometry yields the estimation of R_i at any pressure (R_{ipx}) based on the following equations.

$$\pi(R_o^2 - R_i^2)_{Px} = \pi(R_o^2 - R_i^2)_{Po} \quad [3.7]$$

$$R_{i_{Px}} = \sqrt{R_{o_{Px}}^2 - R_{o_{Po}}^2 + R_{i_{Po}}^2} \quad [3.8]$$

Previous estimations of R_i using these assumptions, specifically examined for various blood vessels over a wide range of pressure conditions, were found to be within a mean of less than 1% of actual R_i measurements [210]. Knowledge of R_i (estimated) and R_o (measured) for each pressure allows for additional characterization of tissue material properties, as discussed within sections 3.2.2.8-9.

3.2.2.5 Urethra Compliance. The bulk elastic tissue compliance was calculated for both the active and passive states. Compliance (C) is defined as the fractional change in lumenal volume that occurs in response to changes in pressure, approximated as

$$C = \left(\frac{D_{\max} - D_{\min}}{D_{\min}} \right) * \left(P_{\max} - P_{\min} \right)^{-1} \quad [3.9]$$

where D_{max} and D_{min} represent the measured diameters corresponding to the maximum and minimum pressures, P_{max} and P_{min}, used to define the range over which the compliance is calculated. Based on the true mathematical definition, the diameters used in this calculation should represent those of the inner lumen (ID). However, it has been previously established that the use of OD in these calculations, which is more amenable to direct measurement, does not result in significant deviations when compared to those obtained using ID; specifically, for cases in which the tissue thickness to radius ratio is small ($t/R \leq 0.05$) [211]. Compliance was calculated from both OD and ID separately, and this thin-wall assumption was investigated based on estimations of this ratio for the urethra.

For calculation of overall tissue compliance, diameters correspond to the maximum (P_{max}, 20 mmHg) and minimum (P_{min}, 0 mmHg) applied pressures, respectively. However, since the overall compliance parameter does not account for the differential responses seen at lower pressures, stepwise compliance over smaller pressure ranges was also examined. These stepwise compliance values were determined in an identical manner, where the diameters correspond to the maximum and minimum pressure values taken at 4 mmHg incremental pressure ranges (0-4 mmHg, 4-8 mmHg, etc.).

3.2.2.6 <u>Beta (β)-Stiffness</u>. Compliance can be used to quantitatively express the relative level of tissue stiffness, but must be carefully defined according to the pressure range over which it applies. This is due to the highly non-linear nature of soft tissue P-D responses that generally result in rapid changes in such values. In an attempt to overcome this non-linearity, a dimensionless stiffness parameter (β) has been defined and has been frequently used in the study of blood vessel biomechanics [181]. This single parameter has been used to describe the structural stiffness of vessels and, unlike compliance, incorporates all of the measured P-D values over the range of physiologic pressure examined. It is defined as follows:

$$\ln\left(\frac{P}{P_s} \right) = \beta \left(\frac{D}{D_s} - 1 \right) \quad [3.10]$$

where P_s and D_s are a user-defined standard pressure and corresponding diameter, respectively, which is chosen by the investigator to be within the average physiologic pressure range. P and D are the paired pressure and corresponding measured diameter. $Ln(P/P_s)$ is plotted versus $(D/D_s - 1)$, and β-values are determined from the fitted slope of this linearized data. For the β-stiffness values presented, standard pressure and corresponding OD were

taken at 8 mmHg, and linear regression was performed using Excel. This standard pressure generally resulted in the best linear fit, as determined by r^2 values. It should be noted that the first pressure step (from 0-2 mmHg) has no influence on the estimation of this parameter (since ln 0 is undefined).

It is apparent that, as a consequence of the logarithmic transformation of the P-D data, reasonable β-values can only be obtained for tissues that exhibit exponential P-D responses (based on reasonable fit to linear regression). This limited the use of the β-stiffness parameter primarily to comparison of passive tissue state responses. For tissues in which muscle activity was evoked, a generally poor fit was observed due to the tissues ability to resist deformation at the lower applied pressures.

3.2.2.7 Muscle Contraction Parameters. Parameters descriptive of the relative contractile function of the active muscle element(s) over the entire applied pressure range were also obtained from the P-D data. A measure of muscle contraction capacity can be obtained from areas related to the respective active and passive P-D data curves (Figure 3.10A). The ratio of the area between the active and passive curves (A1) to the area under the passive curve alone (A2), termed the total contraction capacity (TCC), may be considered as the relative ratio in the work performed by the activated muscle to the elastic energy stored by the passive elements of the tissue alone [207]. In order to calculate these areas, the OD data was normalized to the initial diameter value (i.e. $D/D_0=1.0$ at P=0 mmHg) to obtain a common starting point. Each set of active and passive P-D data was then fit separately to a third-order polynomial function ($y=ax^3+bx^2+cx+d$) using non-linear regression (SigmaStat, v2.0). This regression uses an iterative algorithm (Marquardt-Levenberg) resulting in the 'best-fit' values for each coefficient (a,b,c,d) through the minimization of the sum of the squared differences between the observed and predicted values for the dependent variable (y, pressure). Fitting to an exponential function was also attempted, particularly for the passive data, but often did not converge and displayed a lower overall fit compared to the polynomial function ($r^2<0.96$ vs. $r^2>0.99$). Once the coefficients were determined the function describing the P-D curve was integrated, over the same normalized-diameter range for each paired passive and active data set, to obtain the representative areas under each respective fitted-curve. The lower limit was taken to be the initial normalized diameter starting point (i.e. 1.0), and the upper limit taken to be the maximum active normalized diameter value (at P=20 mmHg). Since the active tissue deformed to a lesser degree than the passive, this maximum active normalized diameter was chosen as the upper integration limit so that the active curve did not have to be extrapolated.

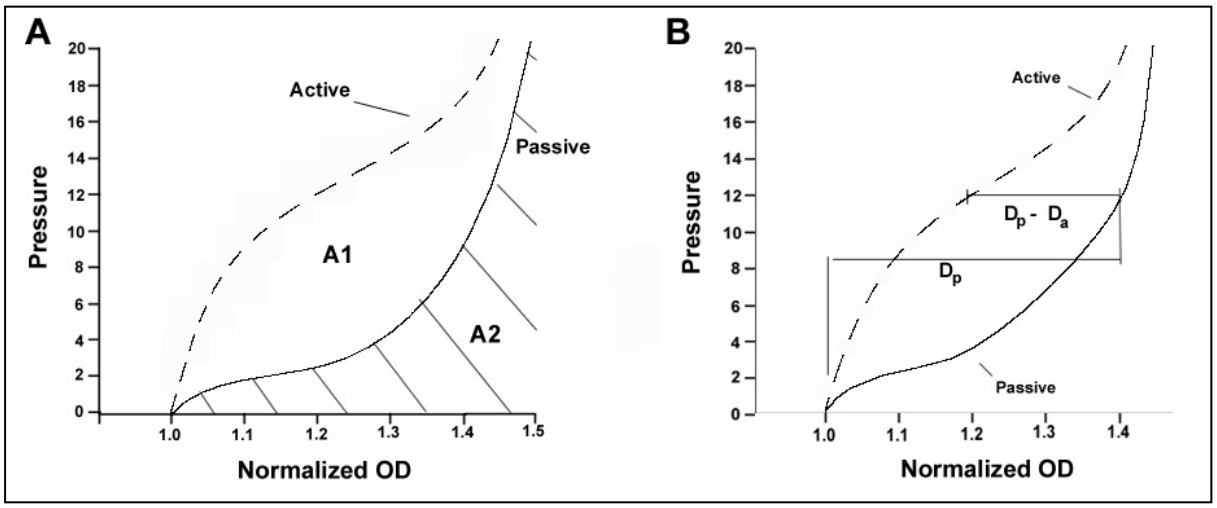

Figure 3.10 Illustration of two measures of contractile function obtained from pressure-diameter data. The contraction capacity (A) is a single dimensionless value representative of the ratio of the total area produced by muscle contraction (A1) to the total area produced by the passive tissue alone (A2) over the entire pressure range. The functional contraction ratio (B), computed separately for each applied pressure, defines the dimensionless ratio of the normalized distance between the active and passive tissue created by the muscle contraction relative to the passive distance. Adapted from [207].

A separate measure of relative contraction was also obtained from the P-D responses. The difference between the measured passive and active diameters, for a given pressure, provides an indication of the relative degree of isobaric contraction for a given muscle component(s). The functional contraction ratio (FCR) was previously defined as the difference between the passive and active diameters (D_p-D_a) relative to the passive diameter (D_p) [207], as shown in Figure 3.10B. This ratio (D_p-D_a/D_p) was calculated for each pressure step from the normalized P-D data for each tissue activation state as a measure of the relative pressure dependence on the contraction capacity.

3.2.2.8 <u>Conversion to Stress/Strain and Estimation of Maximum Stress Generation</u>. The parameters described in sections 3.2.2.5-7 may provide useful information for characterizing relative tissue specimen properties, such as active- and passive-state stiffness. However, these descriptive parameters do not account for the thickness of the tissue wall, and as a consequence are not rigorous representations of the inherent material properties of the tissue. In the experimental system described here, variations in tissue thickness from both known (axial position) and potential (tissue dissection technique) sources may influence the value of such parameters. Thus, a more complete biomechanical characterization is obtained by accounting for changes in specimen geometry for all applied stress

(pressure) conditions. This allows for the description of the innate material properties of the tissue and associated stress-strain behavior which, by mathematical definition, are independent of such concerns.

As briefly mentioned in section 3.2.2.5, a number of simplifying assumptions can be made for cases in which t/r <0.05-0.1. For such cases, the tissue may be treated mathematically as a thin-walled vessel in which variations of tissue stresses in the radial direction (i.e. within the wall of the tissue) may be neglected. However, for the urethra preparation described here t/r was generally greater than 0.5, and thus appropriate characterization requires that stresses be defined with respect to their radial position. Circumferential stress (σ_θ) within a thick-walled, linearly elastic, isotropic cylinder as a function of any radial position (r) within the wall has been previously derived and is given below:

$$\sigma_\theta = P\left(\frac{R_i^2}{R_o^2 - R_i^2}\right)\left(1 + \frac{R_o^2}{r^2}\right) \qquad [3.11]$$

where P is the internal (transmural) pressure and R_i and R_o are the previously defined estimated and measured inner and outer radius, respectively. Along with the equation describing radial stress distribution, these relationships are collectively known as the Lame equations [211]. Derivation of equation 3.11 from a force balance in the radial direction is provided within Appendix A. Circumferential engineering strain, ε_θ, is defined from the change in a given radius (Δr) from its initial position (r_o) as follows.

$$\varepsilon_\theta = \frac{2\pi(r_o + \Delta r) - 2\pi r_o}{2\pi r_o} = \frac{\Delta r}{r_o} \qquad [3.12]$$

Using these equations, urethra mid-wall $\sigma_\theta/\varepsilon_\theta$ responses were calculated and this information was subsequently used to determine the maximum stress generated by each activated muscle component. Since conversion of the data did not result in coinciding active and passive values for either σ_θ or ε_θ, non-linear regression was used to fit the data to either an exponential ($y=a*\exp^{bx}$; active striated and all passive responses) or a third-order polynomial function ($y=ax^3+bx^2+cx$; active smooth and smooth-striated responses), again using SigmatStat. Maximum σ_θ generated by the active muscle component alone for each tissue was determined as the maximum difference between the active and passive fitted σ_θ values, determined at 0.02 strain intervals. Fitted $\sigma_\theta/\varepsilon_\theta$ responses, and subsequent estimation of maximum σ_θ, were performed within the limits of the experimentally-observed strain range (i.e. no extrapolation).

3.2.2.9 Incremental Elastic Modulus. Due to the large and non-linear deformations exhibited by the urethra, adequate mechanical descriptions of σ/ε behavior may be appropriately performed using incremental parameters. Incremental elastic moduli can be used to relate smaller changes in strain with corresponding changes in stress using classic linear theories of mechanics by segmenting the overall large deformation response into a series of small deformations. An expression for incremental elastic modulus was developed by Hudetz [212] in order to characterize the elastic stiffness of an axisymmetric, cylindrical orthotropic and incompressible vessel in which the axial length is held constant:

$$E_{inc} = \frac{\Delta P}{\Delta R_o}\frac{2R_i^2 R_o}{R_o^2 - R_i^2} + \frac{2PR_o^2}{R_o^2 - R_i^2} \qquad [3.13]$$

where ΔP and ΔR_o are the incremental changes in transmural pressure and outer radius. R_i, R_o and P are the inner and outer radius and pressure at the beginning of the increment, respectively. Importantly, this expression incorporates a necessary correction (second term) for the presence of initial stress when defining the moduli, which was absent from earlier incremental models based solely on Young's modulus as defined by classic linear theory [213] Absence of this term can lead to underestimation of stiffness [212]. The modulus defined by equation 3.13 complexly characterizes both the radial and circumferential stiffness as a single material constant. It is used here to quantify the effect of muscle activation on the composite stiffness of the urethra with regard to 2 mmHg incremental increases in intralumenal pressure.

3.2.2.10 Animals. All animals were housed in either the Rangos Research Center Animal Facility of the Children's Hospital of Pittsburgh or at the University of Pittsburgh Biomedical Science Tower under the supervision of the Department of Laboratory Animal Resources. The policies and procedures of the animal laboratory are in accordance with those detailed in the guide for the "Care and Use of Laboratory Animals" published by the US Department of Health and Human Services. Protocols used for these experiments were approved by the Animal Research and Care Committee of the Children's Hospital of Pittsburgh and the Institutional Animal Care and Use Committee of the University of Pittsburgh (Protocols 24/01 and 0208766, respectively).

3.2.2.11 Statistical Analysis. Comparison of parameters between active and corresponding passive tissue states was performed using paired Student's t-test, or the equivalent non-parametric Wilcoxon signed rank test. This included comparisons between the following measured and calculated parameters: OD and ID at each pressure, overall and stepwise compliance, and incremental modulus at specified pressure ranges. Comparison of parameters

among active tissue states (smooth, striated, and smooth-striated), or separately among passive tissue states, were performed using using one-way ANOVA with Student-Newman-Keuls post-hoc pairwise comparisons, or the equivalent nonparametric ANOVA on ranks with Dunn's post hoc analysis. This included comparisons of: overall and stepwise compliance, β-stiffness, total contraction capacity (TCC), functional contraction ratio (FCR) at each applied pressure (separately), and incremental modulus at each pressure range (separately). The Pearson Product Moment was used to determine the strength of association between local striated muscle content and the TCC and maximum generated stress. p-values less than 0.05 are reported as significant, and data is expressed as mean ± SEM. All comparisons were performed using SigmaStat (v2.0; Jandel Scientific) statistical software.

3.2.3 Results

3.2.3.1 Pressure-Diameter Responses. Average P-D plots displaying responses collected within the mid region for all three active muscle states (smooth only, n=8; striated only, n=6; and smooth-striated, n=6), and their corresponding passive state, are provided within Figures 3.11 and 3.12. Plots based on measured OD responses (Figure 3.11) are qualitatively similar to those based on estimated ID responses (Figure 3.12), however they are quantitatively distinct in terms of the relative deformation occurring at the outer and inner surfaces of the tissue respectively. Significantly lower measured OD values were observed for tissues in which the smooth muscle component was activated for all applied pressures in comparison to paired passive responses (Figure 3.11A). Striated muscle activation alone (Figure 3.11B) resulted in significantly lower values from 4-16 mmHg (p=0.058, 2 mmHg; 0.063, 18 mmHg; 0.156, 20 mmHg), and combined smooth and striated activation (Figure 3.11C) resulted in significantly lower values at all applied pressures with the exception of the lowest applied pressure (p=0.063, 2 mmHg). Examining these same responses in terms of estimated ID, activation of smooth muscle (Figure 3.12A) exerted a significant influence over the 0-14 mmHg pressure range (p=0.139, 16 mmHg; 0.229, 18 mmHg; 0.293, 20 mmHg). However with striated muscle activation alone (Figure 3.12B), a significant difference was observed only at 4 mmHg (p=0.053, 2 mmHg; and 0.063, 0.063, 0.313, 1.00, 0.688, 0.563, 0.438, 0.438 from 6-20 mmHg, respectively). Activation of both muscle components (Figure 3.12C) demonstrated significant differences in ID from 4-12 mmHg (p=0.063, 2 mmHg; 0.057, 0.362, 0.657, 0.679 from 14-20 mmHg, respectively).

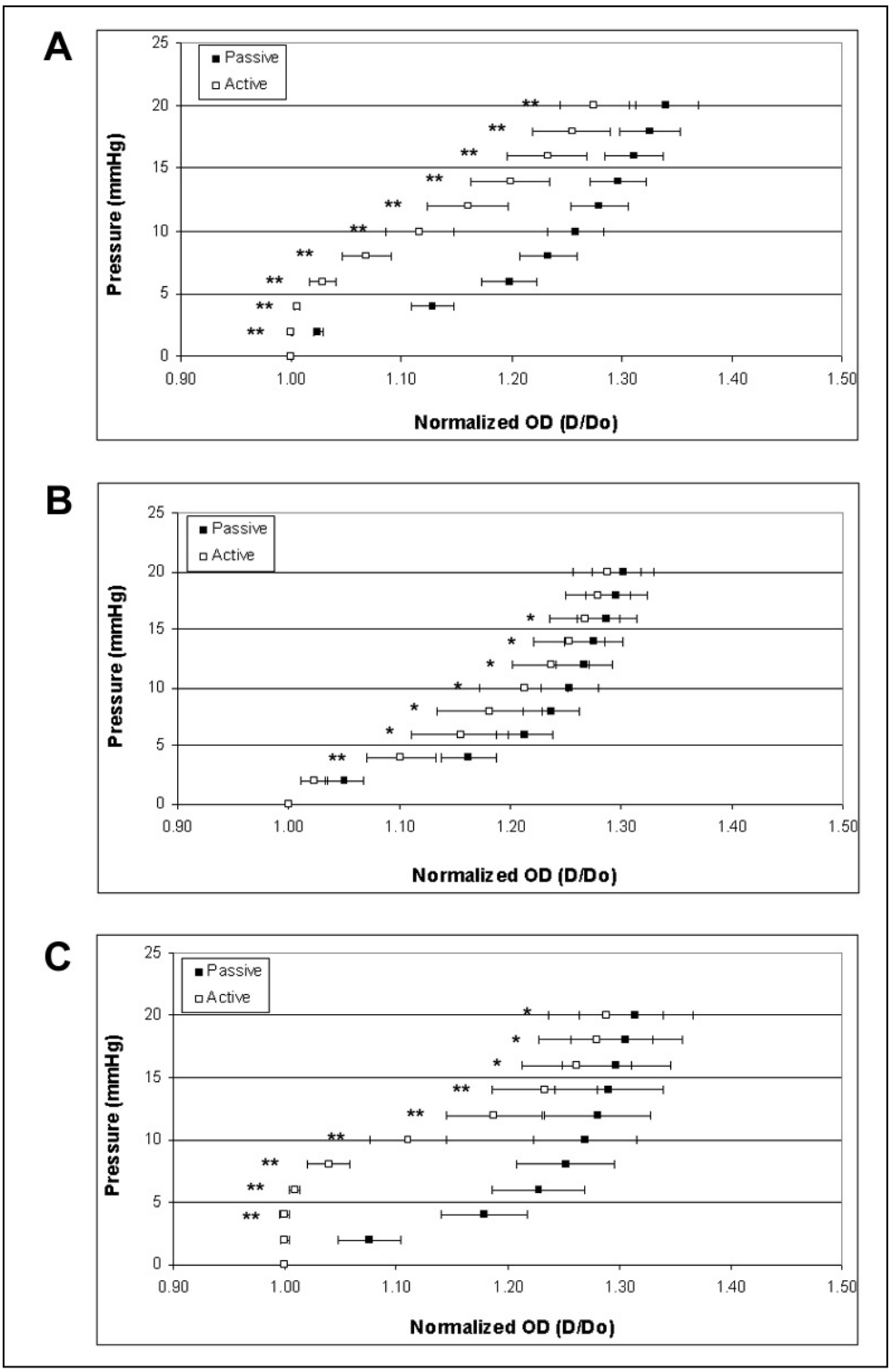

Figure 3.11 Average pressure versus normalized outer diameter (OD) responses. Active tissue responses in the presence of smooth muscle activity alone (A), striated muscle activity alone (B), and combined smooth and striated muscle activity (C). (*$p<0.05$, **$p<0.01$)

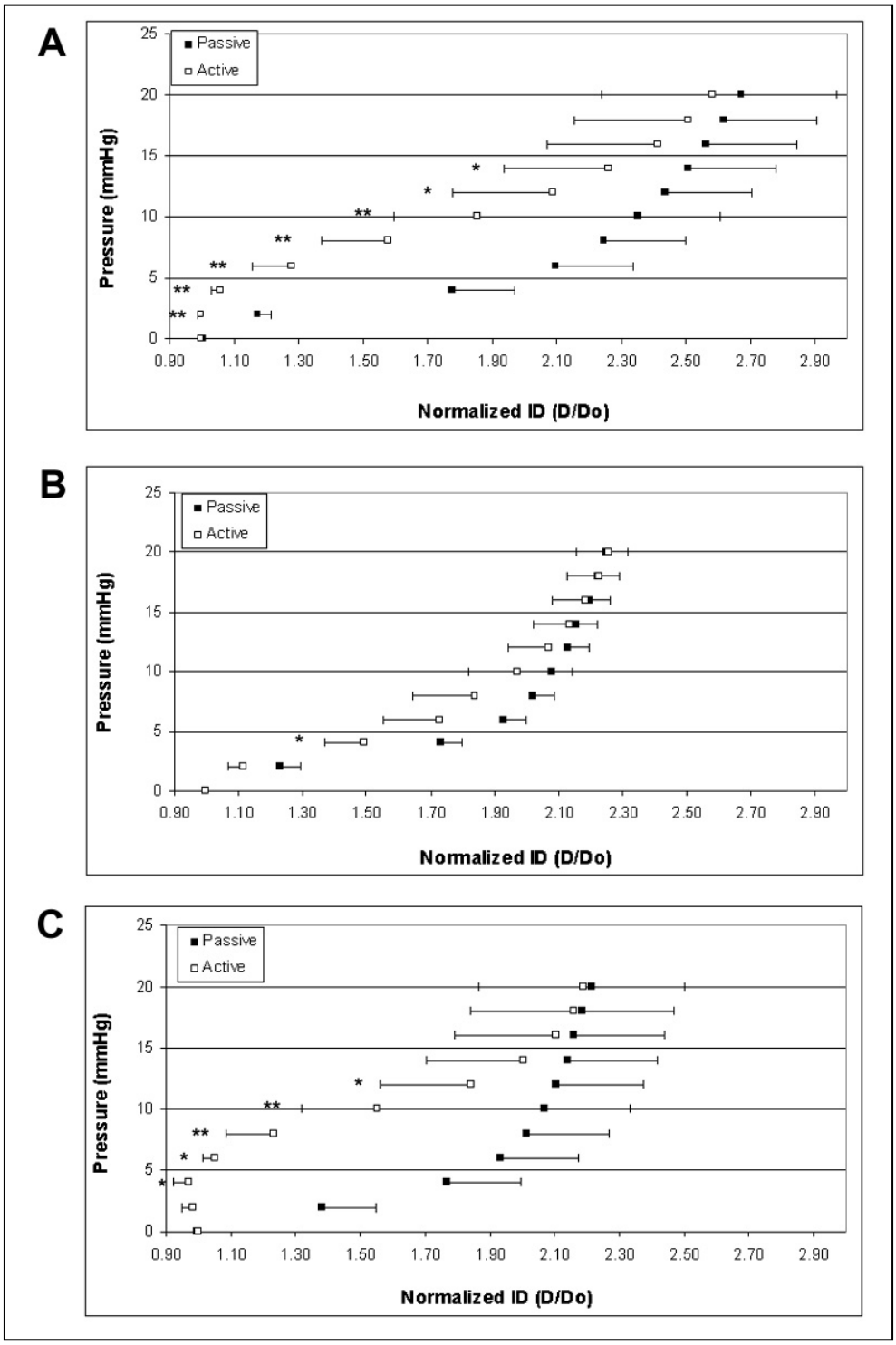

Figure 3.12 Average pressure versus normalized inner diameter (ID) responses. Active tissue responses in the presence of smooth muscle activity alone (A), striated muscle activity alone (B), and combined smooth and striated muscle activity (C). (*$p<0.05$, **$p<0.01$)

3.2.3.2 Compliance. It is apparent that the mid region P-D responses in either state are highly non-linear, an expected response from soft tissue. With the muscle components activated, the P-D curve is sigmoidal in shape as the tissue resists deformation at the initial applied pressure steps. This response is much more pronounced in the presence of smooth muscle activation. In contrast, following elimination of muscle-induced tone with calcium chelation (EDTA), an immediate and large deformation is seen even at the low applied pressures, with a progressive stiffening as pressure is increased. Quantitative description of these P-D responses can be performed by comparing measures of tissue compliance (Tables 3.1-3.3).

Table 3.1 Overall (0-18 mmHg) and stepwise compliance (4 mmHg increments) values for urethra tissue with smooth muscle activated (active), and following elimination of all muscle activity (passive). Values listed are means ± SEM (x 10^{-3} $mmHg^{-1}$).

Smooth Muscle	**Outer Diameter (OD)**			**Inner Diameter (ID)**		**Significance**
Pressure Range (mmHg)	**Active**	**Passive**	**Significance Active vs. Passive**	**Active**	**Passive**	**(p-value) Active vs. Passive**
0 - 20	14±2	17±1	<0.01	79±17	84±15	0.332
0 - 4	1±1	31±5	<0.01	15±7	194±48	<0.01
4 - 8	16±5	23±2	0.240	119±43	66±10	0.266
8 - 12	21±4	10±2	<0.05	75±15	22±6	<0.01
12 - 16	16±3	6±2	<0.01	42±8	13±3	<0.01
16 - 20	9±3	6±1	0.547	21±8	11±3	0.109

Table 3.2 Overall (0-18 mmHg) and stepwise compliance (4 mmHg increments) values for urethra tissue with striated muscle activated (active), and following elimination of all muscle activity (passive). Values listed are means ± SEM (x 10^{-3} $mmHg^{-1}$).

Striated Muscle	**Outer Diameter (OD)**			**Inner Diameter (ID)**		**Significance**
Pressure Range (mmHg)	**Active**	**Passive**	**Significance Active vs. Passive**	**Active**	**Passive**	**(p-value) Active vs. Passive**
0 - 20	14±1	15±1	0.156	63±5	62±3	0.438
0 - 4	25±7	41±6	<0.01	123±28	183±15	<0.05
4 - 8	18±4	16±1	0.438	54±14	42±4	0.482
8 - 12	12±4	6±1	<0.05	45±24	14±2	<0.05
12 - 16	6±2	4±0.4	<0.05	15±5	8±1	<0.05
16 - 20	4±0.4	3±0.1	<0.05	9±1	6±0.4	<0.05

Table 3.3 Overall (0-18 mmHg) and stepwise compliance (4 mmHg increments) values for urethra tissue with both smooth and striated muscle activated (active), and following elimination of all muscle activity (passive). Values listed are means ± SEM (x 10^{-3} $mmHg^{-1}$).

Smooth/Striated Muscle	**Outer Diameter (OD)**			**Inner Diameter (ID)**		**Significance**
Pressure Range (mmHg)	**Active**	**Passive**	**Significance Active vs. Passive**	**Active**	**Passive**	**(p-value) Active vs. Passive**
0 - 20	14±3	16±3	<0.05	60±16	61±15	0.533
0 - 4	0.1±1	45±10	<0.01	-7±12	194±59	<0.05
4 - 8	10±6	15±2	0.406	82±65	35±4	0.563
8 - 12	36±6	6±1	<0.01	120±18	11±1	<0.01
12 - 16	16±2	3±0.3	<0.05	36±5	7±1	<0.01
16 - 20	5±0.4	3±0.2	<0.05	10±1	6±0.3	<0.01

As mentioned in section 3.2.2.5, the use of OD measurements in determining compliance is dependent upon an assumption of a thin tissue wall (t/r ratios <0.05-0.1). Estimated t/r ratios for tissues investigated here are well beyond the thin-walled assumption limits (by data set: smooth, 0.60±0.04; striated, 0.53±0.02; smooth-striated, 0.56±0.02; estimates based on passive R_o at p=0 mmHg). As a result, the OD and ID calculated compliance values differ by as much as an order of magnitude, although this only minimally influenced statistical comparisons between

the passive and active tissue states (differences noted: smooth, 0-20 mmHg, and smooth-striated, 0-20 mmHg; changed from significant to non-significant in each case). Nonetheless, the ID-based compliance values are more representative of the true mathematical definition, and thus are used for statistical comparisons. No difference in ID overall (0-20 mmHg) compliance values were observed between the paired active and passive states regardless of muscle component activation. In addition, no difference in these overall values were observed through multiple comparison of the various active tissue states ($p=0.596$). Stepwise compliance demonstrates a differential response between all active and corresponding passive states within the 0-4 mmHg range. Also within this range, by multiple comparison, a significantly lower compliance is observed for tissue in which both smooth and striated muscle were activated compared to striated activation alone. No difference in stepwise compliance between any active and passive states were observed for the 4-8 mmHg range, although it is obvious from the P-D curves that significant differences exist in the degree of deformation that has occurred to this point. The net negative value for the smooth-striated tissue is representative of the tissue decreasing its ID in response to the initial applied pressures. By multiple comparison, there was no difference among active tissue compliance within the 4-8 mmHg range ($p=0.598$). By 8-12 mmHg of applied intralumenal pressure the passive tissue, which has already undergone a large deformation, continues its rapid stiffening while the active tissue begins to rapidly lose its ability to resist deformation (particularly for both smooth muscle-activated sets of tissues). Thus compliance values within this range are significantly lower for the passive tissue compared to paired active responses for all muscle activation states. This behavior continues for the remainder of the pressure ranges, as tissues in both the active or passive states exhibit decreases in compliance. Significantly lower values are observed within each compliance range for the passive state for comparisons above 8 mmHg (with one exception, active smooth muscle alone from 16-20 mmHg). Multiple comparisons among all active tissues revealed only a significant difference between smooth muscle alone and striated muscle alone within the 12-16 mmHg range.

Comparison of passive compliance values among the three muscle activation protocols used was performed as a measure of the uniformity of the passive state responses, regardless of prior muscle activation. No difference in overall compliance was observed among passive tissues ($p=0.429$), however a few significant differences among stepwise comparisons were noted (smooth vs. smooth-striated passive tissues for 4-8 and 8-12 mmHg).

3.2.3.3 β-stiffness. The average β-stiffness parameters, which incorporate all of the P-D data points over the pressure range examined, were not different among passive tissues regardless of prior muscle activation ($p=0.226$;

smooth muscle only, 10.1±1.1; striated muscle only, 11.6±0.4; and smooth-striated muscle, 12.7±1.2). The transformed passive data from which the β-stiffness was obtained exhibited a good linear fit (r^2; smooth, 0.966±0.013; striated, 0.957±0.006; smooth-striated, 0.961±0.007) which passed through the origin, corresponding to the chosen standard pressure (8 mmHg). In contrast, attempts to transform the active state data, particularly in the presence of smooth muscle activity, was less successful (r^2; smooth, 0.797±0.057; smooth-striated, 0.790±0.018) due to the overall non-exponential P-D responses caused by the strong initial resistance to deformation at low pressures (Figure 3.13). An optimal linear fit would pass through the origin, occurring at the reference pressure data point. A more reasonable fit was observed for striated muscle activity alone (r^2, 0.932±0.030), however the influence of the muscle seen at low pressures was not reflected in this stiffness parameter (β = 9.7±0.8).

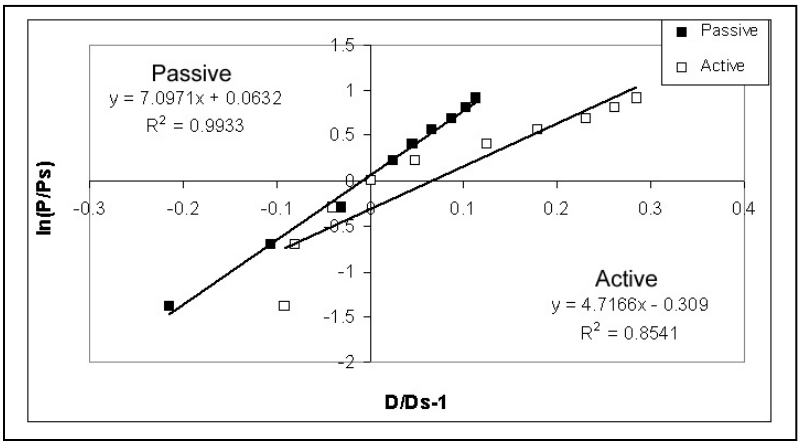

Figure 3.13 Transformation and linear regression of P-D data from a smooth muscle-active and corresponding passive tissue state, for estimation of β-stiffness.

3.2.3.4 **Contraction Capacity**. The relative difference between the mid region P-D passive and active responses (Figures 3.11-3.12) is not easily appreciated through description of the data by compliance values, and further could not be reasonably obtained from β-values with its requisite exponential response. From the P-D data, a single quantitative parameter (TCC) representative of contractile function over the entire pressure range was examined. In order to obtain this parameter, non-linear regression to fit the active and passive data to a third-order polynomial function was performed (r^2: striated, 0.977±0.020 and 0.996±0.001; smooth, 0.954±0.013 and 0.994±0.002; smooth-striated, 0.941±0.015 and 0.993±0.002, for active and passive data fits, respectively). By multiple comparison a

significant difference in contraction, as defined by TCC (Figure 3.14A), was observed between tissues in which striated muscle alone was activated compared to those in which both smooth and striated muscle was activated (striated, 0.43±0.19; smooth, 1.35±0.29; smooth-striated, 1.82±0.46). No such difference was apparent for smooth muscle-activated tissues in the presence or absence of striated muscle activity.

The FCR parameter allows comparison of contractile function between the activated muscle elements at each applied pressure step (Figure 3.14B). Defined by this parameter, both striated and smooth muscle exhibit their maximal influence within approximately the same pressure range (from 4 to 8 mmHg). However smooth muscle activation, either with or without concomitant striated activity, resulted in a significantly increased contraction within the 4 to 14 mmHg range, and again at 20 mmHg, in comparison to striated activation alone (non-significant multiple comparisons: p=0.141, 0.051, and 0.055 at 2, 16, and 18 mmHg, respectively). No detectable difference for smooth muscle activated tissues in the presence or absence of striated muscle activity was observed.

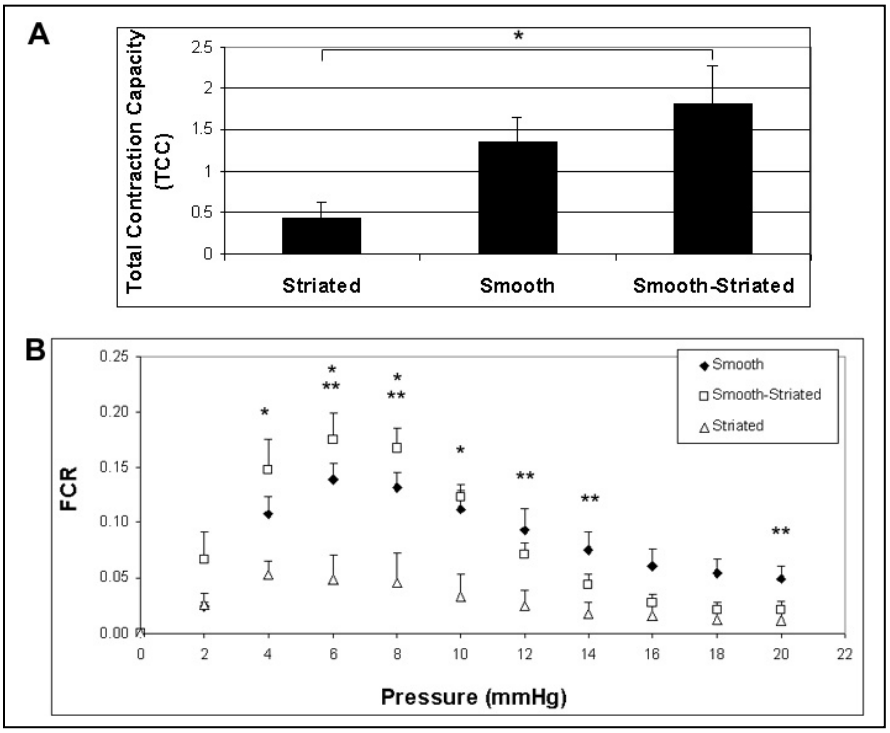

Figure 3.14 P-D-derived measures of relative muscle contractile function within the mid region over the entire applied pressure range (A), or at each pressure individually (B). (A: *, $p<0.05$ striated vs. smooth striated; B: *, $p<0.05$ striated vs. smooth-striated, and **, $p<0.05$ striated vs. smooth)

3.2.3.5 Maximum Stress Generation. Mid-wall $\sigma_\theta/\varepsilon_\theta$ responses obtained directly from experimental measurements (at both mid and distal regions) for all activated, and corresponding passive, tissue states are provided within Appendix B. The mid region data was used to calculate the maximum circumferential stress generated by each muscle component through a fit of these responses to either exponential or third-order polynomial functions. The best fit for tissue with active striated muscle, as well as all passive tissues, was obtained using an exponential function (r^2: striated active, 0.994±0.003; striated passive, 0.996±0.001; smooth passive, 0.993±0.002; smooth-striated passive, 0.995±0.001), whereas the best fit for smooth and smooth-striated active tissues was obtained using the polynomial function (0.985±0.007 and 0.987±0.004). An example of fitted passive and active $\sigma_\theta/\varepsilon_\theta$ data for each of the activation protocols is shown in Figure 3.15. Also shown is the difference between these responses, which is representative of that which would be observed from the activated muscle component alone. From the striated-only, smooth-only, and smooth-striated tissues, the average maximum σ_θ determined in this manner was 748±379, 2229±409, and 2335±239 N/m^2, occurring at a similar degree of mid-wall strain for each (ε_θ=0.42±0.04, 0.47±0.08, and 0.40±0.10, respectively). In addition, the presence of active smooth muscle allowed the tissue to generate a substantial amount of stress at a low, and wider range of, strain.

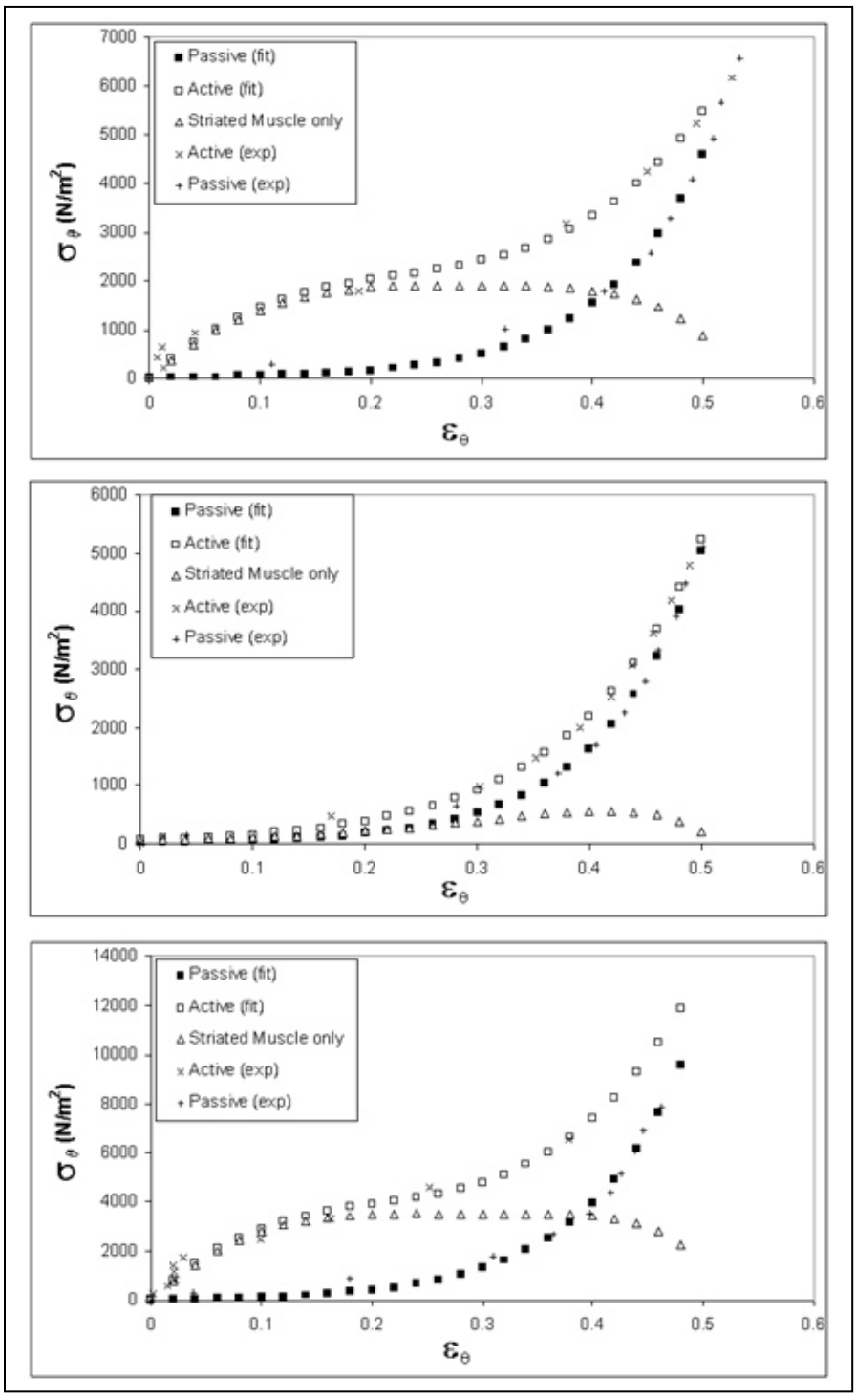

Figure 3.15 Examples of fitted passive and active mid-wall circumferential stress(σ_θ)-strain (ε_θ) responses, and corresponding active muscle-only responses, for the three activation protocols: smooth only (top), striated-only (middle), and smooth-striated (bottom).

3.2.3.6 Incremental Elastic Modulus. From examining the $\sigma_\theta/\varepsilon_\theta$ responses (contained within Appendix B), it is apparent that the muscle-activated tissues exhibit a stiffer response at low strains when compared to their corresponding induced passive states. In fact, in several instances, contraction of the tissue against the lower applied pressures resulted in a net negative slope seen in both the P-D and corresponding $\sigma_\theta/\varepsilon_\theta$ plots. This resulted in a negative incremental modulus (E_{inc}) for these tissues, which does not correspond to any physical meaning in terms of mechanical properties. For this reason, average modulus values for the first 8 mmHg are excluded from this discussion.

Average E_{inc}, determined at 2 mmHg pressure increments, was lower for active tissues compared to corresponding passive tissues regardless of the muscle component activated for all pressures greater than 8 mmHg (Figure 3.16). This reflects the rapid stiffening of passive tissues at higher pressures, also observed in measures of compliance presented earlier. The presence of activated striated muscle significantly affected the E_{inc} of the tissue at pressures up to 14 mmHg ($p=0.327$, 0.144, 0.889 vs. passive tissue at 14-16, 16-18, and 18-20 mmHg, respectively). In contrast, the presence of activated smooth muscle had a significant influence on E_{inc} values up to 16 mmHg for smooth muscle alone, and up to 18 mmHg for both smooth and striated activation ($p=0.315$, 0.084 for smooth only at 16-18 and 18-20 mmHg; $p=0.398$ for smooth-striated at 18-20 mmHg). Striated muscle-activated tissues demonstrated significantly higher values than both smooth and smooth-striated activated tissues from 8-14 and 18-20 mmHg ($p=0.393$ and 0.874, at 14-16 and 16-18 mmHg, respectively). This is representative of the more rapid stiffening of the striated activated tissues, due to the lower initial resistance to deformation imparted by the striated component. Multiple comparison of E_{inc} values among all passive tissues demonstrated the uniformity of these responses regardless of prior muscle activation (only significant difference, smooth vs. smooth-striated from 10-12 mmHg; $p=0.110$, 0.314, 0.109, 0.112, 0.338 for remaining pressure increments, respectively). This verifies that the differences observed between the various activated muscle states of the tissue was not due to underlying differences in passive responses.

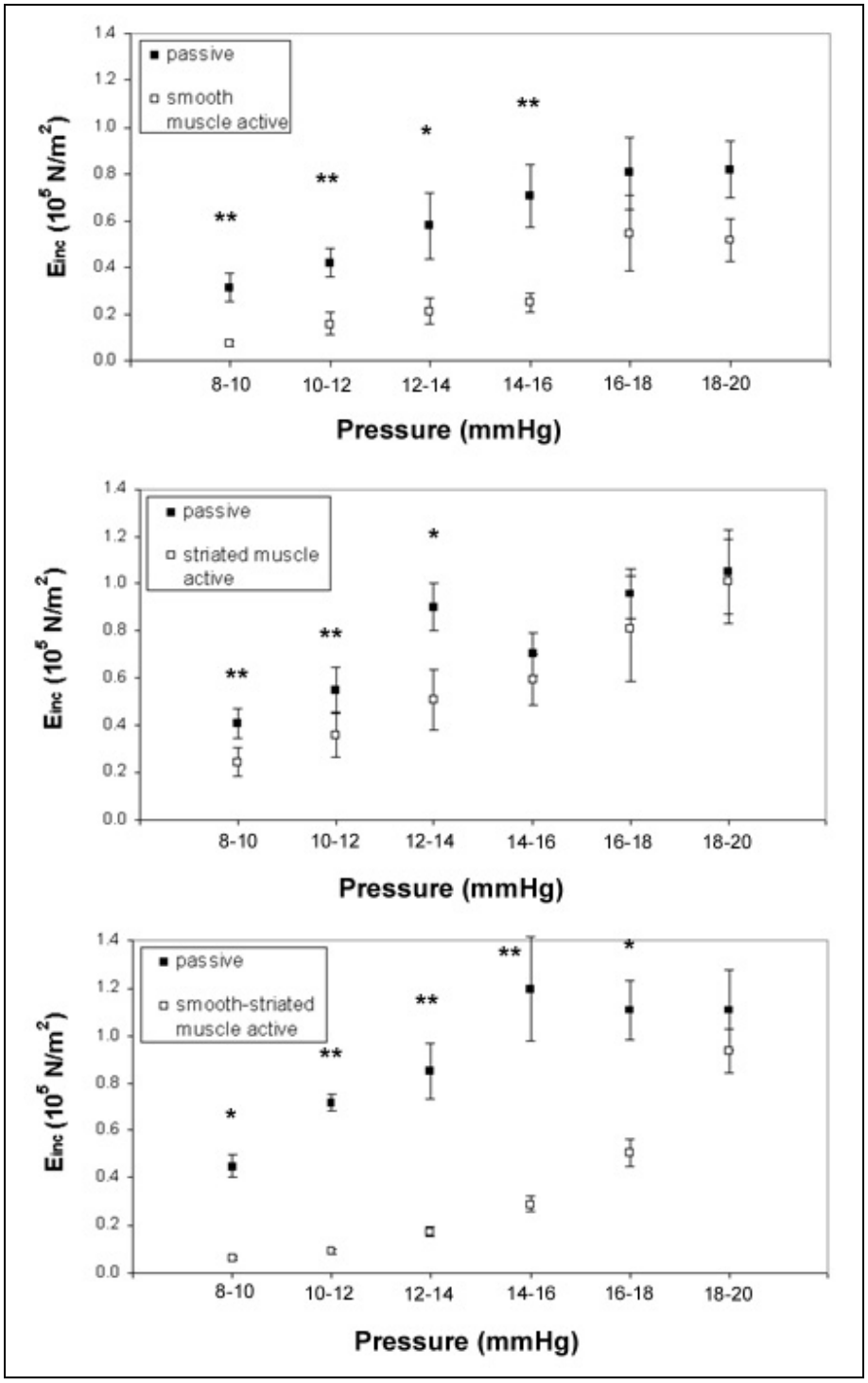

Figure 3.16 Incremental elastic modulus, E_{inc}, for smooth (top), striated (middle), and smooth-striated (bottom) activated tissues and their corresponding induced passive state, taken at 2 mmHg increments. *p<0.05, **p<0.01.

3.2.3.7 Regional P-D Responses and Muscle Orientation. Thus far, only the mid region has been considered in the biomechanical characterization of the urethra. Experiments utilizing the three muscle activation protocols were also performed at the distal axial region of the urethra, to examine potential consequences from changing anatomical structure (specifically, striated muscle content).

In response to increasing intralumenal pressure within the distal region, activation of striated muscle alone again resulted in some initial resistance to deformation (Figure 3.17A), similar to that seen at the mid region. However, a shift in this response to that of active dilation, reflected as a crossing of the active and passive P-D curves, was observed near 4-6 mmHg. Subsequent examination of distal region responses for tissues in which smooth muscle alone (Figure 3.17B), or in which both smooth and striated muscle (Figure 3.17C) was activated, revealed a similar behavior. The switch from active closure to active opening for these tissues occurred at an applied pressure near 10 mmHg. It should also be noted that the distal passive responses appear to be somewhat stiffer, reaching maximum normalized diameters of ~1.2, compared to those within the mid region.

Due to the highly variable responses observed between the mid and distal regions, muscle fiber orientation was examined more closely. As demonstrated in Figure 3.18, and as previously discussed within section 3.1, the striated muscle layer within the mid region contains a prevailing alignment of myofibers in the circumferential direction. In contrast, the striated myofibers found within the distal region are a mixture of those aligned in both the circumferential and longitudinal (axial) directions. Inspection of the smooth muscle layers within the mid region also reveals a predominant circumferentially-oriented muscle layer, along with some longitudinally-distributed fibers closer to the lumen of the tissue. Within the distal region however, this circumferential smooth muscle layer is less prevalent, while longitudinally-arranged fibers appear to comprise an increasing portion of the smooth muscle content.

3.2.3.8 Striated Muscle Influence on Measured Urethral Properties. The variable responses observed within the distal region, both active and passive, along with the mixed orientation of the muscle fibers contained within this region precluded the use of such data in obtaining biomechanical parameters to be used in combination with those obtained at the mid region. Thus, comparison of such parameters based on the degree of striated muscle content alone was limited to the mid region, displaying a considerably more uniform alignment of myofibers, but which

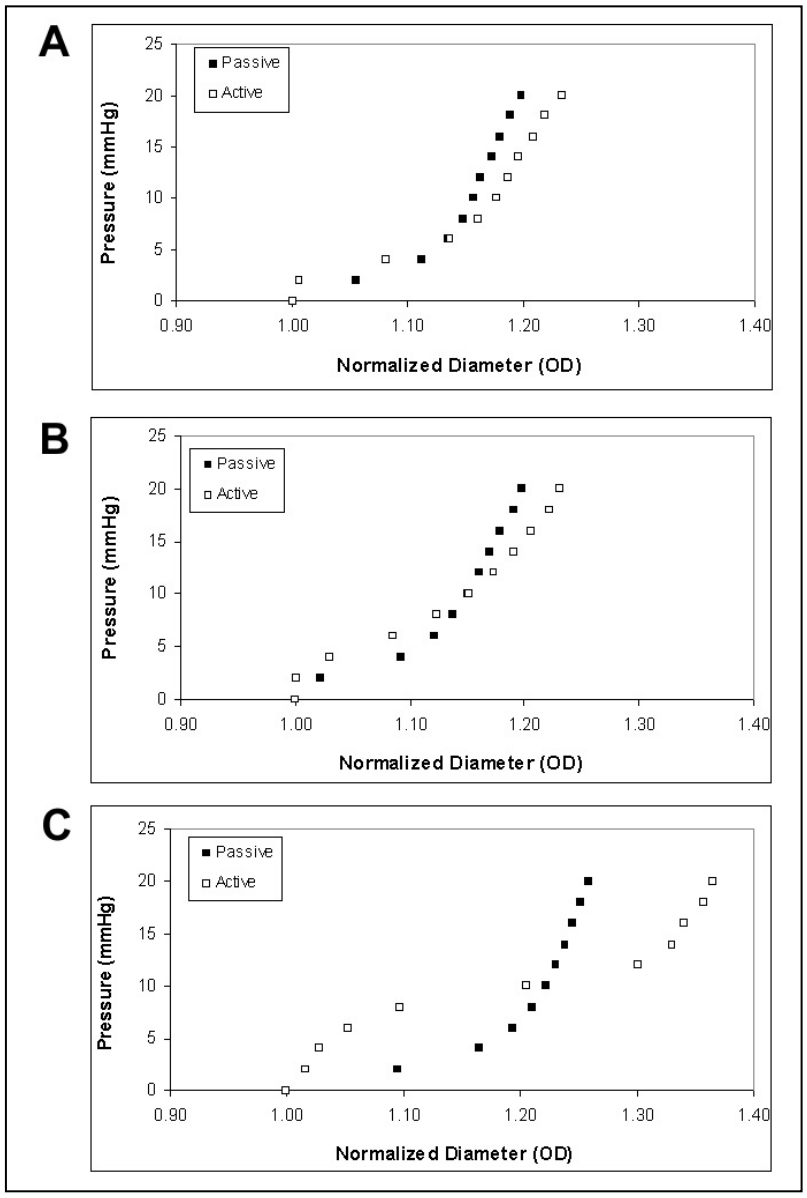

Figure 3.17 Pressure-normalized diameter responses obtained at the distal region of the urethra for tissues in which striated muscle alone (A), smooth muscle alone (B), or smooth-striated muscle together (C), were stimulated. Corresponding passive tissue responses are also shown, which demonstrate the active muscle conversion from a net closure to a net opening response.

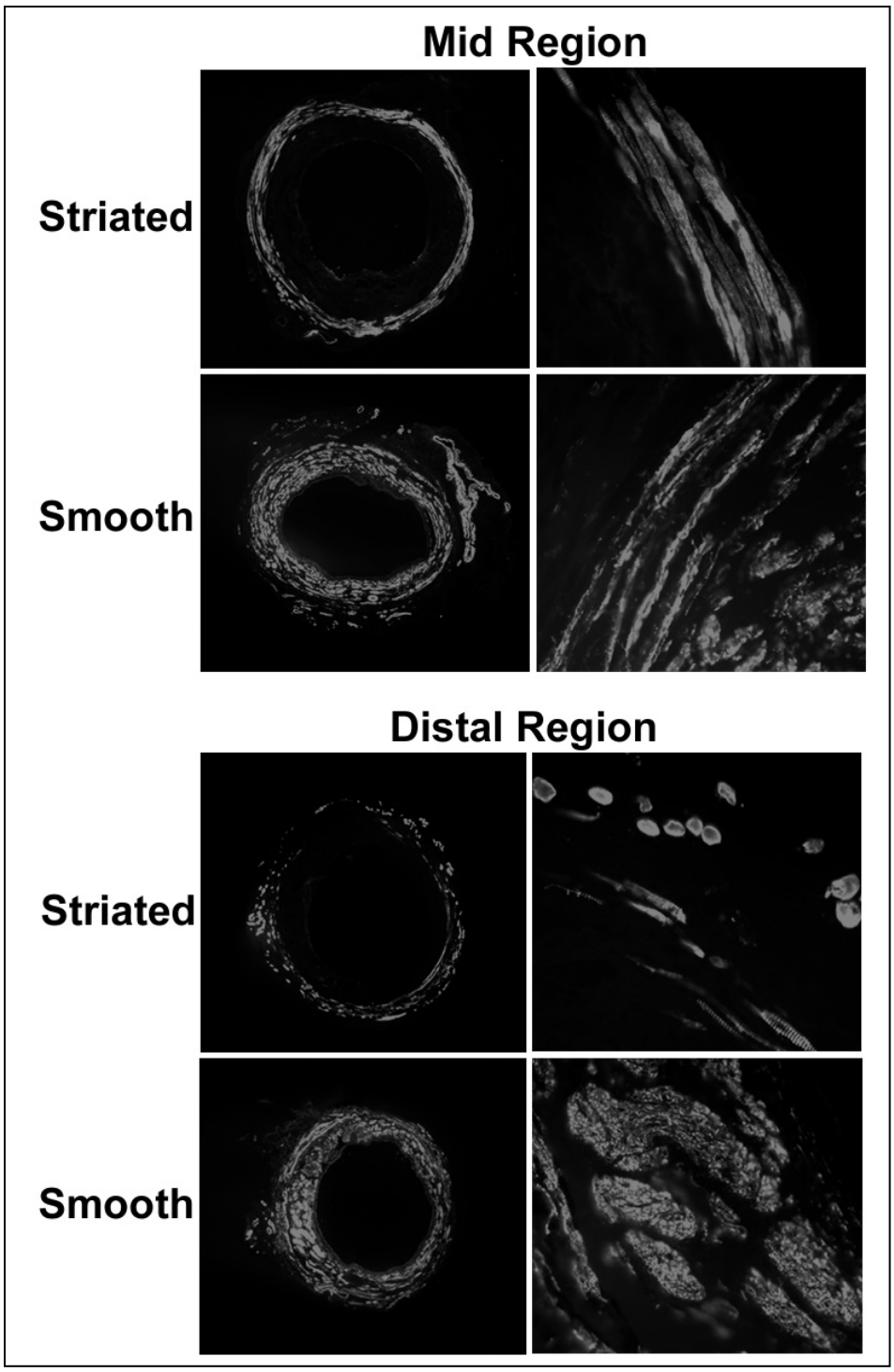

Figure 3.18 Immunofluorescent-labeled cross-sections of mid and distal portions of the female rat urthera, representative of the muscle orientations found within each region. Predominant circumferential layers of both smooth and striated muscle are apparent within the mid region, while the distal region displays a circumferential/longitudinal mixture. Striated muscle revealed with both fast and slow myosin heavy chain and smooth muscle with α-smooth muscle actin. Images taken at 40x (left), and 400x (right).

also consequently limited the range over which such a determination could be made. The influence of this volume fraction on the tissue to generate maximum circumferential stress and to assist in maintaining closure over the range of applied intralumenal pressure, as defined by the total contraction capacity (TCC), is provided within Figure 3.19. Within the mid region, increases in these experimentally-derived parameters are more apparent for tissues in which only the striated muscle was activated. A significant positive correlation is observed between volume fraction and TCC (for maximum stress, p=0.061). For tissues in which both smooth and striated muscle were activated simultaneously, little influence of striated activation is observed (p=0.678 and 0.859, for TCC and maximum stress, respectively).

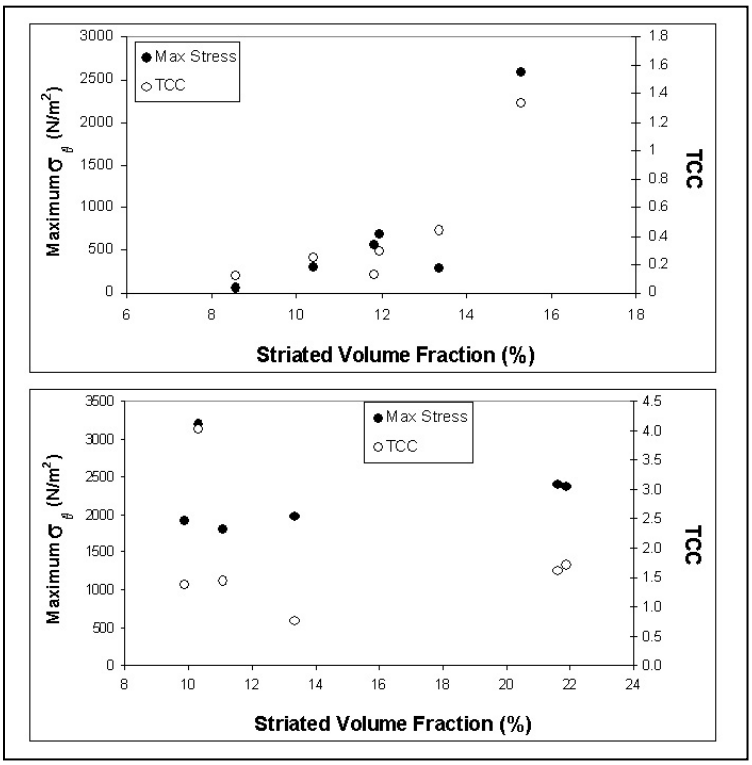

Figure 3.19 Experimentally-determined dependence of local striated muscle content with regard to maximum circumferential stress generated (σ_θ) and the total contraction capacity index (TCC). Tissues in which striated muscle was activated alone (top) or in which striated muscle was activated in addition to smooth muscle (bottom) are shown.

3.2.4 Discussion

Various parameters characterizing the biomechanical properties of the intact urethra were obtained from *ex vivo* experimental measures of changes in tissue diameter (OD) in response to increases in intralumenal pressure. These included compliance, β-stiffness, total contraction capacity (TCC), functional contraction ratio (FCR), incremental elastic modulus, and maximum circumferential stress generation. Experiments performed in the presence or absence of selected muscle activity permitted the determination of the relative influence of each muscle component, smooth or striated, in regard to each of these parameters. Results of these experiments demonstrate that the smooth muscle exhibited a greater influence on the functional responses of the urethra tissue, which in turn resulted in significant changes in tissue mechanical properties. The striated muscle also affected these responses, although to a lesser degree. Attempts to investigate the influence of variations in the amount of local striated muscle on these parameters revealed that the orientation of these muscle fibers, as well as those of the smooth muscle, may have a significant impact upon the urethral closure mechanism. The influence of striated muscle content on local urethra closure function was only revealed in the absence of overshadowing smooth muscle activity. Together these results enhance the overall understanding of the structure-function relationship of the individual components comprising the urethra. In addition, with regard to uromyoplasty therapy, they also establish a mechanism for further investigating the relative importance of the striated muscle layer and for evaluating local changes in biomechanical properties that may result from localized cellular transplantation.

Overall, biomechanical parameters previously used to characterize vascular tissue responses may also be applied to investigate urethra tissue properties. One exception to this was the β-stiffness, which could not be adequately utilized for active tissues due to the lack of exponential P-D responses and subsequent poor fit of the transformed data. Nonetheless, comparison of β-values obtained from passive urethra tissues provided an assurance that changes in these underlying responses were not responsible for the observed differences between the active states with regard to the other parameters. Similar multiple comparisons of compliance and incremental modulus also verified the reproducibility of the passive responses and measurements within the mid region. Although no similar data exists for urethra tissue, the passive urethra β-values obtained in this study are similar to those reported for carotid and other large-conduit human arteries (i.e. thoracic and abdominal aortas) within their respective physiologic pressure ranges [181].

Utilization of the three experimental muscle activation protocols allowed for direct comparison of parameters associated with either striated or smooth muscle activation alone, as well as an indirect measure of the relative effects that could obtained through the addition of the second muscle component. In comparison to passive tissues, induction of either muscle component acting alone resulted in significant changes in the biomechanical properties of the tissue. This is reflected in measured changes in compliance and incremental modulus, although striated muscle had a minimal effect on the latter. However, in comparing all activated tissue states, the addition of an active striated component to smooth muscle-activated tissues had little additional effect on the observed responses. This is reflected in the lack of significant differences in many of the parameters examined (TCC, FCR, and incremental modulus) when comparing smooth-only to smooth-striated activated tissues. In contrast, comparison of striated-only to smooth-striated activated tissues reveals the significant influence of smooth muscle supplementation, as demonstrated by significant differences in these same parameters. Not surprisingly, the average maximum circumferential stress generated by the striated component alone was approximately one-third of that generated by the smooth muscle. Addition of the striated component resulted in only a 5% increase, on average, in the maximum stress above that which could be generated through the smooth muscle alone. These maximum stress values are considerably less than those previously reported for skeletal muscle (~50x less; 2.0-2.5 x 10^5 N/m^2 [201]) and for arterial vascular smooth muscle (~15-30x less; 1 x 10^5 - 3.5 x 10^5 N/m^2 [206, 214]), when corrected for actual muscle volume occupied. Arterial vessels are however exposed to a physiologic pressure range that is an order of magnitude higher than that of the urethra which may help to explain, at least in part, these deviations. It should also be mentioned that although no similar data exists with regard to the urethra, the incremental elastic modulus values obtained within this study for both the passive and active tissue states compares favorably with passive and active values obtained for rat carotid and tail arteries at similar pressures from similarly aged animals (< 50 mmHg; < 2-3 x 10^5 N/m^2 [205, 215, 216]). In addition, reported compliance (distensibility) values based on external diameter measurements for passive human cerebral and carotid arteries also compares favorably with the passive state urethral values reported here following exposure to similar pressures (~8-10 $mmHg^{-1}$ up to 25 mmHg [217], compared to <17 $mmHg^{-1}$ up to 20 mmHg). Such comparisons provide us with some assurance that the values obtained here are within the range of those previously described for other tubular biologic structures obtained using similar methodology.

From the TCC index, which provides a measure of muscle responsiveness over the entire applied pressure range, the striated muscle was approximately one-third as effective as the smooth muscle in resisting deformation. Correspondingly, in reference to smooth muscle alone, the TCC index increased by one-third following the addition of the striated component. Previous *in vivo* investigations attempting to define the relative contribution of the striated musculature in the generation of urethral closure pressures have varied greatly. Estimates of striated contribution to the urethral pressure profile (for UPP methodology see section 1.5.1), performed in the canine, have ranged from one-third [218] to over one-half [219]. In contrast, others have been unable to detect any significant influence by this component [220]. The results presented here suggest that the striated muscle is contributing no more than one-third of the urethra's ability to maintain closure at the mid-region. However, it should also be mentioned that inherent experimental factors in the chemical activation of the striated muscle may have contributed to the comparatively low impact of this component in the responses observed. The use of alternative methodology for inducing contractions, along with other concerns over the experimental measurements performed, is discussed in greater detail within section 4.4.2.

Of direct importance to uromyoplasty therapy is the dependence of urethral mechanical properties with regard to the local content of striated muscle. Originally, the natural changes in striated volume fraction that were observed along the axial length were intended to be exploited in order to gauge the magnitude of this dependence. However, as shown within the distal region, corresponding changes in fiber orientation coinciding with axial position likely cannot be ignored in determining this association. It may be rather unrealistic therefore to not only estimate the fraction of circumferentially-oriented fibers within a mixture of various fiber alignments but to also account for potential counteracting effects of the non-circumferential fibers as well; even at the lower pressure ranges in which resistance to dilation was observed. As a result, in attempting to determine this association, observations were limited to variations seen over a small axial length (~4-5 mm) located within the mid region. From these experiments, correlation between the amount of striated muscle present and the TCC index was observed for tissues in which the striated muscle alone was stimulated. There was no such correlation for tissues in which both smooth and striated muscle were activated simultaneously. In the presence of smooth muscle this may be reflective of the limitations in the sensitivity of the current experimental apparatus and protocol to detect smaller changes in such responses.

The effect of muscle fiber orientation was not initially a subject of experimental inquiry. However, the results of the distal experiments presented here suggest that alignment may be an important variable to consider, particularly for regenerated tissues. A number of suggested mechanisms of assisted urethral opening during micturition have been proposed. One such mechanism is that the urethra is normally maintained in the closed position through spontaneous smooth and striated muscle activity, and is then actively relaxed for micturition primarily through the actions of NO [199]. Also, based on differences in observed maximal myofiber shortening velocity, it has also been previously hypothesized that the longitudinally-oriented smooth muscle layer actively participates in the opening of the urethra during micturition [221]. Conversely, it has been argued that the contraction of this longitudinal muscle layer would be counteractive to lumenal opening due to an increase in myofiber thickness associated with its shortening, and therefore this layer also assists in closure [106]. The P-D results presented here, along with the corresponding histology documenting muscle fiber alignment, suggest an active role for both smooth and striated muscle in urethral opening, as detected within the distal region. The crossing of the active and passive P-D curves was somewhat unexpected and may potentially be explained, at least in part, by the simultaneous activation of both circumferential and longitudinal fibers by virtue of the non-selective pharamacologic stimulation utilized. Activated simultaneously, the forces generated by the longitudinal myofibers would not directly oppose those generated by the circumferentially-oriented fibers, however they presumably would alter the net orientation of force development. It is interesting that the conversion from active closure to active opening corresponded with the same pressure range in which a decline in the FCR parameter for each muscle element was observed (~4-6 mmHg for striated, ~10 mmHg for smooth and smooth-striated activation). This further suggests that some mechanism of active opening may become evident once the circumferentially-generated force is overcome. Under such a scenario, the sequence of activation of the various muscle layers may have significant physiologic consequences. *In vivo* studies in the greyhound have suggested a separate innervation of longitudinally- and circumferentially-oriented smooth muscle, with the former primarily under the control of cholinergic innervation and the latter under control of adrenergic innervation [199]. Active opening in the distal region was observed here in preparations involving joint or independent cholinergic and adrenergic stimulation. Longitudinal muscle fibers are also present to some extent throughout the axial length of the urethra, although in relative terms appears to be greatly reduced within the sphincter-like mid region. Within this region the presumed effects of the longitudinal muscle, which may act on the entire length of the urethra, does not appear to be sufficient enough to

alter the active closure observed over the entire pressure range. However, it cannot be excluded that the simultaneous activation of these muscle fibers may have acted to reduce these closure responses.

3.3 Conclusions

A new method of evaluating the *ex vivo* physiologic function and biomechanical properties of specific segments of the intact urethra has been validated, and subsequently utilized in the investigation of smooth and striated muscle contributions to overall urethral mechanical properties. Due to the ability of the experimental system to perform regional evaluations, validation of chemically-evoked muscle responses was first examined with respect to axial variations in urethral muscle composition. Smooth and striated muscle responsiveness to specific agonists resulted in isobaric contractions that corresponded with local histologic observations regarding the quantity of each muscle component present. The ability to pharmacologically control smooth muscle activity was demonstrated through nitric oxide-mediated manipulations (Nω-Nitro-L-arginine and sodium nitroprusside) as well as direct alpha-adrenergic receptor stimulation (phenylephrine). Likewise, striated muscle activity was demonstrated through direct nicotinic receptor stimulation (acetylcholine), although coinciding muscarinic-mediated smooth muscle activation was also observed. Nonetheless, the ability to specifically activate or inactivate either of these components was confirmed through additional blocking studies. Aside from validating the experimental model, these controlled responses permitted pharmacologic protocols to be established in which specific activation of either muscle component could be ensured.

From measurements of pressure-diameter responses a number of parameters representing the biomechanical properties (compliance, β-stiffness, incremental modulus) or contractile ability (total contraction capacity, functional contraction ratio, maximum circumferential stress) of the isolated urethra tissue, within a physiologic range of incrementally-applied intralumenal pressures, were examined. These allowed the quantitative characterization and comparison of urethral responses in the presence or absence of selected muscle activity, specifically within the mid-urethra. From these investigations, both smooth and striated muscle significantly influenced the urethra's ability to resist deformation when compared to passive tissue, devoid of muscle activity. However, smooth muscle had a significantly larger effect on this ability as reflected in each of the parameters

examined. This was further confirmed through examination of tissues in which both muscles were activated simultaneously. Results indicate an association between the local content of striated muscle and the ability of the tissue to perform work to actively resist deformation. Additional attempts to more accurately define this association were diminished by concerns over muscle fiber orientation with axial position, particularly within the distal region in which this alignment became less dominated by circumferentially-aligned fibers. Within this region an apparent shift from active closure to active opening occurred, in the presence of both smooth and/or striated muscle activation, coincident with increasing intralumenal pressure. Importantly, these results indicate that the relative orientations of the muscle layers may have a significant impact upon the closure function of the urethra.

4.0 DISCUSSION

4.1 Clinical Significance

The clinical significance of the results presented can be viewed from both a pre-injection and post-injection standpoint. Previous experience in myogenic cell transplantation for the treatment of muscular dystrophy has taught a valuable lesson to those undertaking a similar approach for the treatment of other muscle or non-muscle disorders (i.e. through gene therapy): cell selection is critical in achieving a successful clinical outcome. This is particularly evident within the myogenic lineage, which contains its own progenitor cell pool that has been demonstrated by numerous investigators to be highly heterogeneous. Here it is further demonstrated that this heterogeneity can result in a greater than ten-fold difference in skeletal myofiber regeneration following transplantation into dystrophic animals. However, the positive identification of the most efficient progenitors cannot rely solely on *in vivo* outcomes. For translation of experimental animal results to clinical application, reliable *in vitro* selection criteria must be established and must be non-species specific. The results presented here demonstrate that the use of cell surface markers, while clinically attractive and currently accepted within the hematopoietic community, may not be dependable for use in the myogenic lineage. In particular, lack of conserved protein expression between species, inconsistent regeneration results within the same animal model, and temporal fluctuations in surface protein expression may limit their utility. As an alternative, cell behavioral properties appear to be more promising in this regard. *In vitro* behavioral characteristics under imposed conditions which challenge the propensity of a myogenic progenitor cell to choose either a proliferation or differentiation pathway may provide a means for distinguishing cells that retain their mitotic capacity following transplantation. This *in vivo* expansion of donor cells may indeed be a critical variable, along with survival, in the regeneration process. Incorporating such behavioral criteria into cell isolation and/or purification schemes, within a timely fashion, may yield significant returns in the clinical myogenic transplantation setting.

While the amount of striated regeneration may be dictated through cell selection, the extent of biomechanical influence imposed by this new muscle will dictate the urethra's ability to maintain closure when challenged by increases in stress. Although further work is required in this area, results of the biomechanical analysis performed here coincide with previous findings suggesting that the striated layer acts as an adjunct closure

mechanism to the more influential smooth muscle layer. It follows that a significant amount of striated regeneration may be necessary in order to have a significant clinical impact in improving active closure function. This places additional emphasis on the ability to identify adult donor populations that will efficiently and effectively regenerate this muscle layer. Further, the results presented indicate that the proper circumferential alignment and innervation of newly-created myofibers may be critical variables to the success of urethral muscle regenerative strategies.

In the clinical setting, devising effective therapeutic strategies relies upon first understanding the underlying cause(s) of dysfunction. Subsequent evaluation of such of therapies should be performed at the level and manner in which the treatment exerts its influence. With regard to SUI and uromyoplasty treatment, this involves performing investigations at the urethral tissue level to understand biomechanical changes occurring in a regional manner. Currently, the experimental means to perform such investigations are lacking. It is believed that the *ex vivo* experimental model described here fill this void and presents researchers with a new tool to investigate local physiologic and related biomechanical function. Importantly, the results presented demonstrate this model's utility in understanding how each constituent component affects the overall ability of the tissue to perform its intended task; thus making it applicable to a wide range of investigations seeking to gain insight into urethra function, dysfunction, and progression of disease states.

4.2 Advantages of Methodology

Aside from those already briefly discussed within their respective methods and discussion sections, some particular advantages associated with the methods used are worth mentioning.

4.2.1 Isolation and Evaluation of Efficient Myogenic Progenitors

In order to investigate sources of variable regenerative efficiency, one must first be able to obtain populations displaying heterogeneous regenerative behavior. Use of the preplate technique permitted such populations to be obtained, displaying this heterogeneity in terms of their relative myogenic commitment toward

differentiation. The isolation of the MDSC populations from the late preplates allowed for a wide range of regenerative behavior to be investigated.

Combining the time-lapsed microscopic imaging system with immunofluorescence labeling provided both temporal information on cell population expansion and fusion capacity, as well as more detailed information on the differentiation status of individual myogenic nuclei, respectively. From brightfield observations alone it is inherently difficult to determine the actual number of nuclei comprising the multinucleated myotube structures. Immunofluorescence nuclear labeling, together with MHC labeling, provided a clear, definitive and easily-identifiable measure of population differentiation status. Together these methodologies allowed a more detailed distinction in cell behavior to be made between the various myogenic populations. Other advantages of the novel imaging system used, particularly with regard to myogenic cultures, became apparent. It is often assumed that, within myogenic cultures, cellular elongation is a consequence of prior mononuclear cell fusion and subsequent myotube formation. However in many instances, as was made possible only through the use of the time-lapsed imaging system described here, the appearance of such elongated structures was not necessarily the result of cellular differentiation and fusion. Through standard brightfield imaging, transient observations of cultures at discrete sampling intervals would not permit the accurate evaluation and scoring of cellular fusion events. Using the bioinformatic cell imaging system (although reported at 12 hour intervals for brevity) permitted the monitoring of each selected image field at 10 minute sampling intervals, allowing a greater discrimination of cell division and fusion behavior to be made and in a temporal fashion within the same image field. This is reflected in the conformity between the 96 hour fusion data obtained through both brightfield and immunofluorescence imaging methodologies. Further, this imaging system also permitted cellular division times to be measured through direct observations, rather than through calculations which are often based on numerous assumptions.

4.2.2 *Ex vivo* Urethra Biomechanical Evaluation

In vivo administration of agonists and antagonists to ascertain functional contributions of constituent urethral components can affect surrounding muscular support structures, which makes it inherently difficult to attribute responses to specific urethral components. *In vitro* observations allow examination of urethral tissue specifically, the majority of such investigations utilizing strip or segmented ring preparations (section 1.5).

However, in theory, whole preparations offer advantages over conventional segmented tissue methods owing to the retention of the natural tubular tissue structure with minimal damage or disruption of muscle and structural fibers, as well as exposure to physiologic loading conditions (i.e. pressure applied radially outward from the lumen). As the muscle contracts, both it and the associated connective tissue shorten until a new equilibrium between the distending and retractive forces are reached. Considering the geometry of an idealized cylindrical urethra segment (Figure 4.1), these forces can be described by the following equations:

$$F_{distending} = P_t dA = P_t 2 r_i \Delta z \quad [4.1]$$

$$F_{retractive} = \sigma_\theta dA = \sigma_\theta 2h\Delta z \quad [4.2]$$

in which h is thickness, r_i is inner radius, P_t is transmural pressure, and Δz is axial length. In such a configuration, changes in circumferential length will result in simultaneous changes in radius, thickness and circumferential stresses. Thus, at any given distending pressure, the establishment of a new equilibrium is a complex process that is dependent upon both the strength of the active contraction of the muscle and the specific geometry and dimensions of the tissue [214]. These same relationships cannot be realized when utilizing strip studies, and may be

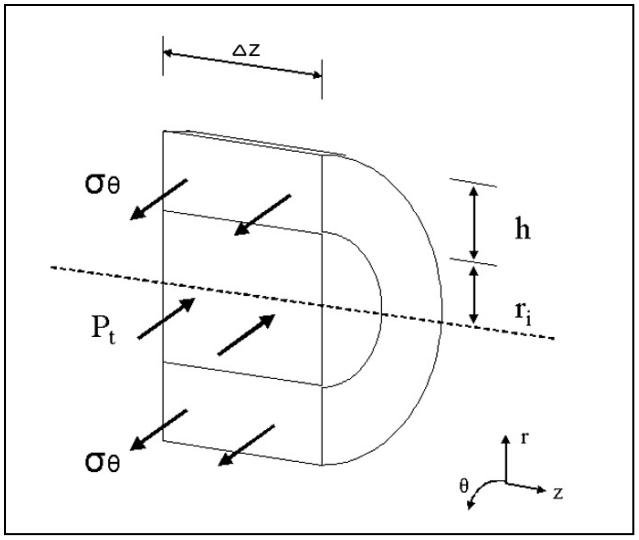

Figure 4.1 Forces acting on a segment of cylindrical tissue. Adapted from [211].

compromised when using small tissue segments. One previously described whole-mounted system has been used to characterize overall urethral closure function through the measurement of parameters that are based on fluid flow resistance through the entire urethra [80, 128, 130]. This overall characterization, however, is not unlike that which could be obtained in the *in vivo* setting. In contrast, strip or ring studies offer the ability to investigate specific axial regions of interest, which is critical for the study of regional functional responses as well as, for example, determining potential effects of therapies targeted to a particular segment of tissue. This is particularly relevant for the evaluation of the experimental regionally-targeted therapy discussed here. However, one potential concern regarding conventional strip preparations is the size of the strip in relation to the treated area of tissue, which could result in a dilution of the measured potential beneficial effects occurring at one specific location along the tissue. Unlike any of the previous systems described in the literature, the *ex vivo* experimental system described here permits regional measurements to be made, by precise adjustments in the positioning of the laser micrometer, while also retaining the whole tissue configuration. Furthermore, unlike conventional measurements of force, the currently described system permits contractile function of the tissue to be assessed, via diameter measurements, during application of a wide range of applied intralumenal (transmural) pressure loads. This allows various mechanical parameters of the tissue to be readily derived from these responses, as demonstrated within section 3.2. In contrast, by performing only force measurements as in conventional strip or ring studies, one would only be able to infer to what extent a therapeutic-induced change in force may impart on the functional ability of the tissue to withstand increases in loading. Such responses are indeed due to the mechanical properties of the tissue that are imposed by the constituent passive and active elements that comprise it, and current force-only measurement systems are not designed to define either whole tissue or constituent mechanical properties. Defining the relative contributions of each of these elements, both passive and active, allows for a more complete understanding of the function of the tissue, particularly in situations in which one of these elements has been compromised (eg. disease or injury) or is manipulated for therapeutic benefit (eg. uromyoplasty).

4.3 Disadvantages and Limitations of Methodology

4.3.1 Isolation and Evaluation of Efficient Myogenic Progenitors

Overall, both MACS and FACS cell separation techniques resulted in a surface protein-specific isolation of viable myogenic progenitors capable of skeletal myofiber regeneration. In terms of the cell separation processes themselves however a more distinct, or cleaner, separation between positive and negative selected fractions was accomplished through the use of FACS separation. This technique affords the ability to eliminate cell populations that are expressing a lesser degree of the protein of interest, such as those in the process of upregulating or downregulating the protein. Consequently, when labeling such cells with antibodies, these cells fall close to the thresholds established to discriminate between clear positive and negative fractions. In contrast to FACS, the nature of the MACS separation dictates that all of the cells passing through the separation column must be collected into either the positive or negative fraction. As shown in Figure 2.9, for the MACS Sca-1 evaluation, these 'borderline' positive cells were retained within the negative fraction. This lack of clean separation has the potential to contribute to the inability to detect differences in regenerative efficiencies, although admittedly there is also a considerable degree of unknown variability in the transplantation process itself. (It should be mentioned however that several advantages in using the MACS technique were also observed, such as increased cell viability and cell yield, which became particularly important when working with smaller cell numbers.)

Aside from the technical aspects of the cell separation methods selected in this study, several factors make identification and comparison of directly-isolated cells versus tissue-cultured cells inherently difficult. Patterns of expression of both proteins examined here have been observed to change rapidly in culture, as demonstrated in section 2.2.3.3 [140, 146]. Thus, it cannot be excluded that other variations in protein expression not examined are also occurring that may have a direct effect on cell behavior. When placed *in vitro*, expansion and/or activation of quiescent progenitor populations may likely occur, potentially through co-culturing effects, and subsequently may have important implications in terms of regeneration. Evidence for such an effect is provided by the emergence and expansion of the MDSC population within culture, which appears to initially remain in a quiescent state until stimulated by, as yet, unknown factors. Further, no directly-isolated population approached the level of regenerative efficiency of the MDSC population obtained through culturing, even though by all reasoning this population of cells

should have been included in at least one of the directly-isolated cell fractions. Finally, it has also been suggested that potential histocompatibility alterations of donor cells may be caused by exposure to tissue culture and proteolytic harvesting conditions [72]. Thus, myogenic progenitors obtained from either direct or cultured isolation methods may need to be evaluated independently.

The method of evaluating regenerative efficiency should be discussed with regard to its ability to characterize the regeneration process. An efficiency index was assigned through measures of regenerated myofiber number, independent of size, as opposed to accounting for the area occupied by the myofibers. Conversion of histological data from myofiber number to area is not likely to significantly alter the results presented, since myofiber size distributions were very similar among cell populations. However neither method, based on histological sectioning, is easily amenable to accounting for the length of the new or restored myofibers and thus provides only a two-dimensional view of the regenerative process. Factors such as individual myofiber length would be extremely difficult to estimate, even from tightly controlled serial histology sections, and would require a sophisticated three-dimensional reconstruction. This would not be practical for larger-scale studies with multiple group comparisons such as those performed here. Alternative methods, such as Western-blotting, to determine the total amount of dystrophin contained within injected muscles could be used to quantitatively assess regeneration. However, this method is indirect and may be subject to potential variations in dystrophin gene expression, not unlike that which may be encountered when attempting to use an inducible-reporter gene. Measurements based on the presence of dystrophin expression, such as the currently-used methodology, provide a measure of transplanted cell participation in the regeneration process as a whole, since the appearance of dystrophin-competent myofibers may result from both the conversion of already existing myofibers, through donor-host fusion, as well as the formation of new myofibers from both donor-donor and donor-host cell fusion. Comparison of the size distribution of dystrophin myofibers relative to those of control non-injected muscle provides us with an indirect and relative assessment of the probable route taken by the injected cells (i.e. new myofiber formation). In either case, at this point it would be difficult to argue whether augmentation of muscle mass through addition of nuclei to existing fibers, or alternatively the generation of new myofibers, would be most beneficial in the urethral physiologic setting. Since muscle cross-sectional area is proportional to the potential force that may be generated, either mechanism may be beneficial.

Aside from the number of dystrophin-positive myofibers, the determination of the regeneration index was based on an estimation of the number of transplanted myogenic cells through concomitant assessment of desmin

expression. This assumes that desmin-negative cells are not capable of participating in this process. However, it is obvious that transplantation of the primarily desmin-negative MDSC population described here indeed results in robust regeneration. It is currently unclear which population(s) within the MDSC cultures may or may not directly participate in myofiber formation and thus regeneration capacity, for this population only, was based upon the entire number of MDSC cells injected. Thus this may actually result in an underestimation in the efficiency of the responsible cells within this population. For the other muscle-derived populations examined, both cultured and directly-isolated, the presence of myogenically-competent desmin-negative cells also cannot be excluded and therefore may result in an artificially-high estimation of their apparent efficiency. Other observations of skeletal muscle-derived cells, expressing various combinations of both Sca-1 and CD34, which do not appear to be myogenic (desmin-negative) but are capable of regenerating myofibers have been reported [38, 144]. Nonetheless, while possible, this most likely occurs at a very low frequency.

The particular method(s) selected to assess protein expression is often based on the detection sensitivity required and the degree of quantitative information that is desired. MRF protein expression within the cell populations examined here was assessed primarily through immunofluorescence labeling and microscopic imaging. While this method permits an estimation of the percentage of cells within a population expressing the particular protein of interest, it does not readily permit distinctions in the level of such expression to be made. As mentioned previously, within section 1.1.2, relative levels of early-stage MRF expression are thought to play an important role in the balanced regulation between differentiation and proliferation. Therefore, in combination with immunofluorescence, methods which provide a quantitative measure of such expression may provide further distinction between progenitor populations beyond that which was reported here. A more rigorous evaluation of expression may include combinations of Western blotting (transcribed protein), RT-PCR (mRNA), and flow cytometry (transcribed protein).

4.3.2 *Ex vivo* Urethra Biomechanical Evaluation

The pressure range used in this study corresponded with previously reported ranges of voiding pressures in the female rat. However, in the physiologic setting the urethra is surrounded by numerous external support structures, which are obviously not present during *ex vivo* testing. Through previous knowledge of maximum flow

rate and intrabladder pressure in the female rat (14.6 mL/min and 33 mmHg, respectively [204]), and based on measures of *in vivo* length obtained in this study (20 mm), maximum internal radius during micturition (viscosity of urine ~ 1 cP) can be estimated through the Hagan-Poiseuille Law assuming a cylindrical lumen geometry. Under these idealized conditions, this law ($r^4=8L\mu Q/\pi\Delta P$) predicts that the urethra lumen opens to a radius of approximately 0.23 mm. Examination of the P-D (ID) data for each muscle activation protocol revealed that this inner radius was generally achieved through application of approximately 0-4 mmHg for striated muscle-activated tissues, and 4-6 mmHg for smooth muscle-activated tissues. From examination of FCR data, a decline in the muscle-induced contractile function of the tissue corresponds with an increasing strain beyond this predicted physiologic range. These experimental results, together with the estimated maximal physiologic urethral radius, suggest that the surrounding tissues play a significant supportive role in the deformation of the tissue. Thus, future *ex vivo* investigation of the isolated urethra using this experimental system should be performed using lower pressures to ensure that the tissue remains within the relevant physiologic strain range.

Slow-twitch striated muscle fibers within the urethra are traditionally considered to aid in the generation of sustained tone during bladder filling while the fast-twitch are considered more likely to be recruited in a reflex manner, such as in response to transient increases in intravesical pressure. Although the female rat is an acceptable model to perform functional urethra studies, the predominantly fast nature of the striated muscle observed in the young rats utilized here is contradictory to histological findings in both the human and in older rats [87, 194], as discussed in section 3.1. The abbreviated duration of ACh-induced contractions from several notable sources, presumably a rapid fatigueability of fast striated muscle in combination with desensitization of nicotinic receptors, may have contributed to a large underestimation of the striated muscle contribution within functional mechanical assays reported in this study. Preliminary experiments (presented in section 3.1) demonstrated the length of maximal striated contraction to be on the same order of time required to complete the incremental pressure testing (Figure 3.9). This left little room for error in the initiation of the P-D measurements. Further, no method of assessing uniform strength of contraction during application of these pressures was possible. The large priming volume of the system, together with the chemically-evoked receptor desensitization, precluded the possibility of challenging the contractile function of the tissue prior to initiation of the mechanical testing protocol. As an alternative to chemical stimulation, modification of the current experimental apparatus for electrical stimulation of muscle may significantly reduce the possibility of variability, particularly for striated muscle experimentation, with

regard to both of these issues. Previous studies of greyhound urethra strip preparations using electrical field stimulation demonstrate the ability to induce repeatable striated contractions through both intermittent or continuous stimulation over extended periods of time, with minimal or no dropoff in force production [222]. Further, these contractions were shown to be relatively maintained despite the striated layer being comprised of over 90% type II (fast, glycolytic) fibers within this particular animal model, similar to the histological findings in the rat model presented here.

There are several sources of experimental error that are inherent to the experimental system in its current form. The incremental pressure steps used in ultimately determining urethra mechanical properties (section 3.2) were performed by manual adjustment of a fluid reservoir (such that 2 mmHg=1.07 inches increase in reservoir height). Unfortunately, this variability could not be accounted for in the present system as the pressure transducers were not sensitive enough to distinguish small variations in pressure (<1-2 mmHg). This variability however is most likely small compared to that generated between-samples from a number of sources related to the dissection and handling of the tissue and, perhaps most importantly, mounting the urethra into the experimental testing system. Following dissection, *in vivo* axial length of the tissue must be measured prior to its removal from the transport catheter and then duplicated by re-securing it to the tubing contained within the tissue bath. This introduces error in re-establishing the correct axial length, and hence the correct axial strain of the tissue. It has been shown previously, for arterial segments, that longitudinal stretch can alter both the basal muscle tone of the tissue as well as the compliance [184]. Alternatively, securing the tissue to a mountable apparatus at the time of dissection may significantly reduce this associated error. Experiments that were performed to compare axial regions of the urethra could not be performed on the same tissue, and thus each measurement was subject to all sources of between-specimen variability. A measurement system to examine all three regions simultaneously would allow for paired comparisons, while at the same time also reduce the number of animals needed to generate significant sample sizes. Additionally, a computer-controlled stepper mechanism could be added to the system to increase the precision of the applied pressure increments over a smaller range (e.g. 0-10 mmHg at 1 mmHg increments) which, as mentioned previously, would expose the urethra to a more physiologic strain range in the absence of external supporting tissue. Automated control of pressure steps should also allow the time interval between step increments to be reduced significantly, which would additionally reduce the potential for muscle fatigue during testing and provide a more

physiologically-relevant simulation of transient stress episodes. In its present form, longer time intervals (10 sec/step) were used to minimize the error associated with manual pressure increases.

As briefly mentioned within section 3.2.2.1, the pH range under which the biomechanical experiments were performed was slightly acidic. Intracellular pH has been shown to change at a ratio of 0.73 per unit of extracelluar pH change and thus provides some buffering [202]. However, severe acidosis may interfere with increases in intracellular calcium and lead to hyperpolarization of membranes by increasing potassium conductance, which subsequently would interfere with voltage-dependent calcium channels. Thus, either of these mechanisms could lead to decreased muscle contractile function. That being stated, under similar experimental acidic conditions, and even more severe (pH, 6.9), changes in PE-induced contractions of trabecular smooth muscle were only noticeable within a very low concentration range (<10μM) [202]. In addition, studies performed utilizing striated muscle under acidic conditions, through the addition of large amounts of lactic acid, failed to demonstrate an inhibitory effect on contractile function [203]. Concerns over proper oxygenation appear to be more relevant when examining contractility, as both smooth and striated muscle has been shown to be sensitive to ischemia [223]. Nonetheless, appropriate adjustments to buffering of bathing media, or use of alternative buffer solutions (eg. Krebs-Ringer) to control shifts in pH should be taken into consideration when performing future studies with this system and when altering gas perfusion.

Evaluation of the intact urethra represents a major advantage over current methodologies. However, one initial concern in attempting to evaluate potential functional differences within relatively small regions along the axial length is the potential effect of tension transition from neighboring regions, which could interfere in such measurements. In an attempt to alleviate such concerns, a pilot study was performed to examine distal region contractile function following crush damage to the mid region (performed with a hemostat). It could be expected that strong contractions within the sphincter-like mid region may potentially have an effect on measurements made on the distal portion of the tissue. However, the distal contraction results following mid-crush were within the range obtained from the non-crush experiments; while the crushed mid region demonstrated a large dilation with applied pressure. While these initial observations are reassuring, at this time such potential effects cannot be totally excluded.

Aside from issues related to experimental and data collection methodologies, many of which may be reduced through the implementation of new procedures and improvements to the experimental apparatus as

described, errors in data analysis and estimation of non-directly measured parameters must also be considered at this time (e.g. thickness and inner radius, which directly impact estimations of stress and incremental modulus). As mentioned in section 3.2.2.4, error associated with the calculation of the inner radius from an assumption of incompressibility has been shown to be small (<1%). However, the validity of such an assumption has only been challenged for vascular tissues, and further was examined at lower strains than those observed here. Further, such an estimation of inner radius is also reliant upon an accurate determination of tissue thickness, obtained from histology. This thickness value utilized in this estimation was obtained through manual determination of outer and inner tissue boundaries, and represents an average wall thickness obtained through an assumption of an idealized cylindrical geometry. Further, this histology-based parameter is reliant upon an accurate re-establishment of *in vivo* length following removal of the tissue from the experimental apparatus, as discussed previously.

We must also consider the estimation of circumferential stress from experimental pressure-diameter data through the use of the Lame equation, which is subject to a number of simplifying assumptions. For the sake of comparison such data is only presented here at one idealized radial position within the tissue wall (mid-wall). Alternatively, other simplified determinations of circumferential stress have also been performed using thin-walled theory ($\sigma_\theta = P*r_i/h$; where h=thickness), resulting in an estimated stress averaged over the entire wall thickness [205, 216]. It is noted that in either case such equations are based on linear mechanics theory and assume that the tissue is composed of a single homogenous isotropic material. In reality, each of the constituent layers of the urethra, and biologic tissues in general, are most likely anisotropic or orthotropic. Further these equations are based upon an assumption of a uniform cylindrical shape, which is also clearly an idealized situation. Each of these assumptions simplifies the derivation of the equations and results in expressions for stress dependent only upon the tissue geometry and the applied pressure. However, the idealized situations represented by these equations are far from reality in most cases when describing biologic tissues, and thus the validity of values obtained should be taken in this context. In addition, in future studies, we should consider other attempts in the literature to perhaps more closely represent the biologic situation.

It is obvious through examination of histology that the urethra is composed of various distinct muscle and non-muscle layered components, each with discrete material properties. Indeed, the mechanical behavior of multi-component structures like the urethra will ultimately depend upon the individual mechanical properties of its constituent components, their relative content, and the manner in which they are coupled. Accounting for such

heterogeneity throughout the tissue wall requires more rigorous modeling of stress distribution. One such model, found within the vascular biomechanics literature, attempts to define the changes in stress distribution of bioresorbable vascular prostheses that occur as the healing process elicits changes in the thickness and elastic modulus of the various constituent layers [224]. Use of such a model most likely results in a more realistic interpretation of stress distributions throughout the wall of the tissue, through the representation of the tissue as a heterogeneous three-layer composite. However, it too is based upon the Lame equations, which were derived using classical infinitesimal linear deformation theory (generally valid for strains <10%). As demonstrated here for the urethra many biologic tissues readily deform in a finite and non-linear manner, thus again restricting the application and validity of such models. More complicated two-layer models have been proposed to account for this non-linearity through inclusion of more complicated descriptions of finite deformations [225]. While such non-linear models may in theory allow more accurate representations of tissue responses, it is also important to mention that the inclusion of additional parameters come at a cost of potential exposure to additional experimental error and assumptions. For instance, incorporation of material non-linearity requires inclusion of an assumed form of the strain energy density function. In addition, in either the linear or non-linear case, utilization of such models requires prior definition of mechanical properties for each of the representative layers of the tissue. For the linear model, this requires a single elastic modulus to be defined for each component. For the non-linear model, extensive experimentation to accurately define mechanical properties over the large deformation range would be necessary.

Future attempts to make more accurate and detailed biomechanical evaluations of urethral tissue responses should also include evaluation of potential residual stresses and strains within the tissue. In the estimation of stress performed here it was assumed that the no-load and zero-stress states were equivalent. The no-load condition defines the tissue state in which the applied transmural pressure is zero. The zero-stress state defines the stress-free state of the tissue, which does not implicitly occur under no-load. In fact, for vascular tissues, this is demonstrated by the fact that segments of vessels cut in the axial direction expand to varying characteristic opening angles depending upon the strain distribution that exists in the no-load state. It has been shown that vessels exhibiting this behavior are under a compressive residual strain near their inner surface and a tensile residual strain near the outer surface, thus explaining this opening characteristic in the absence of any applied forces. By ignoring residual stresses/strains, Fung et al. [226] demonstrated that an overestimation and underestimation of strain will occur at the inner and outer radii, respectively (with the inner an outer surfaces demonstrating the largest degree of error; this

effect is minimized near the mid-wall). It is not currently known whether the urethra is similar to blood vessels in this manner. However this issue should be pursued to eliminate the potential error associated with the presence of residual stresses/strains, particularly for cases in which detailed stress distribution information throughout the urethra wall is desired.

4.4 Future Work

4.4.1 Isolation and Identification of Efficient Myogenic Progenitors

Aside from those already mentioned within previous sections, further experimentation is necessary to validate the hypothesis generated here regarding the influence of progenitor cell differentiation and proliferation behavior in their capacity to regenerate skeletal muscle. This includes both general experimentation, to further corroborate the evidence presented, as well as more specific studies to address the mechanisms behind the differential control of such processes. Obviously, translation of such work toward clinically meaningful outcomes will require the use of human-derived myogenic populations in future experiments.

As a follow-up to the work described here, *in vivo* experimentation has already been initiated to further investigate the temporal sequence of donor cell behavior following injection. As an example, although semi-quantitative, tracking cellular position and mitotic cycle status *in vivo* may be accomplished through the combination of inducible reporter-gene techniques and specific labels of cell division. Following implantation of transduced donor cells, the host animal can be injected systemically at timepoints of interest with bromodeoxyuridine, which is incorporated into the DNA of dividing cells during the S phase of the cell cycle. Double-labeling of muscle tissue sections for both donor cell and dividing cell markers would reveal the location and mitotic status of the injected population of interest. Additionally, a more direct study of *in vivo* proliferation characteristics and its subsequent effects on regeneration outcomes could be performed through similar transplantation experiments to those described here, but in combination with exposure to substances known to limit or prevent cell proliferation. As an example, exposure of myoblasts to the protein myostatin, a member of the transforming growth factor-beta superfamily, has been shown to drastically decrease proliferation through arrest of the cells in the G_1 phase of the cell cycle [227]. A similar effect may be achieved through the transduction of cells

with vectors designed to induce constituitively high levels of MyoD or, perhaps more directly, specific cyclin-dependent kinase inhibitors. Implantation of the various progenitor populations both with and without imposed limitations on expansion capacity would allow perhaps a more direct assessment of the importance of *in vivo* expansion to myofiber production. If this cellular characteristic were indeed influential, as has been suggested by the results presented here, it would follow that such limitations would have a significant impact on the regeneration ability of the most efficient populations (e.g. MDSC) and little impact on the least efficient (e.g. EP).

Additional experimental work to study the link between myogenic differentiation status and regeneration capacity, in a more direct fashion, would build upon and presumably strengthen the work presented here. Unfortunately, as many regulational transcription factors (i.e MRFs) are nuclear-localized, it is not possible to utilize antibody-mediated sorting methods to separate viable myogenic cells based on expression of these proteins. However, construction of viral vectors encoding for fluorescent proteins under the control of MRF-specific promoters would permit the utilization of FACS to achieve such separation. Results of transplantations performed utilizing such populations might enable the identification of specific points within the sequence of myogenic regulatory gene expression beyond which effective regeneration may not be achievable. Taken together with previous *in vitro* studies that have provided a clear linkage between MRF expression and cell cycle entry, described within section 1.1.2, all of these future experiments may provide evidence of such a linkage in the *in vivo* setting within the context of myogenic regeneration.

Aside from these MRF relationships, the biochemical effects of CD34 expression on proliferation and differentiation pathways invites further investigation. Although MRF regulation of protein expression controlling the myogenic differentiation program is no doubt a central determinant of cell fate, the observed behavioral differences between the CD34 sorted populations in the absence of discernable differences in MRF expression suggest that there may be still other unknown influential pathways involved. Examining possible biochemical connections between CD34 and cell cycle regulators, also interconnected with differentiation, would be a logical first step.

Although the experiments performed here became focused on the effects of differentiation, it is also acknowledged that a number of other potential variables may additionally affect regeneration outcomes. In order to fully examine the cause(s) of differential regeneration, further experimentation must be performed to more adequately weigh the influence of all such variables. As previously mentioned in section 1.2.2, a rapid demise of

donor cells has been previously observed and has been implicated as one of the reasons for the lack of success in myoblast transfer therapy for the treatment of muscular dystrophies. A number of causes of short-term cell loss are possible, involving non-specific inflammatory, necrotic, or apoptotic pathways. However, performing such investigations is challenging, as many potentially influential factors are interrelated. For example, evidence of positive effects on survival are seen following the induction of heat shock proteins and their associated upregulation of anti-apoptotic proteins (e.g. Bax/Bcl-2), which has resulted in increased myogenic cellular survival and engraftment by up to two-fold [228]. It has also been shown that induction of certain cyclin-dependent kinase inhibitors, such as p21, also result in the induction of anti-apoptotic proteins, thus implying that cell survival is negatively linked to proliferation and positively linked to differentiation [229]. However, in contrast to this association, efficient MDSC populations which readily proliferate have also been shown to express what appear to be high levels of anti-apoptotic proteins [39]. This is also in contrast to the experimental results presented here, since a mechanism of improved regenerative performance coinciding with delayed differentiation and proliferation would seemingly also lead to exposure of cells to possible mechanisms of apoptotic destruction. Nevertheless, preliminary results indicate that apoptosis does occur at the site of transplantation shortly following injection (Figure 4.2), emphasizing the need for further dissection of early cell survival mechanisms and their subsequent influence on transplantation outcomes. Indeed, separating such effects from specific host immune elimination is more relevant to the application of the proposed uromyoplasty therapy, which is at least initially intended to be applied in an autologous fashion. However, aside from these short-term survival effects, the potential for donor-derived myofiber innervation may also have a significant impact on the longer-term survival of newly formed myofibers. Interestingly, this dependence appears to vary widely among different muscle types and locations, to an extent such that predictions of myofiber survival within a particular tissue based solely on this criterion would not be realistic [230]. The presence of both sensory and motor neurons, as well as Schwann cells or their released proteins, are thought to be essential for successful innervation and therefore may contribute to this spatial dependence [231]. In this regard, independent confirmation within the urethral environment must be established through continued study of myofiber persistence in relation to innervation before any conclusions regarding the long-term outcome and functionality of new tissue resulting from cellular uromyoplasty therapy can be made.

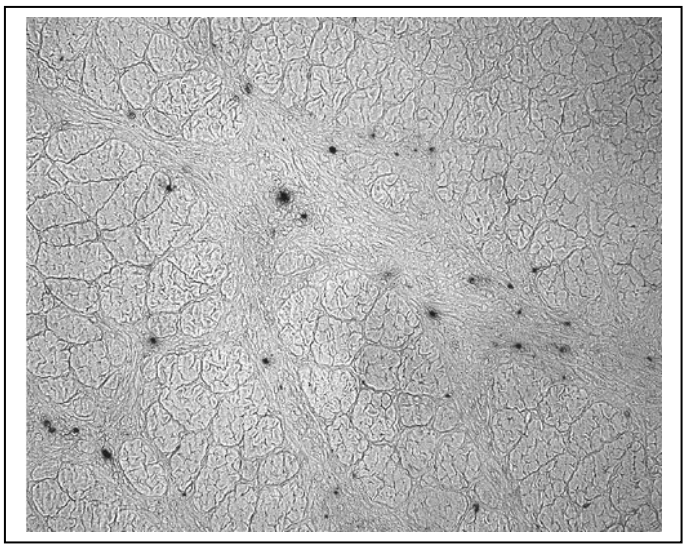

Figure 4.2 Evidence of apoptosis at the site of donor cell (EP) transplantation, 48 hours post-injection. Apoptotic cells (dark) are revealed by peroxidase staining following the labeling of DNA fragments generated by activated endonucleases (TUNEL method). Image taken at 200x magnification.

4.4.2 *Ex vivo* Urethra Biomechanics

As mentioned, certain modifications to the experimental system would most likely reduce the overall variability associated with the P-D measurements and improve control over muscle activation, and as such should be implemented prior to further experimentation. This includes outfitting the experimental system with mechanisms to provide precise applied pressure increments over a smaller range as well as switching from chemical to electrically-evoked muscle stimulation.

Further study of the relative influence of urethra constituent muscle components would build upon the work presented here, and would aid the urologic community in better understanding continence mechanisms. More specifically, in regard to uromyoplasty, the issue of regenerated striated muscle functionality is a scientific priority as it provides the foundation for applying this type of therapy to restore tissue function rather than alternative passive bulking options. Therefore, it follows that future experimentation be performed with the intent of resolving the mechanism of observed improvements in leak point measures, as well as to further investigate whether characterization of urethral mechanical responses can be utilized in a predictive fashion to estimate the potential

clinical benefit of cellular therapy. With this in mind, experiments to better understand and correlate the dependence of urethral biomechanics on the amount of local striated muscle would be beneficial. Unlike other currently available techniques, the methodology described here may be capable of delineating passive and active contributions to overall urethra mechanical properties. Urethral tissue resistance to deformation may be thought of as a composite of the individual contributions from the various constituent tissue components. Attempting to break down total tissue responses into the sum of those contributed by all of the individual passive and active constituent components of the tissue assumes a somewhat straightforward, or linear, interaction between these constituents. In contrast to this reductionism approach, it may be more realistic to initially attempt to predict the mechanical response of whole tissues following changes in a single component under specific loading conditions. For the purpose of predicting the mechanical benefit of augmenting a specific component within the tissue, in this case striated muscle, it may be beneficial to initially start with simplistic models involving minimal constituent terms. Using circumferential stress and strain parameters, obtained through similar methodology as already described, we can attempt to apply material composite theory to account for individual material contributions to the overall stress response. Assuming a no slippage condition between the components of the composite material, equal strain will be experienced by the composite as a whole and subsequently by each individual component. Thus, the load carried by the composite (P_c) is shared between the separate components (indicated as 1 and 2) and is additive. The total load carried by the composite, written in terms of the individual stress components and their corresponding cross-sectional areas (CSA), is given by the equation below.

$$P_c = \sigma_c * CSA_c = \sigma_1 * CSA_1 + \sigma_2 * CSA_2 \quad [4.3]$$

By assuming that the fibers that run through the composite are homogeneous, in the circumferential direction, the volume fraction (V) is equal to the area fraction such that this relationship can now be written as follows.

$$\sigma_c = \sigma_1 * V_1 + \sigma_2 * V_2 \quad [4.4]$$

With respect to the strain, which is assumed to be experienced equally for each component of the composite, the differentiation of the stresses with respect to the strain gives the material properties of each of the composite components:

$$\frac{d\sigma_c}{d\varepsilon_c} = \frac{d\sigma_1}{d\varepsilon_1} * V_1 + \frac{d\sigma_2}{d\varepsilon_2} * V_2 \quad [4.5]$$

$$E_c = E_1 * V_1 + E_2 * V_2 \quad [4.6]$$

where E is the material elastic modulus, in this case in the circumferential direction [232]. As a first attempt, application of composite theory to urethral tissue can be applied using similar simplified forms as described above. For example, in the active tissue state, the tissue components can be broken down to include the passive ECM (component 1) and the active striated muscle (component 2). In this simplified form it could initially be assumed that these ECM and the active cellular contributions dominate the response. Passive cellular cytoskeletal contributions from smooth muscle and its interactions with the ECM can be included as part of the generalized ECM component rather than considered separately. Similarly, in the passive state, the total tissue response can be thought of as resulting from contributions of the passive ECM/smooth muscle (component 1) and the passive striated muscle (component 2). For both cases, this type of model is based on small strain linear elastic behavior and thus should be applied to regions of the stress/strain response corresponding to <10-15% strain. In this region, based on preliminary results, a relatively linear response can be expected. Modifications to the experimental system to reduce the pressure range applied, and use of smaller pressure increments, will allow more experimental data to be collected within this small strain range. However, even in this simplified form, additional assumptions must be made in order to perform this type of analysis. The muscle fiber arrangement is considered to be preferentially circumferential and does not vary from sample to sample. In addition, it must be assumed that the fibers are uniform in their individual strengths. Statistical models to account for the cumulative weakening of composite structures, as individual fibers fail at increasing loads, have been proposed to account for stress redistribution in composites, but would be difficult to apply in this setting. As mentioned, other stress generating components can be considered negligible or lumped-in with other terms for simplification. Direct measures of the interaction of cytoskeletal components with the ECM would require additional experimentation using agents that disrupt the cytoskeletal structure of the cells, perhaps by destruction of the cellular actin filament structure [233].

The benefit of applying the type of analysis described above is that it may help us to better understand the relative passive and active influence of the striated muscle layer. Measurements made in the presence of variations in local striated composition would be required to effectively determine this influence. However, as demonstrated here, variations in striated myofiber orientation likely prohibit the use of the natural axial variations in striated muscle content that occur within the urethra to be used for this purpose. Alternatively, injury models to reduce the amount of striated muscle could allow such a determination to be made at a single axial location, most logically the

mid region. Fortunately, such injury models have been previously investigated by researchers attempting to create conditions to mimic SUI in animal models. Common models to induce loss of striated muscle in the female rat involve transection [187], crush [234], or cauterization to damage the pudendal nerve which specifically innervates this muscle layer. Other methods involve direct administration of myotoxic agents [120]. This type of study may potentially be effectively combined with *in vivo* measures of continence function in the investigation of uromyoplasty therapy. As outlined in Figure 4.3, correlation of *in vivo* physiologic measures such as leak point pressure with *ex vivo* biomechanical parameters and histological evidence of tissue structural changes would provide a solid foundation for delineating the role of the striated muscle and the subsequent consequences of cell injection therapy. However, a major assumption for extension of such results to cases in which the striated muscle is regenerated through transplantation requires that the new tissue be as functionally-integrated as the native tissue. Experimentally-obtained data utilizing treated tissue would be needed to verify the validity of such assumptions and determine whether simplistic determinations of muscle area can be translated into models to predict physiologic outcomes.

For the composite model discussed above, an account of heterogeneity in material properties throughout the tissue wall is accomplished simply through an inclusion of the relative volume fraction of each separate material component. This would imply that the individual components are evenly distributed throughout the wall thickness. Through examination of histology it is obvious that the various major urethra components (striated muscle, smooth muscle, inner submucosa) are arranged in a concentrically layered manner. As mentioned within 4.3.2, alternative models accounting for material heterogeneity in a layered cylindrical model have been proposed, and may permit a more accurate physiologic representation of the urethra. Using this model, presented by Vorp et al. [224], the stress distribution throughout the thickness of the wall is dependent upon the inner and outer pressures acting on the complex and on the mechanical properties and thickness of each layer. This type of a model, based upon histologic measurements and previously reported material property values (elastic moduli) of muscle and similarly-structured connective tissue components, could be beneficial at the least with regard to estimating the hypothetical effects of increased striated muscle layer thickness on overall stress distribution. Incorporation of measured material values of the various urethral components, obtained through future direct experimentation, could be added later to improve upon the model's quality.

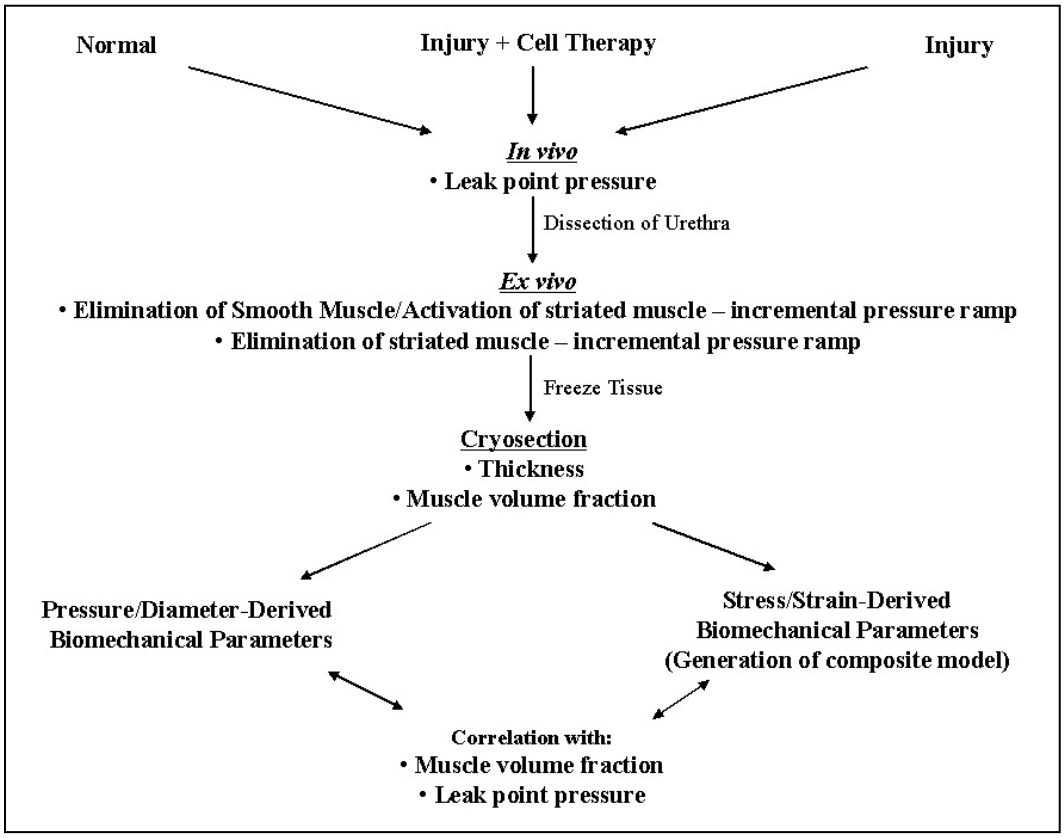

Figure 4.3 Proposed experimental protocol for establishing the influence of striated muscle in the biomechanical properties of the urethra, in relation to physiologic measures of continence.

5.0 CONCLUSIONS

The prevalence of SUI among the aging female population is so high that it is often considered inevitable. Development of this condition, while not life-threatening, can be associated with severe psychological distress and represents a considerable financial burden to the health care community in caring for the elderly population. The importance of the urethral striated muscle layer in maintaining continence has been previously demonstrated through numerous physiologic studies, and damage to this muscle has been implicated in the immediate and delayed onset of SUI. Thus, methods to restore or augment this muscle layer have the potential to create functional improvements in urethral continence securing ability, as opposed to other therapeutic options leading to the creation of bulking obstructions which may or may not persist and which do not address the underlying pathology of the condition.

Regeneration of striated (skeletal) muscle fibers in response to injury is made possible by the presence of resident myogenic progenitor cells. Previously, transplantation of these progenitors has been proposed as a potential treatment for muscle diseases. From a research standpoint, the overwhelming majority of such investigations have focused on the regeneration of motor skeletal muscle to augment the expression of a missing and crucial structural protein, dystrophin, resulting in the pathogenesis of muscular dystrophy. It follows that previous knowledge and experience gained from the use of such technology in the field of muscular dystrophy could be applied for the successful treatment of SUI. Although this concept seems relatively straightforward, and the smaller scale regenerative task at hand seems significantly easier, a number of relevant scientific concerns remain unaddressed. Despite the tremendous amount of research performed in the field of myogenic cell transplantation, little progress has been made in the isolation and identification of progenitors that are capable of tolerating the initial transplantation environment and effectively regenerating clinically-relevant quantities of muscle. Moreover, as opposed to motor skeletal (striated) muscle with a clearly defined and measurable physiologic function, the quantitative role of striated muscle within the urethra remains unclear.

To address the first of these deficiencies, the preplating isolation technique was used to obtain populations that displayed variable abilities to regenerate skeletal myofibers, assessed through the appearance of dystrophin within dystrophic animals following transplantation. A wide range of regeneration ability between isolated populations was observed, however the most efficient population was also the most difficult to obtain, through a laborious culturing procedure. Variable surface protein expression was confirmed among the isolated populations

and provided the basis for investigating whether such proteins had a predictive value in identifying the most efficient progenitors prior to their implantation. However, the proliferation and differentiation behavior of cells within these isolated populations was observed to be superior to these surface markers in this regard. Further, associations between behavior and regenerative quality spanned cells obtained from several species. These results contribute to the growing evidence of underlying behavioral differences that exist between various myogenic progenitors, while also providing evidence that these differences may significantly impact their functional capabilities post-transplantation and thus their utility in regenerative therapies. Further understanding of variability in proliferation and differentiation processes may allow their exploitation for therapeutic benefit. This may indeed represent a significant advancement in an otherwise relatively stagnant field that has struggled to understand the critical variables controlling successful regeneration.

Using an *ex vivo* urethra preparation in combination with an experimental apparatus that had been specifically designed for investigating vascular biomechanics, characterization of regional urethral mechanical properties was performed. It is believed that this represents the first study of its kind, and as such represents a significant advancement in the field by providing a tool in which to relate local urethral tissue structure to mechanical function. Indeed, it was shown that local contractile function could be related to quantitative histological measurements of regional muscle content. Establishing pharmacologic protocols that would allow the specific activation or de-activation of the smooth and/or striated muscle constituents was fundamental to performing studies in which passive and active element contributions to such responses could be evaluated. Measurement of tissue deformation resulting from increasing applied intralumenal pressures allowed quantitative and descriptive parameters describing the contractile capability of each muscle component and its subsequent influences on regional mechanical tissue properties to be obtained. From these measurements, smooth muscle exerted a significantly greater influence on these responses within the mid region in comparison with striated muscle, which corresponded with smooth muscle's ability to generate a higher degree of circumferential stress over a wider range of strain. This would suggest that, in relative terms, a large degree of striated muscle regeneration may be required to elicit significant biomechanical changes. However, the relatively small size of the urethra as a whole, and specifically the functional sphincter region, provides hope that regenerative strategies will be sufficient enough to achieve clinically-relevant outcomes. Not to be overlooked, these outcomes may be highly dependent upon the placement of the cellular grafts and the relative orientation of the regenerated muscle fibers. It should also be mentioned that, as with

most experimental endeavors, the methodology used in the collection of the biomechanical data is currently not without limitations. The most relevant of which was the activation of the striated muscle which may have led to the underestimation of its mechanical relevance to the urethra. Improvements in the system, as suggested, should permit future urethra biomechanical investigations to solidify the structure-mechanical function relationship of normal and therapeutically-treated tissue.

APPENDICES

Appendix A

Non-exponential Growth Model

Within many primary and non-primary cell cultures, a fraction of the cell population often remains in a non-dividing state. To account for this fraction in describing cell population growth, a non-exponential growth model has been proposed by Sherley. This model uses two characteristics of mitotically-active cells to describe the grow kinetics of a cell population, the mitotic fraction (α) and the cell division time (DT). To simplify the mathematical description of non-exponential growth, the following assumptions are made: 1) cells undergo asymmetric divisions, such that the probability of a dividing cell giving rise to a non-dividing cell is constant (i.e. α remains constant), 2) DT of the mitotically-active fraction remains constant over the period of interest, and 3) non-dividing cells do not re-enter the cell cycle. The validity of these assumptions has been discussed within the myogenic cell compartment [235]. Starting with an initial number of cells, N_o, the number of cells at any subsequent doubling time interval can be described by the following:

$$N_1 = 2\alpha N_o + (1-\alpha)N_o \qquad [A1]$$

where the first term represents the mitotically-active fraction and the second term represents the non-mitotically-active fraction. With the assumptions outlined above in mind, it follows that subsequent intervals may be described as follows.

$$N_2 = 2\alpha(2\alpha N_o) + (1-\alpha)(2\alpha N_o) + (1-\alpha)N_o \qquad [A2]$$

$$N_i = 2\alpha^i N_o + (1-\alpha)2\alpha^{i-1} N_o + (1-\alpha)^o N_o \qquad [A3]$$

Expansion of the terms and simplification leads to the following expression.

$$N_i = N_o\left[0.5 + 0.5\sum_{i=0}^{n}(2\alpha)^i\right] \qquad [A4]$$

The following identity (A5) can be used to put the equation into its final form, equation A6.

$$a\sum_{i=0}^{n} x^i = a\frac{1-x^{n+1}}{1-x} \qquad [A5]$$

$$N = N_o\left[0.5 + \frac{1-2\alpha^{(t/DT)+1}}{2(1-2\alpha)}\right] \qquad \text{[A6]}$$

Appendix B

Thick-Walled Circumferential Stress

Variation of stresses in the radial direction (i.e. $\sigma_\theta(r)$, $\sigma_r(r)$) cannot be neglected with thick-walled vessels [211]. A force balance in the radial direction, on a differential element of thickness dz and with radial and circumferential stresses acting upon the element contained within a thick cylindrical-shaped tissue wall (see Figure A.1), yields the following equation.

$$(\sigma_r + d\sigma_r)(r + dr)d\theta dz - \sigma_r r d\theta dz - 2\sigma_\theta dr dz \sin\frac{d\theta}{2} = 0 \qquad [A7]$$

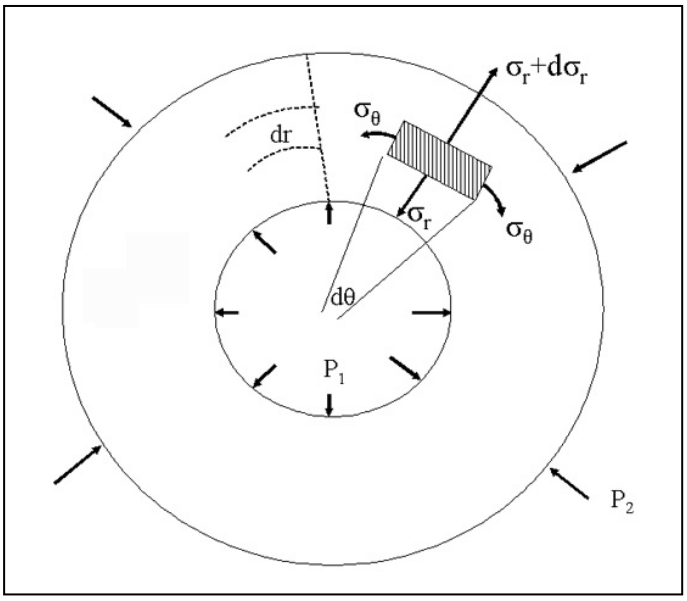

Figure A.1 Stresses acting on a differential element within a cylindrical-shaped tissue segment. Adapted from [211].

This equation is expanded and simplified from discarding higher-order differential terms, and by applying an approximation of sin dθ/2 = θ/2 for a small differential element (e.g. small θ). Dividing all terms by rdrdθdz yields the simplified equilibrium equation.

$$\frac{d\sigma_r}{dr} + \frac{(\sigma_r - \sigma_\theta)}{r} = 0 \qquad \text{[A8]}$$

For displacement, du, in the radial direction, the radial (ε_r) and circumferential (ε_θ) strains are given by the following equations.

$$\varepsilon_r = \frac{du}{dr} \qquad \text{[A9]}$$

$$\varepsilon_\theta = \frac{2\pi(r+u) - 2\pi r}{2\pi r} = \frac{u}{r} \qquad \text{[A10]}$$

Further, the stress-strain relationship can be represented by the following generalized Hooke's law relationships for an isotropic material

$$\varepsilon_r = \frac{\sigma_r}{E} - \frac{\upsilon\sigma_\theta}{E} - \frac{\upsilon\sigma_z}{E} \qquad \text{[A11]}$$

$$\varepsilon_\theta = \frac{\sigma_\theta}{E} - \frac{\upsilon\sigma_r}{E} - \frac{\upsilon\sigma_z}{E} \qquad \text{[A12]}$$

where E is the elastic modulus and υ is the Poisson's ratio (lateral strain/axial strain; such that deformation in one direction will result in corresponding balancing deformations in the transverse directions). These equations also incorporate an assumption of homogeneity such that E is the same at every point in the material (allowing for the principle of superposition to be applied). Rearranging A11 and A12 and simplifying (σ_z=0) yields the following expressions.

$$\sigma_r = E\varepsilon_r + \upsilon\sigma_\theta \qquad \text{[A13]}$$

$$\sigma_\theta = E\varepsilon_\theta + \upsilon\sigma_r \qquad \text{[A14]}$$

Substituting equation A14 into A13, and similarly A13 into A14, yields

$$\sigma_r = \frac{E}{1-\upsilon^2}(\varepsilon_r + \upsilon\varepsilon_\theta) \qquad \text{[A15]}$$

and similarly

$$\sigma_\theta = \frac{E}{1-\upsilon^2}(\varepsilon_\theta + \upsilon\varepsilon_r) \qquad \text{[A16]}$$

Substitution of equations A9 and A10 into equations A15 and A16 yields the following stress-strain relationships.

$$\sigma_r = \frac{E}{1-\upsilon^2}\left(\frac{du}{dr} + \upsilon\frac{u}{r}\right) \quad [A17]$$

$$\sigma_\theta = \frac{E}{1-\upsilon^2}\left(\frac{u}{r} + \upsilon\frac{du}{dr}\right) \quad [A18]$$

Substitution of A17 and A18 into the equilibrium equation, A8, yields A19.

$$\frac{d\left(\frac{du}{dr} + \upsilon\frac{u}{r}\right)}{dr} + \frac{\left(\frac{du}{dr} + \upsilon\frac{u}{r}\right) - \left(\frac{u}{r} + \upsilon\frac{du}{dr}\right)}{r} = 0 \quad [A19]$$

Not that the constants E and υ (which is taken to be a constant 0.5 for incompressible materials) are eliminated from the equation. Expansion of the terms in A19 lead to the following generalized equations for radial displacement, u=u(r).

$$\frac{du^2}{dr^2} + \frac{1}{r}\frac{du}{dr} - \frac{u}{r^2} = 0 \quad [A20]$$

which can be re-written as

$$\frac{d}{dr}\left[\frac{1}{r}\frac{d}{dr}(ur)\right] = 0 \quad [A21]$$

Integrating equation A21 yields

$$u(r) = c_1 r + \frac{c_2}{r} \quad [A22]$$

Substituting A22 into the stress-strain relationships given by equations A17 and A18

$$\sigma_r = \frac{E}{1-\upsilon^2}\left[c_1(1+\upsilon) - c_2\frac{(1-\upsilon)}{r^2}\right] \quad [A23]$$

$$\sigma_\theta = \frac{E}{1-\upsilon^2}\left[c_1(1+\upsilon) + c_2\frac{(1-\upsilon)}{r^2}\right] \quad [A24]$$

Evaluation of the integration constants c_1 and c_2 is performed by applying boundary conditions at the inner (i) and outer (o) cylinder surfaces; $\sigma_r=-P_1$ at $R=R_i$ and $\sigma_r=-P_2$ at $R=R_o$. These conditions state that the radial stress at each

surface is equal to the pressure acting at each respective surface, and both are negative since the pressures are acting into the surface. Substituting the boundary conditions into equation A23

$$-P_1 = \frac{E}{1-\upsilon^2}\left[c_1(1+\upsilon) - c_2\frac{1-\upsilon}{R_i^2}\right] \quad [A25]$$

$$-P_2 = \frac{E}{1-\upsilon^2}\left[c_1(1+\upsilon) - c_2\frac{1-\upsilon}{R_o^2}\right] \quad [A26]$$

these equations can be solved to yield expressions for the integration constants. For simplification, let $A=E/1-\upsilon^2$, $B=1+\upsilon$, and $D=1-\upsilon$. Subtraction of A26 from A25 yields

$$P_2 - P_1 = ADC_2\left(\frac{1}{R_o^2} - \frac{1}{R_i^2}\right) \quad [A27]$$

Rearranging A27 yields

$$c_2 = \frac{1}{AD}\left[\frac{R_i^2 R_o^2(P_1 - P_2)}{R_o^2 - R_i^2}\right] \quad [A28]$$

and substitution of A28 back into A25 results in a similar expression for c_1.

$$c_1 = \frac{1}{AB}\left(\frac{P_1 R_i^2 - P_2 R_o^2}{R_o^2 - R_i^2}\right) \quad [A29]$$

Substitution for A,B, and D results in the final expressions for the integration constants.

$$c_1 = \frac{1-\upsilon}{E}\left[\frac{P_1 R_i^2 - P_2 R_o^2}{R_o^2 - R_i^2}\right] \quad [A30]$$

and

$$c_2 = \frac{1+\upsilon}{E}\left[\frac{R_i^2 R_o^2 (P_1 - P_2)}{R_o^2 - R_i^2}\right] \quad [A31]$$

We can now substitute A30 and A31 into equation A24 to obtain an expression for radial σ distribution throughout the thickness of the cylinder wall.

$$\sigma_\theta(r) = P_1\left(\frac{R_i^2}{R_o^2 - R_i^2}\right)\left(1 + \frac{R_o^2}{r^2}\right) - P_2\left(\frac{R_o^2}{R_o^2 - R_i^2}\right)\left(1 + \frac{R_i^2}{r^2}\right) \quad [A32]$$

This equation may be simplified further for cases in which transmural pressure (P) is specified as the internal pressure, P_1. Thus, $P_2=0$ may be substituted, resulting in the simplified form.

$$\sigma_\theta(r) = P\left(\frac{R_i^2}{R_o^2 - R_i^2}\right)\left(1 + \frac{R_o^2}{r^2}\right) \qquad \text{[A33]}$$

As predicted by the equation A33, σ_θ decreases with increasing radial position toward the outer cylindrical surface (increasing r). This is intuitive since the circumferential strain is the largest near the inner surface and the smallest near the outer surface of the cylinder.

Appendix C

Pressure-Diameter and Stress-Strain (Mid-wall) Responses

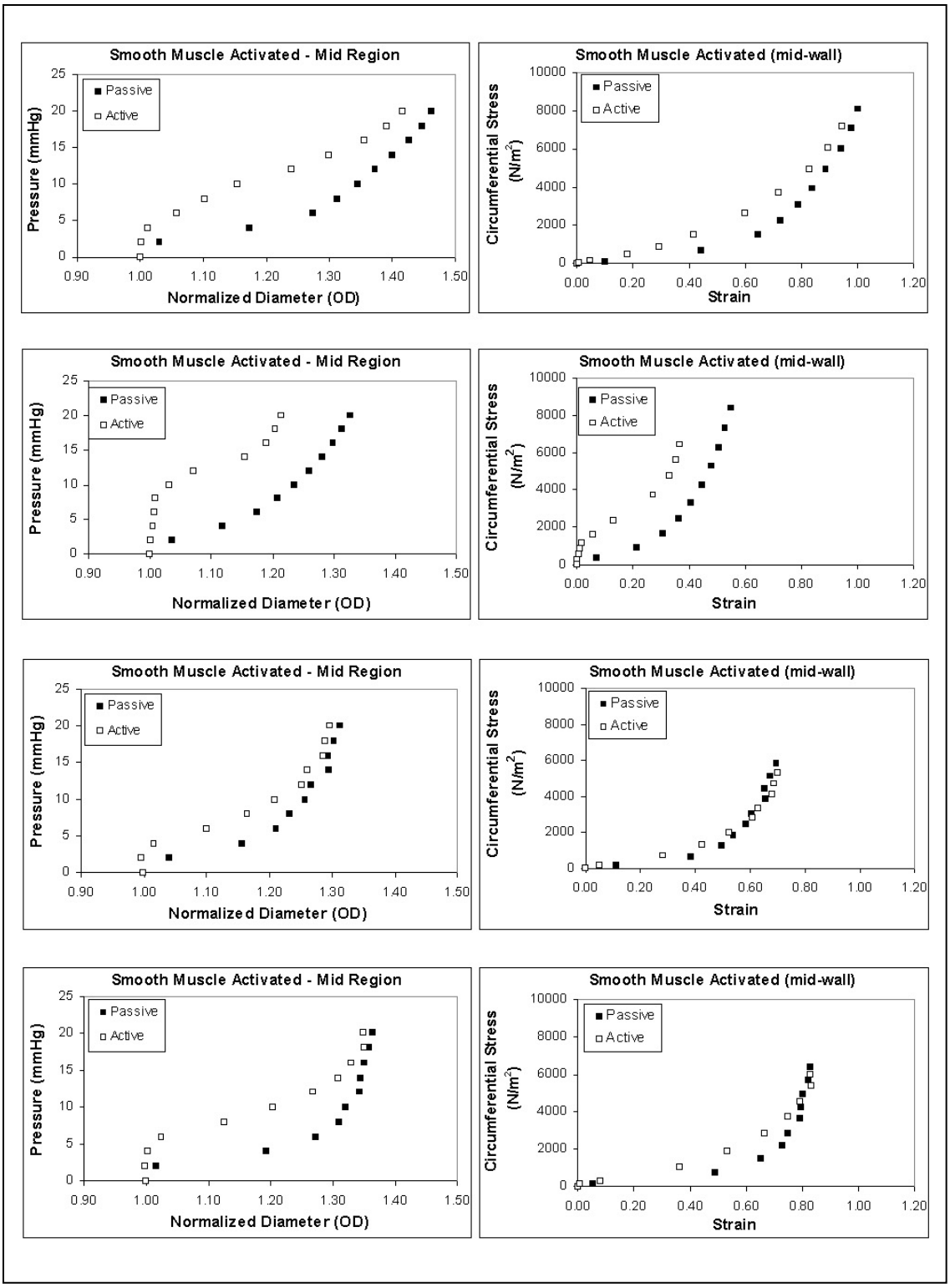

Figure A.2 Smooth muscle only pressure-diameter and mid-wall stress-strain responses.

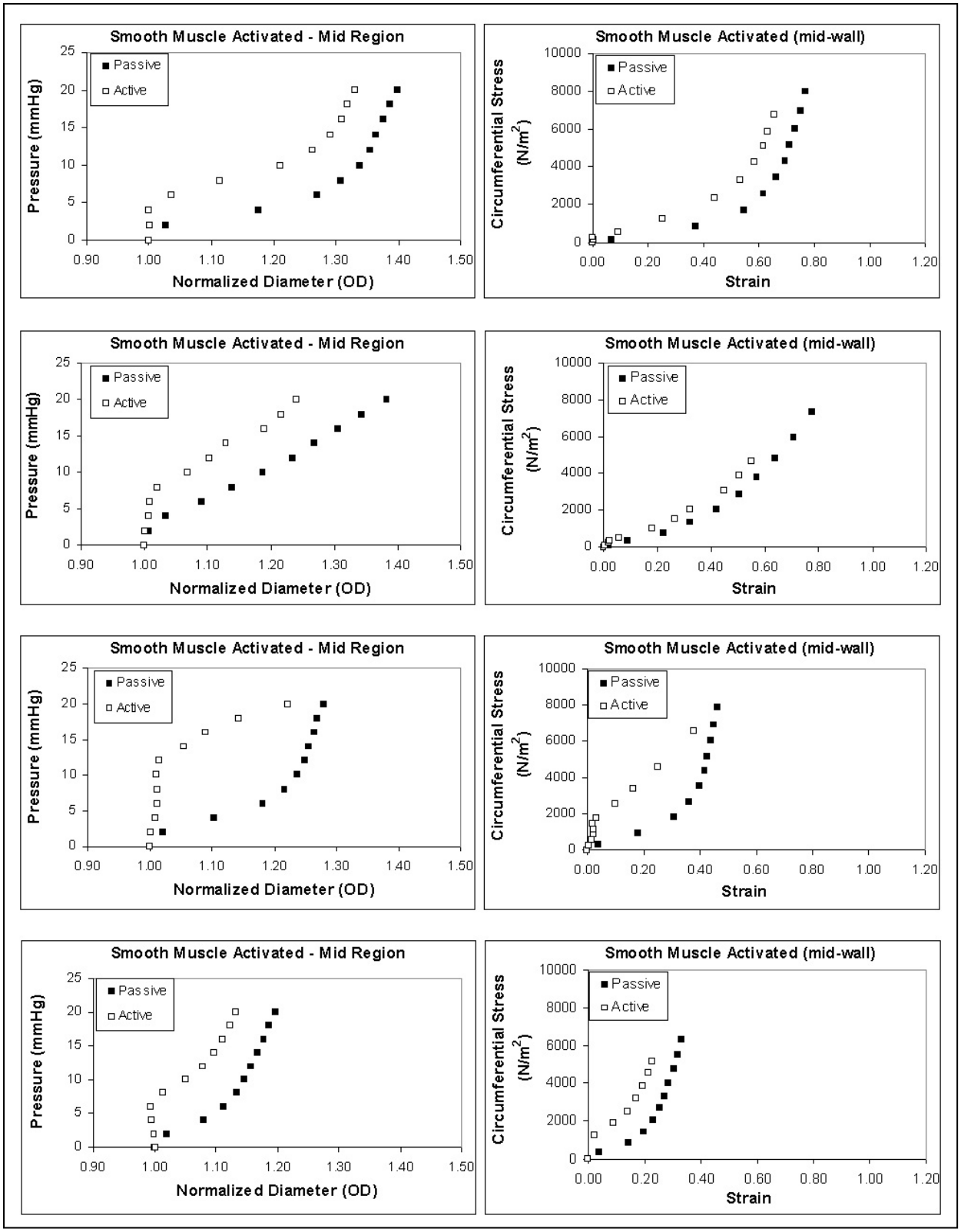

Figure A.3 Smooth muscle only pressure-diameter and mid-wall stress-strain responses, continued.

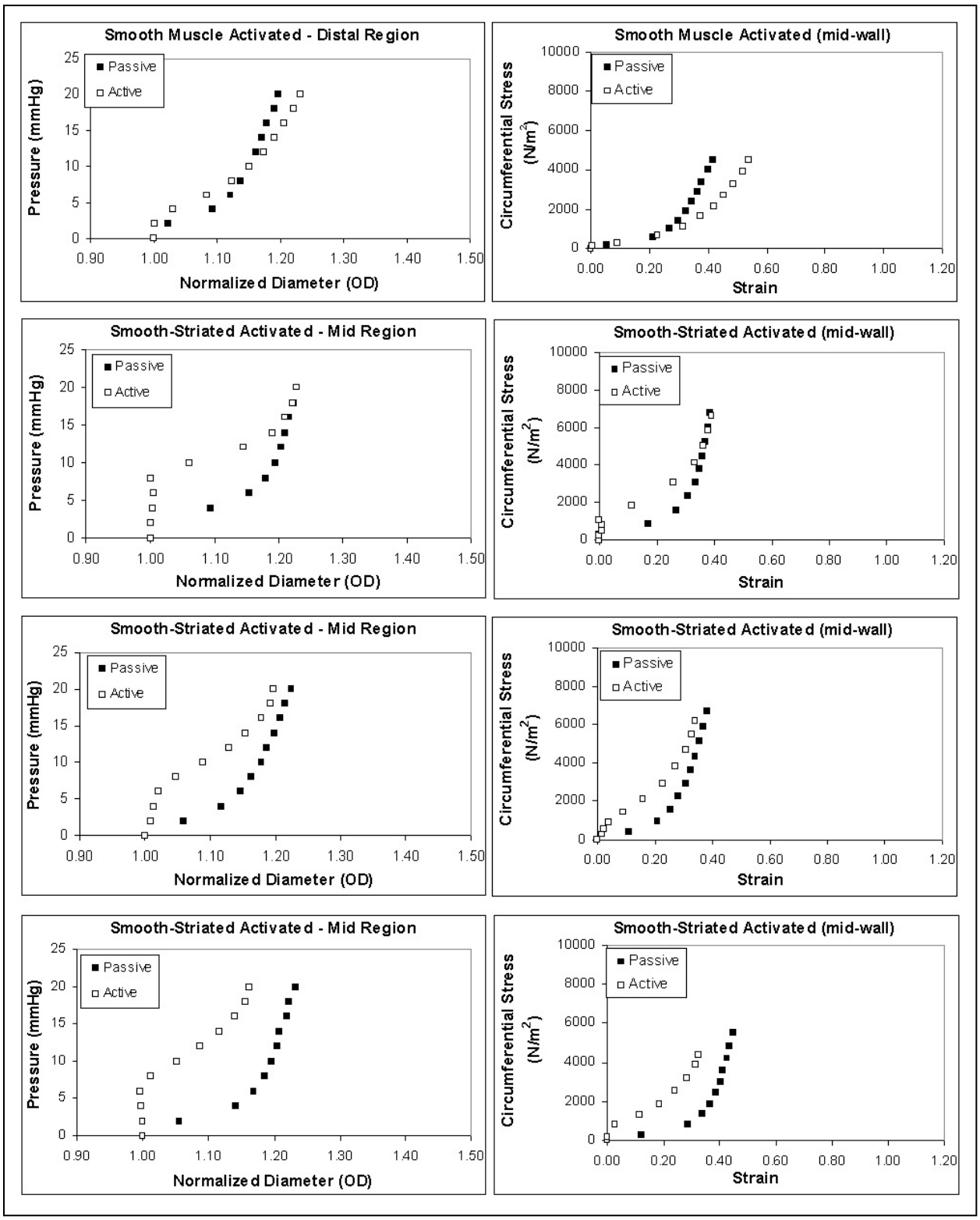

Figure A.4 Smooth muscle only and smooth-striated muscle pressure-diameter and mid-wall stress-strain responses.

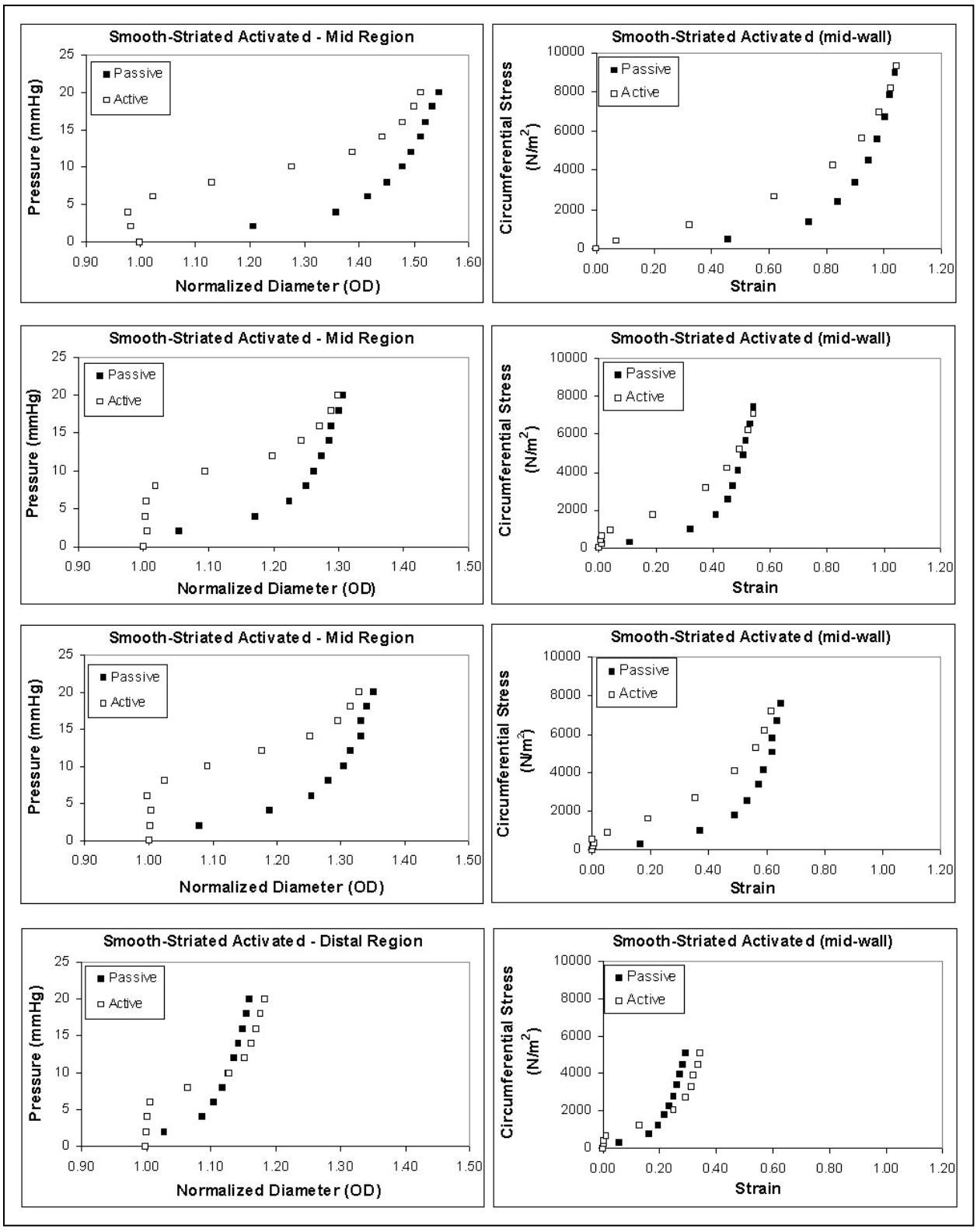

Figure A.5 Smooth-striated muscle pressure-diameter and mid-wall stress-strain responses, continued.

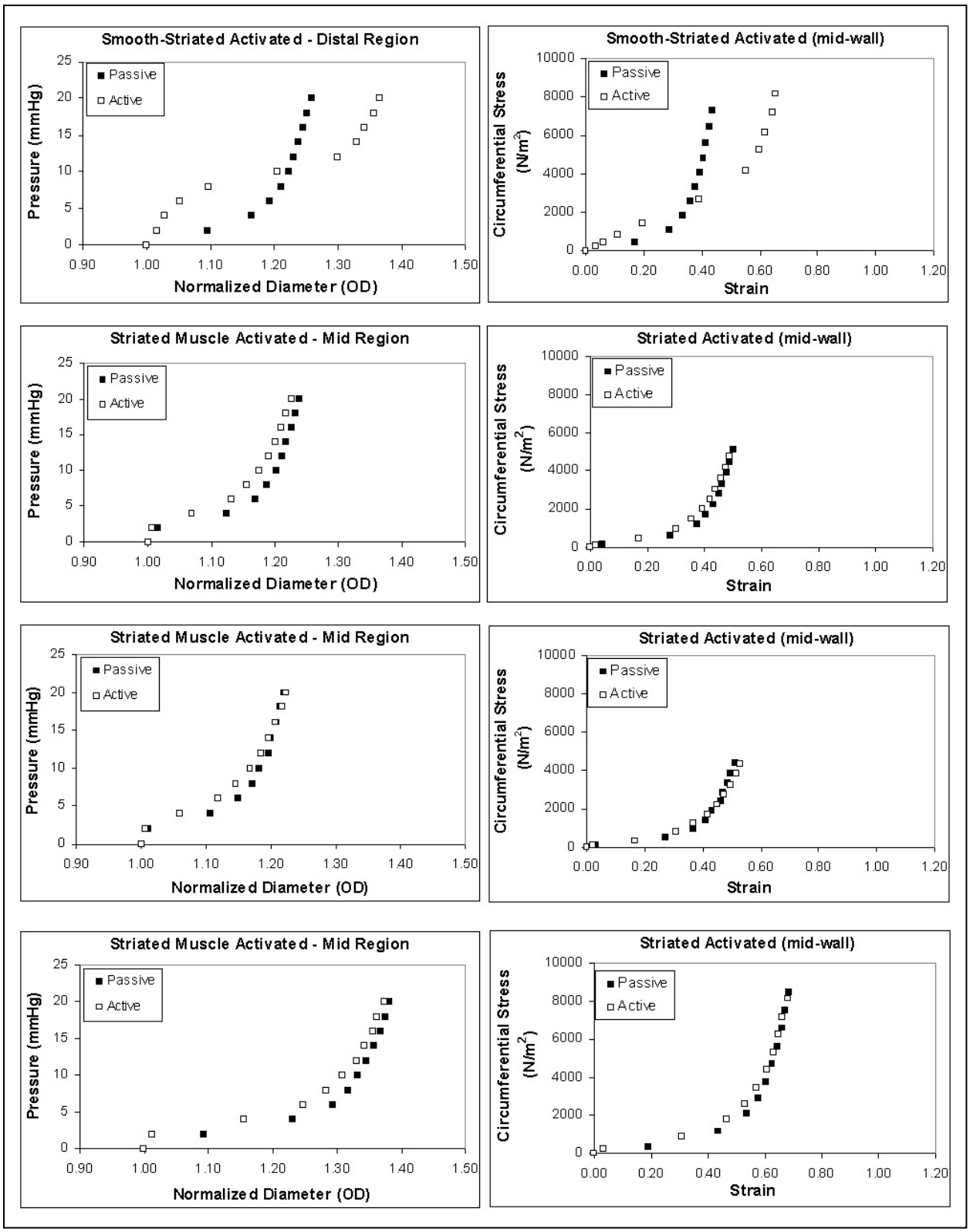

Figure A.6 Smooth-striated and striated muscle only pressure-diameter and mid-wall stress-strain responses.

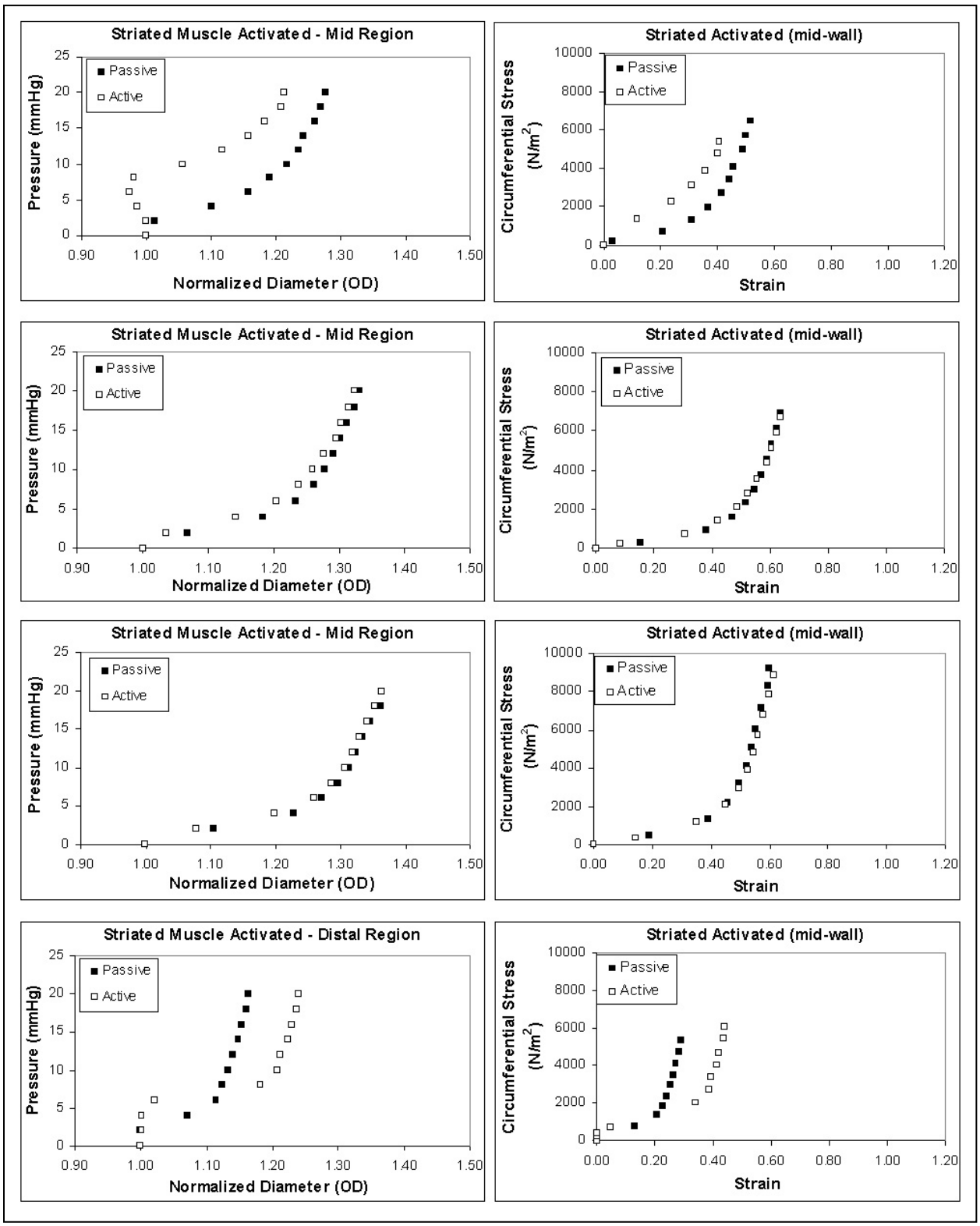

Figure A.7 Striated muscle only pressure-diameter and mid-wall stress-strain responses, continued.

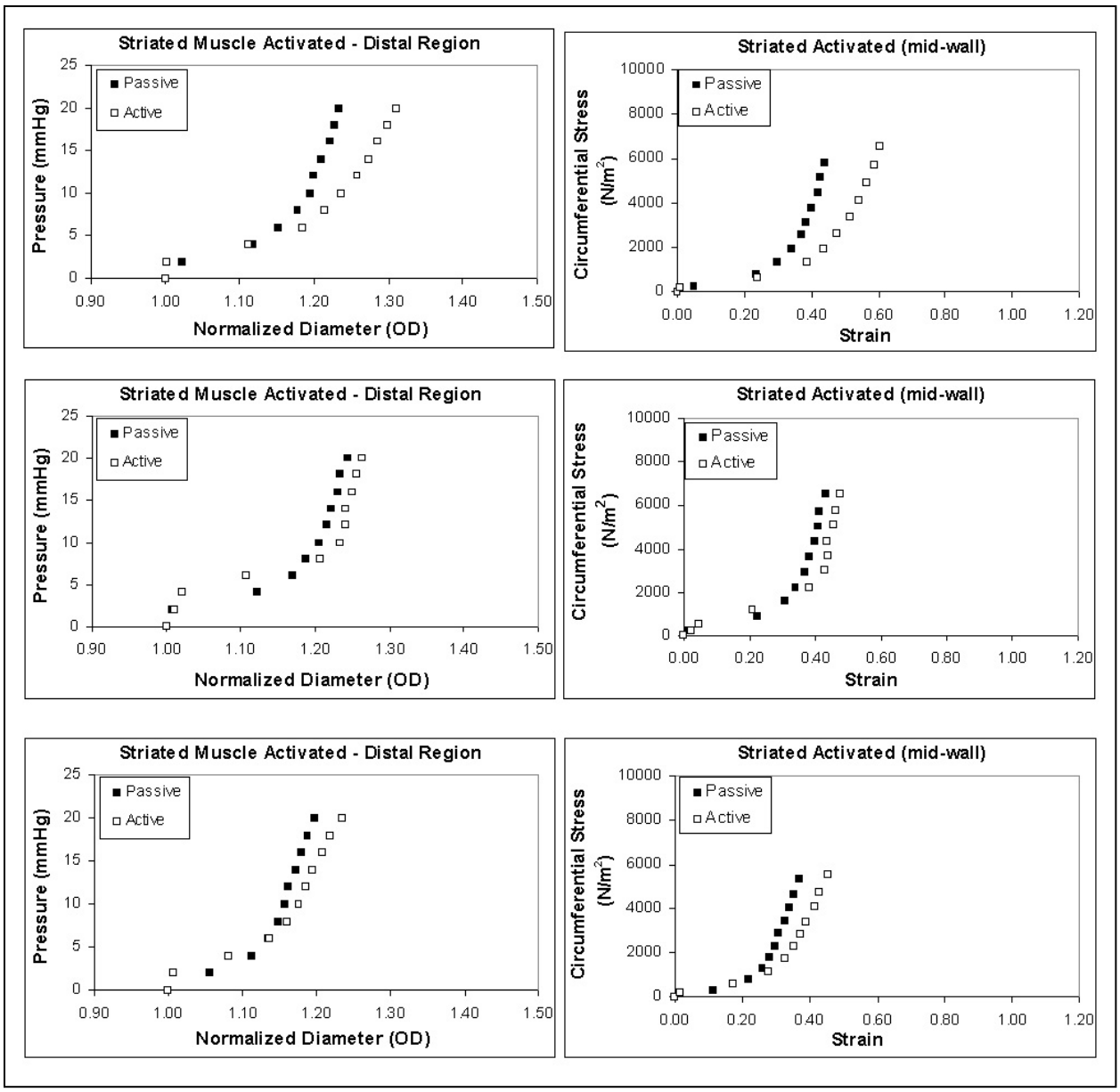

Figure A.8 Striated muscle only pressure-diameter and mid-wall stress-strain responses, continued.

BIBLIOGRAPHY

[1] A. Mauro, "Satellite cells of skeletal muscle fibers," *Journal of Biochemistry and Biophysical Cytology*, vol. 9, pp. 493-8, 1961.

[2] R. Bischoff, "The satellite cell and muscle regeneration," in *Myology*, A. G. Engel, and C. Franszini-Armstrong, Eds. New York: McGraw-Hill, 1994, pp. 97-118.

[3] B. H. Lipton, and E. Schultz, "Developmental fate of skeletal muscle satellite cells," *Science*, vol. 205, pp. 1292-4, 1979.

[4] K. Goldring, T. Partridge, and D. Watt, "Muscle stem cells," *J Pathol*, vol. 197, pp. 457-67, 2002.

[5] Z. Dvir, "Biomechanics of muscle," in *Clinical biomechanics.*, Z. Dvir, Eds. New York: Churchill Livingstone, 2000, pp. 83-102.

[6] D. D. Cornelison, and B. J. Wold, "Single-cell analysis of regulatory gene expression in quiescent and activated mouse skeletal muscle satellite cells," *Dev Biol*, vol. 191, pp. 270-83, 1997.

[7] J. R. Beauchamp, L. Heslop, D. S. Yu, S. Tajbakhsh, R. G. Kelly, A. Wernig, M. E. Buckingham, T. A. Partridge, and P. S. Zammit, "Expression of cd34 and myf5 defines the majority of quiescent adult skeletal muscle satellite cells," *J Cell Biol*, vol. 151, pp. 1221-34, 2000.

[8] N. Yoshida, S. Yoshida, K. Koishi, K. Masuda, and Y. Nabeshima, "Cell heterogeneity upon myogenic differentiation: Down-regulation of myod and myf-5 generates 'reserve cells'," *J Cell Sci*, vol. 111 (Pt 6), pp. 769-79, 1998.

[9] P. Seale, and M. A. Rudnicki, "A new look at the origin, function, and "stem-cell" status of muscle satellite cells," *Dev Biol*, vol. 218, pp. 115-24, 2000.

[10] P. Seale, L. A. Sabourin, A. Girgis-Gabardo, A. Mansouri, P. Gruss, and M. A. Rudnicki, "Pax7 is required for the specification of myogenic satellite cells," *Cell*, vol. 102, pp. 777-86, 2000.

[11] L. A. Megeney, and M. A. Rudnicki, "Determination versus differentiation and the myod family of transcription factors," *Biochem Cell Biol*, vol. 73, pp. 723-32, 1995.

[12] H. Weintraub, "The myod family and myogenesis: Redundancy, networks, and thresholds," *Cell*, vol. 75, pp. 1241-4, 1993.

[13] M. Kitzmann, G. Carnac, M. Vandromme, M. Primig, N. J. Lamb, and A. Fernandez, "The muscle regulatory factors myod and myf-5 undergo distinct cell cycle-specific expression in muscle cells," *J Cell Biol*, vol. 142, pp. 1447-59, 1998.

[14] A. B. Firulli, and E. N. Olson, "Modular regulation of muscle gene transcription: A mechanism for muscle cell diversity," *Trends Genet*, vol. 13, pp. 364-9, 1997.

[15] M. Kitzmann, and A. Fernandez, "Crosstalk between cell cycle regulators and the myogenic factor myod in skeletal myoblasts," *Cell Mol Life Sci*, vol. 58, pp. 571-9, 2001.

[16] J. M. Zhang, Q. Wei, X. Zhao, and B. M. Paterson, "Coupling of the cell cycle and myogenesis through the cyclin d1-dependent interaction of myod with cdk4," *Embo J*, vol. 18, pp. 926-33, 1999.

[17] C. J. Sherr, "G1 phase progression: Cycling on cue," *Cell*, vol. 79, pp. 551-5, 1994.

[18] D. C. Ludolph, and S. F. Konieczny, "Transcription factor families: Muscling in on the myogenic program," *Faseb J*, vol. 9, pp. 1595-604, 1995.

[19] J. D. Molkentin, and E. N. Olson, "Defining the regulatory networks for muscle development," *Curr Opin Genet Dev*, vol. 6, pp. 445-53, 1996.

[20] R. L. Perry, and M. A. Rudnick, "Molecular mechanisms regulating myogenic determination and differentiation," *Front Biosci*, vol. 5, pp. D750-67, 2000.

[21] P. L. Puri, and V. Sartorelli, "Regulation of muscle regulatory factors by DNA-binding, interacting proteins, and post-transcriptional modifications," *J Cell Physiol*, vol. 185, pp. 155-73, 2000.

[22] J. B. Miller, L. Schaefer, and J. A. Dominov, "Seeking muscle stem cells," *Curr Top Dev Biol*, vol. 43, pp. 191-219, 1999.

[23] L. A. Sabourin, and M. A. Rudnicki, "The molecular regulation of myogenesis," *Clin Genet*, vol. 57, pp. 16-25, 2000.

[24] J. Rantanen, T. Hurme, R. Lukka, J. Heino, and H. Kalimo, "Satellite cell proliferation and the expression of myogenin and desmin in regenerating skeletal muscle: Evidence for two different populations of satellite cells," *Lab Invest*, vol. 72, pp. 341-7, 1995.

[25] E. Schultz, "Satellite cell proliferative compartments in growing skeletal muscles," *Dev Biol*, vol. 175, pp. 84-94, 1996.

[26] A. Baroffio, M. L. Bochaton-Piallat, G. Gabbiani, and C. R. Bader, "Heterogeneity in the progeny of single human muscle satellite cells," *Differentiation*, vol. 59, pp. 259-68, 1995.

[27] A. Baroffio, M. Hamann, L. Bernheim, M. L. Bochaton-Piallat, G. Gabbiani, and C. R. Bader, "Identification of self-renewing myoblasts in the progeny of single human muscle satellite cells," *Differentiation*, vol. 60, pp. 47-57, 1996.

[28] G. Molnar, M. L. Ho, and N. A. Schroedl, "Evidence for multiple satellite cell populations and a non-myogenic cell type that is regulated differently in regenerating and growing skeletal muscle," *Tissue Cell*, vol. 28, pp. 547-56, 1996.

[29] E. Schultz, and B. H. Lipton, "Skeletal muscle satellite cells: Changes in proliferation potential as a function of age," *Mech Ageing Dev*, vol. 20, pp. 377-83, 1982.

[30] E. Schultz, and D. L. Jaryszak, "Effects of skeletal muscle regeneration on the proliferation potential of satellite cells," *Mech Ageing Dev*, vol. 30, pp. 63-72, 1985.

[31] E. E. Spangenburg, M. V. Chakravarthy, and F. W. Booth, "P27kip1: A key regulator of skeletal muscle satellite cell proliferation," *Clin Orthop*, vol. pp. S221-7, 2002.

[32] A. Asakura, M. Komaki, and M. Rudnicki, "Muscle satellite cells are multipotential stem cells that exhibit myogenic, osteogenic, and adipogenic differentiation," *Differentiation*, vol. 68, pp. 245-53, 2001.

[33] B. M. Deasy, and J. Huard, "Gene therapy and tissue engineering based on muscle-derived stem cells," *Curr Opin Mol Ther*, vol. 4, pp. 382-9, 2002.

[34] L. De Angelis, L. Berghella, M. Coletta, L. Lattanzi, M. Zanchi, M. G. Cusella-De Angelis, C. Ponzetto, and G. Cossu, "Skeletal myogenic progenitors originating from embryonic dorsal aorta coexpress endothelial and myogenic markers and contribute to postnatal muscle growth and regeneration," *J Cell Biol*, vol. 147, pp. 869-78, 1999.

[35] G. Cossu, and F. Mavilio, "Myogenic stem cells for the therapy of primary myopathies: Wishful thinking or therapeutic perspective?," *J Clin Invest*, vol. 105, pp. 1669-74, 2000.

[36] E. Gussoni, Y. Soneoka, C. D. Strickland, E. A. Buzney, M. K. Khan, A. F. Flint, L. M. Kunkel, and R. C. Mulligan, "Dystrophin expression in the mdx mouse restored by stem cell transplantation," *Nature*, vol. 401, pp. 390-4, 1999.

[37] K. A. Jackson, T. Mi, and M. A. Goodell, "Hematopoietic potential of stem cells isolated from murine skeletal muscle," *Proc Natl Acad Sci U S A*, vol. 96, pp. 14482-6, 1999.

[38] Y. Torrente, J. P. Tremblay, F. Pisati, M. Belicchi, B. Rossi, M. Sironi, F. Fortunato, M. El Fahime, M. G. D'Angelo, N. J. Caron, G. Constantin, D. Paulin, G. Scarlato, and N. Bresolin, "Intraarterial injection of muscle-derived cd34(+)sca-1(+) stem cells restores dystrophin in mdx mice," *J Cell Biol*, vol. 152, pp. 335-48, 2001.

[39] J. Y. Lee, Z. Qu-Petersen, B. Cao, S. Kimura, R. Jankowski, J. Cummins, A. Usas, C. Gates, P. Robbins, A. Wernig, and J. Huard, "Clonal isolation of muscle-derived cells capable of enhancing muscle regeneration and bone healing," *J Cell Biol*, vol. 150, pp. 1085-100, 2000.

[40] R. G. Bateson, D. F. Woodrow, and J. C. Sloper, "Circulating cell as a source of myoblasts in regenerating injured mammalian skeletal muscle," *Nature*, vol. 213, pp. 1035-6, 1967.

[41] C. N. Pagel, and T. A. Partridge, "Covert persistence of mdx mouse myopathy is revealed by acute and chronic effects of irradiation," *J Neurol Sci*, vol. 164, pp. 103-16, 1999.

[42] T. A. Partridge, "Cells that participate in regeneration of skeletal muscle," *Gene Ther*, vol. 9, pp. 752-3, 2002.

[43] Z. Qu-Petersen, B. Deasy, R. Jankowski, M. Ikezawa, J. Cummins, R. Pruchnic, J. Mytinger, B. Cao, C. Gates, A. Wernig, and J. Huard, "Identification of a novel population of muscle stem cells in mice: Potential for muscle regeneration," *J Cell Biol*, vol. 157, pp. 851-64, 2002.

[44] E. P. Hoffman, R. H. Brown, and L. M. Kunkel, "Dystrophin: The protein product of the duchene muscular dystrophy locus.," *Biotechnology*, vol. 24, pp. 457-66, 1992.

[45] E. Bakker, and G. van Ommen, "Duchenne and becker dystrophy," in *Neuromuscular disorders : Clinical and molecular genetics*, A. E. Emery, Eds. New York: Wiley and Sons, 1998, pp. 59-85.

[46] K. P. Campbell, and S. D. Kahl, "Association of dystrophin and an integral membrane glycoprotein," *Nature*, vol. 338, pp. 259-62, 1989.

[47] E. Bonilla, C. E. Samitt, A. F. Miranda, A. P. Hays, G. Salviati, S. DiMauro, L. M. Kunkel, E. P. Hoffman, and L. P. Rowland, "Duchenne muscular dystrophy: Deficiency of dystrophin at the muscle cell surface," *Cell*, vol. 54, pp. 447-52, 1988.

[48] B. J. Petrof, J. B. Shrager, H. H. Stedman, A. M. Kelly, and H. L. Sweeney, "Dystrophin protects the sarcolemma from stresses developed during muscle contraction," *Proc Natl Acad Sci U S A*, vol. 90, pp. 3710-4, 1993.

[49] B. Weller, G. Karpati, and S. Carpenter, "Dystrophin-deficient mdx muscle fibers are preferentially vulnerable to necrosis induced by experimental lengthening contractions," *J Neurol Sci*, vol. 100, pp. 9-13, 1990.

[50] M. Grounds, T. A. Robertson, C. A. Mitchell, and J. M. Papadimitiou, "Necrosis and regeneration in dystrophic and normal skeletal muscle," in *Duchenne muscular dystrophy: Animal models and genetic manipulation*, B. A. Kakulas, Eds. New York: Raven Press, 1992, pp. 141-50.

[51] J. T. Vilquin, V. Brussee, I. Asselin, I. Kinoshita, M. Gingras, and J. P. Tremblay, "Evidence of mdx mouse skeletal muscle fragility in vivo by eccentric running exercise," *Muscle Nerve*, vol. 21, pp. 567-76, 1998.

[52] N. Deconinck, T. Ragot, G. Marechal, M. Perricaudet, and J. M. Gillis, "Functional protection of dystrophic mouse (mdx) muscles after adenovirus-mediated transfer of a dystrophin minigene," *Proc Natl Acad Sci U S A*, vol. 93, pp. 3570-4, 1996.

[53] L. Yang, H. Lochmuller, J. Luo, B. Massie, J. Nalbantoglu, G. Karpati, and B. J. Petrof, "Adenovirus-mediated dystrophin minigene transfer improves muscle strength in adult dystrophic (mdx) mice," *Gene Ther*, vol. 5, pp. 369-79, 1998.

[54] T. A. Partridge, J. E. Morgan, G. R. Coulton, E. P. Hoffman, and L. M. Kunkel, "Conversion of mdx myofibres from dystrophin-negative to -positive by injection of normal myoblasts," *Nature*, vol. 337, pp. 176-9, 1989.

[55] J. E. Morgan, E. P. Hoffman, and T. A. Partridge, "Normal myogenic cells from newborn mice restore normal histology to degenerating muscles of the mdx mouse," *J Cell Biol*, vol. 111, pp. 2437-49, 1990.

[56] E. Gussoni, G. K. Pavlath, A. M. Lanctot, K. R. Sharma, R. G. Miller, L. Steinman, and H. M. Blau, "Normal dystrophin transcripts detected in duchenne muscular dystrophy patients after myoblast transplantation," *Nature*, vol. 356, pp. 435-8, 1992.

[57] J. Huard, J. P. Bouchard, R. Roy, F. Malouin, G. Dansereau, C. Labrecque, N. Albert, C. L. Richards, B. Lemieux, and J. P. Tremblay, "Human myoblast transplantation: Preliminary results of 4 cases," *Muscle Nerve*, vol. 15, pp. 550-60, 1992.

[58] R. G. Miller, K. R. Sharma, G. K. Pavlath, E. Gussoni, M. Mynhier, A. M. Lanctot, C. M. Greco, L. Steinman, and H. M. Blau, "Myoblast implantation in duchenne muscular dystrophy: The san francisco study," *Muscle Nerve*, vol. 20, pp. 469-78, 1997.

[59] J. Huard, R. Roy, J. P. Bouchard, F. Malouin, C. L. Richards, and J. P. Tremblay, "Human myoblast transplantation between immunohistocompatible donors and recipients produces immune reactions," *Transplant Proc*, vol. 24, pp. 3049-51, 1992.

[60] J. P. Tremblay, J. P. Bouchard, F. Malouin, D. Theau, F. Cottrell, H. Collin, A. Rouche, S. Gilgenkrantz, N. Abbadi, M. Tremblay, and et al., "Myoblast transplantation between monozygotic twin girl carriers of duchenne muscular dystrophy," *Neuromuscul Disord*, vol. 3, pp. 583-92, 1993.

[61] Y. Ohtsuka, K. Udaka, Y. Yamashiro, H. Yagita, and K. Okumura, "Dystrophin acts as a transplantation rejection antigen in dystrophin-deficient mice: Implication for gene therapy," *J Immunol*, vol. 160, pp. 4635-40, 1998.

[62] J. Huard, G. Acsadi, A. Jani, B. Massie, and G. Karpati, "Gene transfer into skeletal muscles by isogenic myoblasts," *Hum Gene Ther*, vol. 5, pp. 949-58, 1994.

[63] J. P. Tremblay, F. Malouin, R. Roy, J. Huard, J. P. Bouchard, A. Satoh, and C. L. Richards, "Results of a triple blind clinical study of myoblast transplantations without immunosuppressive treatment in young boys with duchenne muscular dystrophy," *Cell Transplant*, vol. 2, pp. 99-112, 1993.

[64] J. R. Mendell, J. T. Kissel, A. A. Amato, W. King, L. Signore, T. W. Prior, Z. Sahenk, S. Benson, P. E. McAndrew, R. Rice, and et al., "Myoblast transfer in the treatment of duchenne's muscular dystrophy," *N Engl J Med*, vol. 333, pp. 832-8, 1995.

[65] A. M. Neumeyer, D. Cros, D. McKenna-Yasek, A. Zawadzka, E. P. Hoffman, E. Pegoraro, R. G. Hunter, T. L. Munsat, and R. H. Brown, Jr., "Pilot study of myoblast transfer in the treatment of becker muscular dystrophy," *Neurology*, vol. 51, pp. 589-92, 1998.

[66] Y. Fan, M. Maley, M. Beilharz, and M. Grounds, "Rapid death of injected myoblasts in myoblast transfer therapy," *Muscle Nerve*, vol. 19, pp. 853-60, 1996.

[67] J. R. Beauchamp, J. E. Morgan, C. N. Pagel, and T. A. Partridge, "Quantitative studies of efficacy of myoblast transplantation," *Muscle Nerve*, vol. 18 (Suppl), pp. 261, 1994.

[68] J. R. Beauchamp, J. E. Morgan, C. N. Pagel, and T. A. Partridge, "Dynamics of myoblast transplantation reveal a discrete minority of precursors with stem cell-like properties as the myogenic source," *J Cell Biol*, vol. 144, pp. 1113-22, 1999.

[69] I. Kinoshita, J. Huard, and J. P. Tremblay, "Utilization of myoblasts from transgenic mice to evaluate the efficacy of myoblast transplantation," *Muscle Nerve*, vol. 17, pp. 975-80, 1994.

[70] B. Guerette, I. Asselin, D. Skuk, M. Entman, and J. P. Tremblay, "Control of inflammatory damage by anti-lfa-1: Increase success of myoblast transplantation," *Cell Transplant*, vol. 6, pp. 101-7, 1997.

[71] I. Kinoshita, J. T. Vilquin, B. Guerette, I. Asselin, R. Roy, and J. P. Tremblay, "Very efficient myoblast allotransplantation in mice under fk506 immunosuppression," *Muscle Nerve*, vol. 17, pp. 1407-15, 1994.

[72] G. M. Smythe, S. I. Hodgetts, and M. D. Grounds, "Problems and solutions in myoblast transfer therapy," *J Cell Mol Med*, vol. 5, pp. 33-47, 2001.

[73] S. I. Hodgetts, M. W. Beilharz, A. A. Scalzo, and M. D. Grounds, "Why do cultured transplanted myoblasts die in vivo? DNA quantification shows enhanced survival of donor male myoblasts in host mice depleted of cd4+ and cd8+ cells or nk1.1+ cells," *Cell Transplant*, vol. 9, pp. 489-502, 2000.

[74] F. Merly, C. Huard, I. Asselin, P. D. Robbins, and J. P. Tremblay, "Anti-inflammatory effect of transforming growth factor-beta1 in myoblast transplantation," *Transplantation*, vol. 65, pp. 793-9, 1998.

[75] Z. Qu, L. Balkir, J. C. van Deutekom, P. D. Robbins, R. Pruchnic, and J. Huard, "Development of approaches to improve cell survival in myoblast transfer therapy," *J Cell Biol*, vol. 142, pp. 1257-67, 1998.

[76] T. Partridge, "The current status of myoblast transfer," *Neurol Sci*, vol. 21, pp. S939-42, 2000.

[77] A. Elbadawi, "Functional anatomy of the organs of micturition," *Urol Clin North Am*, vol. 23, pp. 177-210, 1996.

[78] A. Massey, and P. Abrams, "Urodynamics of the female lower urinary tract," *Urol Clin North Am*, vol. 12, pp. 231-46, 1985.

[79] S. A. MacDiarmid, "Incontinence after radical prostatectomy: Pathophysiology and management," *Curr Urol Rep*, vol. 2, pp. 209-13, 2001.

[80] J. G. Lee, A. J. Wein, and R. M. Levin, "Effects of pregnancy on urethral and bladder neck function," *Urology*, vol. 42, pp. 747-52, 1993.

[81] Agency for Healthcare Policy and Research, US Department of Health and Human Services, "Urinary incontinence in adults - clinical practice guidelines.," Rockville, MD, 1996.

[82] A. J. Macaulay, R. S. Stern, and S. L. Stanton, "Psychological aspects of 211 female patients attending a urodynamic unit," *J Psychosom Res*, vol. 35, pp. 1-10, 1991.

[83] J. A. Gosling, "The structure of the female lower urinary tract and pelvic floor," *Urol Clin North Am*, vol. 12, pp. 207-14, 1985.

[84] T. M. Oelrich, "The striated urogenital sphincter muscle in the female," *Anat Rec*, vol. 205, pp. 223-32, 1983.

[85] D. P. Keane, and S. O'Sullivan, "Urinary incontinence: Anatomy, physiology and pathophysiology," *Baillieres Best Pract Res Clin Obstet Gynaecol*, vol. 14, pp. 207-26, 2000.

[86] P. Thind, "The significance of smooth and striated muscles in the sphincter function of the urethra in healthy women," *Neurourol Urodyn*, vol. 14, pp. 585-618, 1995.

[87] A. F. Brading, C. H. Fry, C. A. Maggi, M. Takeda, R. Wammack, N. P. Wilklund, B. Uvelius, and G. Gabella, "Cellular biology," in *Incontinence*, P. Abrams, S. Khoury, and A. Wein, Eds. Plymouth UK: Health Publications Ltd, 1999, pp. 59-104.

[88] A. Carlile, I. Davies, A. Rigby, and J. C. Brocklehurst, "Age changes in the human female urethra: A morphometric study," *J Urol*, vol. 139, pp. 532-5, 1988.

[89] D. Perucchini, J. O. DeLancey, J. A. Ashton-Miller, A. Galecki, and G. N. Schaer, "Age effects on urethral striated muscle. Ii. Anatomic location of muscle loss," *Am J Obstet Gynecol*, vol. 186, pp. 356-60, 2002.

[90] D. Perucchini, J. O. DeLancey, J. A. Ashton-Miller, U. Peschers, and T. Kataria, "Age effects on urethral striated muscle. I. Changes in number and diameter of striated muscle fibers in the ventral urethra," *Am J Obstet Gynecol*, vol. 186, pp. 351-5, 2002.

[91] T. Rud, "Urethral pressure profile in continent women from childhood to old age," *Acta Obstet Gynecol Scand*, vol. 59, pp. 331-5, 1980.

[92] J. M. van Geelen, W. A. Lemmens, T. K. Eskes, and C. B. Martin, Jr., "The urethral pressure profile in pregnancy and after delivery in healthy nulliparous women," *Am J Obstet Gynecol*, vol. 144, pp. 636-49, 1982.

[93] R. E. Allen, G. L. Hosker, A. R. Smith, and D. W. Warrell, "Pelvic floor damage and childbirth: A neurophysiological study," *Br J Obstet Gynaecol*, vol. 97, pp. 770-9, 1990.

[94] H. Koelbl, J. Mostwin, J. P. Boiteaux, E. Macarak, E. Petri, W. Schafer, and O. Yamaguchi, "Pathophysiology," in *Incontinence*, P. Abrams, L. D. Cardozo, S. Khoury, and A. Wein, Eds. Plymouth, OK: Health Publication Ltd., 2002, pp. 205-41.

[95] D. S. Hale, J. T. Benson, L. Brubaker, M. C. Heidkamp, and B. Russell, "Histologic analysis of needle biopsy of urethral sphincter from women with normal and stress incontinence with comparison of electromyographic findings," *Am J Obstet Gynecol*, vol. 180, pp. 342-8, 1999.

[96] P. Thind, and G. Lose, "The effect of bilateral pudendal blockade on the adjunctive urethral closure forces in healthy females," *Scand J Urol Nephrol*, vol. 28, pp. 249-55, 1994.

[97] P. Thind, and G. Lose, "The effect of bilateral pudendal blockade on the static urethral closure function in healthy females," *Obstet Gynecol*, vol. 80, pp. 906-11, 1992.

[98] G. Lose, and H. Colstrup, "Mechanical properties of the urethra in healthy and stress incontinent females: Dynamic measurements in the resting urethra," *J Urol*, vol. 144, pp. 1258-62, 1990.

[99] E. Versi, L. D. Cardozo, J. W. Studd, M. Brincat, T. M. O'Dowd, and D. J. Cooper, "Internal urinary sphincter in maintenance of female continence," *Br Med J (Clin Res Ed)*, vol. 292, pp. 166-7, 1986.

[100] D. A. Richardson, "Overflow incontinence and urinary retention," *Clin Obstet Gynecol*, vol. 33, pp. 378-81, 1990.

[101] J. T. Benson, "New therapeutic options for urge incontinence," *Curr Womens Health Rep*, vol. 1, pp. 61-6, 2001.

[102] K. H. Moore, "Conservative management for urinary incontinence," *Baillieres Best Pract Res Clin Obstet Gynaecol*, vol. 14, pp. 251-89, 2000.

[103] J. A. Ashton-Miller, D. Howard, and J. O. DeLancey, "The functional anatomy of the female pelvic floor and stress continence control system," *Scand J Urol Nephrol Suppl*, vol. pp. 1-7; discussion 106-25, 2001.

[104] K. Paddison, "Complying with pelvic floor exercises: A literature review," *Nurs Stand*, vol. 16, pp. 33-8, 2002.

[105] K. E. Andersson, "Drug therapy for urinary incontinence," *Baillieres Best Pract Res Clin Obstet Gynaecol*, vol. 14, pp. 291-313, 2000.

[106] W. Schafer, "Some biomechanical aspects of continence function," *Scand J Urol Nephrol Suppl*, vol. pp. 44-60; discussion 106-25, 2001.

[107] F. Haab, P. E. Zimmern, and G. E. Leach, "Urinary stress incontinence due to intrinsic sphincteric deficiency: Experience with fat and collagen periurethral injections," *J Urol*, vol. 157, pp. 1283-6, 1997.

[108] E. J. McGuire, and S. F. English, "Periurethral collagen injection for male and female sphincteric incontinence: Indications, techniques, and result," *World J Urol*, vol. 15, pp. 306-9, 1997.

[109] G. J. Jarvis, "Surgery for urinary incontinence," *Baillieres Best Pract Res Clin Obstet Gynaecol*, vol. 14, pp. 315-34, 2000.

[110] R. T. Kershen, R. R. Dmochowski, and R. A. Appell, "Beyond collagen: Injectable therapies for the treatment of female stress urinary incontinence in the new millennium," *Urol Clin North Am*, vol. 29, pp. 559-74, 2002.

[111] A. A. Malizia, Jr., H. M. Reiman, R. P. Myers, J. R. Sande, S. S. Barham, R. C. Benson, Jr., M. K. Dewanjee, and W. J. Utz, "Migration and granulomatous reaction after periurethral injection of polytef (teflon)," *Jama*, vol. 251, pp. 3277-81, 1984.

[112] R. T. Kershen, and A. Atala, "New advances in injectable therapies for the treatment of incontinence and vesicoureteral reflux," *Urol Clin North Am*, vol. 26, pp. 81-94, viii, 1999.

[113] T. Yokoyama, J. Huard, and M. B. Chancellor, "Myoblast therapy for stress urinary incontinence and bladder dysfunction," *World J Urol*, vol. 18, pp. 56-61, 2000.

[114] J. Corcos, and C. Fournier, "Periurethral collagen injection for the treatment of female stress urinary incontinence: 4-year follow-up results," *Urology*, vol. 54, pp. 815-8, 1999.

[115] P. A. Bernier, P. E. Zimmern, M. H. Saboorian, and S. Chassagne, "Female outlet obstruction after repeated collagen injections," *Urology*, vol. 50, pp. 618-21, 1997.

[116] V. C. Smith, T. B. Boone, and L. D. Truong, "Collagen polyp of the urinary tract: A report of two cases," *Mod Pathol*, vol. 12, pp. 1090-3, 1999.

[117] T. Yokoyama, R. Pruchnic, J. Y. Lee, Y. C. Chuang, H. Jumon, N. Yoshimura, W. C. de Groat, J. Huard, and M. B. Chancellor, "Autologous primary muscle-derived cells transfer into the lower urinary tract," *Tissue Eng*, vol. 7, pp. 395-404, 2001.

[118] T. Yokoyama, N. Yoshimura, R. Dhir, Z. Qu, M. O. Fraser, H. Kumon, W. C. de Groat, J. Huard, and M. B. Chancellor, "Persistence and survival of autologous muscle derived cells versus bovine collagen as potential treatment of stress urinary incontinence," *J Urol*, vol. 165, pp. 271-6, 2001.

[119] M. B. Chancellor, T. Yokoyama, S. Tirney, C. E. Mattes, H. Ozawa, N. Yoshimura, W. C. de Groat, and J. Huard, "Preliminary results of myoblast injection into the urethra and bladder wall: A possible method for the treatment of stress urinary incontinence and impaired detrusor contractility," *Neurourol Urodyn*, vol. 19, pp. 279-87, 2000.

[120] R. Yiou, P. Dreyfus, D. K. Chopin, C. C. Abbou, and J. P. Lefaucheur, "Muscle precursor cell autografting in a murine model of urethral sphincter injury," *BJU Int*, vol. 89, pp. 298-302, 2002.

[121] J. Y. Lee, T. W. Cannon, R. Pruchnic, M. O. Fraser, J. Huard, and M. B. Chancellor, "The effects of periurethral muscle derived stem cell injection on leak point pressure in a rat model of stress urinary incontinence," *International J Urogynecol*, vol. pp. in press, 2003.

[122] J. Huard, T. Yokoyama, R. Pruchnic, Z. Qu, Y. Li, J. Y. Lee, G. T. Somogyi, W. C. De Groat, and M. B. Chancellor, "Muscle-derived cell-mediated ex vivo gene therapy for urological dysfunction," *Gene Ther*, vol. 9, pp. 1617-26, 2002.

[123] Y. Homma, J. Batista, S. Bauer, D. J. Griffiths, P. Hilton, G. Kramer, G. Lose, and P. Rosier, "Urodynamics," in *Incontinence*, P. Abrams, L. D. Cardozo, S. Khoury, and A. Wein, Eds. Plymouth, OK: Health Publication Ltd., 2002, pp. 318-72.

[124] P. Abrams, R. Feneley, and M. Torrens, *Urodynamics*. New York: Springer-Verlag, 1983.

[125] G. Lose, "Urethral pressure measurement," *Acta Obstet Gynecol Scand Suppl*, vol. 166, pp. 39-42, 1997.

[126] T. W. Cannon, E. M. Wojcik, C. L. Ferguson, S. Saraga, C. Thomas, and M. S. Damaser, "Effects of vaginal distension on urethral anatomy and function," *BJU Int*, vol. 90, pp. 403-7, 2002.

[127] M. E. Brune, A. B. O'Neill, D. M. Gauvin, S. P. Katwala, R. J. Altenbach, J. D. Brioni, A. A. Hancock, and J. P. Sullivan, "Comparison of alpha 1-adrenoceptor agonists in canine urethral pressure profilometry and abdominal leak point pressure models," *J Urol*, vol. 166, pp. 1555-9, 2001.

[128] H. Y. Kwon, A. J. Wein, and R. M. Levin, "Effect of anoxia on the urethral response to phenylephrine," *J Urol*, vol. 154, pp. 1527-31, 1995.

[129] A. Schroeder, J. Lieb, L. O'Connor, P. Horan, R. Leggett, and R. M. Levin, "Role of calcium and calcium modulation in the control of urethral tone," *Scand J Urol Nephrol Suppl*, vol. pp. 19-25; discussion 106-25, 2001.

[130] A. L. Chun, H. S. Gill, A. J. Wein, and R. M. Levin, "Pharmacological comparison of the isolated whole urethra model to urethral strip methodology," *Pharmacology*, vol. 39, pp. 192-9, 1989.

[131] M. Hassouna, A. Abdel-Hakim, M. Abdel-Rahman, C. Galeano, and M. M. Elhilali, "Response of the urethral smooth muscles to pharmacological agents. I. Cholinergic and adrenergic agonists and antagonists," *J Urol*, vol. 129, pp. 1262-4, 1983.

[132] C. Richler, and D. Yaffe, "The in vitro cultivation and differentiation capacities of myogenic cell lines," *Dev Biol*, vol. 23, pp. 1-22, 1970.

[133] T. A. Rando, and H. M. Blau, "Primary mouse myoblast purification, characterization, and transplantation for cell-mediated gene therapy," *J Cell Biol*, vol. 125, pp. 1275-87, 1994.

[134] C. Webster, G. K. Pavlath, D. R. Parks, F. S. Walsh, and H. M. Blau, "Isolation of human myoblasts with the fluorescence-activated cell sorter," *Exp Cell Res*, vol. 174, pp. 252-65, 1988.

[135] J. L. Lequerica, V. Mirabet, J. A. Montero, C. Hurtado, S. Piquer, and F. Carbonell, "In vitro proliferation, differentiation and immuno-magnetic bead purification of human myoblasts," *Ann Transplant*, vol. 4, pp. 103-8, 1999.

[136] S. Okada, H. Nakauchi, K. Nagayoshi, S. Nishikawa, Y. Miura, and T. Suda, "In vivo and in vitro stem cell function of c-kit- and sca-1-positive murine hematopoietic cells," *Blood*, vol. 80, pp. 3044-50, 1992.

[137] M. Osawa, K. Hanada, H. Hamada, and H. Nakauchi, "Long-term lymphohematopoietic reconstitution by a single cd34-low/negative hematopoietic stem cell," *Science*, vol. 273, pp. 242-5, 1996.

[138] D. S. Krause, M. J. Fackler, C. I. Civin, and W. S. May, "Cd34: Structure, biology, and clinical utility," *Blood*, vol. 87, pp. 1-13, 1996.

[139] L. Carlsson, and L. E. Thornell, "Desmin-related myopathies in mice and man," *Acta Physiol Scand*, vol. 171, pp. 341-8, 2001.

[140] R. J. Jankowski, C. Haluszczak, M. Trucco, and J. Huard, "Flow cytometric characterization of myogenic cell populations obtained via the preplate technique: Potential for rapid isolation of muscle-derived stem cells," *Hum Gene Ther*, vol. 12, pp. 619-28, 2001.

[141] K. Yamazaki, and B. P. Eyden, "Ultrastructural and immunohistochemical observations on intralobular fibroblasts of human breast, with observations on the cd34 antigen," *J Submicrosc Cytol Pathol*, vol. 27, pp. 309-23, 1995.

[142] J. M. Vanderwinden, J. J. Rumessen, M. H. De Laet, J. J. Vanderhaeghen, and S. N. Schiffmann, "Cd34+ cells in human intestine are fibroblasts adjacent to, but distinct from, interstitial cells of cajal," *Lab Invest*, vol. 79, pp. 59-65, 1999.

[143] M. J. MacPhee, R. H. Wiltrout, K. L. McCormick, T. J. Sayers, and A. M. Pilaro, "A method for obtaining and culturing large numbers of purified organ-derived murine endothelial cells," *J Leukoc Biol*, vol. 55, pp. 467-75, 1994.

[144] T. Tamaki, A. Akatsuka, K. Ando, Y. Nakamura, H. Matsuzawa, T. Hotta, R. R. Roy, and V. R. Edgerton, "Identification of myogenic-endothelial progenitor cells in the interstitial spaces of skeletal muscle," *J Cell Biol*, vol. 157, pp. 571-7, 2002.

[145] Z. Qu, and J. Huard, "Matching host muscle and donor myoblasts for myosin heavy chain improves myoblast transfer therapy," *Gene Ther*, vol. 7, pp. 428-37, 2000.

[146] R. J. Jankowski, B. M. Deasy, B. Cao, C. Gates, and J. Huard, "The role of cd34 expression and cellular fusion in the regeneration capacity of myogenic progenitor cells," *J Cell Sci*, vol. 115, pp. 4361-74, 2002.

[147] A. Ferrer, K. E. Wells, and D. J. Wells, "Immune responses to dystropin: Implications for gene therapy of duchenne muscular dystrophy," *Gene Ther*, vol. 7, pp. 1439-46, 2000.

[148] G. Karpati, "Immunological aspects of histoincompatible myoblast transfer into non-tolerant hosts," in *Myoblast transfer therapy*, R. Griggs, and G. Karpati, Eds. New York: Plenum Press, 1990, pp. 31-4.

[149] G. K. Pavlath, T. A. Rando, and H. M. Blau, "Transient immunosuppressive treatment leads to long-term retention of allogeneic myoblasts in hybrid myofibers," *J Cell Biol*, vol. 127, pp. 1923-32, 1994.

[150] J. T. Vilquin, E. Wagner, I. Kinoshita, R. Roy, and J. P. Tremblay, "Successful histocompatible myoblast transplantation in dystrophin-deficient mdx mouse despite the production of antibodies against dystrophin," *J Cell Biol*, vol. 131, pp. 975-88, 1995.

[151] J. Rohwedel, V. Horak, M. Hebrok, E. M. Fuchtbauer, and A. M. Wobus, "M-twist expression inhibits mouse embryonic stem cell-derived myogenic differentiation in vitro," *Exp Cell Res*, vol. 220, pp. 92-100, 1995.

[152] J. S. Greenberger, J. P. Goff, J. Bush, A. Bahnson, D. Koebler, H. Athanassiou, M. Domach, and R. K. Houck, "Expansion of hematopoietic stem cells in vitro as a model system for human tissue engineering," *Orthop Clin North Am*, vol. 31, pp. 499-510, 2000.

[153] B. M. Deasy, Z. Qu-Peterson, J. S. Greenberger, and J. Huard, "Mechanisms of muscle stem cell expansion with cytokines," *Stem Cells*, vol. 20, pp. 50-60, 2002.

[154] J. L. Sherley, P. B. Stadler, and J. S. Stadler, "A quantitative method for the analysis of mammalian cell proliferation in culture in terms of dividing and non-dividing cells," *Cell Prolif*, vol. 28, pp. 137-44, 1995.

[155] G. Cossu, B. Zani, M. Coletta, M. Bouche, M. Pacifici, and M. Molinaro, "In vitro differentiation of satellite cells isolated from normal and dystrophic mammalian muscles. A comparison with embryonic myogenic cells," *Cell Differ*, vol. 9, pp. 357-68, 1980.

[156] L. A. Sabourin, A. Girgis-Gabardo, P. Seale, A. Asakura, and M. A. Rudnicki, "Reduced differentiation potential of primary myod-/- myogenic cells derived from adult skeletal muscle," *J Cell Biol*, vol. 144, pp. 631-43, 1999.

[157] J. R. Florini, D. Z. Ewton, and K. A. Magri, "Hormones, growth factors, and myogenic differentiation," *Annu Rev Physiol*, vol. 53, pp. 201-16, 1991.

[158] J. W. Kimball, *Introduction to immunology*. New York: Macmillan Publishing Co., 1986.

[159] J. R. Florini, D. Z. Ewton, and S. L. Roof, "Insulin-like growth factor-i stimulates terminal myogenic differentiation by induction of myogenin gene expression," *Mol Endocrinol*, vol. 5, pp. 718-24, 1991.

[160] P. Hasty, A. Bradley, J. H. Morris, D. G. Edmondson, J. M. Venuti, E. N. Olson, and W. H. Klein, "Muscle deficiency and neonatal death in mice with a targeted mutation in the myogenin gene," *Nature*, vol. 364, pp. 501-6, 1993.

[161] C. K. Smith, 2nd, M. J. Janney, and R. E. Allen, "Temporal expression of myogenic regulatory genes during activation, proliferation, and differentiation of rat skeletal muscle satellite cells," *J Cell Physiol*, vol. 159, pp. 379-85, 1994.

[162] I. Kinoshita, J. T. Vilquin, and J. P. Tremblay, "Pretreatment of myoblast cultures with basic fibroblast growth factor increases the efficacy of their transplantation in mdx mice," *Muscle Nerve*, vol. 18, pp. 834-41, 1995.

[163] M. Grounds, "The proliferation and fusion of myoblasts in vivo," in *Myoblast transfer therapy*, R. Griggs, and G. Karpati, Eds. New York: Plenum Press, 1990, pp. 101-5.

[164] J. T. Barrett, *Textbook of immunology*. St. Louis: C.V. Mosby Company, 1983.

[165] R. Roy, G. Dansereau, J. P. Tremblay, M. Belles-Isles, J. Huard, C. Labrecque, and J. P. Bouchard, "Expression of major histocompatibility complex antigens on human myoblasts," *Transplant Proc*, vol. 23, pp. 799-801, 1991.

[166] K. Nagaraju, N. Raben, G. Merritt, L. Loeffler, K. Kirk, and P. Plotz, "A variety of cytokines and immunologically relevant surface molecules are expressed by normal human skeletal muscle cells under proinflammatory stimuli," *Clin Exp Immunol*, vol. 113, pp. 407-14, 1998.

[167] H. Wiendl, L. Behrens, S. Maier, M. A. Johnson, E. H. Weiss, and R. Hohlfeld, "Muscle fibers in inflammatory myopathies and cultured myoblasts express the nonclassical major histocompatibility antigen hla-g," *Ann Neurol*, vol. 48, pp. 679-84, 2000.

[168] B. A. Ponder, M. M. Wilkinson, M. Wood, and J. H. Westwood, "Immunohistochemical demonstration of h2 antigens in mouse tissue sections," *J Histochem Cytochem*, vol. 31, pp. 911-9, 1983.

[169] A. M. Emslie-Smith, K. Arahata, and A. G. Engel, "Major histocompatibility complex class i antigen expression, immunolocalization of interferon subtypes, and t cell-mediated cytotoxicity in myopathies," *Hum Pathol*, vol. 20, pp. 224-31, 1989.

[170] R. M. McDouall, M. J. Dunn, and V. Dubowitz, "Expression of class i and class ii mhc antigens in neuromuscular diseases," *J Neurol Sci*, vol. 89, pp. 213-26, 1989.

[171] O. Majdic, J. Stockl, W. F. Pickl, J. Bohuslav, H. Strobl, C. Scheinecker, H. Stockinger, and W. Knapp, "Signaling and induction of enhanced cytoadhesiveness via the hematopoietic progenitor cell surface molecule cd34," *Blood*, vol. 83, pp. 1226-34, 1994.

[172] T. L. Holyoake, and M. J. Alcorn, "Cd34+ positive haemopoietic cells: Biology and clinical applications," *Blood Rev*, vol. 8, pp. 113-24, 1994.

[173] P. Zammit, and J. Beauchamp, "The skeletal muscle satellite cell: Stem cell or son of stem cell?," *Differentiation*, vol. 68, pp. 193-204, 2001.

[174] M. J. Fackler, D. S. Krause, O. M. Smith, C. I. Civin, and W. S. May, "Full-length but not truncated cd34 inhibits hematopoietic cell differentiation of m1 cells," *Blood*, vol. 85, pp. 3040-7, 1995.

[175] D. Schluter, M. Deckert-Schluter, G. Schwendemann, H. Brunner, and H. Hof, "Expression of major histocompatibility complex class ii antigens and levels of interferon-gamma, tumour necrosis factor, and interleukin-6 in cerebrospinal fluid and serum in toxoplasma gondii-infected scid and immunocompetent c.B-17 mice," *Immunology*, vol. 78, pp. 430-5, 1993.

[176] D. L. Simmons, A. B. Satterthwaite, D. G. Tenen, and B. Seed, "Molecular cloning of a cdna encoding cd34, a sialomucin of human hematopoietic stem cells," *J Immunol*, vol. 148, pp. 267-71, 1992.

[177] D. S. Krause, T. Ito, M. J. Fackler, O. M. Smith, M. I. Collector, S. J. Sharkis, and W. S. May, "Characterization of murine cd34, a marker for hematopoietic progenitor and stem cells," *Blood*, vol. 84, pp. 691-701, 1994.

[178] K. A. Jackson, S. M. Majka, G. G. Wulf, and M. A. Goodell, "Stem cells: A minireview," *J Cell Biochem Suppl*, vol. 38, pp. 1-6, 2002.

[179] N. Mahmud, P. Weiss, F. Li, and R. Hoffman, "Primate skeletal muscle contains cells capable of sustaining in vitro hematopoiesis," *Exp Hematol*, vol. 30, pp. 925-36, 2002.

[180] C. Dell'Agnola, C. Rabascio, P. Mancuso, M. Capillo, G. Pruneri, A. Gobbi, S. Minucci, S. Ronzoni, S. Volorio, L. Calabrese, N. Tradati, G. Martinelli, L. Shultz, and F. Bertolini, "In vitro and in vivo hematopoietic potential of human stem cells residing in muscle tissue," *Exp Hematol*, vol. 30, pp. 905-14, 2002.

[181] K. Hayashi, "Experimental approaches on measuring the mechanical properties and constitutive laws of arterial walls," *J Biomech Eng*, vol. 115, pp. 481-8, 1993.

[182] D. A. Vorp, D. A. Severyn, D. L. Steed, and M. W. Webster, "A device for the application of cyclic twist and extension on perfused vascular segments," *Am J Physiol*, vol. 270, pp. H787-95, 1996.

[183] J. Zhao, X. Lu, F. Zhuang, and H. Gregersen, "Biomechanical and morphometric properties of the arterial wall referenced to the zero-stress state in experimental diabetes," *Biorheology*, vol. 37, pp. 385-400, 2000.

[184] M. A. Zulliger, N. T. Kwak, T. Tsapikouni, and N. Stergiopulos, "Effects of longitudinal stretch on vsm tone and distensibility of muscular conduit arteries," *Am J Physiol Heart Circ Physiol*, vol. 283, pp. H2599-605, 2002.

[185] P. O. Andersson, A. Malmgren, and B. Uvelius, "Functional responses of different muscle types of the female rat urethra in vitro," *Acta Physiol Scand*, vol. 140, pp. 365-72, 1990.

[186] W. D. Steers, "Rat: Overview and innervation," *Neurourol Urodyn*, vol. 13, pp. 97-118, 1994.

[187] M. C. Heidkamp, F. C. Leong, L. Brubaker, and B. Russell, "Pudendal denervation affects the structure and function of the striated, urethral sphincter in female rats," *Int Urogynecol J Pelvic Floor Dysfunct*, vol. 9, pp. 88-93, 1998.

[188] J. M. Kerns, M. S. Damaser, J. M. Kane, K. Sakamoto, J. T. Benson, S. Shott, and L. Brubaker, "Effects of pudendal nerve injury in the female rat," *Neurourol Urodyn*, vol. 19, pp. 53-69, 2000.

[189] R. F. Labadie, J. F. Antaki, J. L. Williams, S. Katyal, J. Ligush, S. C. Watkins, S. M. Pham, and H. S. Borovetz, "Pulsatile perfusion system for ex vivo investigation of biochemical pathways in intact vascular tissue," *Am J Physiol*, vol. 270, pp. H760-8, 1996.

[190] B. von Heyden, R. K. Riemer, L. Nunes, G. B. Brock, T. F. Lue, and E. A. Tanagho, "Response of guinea pig smooth and striated urethral sphincter to cromakalim, prazosin, nifedipine, nitroprusside, and electrical stimulation," *Neurourol Urodyn*, vol. 14, pp. 153-68, 1995.

[191] M. Parlani, B. Conte, and S. Manzini, "Nonadrenergic, noncholinergic inhibitory control of the rat external urethral sphincter: Involvement of nitric oxide," *J Pharmacol Exp Ther*, vol. 265, pp. 713-9, 1993.

[192] S. Corvin, H. Strasser, S. T. Boesch, G. Bartsch, and H. Klocker, "Human rhabdosphincter cell culture: A model for videomicroscopy of cell contractions," *Prostate*, vol. 47, pp. 189-93, 2001.

[193] M. Parlani, S. Manzini, A. Argentino-Storino, and B. Conte, "The rat external urethral sphincter an in vitro model to evaluate the activity of drugs on the smooth and striated components of the urinary bladder outlet," *J Pharmacol Toxicol Methods*, vol. 28, pp. 85-90, 1992.

[194] B. Russell, M. Baumann, M. C. Heidkamp, and A. Svanborg, "Morphometry of the aging female rat urethra," *Int Urogynecol J Pelvic Floor Dysfunct*, vol. 7, pp. 30-6, 1996.

[195] B. C. Bennett, M. N. Kruse, J. R. Roppolo, H. D. Flood, M. Fraser, and W. C. de Groat, "Neural control of urethral outlet activity in vivo: Role of nitric oxide," *J Urol*, vol. 153, pp. 2004-9, 1995.

[196] W. C. de Groat, and N. Yoshimura, "Pharmacology of the lower urinary tract," *Annu Rev Pharmacol Toxicol*, vol. 41, pp. 691-721, 2001.

[197] J. O. DeLancey, J. A. Gosling, K. Creed, J. Dixon, V. Delmas, D. Landon, and P. Norton, "Gross anatomy and cell biology of the lower urinary tract," in *Incontinence*, P. Abrams, L. D. Cardozo, S. Khoury, and A. Wein, Eds. Plymouth, UK: Health Publications Ltd., 2002, pp. 19-82.

[198] H. Kakizaki, M. O. Fraser, and W. C. De Groat, "Reflex pathways controlling urethral striated and smooth muscle function in the male rat," *Am J Physiol*, vol. 272, pp. R1647-56, 1997.

[199] B. A. Van der Werf, and K. E. Creed, "Mechanical properties and innervation of the smooth muscle layers of the urethra of greyhounds," *BJU Int*, vol. 90, pp. 588-95, 2002.

[200] W. K. Ovalle, B. H. Bressler, L. G. Jasch, and C. E. Slonecker, "Abnormal distribution of fiber types in the slow-twitch soleus muscle of the c57bl/6j dy2j/dy2j dystrophic mouse during postnatal development," *Am J Anat*, vol. 168, pp. 291-304, 1983.

[201] R. H. Fitts, and J. J. Widrick, "Muscle mechanics: Adaptations with exercise-training," *Exerc Sport Sci Rev*, vol. 24, pp. 427-73, 1996.

[202] I. Saenz de Tejada, N. N. Kim, J. T. Daley, R. Royai, J. Hypolite, G. A. Broderick, F. Garcia-Diaz, and R. Levin, "Acidosis impairs rabbit trabecular smooth muscle contractility," *J Urol*, vol. 157, pp. 722-6, 1997.

[203] O. B. Nielsen, F. de Paoli, and K. Overgaard, "Protective effects of lactic acid on force production in rat skeletal muscle," *J Physiol*, vol. 536, pp. 161-6, 2001.

[204] T. Streng, R. Santti, and A. Talo, "Similarities and differences in female and male rat voiding," *Neurourol Urodyn*, vol. 21, pp. 136-41, 2002.

[205] R. H. Cox, "Comparison of arterial wall mechanics in normotensive and spontaneously hypertensive rats," *Am J Physiol*, vol. 237, pp. H159-67, 1979.

[206] S. E. Greenwald, D. L. Newman, and H. T. Denyer, "Effect of smooth muscle activity on the static and dynamic elastic properties of the rabbit carotid artery," *Cardiovasc Res*, vol. 16, pp. 86-94, 1982.

[207] P. Fridez, A. Makino, H. Miyazaki, J. J. Meister, K. Hayashi, and N. Stergiopulos, "Short-term biomechanical adaptation of the rat carotid to acute hypertension: Contribution of smooth muscle," *Ann Biomed Eng*, vol. 29, pp. 26-34, 2001.

[208] C. J. Wingard, A. K. Browne, and R. A. Murphy, "Dependence of force on length at constant cross-bridge phosphorylation in the swine carotid media," *J Physiol*, vol. 488 (Pt 3), pp. 729-39, 1995.

[209] T. E. Carew, R. N. Vaishnav, and D. J. Patel, "Compressibility of the arterial wall," *Circ Res*, vol. 23, pp. 61-8, 1968.

[210] G. Faury, G. M. Maher, D. Y. Li, M. T. Keating, R. P. Mecham, and W. A. Boyle, "Relation between outer and luminal diameter in cannulated arteries," *Am J Physiol*, vol. 277, pp. H1745-53, 1999.

[211] K. B. Chandran, *Cardiovascular biomechanics*. New York: New York University Press, 1992.

[212] A. G. Hudetz, "Incremental elastic modulus for orthotropic incompressible arteries," *J Biomech*, vol. 12, pp. 651-5, 1979.

[213] D. H. Bergel, "The static elastic properties of the arterial wall," *J Physiol*, vol. 156, pp. 445-57, 1961.

[214] P. B. Dobrin, "Mechanical behavior of vascular smooth muscle in cylindrical segments of arteries in vitro," *Ann Biomed Eng*, vol. 12, pp. 497-510, 1984.

[215] R. H. Cox, and P. P. Bockus Institute, "Comparison of carotid artery mechanics in the rat, rabbit, and dog," *Am J Physiol*, vol. 234, pp. H280-8, 1978.

[216] R. H. Cox, "Basis for the altered arterial wall mechanics in the spontaneously hypertensive rat," *Hypertension*, vol. 3, pp. 485-95, 1981.

[217] A. G. Hudetz, G. Mark, A. G. Kovach, T. Kerenyi, L. Fody, and E. Monos, "Biomechanical properties of normal and fibrosclerotic human cerebral arteries," *Atherosclerosis*, vol. 39, pp. 353-65, 1981.

[218] S. A. Awad, and J. W. Downie, "Relative contributions of smooth and striated muscles to the canine urethral pressure profile," *Br J Urol*, vol. 48, pp. 347-54, 1976.

[219] E. A. Tanagho, F. H. Meyers, and D. R. Smith, "Urethral resistance: Its components and implications. Ii. Striated muscle component," *Invest Urol*, vol. 7, pp. 195-205, 1969.

[220] A. S. Cass, and F. Hinman, Jr., "Constant urethral flow in female dog. I. Normal vesical and urethral pressures and effect of muscle relaxant," *J Urol*, vol. 99, pp. 442-6, 1968.

[221] A. Arner, A. Mattiasson, P. Radzizewski, and B. Uvelius, "Shortening velocity is different in longitudinal and circular muscle layers of the rabbit urethra," *Urol Res*, vol. 26, pp. 423-6, 1998.

[222] B. A. Van der Werf, T. Hidaka, and K. E. Creed, "Continence and some properties of the urethral striated muscle of male greyhounds," *BJU Int*, vol. 85, pp. 341-9, 2000.

[223] G. Bratslavsky, B. Kogan, and R. M. Levin, "Urethra is more sensitive to ischemia than bladder: Evidence from an in vitro rat study," *J Urol*, vol. 165, pp. 2086-90, 2001.

[224] D. A. Vorp, M. L. Raghavan, H. S. Borovetz, H. P. Greisler, and M. W. Webster, "Modeling the transmural stress distribution during healing of bioresorbable vascular prostheses," *Ann Biomed Eng*, vol. 23, pp. 178-88, 1995.

[225] W. W. von Maltzahn, D. Besdo, and W. Wiemer, "Elastic properties of arteries: A nonlinear two-layer cylindrical model," *J Biomech*, vol. 14, pp. 389-97, 1981.

[226] Y. C. Fung, and S. Q. Liu, "Strain distribution in small blood vessels with zero-stress state taken into consideration," *Am J Physiol*, vol. 262, pp. H544-52, 1992.

[227] M. Thomas, B. Langley, C. Berry, M. Sharma, S. Kirk, J. Bass, and R. Kambadur, "Myostatin, a negative regulator of muscle growth, functions by inhibiting myoblast proliferation," *J Biol Chem*, vol. 275, pp. 40235-43, 2000.

[228] K. Suzuki, R. T. Smolenski, J. Jayakumar, B. Murtuza, N. J. Brand, and M. H. Yacoub, "Heat shock treatment enhances graft cell survival in skeletal myoblast transplantation to the heart," *Circulation*, vol. 102, pp. III216-21, 2000.

[229] Y. Fujio, K. Guo, T. Mano, Y. Mitsuuchi, J. R. Testa, and K. Walsh, "Cell cycle withdrawal promotes myogenic induction of akt, a positive modulator of myocyte survival," *Mol Cell Biol*, vol. 19, pp. 5073-82, 1999.

[230] S. D. Hauschka, "Development, anatomy, and cell biology," in *Myology*, A. G. Engel, and C. Franszini-Armstrong, Eds. New York: McGraw-Hill, Inc., 1994, pp. 3-73.

[231] S. Guettier-Sigrist, G. Coupin, J. M. Warter, and P. Poindron, "Cell types required to efficiently innervate human muscle cells in vitro," *Exp Cell Res*, vol. 259, pp. 204-12, 2000.

[232] B. D. Agarwal, and L. J. Broutman, *Analysis and performance of fiber composites*. New York: Wiley and Sons, 1990.

[233] T. Wakatsuki, M. S. Kolodney, G. I. Zahalak, and E. L. Elson, "Cell mechanics studied by a reconstituted model tissue," *Biophys J*, vol. 79, pp. 2353-68, 2000.

[234] K. Sakamoto, G. M. Smith, P. D. Storer, K. J. Jones, and M. S. Damaser, "Neuroregeneration and voiding behavior patterns after pudendal nerve crush in female rats," *Neurourol Urodyn*, vol. 19, pp. 311-21, 2000.

[235] B. M. Deasy, R. J. Jankowski, T. R. Payne, B. Cao, J. P. Goff, J. S. Greenberger, and J. Huard, "Modeling stem cell population growth: Incorporating terms for proliferative heterogeneity," *Stem Cells*, vol. pp. in press.